NUMERICAL ANALYSIS OF THE ELECTRICAL CHARACTERISTICS OF LEAD-FREE PEROVSKITE SOLAR CELL BASED ON METHYLAMMONIUM TIN IODIDE

GEORGE GICHANGA NJEMA

A Thesis Submitted to the Graduate School in Partial Fulfilment of the Requirements for the Master of Science Degree in Chemistry of Egerton University

EGERTON UNIVERSITY

OCTOBER, 2024

DECLARATION AND RECOMMENDATION

Declaration

This thesis is my original work and has not been submitted or presented for examination in any institution.

Signature…… 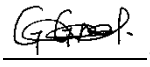 ……. Date……3/10/2024……

George Gichanga Njema

SM11/04066/22

Recommendation

This thesis has been submitted for examination with our approval as University supervisors.

Signature……  …… Date……4/10/2024.....

Prof. Joshua K. Kibet, Ph.D.

Department of Chemistry

Egerton University, Njoro

Signature  Date…....4/10/2024.....

Prof. S. M. Ngari, PhD.

Department of Chemistry

Egerton University, Njoro

COPYRIGHT

DEDICATION

I dedicate this work with deep appreciation to my loving parents, Mr. Duncan Njema Gichanga and Mrs. Julia Wairimu Njema, along with Mr. Sammy Mwangi Njema and Josephine Nyambura Karago. Their steadfast support, encouragement, and prayers have been vital in guiding me to pursue my aspirations and achieve this accomplishment. To my dear wife, Regina Nyokabi your constant love, support, and patience have been my guiding light throughout this journey. To my son, Milan Njema, and my daughters, Millicent Wangui and Michelle Wairimu you are my greatest inspiration. I hope this work shows you that with dedication and perseverance, you can achieve anything. This work is dedicated to all of you, with all my love.

ACKNOWLEDGEMENTS

I am profoundly grateful to the Almighty God for the grace and strength to complete this work. My deepest appreciation goes to Egerton University, particularly the Department of Chemistry, for their invaluable support and the facilities that enabled the success of this study. I am especially thankful to my supervisors, Prof. Joshua K. Kibet and Prof. S. M. Ngari, whose mentorship, unwavering support, and insightful guidance have greatly shaped my academic journey. I extend my heartfelt thanks to my parents, sister, and friends for their continuous prayers, financial, and moral support. I am also grateful to Prof. J.K. Kibet's research group, especially Josephate O. Bosire and Dr. Rono, for fostering a collaborative scientific environment. Prof. Burgelman of the University, Department of Information Systems, Belgium, is highly appreciated for facilitating the use of SCAPS-1D device simulator. Special thanks go to Ms. Salome Wairimu Muturi for her generous material and financial support. I would like to express my heartfelt gratitude to the Egerton University Alumni Association (EUAA) for awarding me the Master's Grant Scholarship. Your support has been invaluable in advancing my research efforts. I am deeply appreciative of the opportunity you have provided to further my academic and professional growth. Lastly, I acknowledge everyone whose cooperation and assistance have contributed to the success of this study. I pray for God’s blessings to all.

ABSTRACT

The desire to decarbonise the global energy system has paved the way for renewable energy alternatives like solar energy, which is more dependable, affordable, inexhaustible, and sustainable. Nonetheless, there are significant challenges associated with stability, durability, and scalability with photovoltaic technologies. By carefully optimizing the interfacial engineering of device architectures, these bottle-necks can be addressed, lowering the cost of fabrication while improving the performance and longevity of the solar cell designs. Solar cell capacitance simulator (SCAPS-1D) was utilized to model the electrical behaviour of perovskite solar cells. Accordingly, this study presents a thorough examination of performance indicators for a range of perovskite solar cell (PSC) configurations, comprising both traditional and innovative architectures. Various hole transport layers (HTLs) and electron transport layers (ETLs) have been tested. The configurations examined include HTL-free architecture, ITO/PC61BM/$CH_3NH_3SnI_3$/Pt, as well as those integrating hole transport materials such as graphene oxide (GO) and Poly(3,4-ethylenedioxythiophene) polystyrene sulfonate (PEDOT:PSS). The simulations recorded impressive photovoltaic parameters – HTL-free configuration, ITO/PC61BM/$CH_3NH_3SnI_3$/Pt, achieved a remarkable PCE of 38.11%, J_{sc} of 35.32 mA/cm², V_{oc} of 1.2168 V, and FF of 88.67%. Another configuration, ITO/PC61BM/$CH_3NH_3SnI_3$/GO/Fe, delivered a PCE of 36.27%, J_{sc} of 34.84 mA/cm², V_{oc} of 1.3462 V, and FF of 77.32%. On the other hand, the cell with the configuration, ITO/PC61BM/$CH_3NH_3SnI_3$/PEDOT:PSS/Mo, gave a PCE of 37.66%. Furthermore, cadmium sulphide (CdS), zinc selenide (ZnSe) and titanium oxide (TiO_2) were investigated as a buffer layer across the HTL-free configuration in order to enhance charge collection, charge transport and minimize recombination losses. The HTL-free design demonstrated significant potential for producing cost-effective and efficient solar cells with outstanding electrical and optical properties. Configurations incorporating GO as the HTL showed remarkable improvements in thermal stability and efficiency, driven by excellent charge separation, low recombination rates, and high quantum efficiency (QE). This work underscores the necessity of developing high-performance, lead-free PSCs to mitigate the environmental and health risks associated with traditional lead-based designs, and offers valuable guidance for the future development of PSC technology.

TABLE OF CONTENTS

LIST OF TABLES

LIST OF FIGURES

LIST OF ABBREVIATIONS AND ACRONYMS

BIPV	Building-integrated photovoltaics
CdS	Cadimium sulphide
CTL	Conjugated transport layer
CZTS	Copper zinc tin sulphide
DC	Direct current
DPSC	Double perovskite solar cell
DSSCs	Dye sensitized solar cells
Ea	Activation energy
ESC	Electron selective contacts
ETL	Electron transport layer
FF	Fill factor
FTO	Fluorine doped tin oxide
HJT	Heterojuctions
HSC	Hole selective contacts
HTL	Hole transport layer
ITO	Indium doped tin oxide
J_{sc}	Short circuit current density
LFDPs	Lead free double perovskite solar cells
MS	Mott-Schottky
NACOSTI	National Commission for Science, Technology and Innovation
OPVs	Organic photovoltaics
PC61BM	[6,6]-Phenyl-C61-butyric acid methyl ester
PCE	Power conversion efficiency
PEDOT:PSS	Poly(3,4-ethelenedioxythiophene) polystyrene sulphonate
PPDI:F_3N	(Poly{[N,N'-bis(2-decyltetradecyl)-naphthalene-1,4,5,8-bis(dicarboximide)-2,6-diyl]-alt-5,5'-(2,2'-bithiophene)
PQDS	Perovskite quantum dot
PERC	Passivated emitter and rear contacts
PLD	Pulsed laser deposition
PSCs	Perovskite solar cells
PV	Photovoltaic
QD	Quantum dot

QDSCs	Quantum dot sensitized solar cells
QE	Quantum efficiency
SCAPS-1D	One dimensional solar cell capacitance simulator
S-Q	Shockley-Quisser
Vsn	Tin vacancies
TCO	Transparent conductive oxide
TOE	Tonne of energy equivalent
TSCs	Tandem solar cells
UV	Ultra – Violet
V_{oc}	Open circuit voltage
ZnOS	Zinc oxysulphide

CHAPTER ONE
INTRODUCTION

1.1 Background information

Maximizing the potential of green energy is crucial for tackling the escalating environmental issues caused by rising pollution from fossil fuels and woody biomass (Raihan & Tuspekova, 2022). Photovoltaic systems are particularly versatile due to their ability to convert solar energy into electricity (El Hammoumi *et al.*, 2022). Perovskite solar cells (PSCs) offer a promising alternative to traditional solar cells due to their potential for low-cost production, lightweight nature, and ease of processing. However, their commercialization is hindered by low stability. To address this issue, polymers are employed to enhance the stability of PSCs, paving the way for the development of more affordable solar cells with improved conversion efficiencies. In this study, optical modelling will be utilized to efficiently and comprehensively model these devices. This approach will aid in identifying new materials and techniques for better designs, eliminating unfavourable component combinations in experimental devices, and ultimately accelerating the advancement of highly efficient organic perovskite solar cells. By carefully analysing the complex interactions among material layers and interfaces within the $MASnI_3$ solar cell architecture, this study aims to optimize electron transport, charge separation, and overall device efficiency. Through innovative interface engineering and precise adjustments to the perovskite layer thickness, this research aspires to unlock the full potential of lead-free PSCs, paving the way for highly efficient and environmentally sustainable solar energy conversion.

This work introduces a novel approach in order to tackle the critical challenges of stability, scalability, and environmental sustainability in PSC technology. By exploring a range of both conventional and innovative PSC configurations, the study emphasizes the importance of optimizing interfacial engineering using buffers and interfacial layers to boost device performance while reducing fabrication costs. One of the standout innovations is the exploration of the HTL-free architecture which has the capability to revolutionise the affordability and simplicity of photovoltaic cells. This underscores the potential for creating highly efficient solar cells without relying on expensive or potentially unstable HTLs, thereby paving the way for more cost-effective solutions. The study also highlights the significant role of graphene oxide (GO) and PEDOT:PSS as hole transport layers. The incorporation of these materials has the potential to improve the thermal stability, charge separation, and overall device efficiency.

Solar cells convert sunlight into electricity, and have evolved through four distinct generations, each with its own advantages and challenges. The first-generation solar cells are characterized by crystalline silicon solar cells, which currently dominate the photovoltaic market with an established efficiency of approximately 25% (Pattelath *et al.*, 2023). The major drawback is enormous cost associated purification of silicon. On the other hand, thin-film solar cells, introduced as the second generation, offer lower material costs but their efficiency is generally lower than that of crystalline silicon cells, typically around 10% to 12% (Chopra *et al.*, 2004). Further, the use of toxic materials such as Cd in some thin-film technologies also raises environmental and disposal concerns.

The third generation introduces emerging technologies that aim to exceed the efficiency limits of traditional cells (Solak & Irmak, 2023). These solar cells use innovative materials like perovskites, organic compounds, and quantum dots, which offer the potential for high efficiency and cost-effective production; however, these technologies face significant challenges, including stability issues that limit their long-term viability. Examples of third-generation solar cells include perovskite cells, which have achieved efficiencies exceeding 25% in laboratory settings, and organic photovoltaics (OPVs), which are flexible and lightweight although they exhibit low efficiencies of around 10%-12% (Alhamada *et al.*, 2023). The fourth generation focuses on hybrid and advanced solar cells that combine the strengths of earlier technologies to achieve high efficiency, low cost, and improved stability. Examples include multi-junction solar cells, which use multiple layers to capture different parts of the solar spectrum and have achieved efficiencies above 40% (Pearce *et al.*, 2024).

Simulation strategies in PSCs are crucial for optimizing device performance, understanding material behaviour, and predicting experimental results. Popular tools like SCAPS-1D, wxAMPS, and TiberCAD focus on solving drift-diffusion equations to model charge transport, recombination, and generation processes within PSCs (Chouchen *et al.*, 2024). These simulation tools enable researchers to investigate how factors such as absorber thickness, band alignment, defect states, and interface properties influence key performance metrics like V_{oc}, FF, and PCE. By modelling various device architectures, including planar and mesoporous designs, researchers can evaluate the effects of different ETLs and HTLs, as well as back contact materials, under varying temperature and illumination conditions. This approach helps streamline experimental efforts, guiding material selection and device optimization for improved stability and efficiency.

According to estimates released in 2019, global energy consumption is projected to rise to 17 billion tonnes of energy equivalent (TOE) by 2035 (Newell *et al.,* 2019). The unprecedented surge in electricity demand is attributed to the rapid growth of the human population and the swift expansion of the industrial and technology sectors (Madhav & Tyagi, 2022). Unfortunately, this has led to a significant dependence on fossil fuels for power generation, further exacerbating the already high pollution levels (Ali & Seraj, 2022). Consequently, promoting sustainable practices and reducing emissions from power production have become increasingly crucial in the energy sector. Solar cell technology is advocated as an eco-friendly solution to the emerging energy challenge due to its abundance of resources, sustainability, renewability, and ease of deployment (Olujobi *et al.,* 2023). The earlier and current generations of solar cell technologies, including those based on silicon and thin films, face several challenges. These include a long energy payback period, higher costs due to the need for purer active materials, material shortages, poor performance in low-light conditions, inflexibility, and issues with opacity and aesthetics. However, next-generation PSCs are being developed as a promising alternative. Lead-free tin halide perovskites, known for their eco-friendly properties, high carrier mobility, and bandgap close to the Shockley-Queisser limit (S-Q), are considered to be particularly promising candidates (Jang *et al.,* 2023).

The quest for solar cells that are non-toxic, highly efficient, and environmentally friendly remains a central focus of scientific research (Ikram *et al.,* 2022). The upcoming generation of PSCs is anticipated to utilize lead-free tin halide perovskites. These materials are expected to offer high mobility, a suitable bandgap close to the S-Q limit, and other environmentally friendly properties (Wu *et al.,* 2022). Another approach to enhancing the stability of perovskite solar cells involves the use of interfacial layers. In a standard perovskite solar cell, an electron-selective contact (ESC) and a hole-selective contact (HSC) interface are formed by placing a perovskite layer between two electron-selective contacts.). Perovskite solar cells could play a significant role in advancing sustainable development objectives by enhancing clean energy generation (SDG 7) and supporting climate action efforts (SDG 13) (Olabi *et al.,* 2023). Therefore, this work contributes immensely towards the global transition in renewable energy, access and uptake in order to a sustainable energy future.

1.2 Statement of the problem

Transitioning to a net-zero pollution future is dependent on overcoming key challenges in solar energy technology. Perovskite solar cells (PSCs) offer promise due to their cost-effectiveness and efficiency, but issues such as lead toxicity and stability must be addressed for environmental sustainability. Enhancing interfacial engineering is vital for improving

efficiency and extending solar panel lifespan. There is need to introduce sophisticated modelling and experimental validation to optimize perovskite solar cells for better performance. This aligns with broader ambitions to advance solar energy technology globally, contributing to cleaner energy sources and climate change mitigation. Perovskite solar cells represent a significant step towards a cleaner and more cost-effective energy future, addressing environmental concerns and meeting growing energy demands. This work underscores a commitment to tackling urgent environmental challenges through innovative technological solutions, and ultimately shaping a sustainable and equitable global energy system.

1.3 Objectives

1.3.1 General objective

To explore the electrical output characteristics of the simulated methylammonium tin iodide perovskite solar cell with the purpose of understanding its efficiency and potential for renewable energy applications.

1.3.2 Specific objectives

i. To determine how different material layers will affect the performance of the solar cell architecture based on methylammonium tin iodide photoactive layer
ii. To calculate numerically the electrical characteristics of the proposed solar cell structure such as current density (J_{sc}), open circuit-voltage (V_{oc}), power conversation efficiency (PCE) and Fill factor (FF).
iii. To compute the optical characteristics of the proposed solar cell architecture based on the optimization of various thicknesses of the perovskite.

1.4 Research questions

i. How will different material layers affect the performance of the proposed solar cell device?
ii. What are the numerical values of the electrical characteristics of the proposed cell architecture?
iii. How do the optical characteristics of the simulated solar cell vary with the thickness of the perovskite?

1.5 Justification

The urgent push for 100% renewable energy, especially through solar power, faces challenges like making perovskite solar cells economically viable and addressing lead toxicity concerns. Overcoming these requires significant investment in improving electron movement and charge separation in solar cell structures. This is crucial for a pollution-free future, as these

barriers affect solar energy system effectiveness, safety, and scalability. While PSCs offer promise due to cost-effectiveness and efficiency, lead contamination and stability issues must be addressed for environmental sustainability. Optimizing interface engineering is also vital for energy conversion efficiency and solar panel lifespan. Solar energy, particularly through perovskite cells, aligns with sustainable development goals (SDGs) and climate action agendas, emphasizing the importance of technological solutions in the face of rising energy demand and climate change. Research focusing on optimizing perovskite absorber layers is essential for advancing solar cell technology and accelerating the transition to sustainable energy.

REFERENCES

Alhamada, T., Hanim, M. A., Saidur, R., Nuraini, A., Hasan, W. W., & Jung, D. (2023). Recent advances in polymer and perovskite based third-generation solar cell devices. *Materials Today: Proceedings*, ***74***(45), 533-539. https://doi.org/10.1016/j.matpr.2022.12.158

Ali, M., & Seraj, M. (2022). Nexus between energy consumption and carbon dioxide emission: evidence from 10 highest fossil fuel and 10 highest renewable energy-using economies. *Environmental Science and Pollution Research*, ***29***(58), 87901-87922.

Chopra, K., Paulson, P., & Dutta, V. (2004). Thin-film solar cells: an overview. *Progress in Photovoltaics: Research and Applications*, ***12***(2-3), 69-92.

Chouchen, B., Mhadhbi, N., Gassoumi, B., Hamdi, I., Hadi, H., der Maur, M. A., Chouaih, A., Ladhari, T., Magazù, S., & Naïli, H. (2024). DFT-Computational Modeling and TiberCAD Frameworks for Photovoltaic Performance Investigation of Copper-Based 2D Hybrid Perovskite Solar Absorbers. *ACS omega*, ***9***(27), 29263-29273.

El Hammoumi, A., Chtita, S., Motahhir, S., & El Ghzizal, A. (2022). Solar PV energy: From material to use, and the most commonly used techniques to maximize the power output of PV systems: A focus on solar trackers and floating solar panels. *Energy Reports*, ***8***(2), 11992-12010.

Hsieh, S., Lin, P.-Y., Lin, I.-H., Beck, D. E., & Lin, C.-H. (2023). Assessing the contribution of semiconductors to the sustainable development goals (SDGs) from 2017 to 2022. *Heliyon*, ***9***(11), 1-15.

Ikram, M., Malik, R., Raees, R., Imran, M., Wang, F., Ali, Salamat.,Maqbool, M. (2022). Recent advancements and future insight of lead-free non-toxic perovskite solar cells for sustainable and clean energy production: A review. *Sustainable Energy Technologies and Assessments*, ***53***(5), 1-51.

Jang, W. J., Jang, H. W., & Kim, S. Y. (2024). Recent Advances in Wide Bandgap Perovskite Solar Cells: Focus on Lead-Free Materials for Tandem Structures. *Small Methods*, ***8***(2), 1-26.

Newell, R., Raimi, D., & Aldana, G. (2019). Global energy outlook 2019: the next generation of energy. *Resources for the Future*, ***1***, 8-19.

Olujobi, O. J., Okorie, U. E., Olarinde, E. S., & Aina-Pelemo, A. D. (2023). Legal responses to energy security and sustainability in Nigeria's power sector amidst fossil fuel disruptions and low carbon energy transition. *Heliyon*, ***9***(7), 1-24.

Pearce, P. M., Halme, J., Jiang, J. Y., & Ekins-Daukes, N. J. (2024). Efficiency limits and design principles for multi-junction coloured photovoltaics. *Energy & Environmental Science*, ***17***(3), 1189-1201.

Pattelath, M. S., Giripunje, S. M., & Verma, A. K. (2023). A Review of Photovoltaic Cell Generations and Simplified Overview of Bifacial Photovoltaic Cell Technology. *Applied Solar Energy*, ***59***(5), 621-646.

Raihan, A., & Tuspekova, A. (2022). Nexus between economic growth, energy use, agricultural productivity, and carbon dioxide emissions: new evidence from Nepal. *Energy Nexus*, ***7***(22), 1-12.

Solak, E. K., & Irmak, E. (2023). Advances in organic photovoltaic cells: A comprehensive review of materials, technologies, and performance. *RSC advances*, 13(18), 12244-12269.

Wu, T., Liu, X., Luo, X., Segawa, H., Tong, G., Zhang, Y.,Han, L. (2022). Heterogeneous FASnI3 absorber with enhanced electric field for high-performance lead-free perovskite solar cells. *Nano-Micro Letters*, ***14***(1), 99.

CHAPTER TWO
LITERATURE REVIEW

2.1 Introduction

The continuous global warming, technological advancement, and improving living conditions worldwide drive the requirement for dependable, safe, and clean energy sources. As a result, traditional fossil fuels are inadequate to sustain the human society's ability to expand sustainably and protect the environment (Wang *et al.,* 2023). For many years, humanity has relied on energy sources that harm the environment, contributing to global warming and climate change, and public health issues. Consequently, intensive scientific research has increasingly focused on identifying sustainable renewable energy solutions. Among the various alternatives, including biofuels, geothermal energy, and nuclear power, solar energy stands out as one of the most viable, reliable, and inexhaustible resources. In essence, a solar cell is a device that harnesses the photovoltaic effect or photochemical reactions to convert light energy directly into electrical energy (Kong *et al.,* 2023).

In recent years, PSCs have garnered significant attention due to their exceptional photovoltaic functionality. The general chemical structure of PSCs is represented as ABX_3, where X is a halogen anion, B is a divalent cation, and A is a monovalent cation, such as potassium or caesium. Materials for perovskites are considered leading candidates for next-generation photovoltaic technology, owing to their unique characteristics, including high electron mobility (up to 800 cm^2/Vs), extended carrier diffusion lengths (exceeding 1 μm), and excellent charge transport properties (Roy *et al.,* 2022). The key distinction between organic absorbers and inorganic photoactive materials lies in their high exciton transport capability (Ghaithi, 2020).

The main challenge in scaling up solar energy production has been its expensive price. However, over the past century, the manufacturing the price of traditional silicon-based solar devices has significantly dropped, from $76.67 per watt in 1977 to as low as $0.36 per watt in 2022 (Sarker *et al.,* 2022). However, the price of manufacturing such a solar device remains 10 to 20 times higher than the cost of energy produced from fossil fuels. Perovskite stands out as a promising photovoltaic technology with the potential to replace traditional silicon solar cells, while also presenting strong rivalry with other cutting-edge solar technologies like dye-sensitized solar cells (Elseman *et al.,* 2020). PSCs are a highly efficient emerging solar cell technology with significant commercial potential to meet global energy needs. Unlike traditional fossil fuels, PSCs harness abundant solar energy and convert it into electricity without causing pollution (Green *et al.,* 2014; Min *et al.,* 2021). Guo *et al.,* (2022) highlight

that PSCs have achieved remarkable advancements, with their PCE surpassing 31.01% in just about a decade. (Sarker *et al.,* 2022), While traditional silicon solar cells achieved 26% efficiency after four decades of research, they face significant challenges such as short lifespans, instability, high production costs, and issues with recombination, reflection, absorption losses, and overall efficiency (Lal *et al.,* 2017; Liu *et al.,* 2020). Conversely, solution-processed perovskite-based solar cells have achieved a PCE of 20% (Li *et al.,* 2016).

The appealing qualities of PSCs lie in their exceptional photovoltaic performance and cost-effective processing methods. PSCs can be readily fabricated using straightforward, methods used locally include dip coating, spin coating, dual-source evaporation, and screen printing (Roy *et al.,* 2020). To surpass the Shockley-Queisser (SQ) limit of 35.5% in perovskite solar cells (PSCs), advancements have been made in tandem perovskite solar cells (Turkevych *et al.,* 2019). Accordingly, PSCs are environmentally friendly in their conversion of solar energy into electricity. Perovskite solar cells hold promise for advancing sustainable development goals, including boosting sustainable energy production (SDG 7) and supporting climate action (SDG 13) (Aljaghoub *et al.,* 2022). Figure 2.1 depicts a picture of a lead-based perovskite.

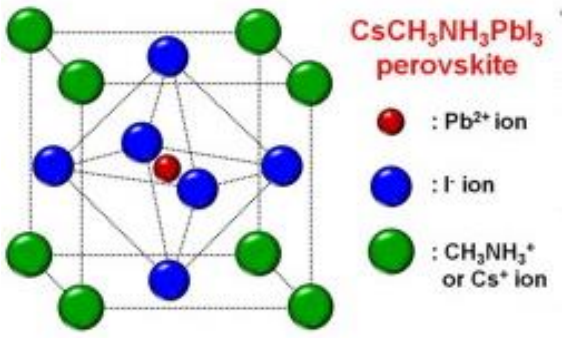

Figure 2.1: Structure of a methylammonium perovskite based on lead (Choi *et al.,* 2014).

The potential of perovskite materials in solar cells is attributed to their exceptional efficiency and stability. The initial perovskite crystal identified was calcium titanium oxide, which shares the same crystal structure as the general class of materials known as perovskites. Perovskite compounds typically follow the chemical formula ABX_3, where 'A' and 'B' represent cations, and 'X' denotes an anion that bonds with both (Cheng *et al.,* 2022; Khirade & Raut, 2022). Perovskite structures can be engineered by integrating a diverse array of components. This flexibility in composition enables scholars to tailor perovskite crystals with a wide spectrum of physical, optical, and electrical properties.

Nowadays, perovskite crystals are utilized in a range of technologies, including solar cells, memory chips, and ultrasound devices. Perovskite solar cells typically feature a basic structure including a hole transport layer (HTL) and an electron transport layer (ETL) into which free electrons and holes are injected. Generally, each cathode and anode in these solar cells are made from fluorine-doped tin oxide (FTO) and indium gallium zinc oxide (IGZO) glass materials, along with a metal back contact.

At present, cell architectures predominantly use either p-type or n-type silicon, with efficiency largely influenced by the busbar configuration, type of junction, or passivation method (Zhou, Su, *et al.,* 2022). Theoretically, positioning the contact grids on the rear of the cell instead of the front can help prevent shading losses, potentially leading to higher efficiencies for inter-digitated back contact (IBC) solar cells. IBC cells, which utilize high-purity n-type silicon, can achieve efficiencies of 20–22%. Additionally, panels incorporating advanced technologies such as passivated emitter and rear contact (PERC) cells made of monocrystalline silicon, heterojunction (HJT) cells, and n-type tunnel oxide passivated contact (TOPCon).have the potential to exceed efficiencies of 21% (Gao *et al.,* 2019). Tandem silicon-perovskite solar cells have achieved theoretical efficiencies of up to 43% and have shown testing efficiencies surpassing 30%. However, these cells are still primarily in the development phase and are not yet widely available commercially (Fang *et al.,* 2021). However, various factors like temperature, shading, panel orientation, and irradiance at the installation site can influence efficiencies. Maximizing electricity output can be achieved by enhancing the solar cell installation's overall efficiency (Mohammadnia *et al.*, 2020).

2.3 Lead-based perovskite solar cells

As a visible light sensitizer, perovskite structures with PCE of 3.8% have previously been employed, specifically those based on methylammonium lead bromide ($CH_3NH_3PbBr_3$) and methylammonium lead iodide ($CH_3NH_3PbI_3$) (Chaudhary *et al.,* 2019; Husainat *et al.,* 2020). Researchers were particularly interested in PSCs due to their affordability and straightforward manufacturing process. In 2019, the PCE of PSCs increased from 3.8% to an impressive 25.2% by 2020 (Su *et al.,* 2020). Lead-based perovskite solar cells exhibit almost perfect optical and electrical properties. Recently, they have surpassed the efficiency of solar cells made from $Cu(In,Ga)(S,Se)_2$, CdTe, and Si, achieving a remarkable efficiency of 23.7%. However, these Pb-based perovskite solar cells face two significant issues: limited stability and high toxicity (Singh & Nagarjuna, 2014). For every parameter, optimization is performed to achieve the highest possible PCE. $CH_3NH_3PbI_3$ has emerged as an excellent light harvester due to its outstanding attributes, which include an ideal band gap, a broad absorption spectrum,

efficient carrier transport, ease of fabrication on flexible substrates, a tunable band gap, and a long diffusion length (Mandadapu *et al.,* 2017).

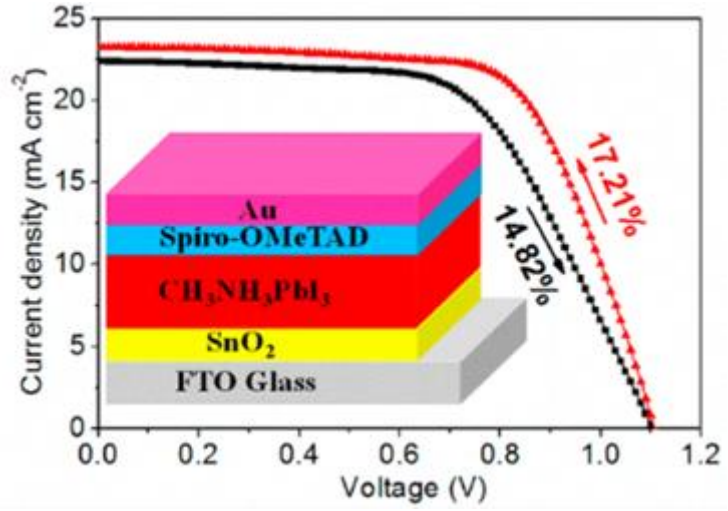

Figure 2.2: Lead halide-based PSC device architecture utilizing SnO_2 as the ETL is shown, with the red line representing the reverse scan and the black line indicating the forward scan (Ke *et al.,* 2015).

Figure 2.2 shows a typical $CH_3NH_3PbI_3$-based solar cell, which includes a p-type (PEDOT: PSS) electrode at the top and an n-type (PC61BM) electrode at the bottom (Ke *et al.,* 2015; Mandadapu *et al.,* 2017). Previous reports have shown that the top-performing planar cell utilizing a SnO_2 ETL achieved an average efficiency of 16.02%, based on measurements taken from both reverse and forward voltage scans, as depicted in Figure 2.2. The exceptional performance of SnO_2 ETLs is credited to the superior characteristics of nanocrystalline SnO_2 films, including effective antireflection properties, appropriate band edge alignment, and high electron mobility (Ke *et al.,* 2015).

Initially, the highest achievable PCE for perovskite solar cells using $CH_3NH_3PbI_3$ was 3.8%.(Liu *et al.,* 2014; Ye *et al.,* 2015) recently, the PCE of perovskite solar cells has improved to 22.1%, driven by innovative fabrication techniques, enhanced band alignment, and more robust cell architectures (Fu *et al.,* 2018; Li *et al.,* 2018). Methylammonium lead halide perovskite materials are readily accessible and can be produced using cost-effective manufacturing methods. However, due to the increasing adoption of photovoltaics, lead has become widely used in the solar cell industry, raising significant environmental and occupational health concerns. If solar panels, especially those made with PSCs, are damaged, lead could potentially leach into the environment, contaminating the air, soil, and groundwater (Ren *et al.,* 2021). The leaching and dispersal of toxic elements like Pb from lead-based PSCs into water, air, and soil could pose significant etiological risks to both animals and plants.

2.4 Lead-free perovskites

Although lead is allowed in solar modules, it would be preferable to find alternatives that maintain the unique optoelectronic properties of lead halide perovskites. Previous research has demonstrated that less toxic ions such as Sn^{2+}, Bi^{3+}, Ge^{2+}, Sb^{3+}, Mn^{2+}, and Cu^{2+} can serve as potential replacements for Pb^{2+} in perovskites to develop new lead-free perovskite solar cells (Nakita *et al.*, 2014; Wang *et al.*, 2021). The addition of these metal cations not only broadens the range of perovskite types but also improves the eco-friendly characteristics of PSCs (Wang *et al.*, 2021). In Sn-based PSCs, the material's absorption coefficient is comparatively high approximately 1.80×10^4 cm^{-1}. However, the primary obstacle to advancing Sn-based PSCs is the oxidation of Sn^{2+} to Sn^{4+} (Wang *et al.*, 2021).

Various methods have been proposed to mitigate the oxidation of Sn to improve its performance; yet managing its chemical stability remains challenging (Wang *et al.*, 2021). A range of non-toxic or minimally toxic perovskite materials has been employed in the creation of lead-free perovskite solar cells that are environmentally friendly, with several exhibiting exceptional optoelectronic properties and device performance (Wang *et al.*, 2021). Tin is considered a crucial alternative to lead to reduce the risk of lead poisoning. Lead can enter the human body, bind to enzymes, and accumulate in soft tissues like the spleen, kidneys, liver, and brain via the bloodstream. This accumulation can lead to lead poisoning, which manifests as functional impairments in the neurological, digestive, and circulatory systems (Mani *et al.*, 2020). Symptoms of lead poisoning usually manifest in most individuals when their exposure exceeds 0.5 mg per day (Cao *et al.*, 2022). A detailed analysis of the fundamental physical properties of Sn-based perovskites, compared to those of Pb-based perovskites, reveals a high degree of similarity. Consequently, these Sn-based materials have the potential to match the efficiency of $APbI_3$ systems (Ke & Kanatzidis, 2019). To achieve this goal, all-inorganic, lead-free, as well as organic-inorganic hybrid and lead-free PSCs have demonstrated both reliability as well as affordability.

Double perovskites with the formula $A_2M{+}M_3{+}X_6$ are being explored alongside the more familiar Sn and Ge-based perovskites. These 3-D materials generally have broader band gaps, approximately 2 eV, and tend to be more stable in air. However, they are characterized by indirect band gaps, forbidden transitions, zero-dimensional electronic properties, and large effective masses for both holes and electrons. These characteristics lead to low exciton mobilities and suboptimal carrier transport. While bismuth-based double perovskite solar cells share some similarities with those made from Cs_2SnI_6, they have not yet achieved high J_{sc} or PCE (Ke & Kanatzidis, 2019). Earlier, the efficiency of tin-based perovskite solar cells

decreased markedly as the cell area increased, owing to the uneven quality of tin perovskite films from a one-step deposition method. This problem has been resolved with the two-step deposition technique, which employs appropriate solvents to achieve better film uniformity and boost cell performance (Liu *et al.*, 2022). Currently, there is a pressing need for novel lead-free perovskite materials with adjustable optical and electrical properties to develop highly efficient and stable lead-free perovskite solar cells.

2.5 Lead-free double perovskite solar cell

Recently, metal halide perovskites have garnered attention as promising semiconductor materials for optoelectronic applications due to their attractive properties. Nonetheless, they face two significant challenges: instability and the presence of toxic lead (Bibi *et al.*, 2021). As a result, lead-free double perovskites (LFDPs) are becoming the favoured choice for photoactive absorbers due to their excellent photovoltaic properties, including inherent chemical stability and environmental friendliness (Kung *et al.*, 2020a). Lead-free halide double perovskite nanocrystals are regarded as highly promising alternatives to lead halide perovskite nanocrystals due to their remarkable features, including non-toxicity, robust internal thermodynamic stability, and versatile, tunable optoelectronic properties (Tang *et al.*, 2021).

Lead-free double perovskites have recently revolutionized photovoltaic research, although a comprehensive understanding of their transport, excitonic, and optical characteristics is still lacking (Jain *et al.*, 2022; Zhang *et al.*, 2021). Jain and colleagues have demonstrated that alloyed LFDPs exhibit a longer exciton lifetime compared to pristine LFDPs. This extended lifetime indicates reduced electron-hole recombination, resulting in higher quantum yield and improved power conversion efficiency in the alloyed materials (Jain *et al.*, 2022). Inorganic halide double perovskites exhibit enhanced stability due to their inorganic counterions (Ghosh *et al.*, 2022). LFDPs are exceptional photoactive layers for efficient solar harvesting due to their enhanced hole and electron mobilities (Jain *et al.*, 2022; Kung *et al.*, 2020b).

Double perovskites have become significant because of their comparable properties to lead halide perovskites, and they demonstrate intriguing optical and morphological characteristics (Ghosh *et al.*, 2022). Despite their potential, LFDPs face several challenges, including low photoluminescence quantum yields, the need for high-temperature synthesis, which complicates device fabrication, and difficulties in tuning their morphology. Nevertheless, double perovskites have recently attracted significant research interest and are growing in popularity as viable substitutes for lead halide perovskites (Ghosh *et al.*, 2022).

At present, the LFDP structure, $Cs_2AgBiBr_6$, is attracting significant attention for its potential use as a light-harvesting component in PSCs (Rai *et al.*, 2021). The numerical simulation of the device configuration, FTO/SnO_2/$Cs_2AgBiBr_6$/P3HT/Au, using SCAPS-1D resulted in a low PCE of 1.81% (Rai *et al.*, 2021). This issue was due to the inadequate band alignment of P_3HT with the perovskite, along with its low carrier mobility and significant charge recombination (Li *et al.*, 2021). The result of defect density on the device's performance was assessed by varying the absorber's defect density from 1×10^{13} cm^{-3} to 1×10^{19} cm^{-3}, using $CuSbS_2$ as the HTL for the most effective device (Rai *et al.*, 2021). Additionally, optimizing the thickness of the double-perovskite layer to 400 nm led to further improvements in the device's photovoltaic performance, achieving peak efficiency with a PCE of 18.18% (Singh *et al.*, 2021). The optimized values were V_{oc} at 1.39 V, J_{sc} at 16.04 mA/cm^2, and FF at 78.34%, indicating that the double-perovskite absorber layer ($Cs_2AgBi_{0.75}Sb_{0.25}Br_6$) is a promising choice for developing a highly efficient Pb-free double-perovskite solar cell (DPSC) (Singh *et al.*, 2021). Figure 2.3 illustrates an improved LFDP solar cell design.

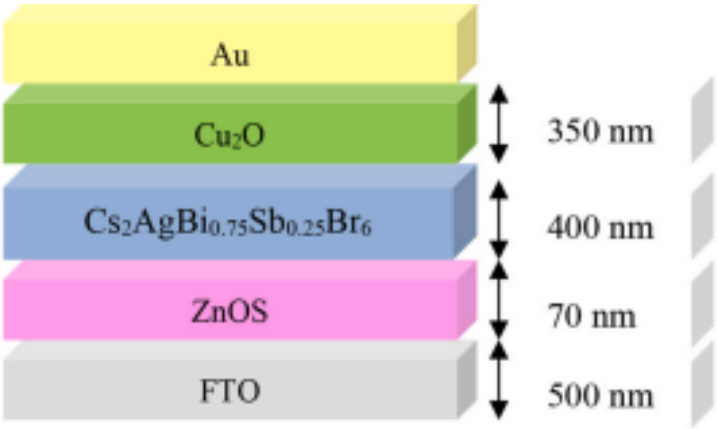

Figure 2.3: Enhanced double perovskite solar cells without lead (Singh *et al.*, 2021)

Tin is a crucial element in lead-free PSCs due to its comparable atomic radius and valence to lead. Consequently, researchers are substituting lead with tin to develop $ASnX_3$ perovskite films (Yan *et al.*, 2022). In contrast to lead-based perovskite solar cells, the highest power conversion efficiency (PCE) achieved by the tin-based device was only 6.4% (Nakita K Noel *et al.*, 2014; Wu *et al.*, 2018). More importantly, Sn^{2+} ion instability in the substance readily transforms into Sn^{4+}, leading to a reduction in photovoltaic performance (Liu *et al.*, 2023). In tin-based perovskites, there is a significant relationship between the molecular hardness of Lewis base molecules and their effectiveness in passivating the material (Yan *et al.*, 2022). By inducing redistribution of charge and saturated phases of hanging charge while reducing the presence of deep band gap states, it is shown how the hardness of the Lewis

adsorbate influences the stabilization of the photovoltaic device (Yan *et al.,* 2022). The initial effect is altering the persistent spatial distribution of tin vacancies (VSn). Creating novel perovskites devoid of lead with adequate intrinsic stability for solar applications remains a significant challenge (Wu *et al.,* 2018).

2.6 Organic-inorganic hybrid solar cell

Lead halide hybrid perovskites, both organic and inorganic, have demonstrated to be ground-breaking optoelectronic semiconductors for a wide range of device applications. However, concerns about their long-term stability and lead toxicity have led to increasing interest in all-inorganic, lead-free perovskites as a viable alternative for use in solar cells and optoelectronic devices (Wang *et al.,* 2019). Halide perovskites are made from inexpensive materials and utilize highly efficient deposition methods that have been previously used in organic electronics (Abate, 2017; Marinova *et al.,* 2017). To leverage the cost-effective manufacturing of organic photovoltaics (OPV) while also benefiting from the inorganic components, which offer tunable absorption spectra, hybrid solar cells combine both organic and inorganic materials.

Organic-inorganic hybrid PSCs have lately gained significant attention within the photovoltaic community. However, recent studies have revealed that the loss of hydrogen due to poor stability can lead to substantial energy losses, potentially making them unreliable over time (Zhang *et al.,* 2021). Hybrid organic-inorganic perovskites have shown solar efficiencies exceeding 25% (Li *et al.,* 2017). The presence of organic molecules containing carbon and hydrogen in the material is crucial for achieving exceptional photovoltaic performance, as these molecules are believed to reduce energy-draining "non-radiative recombination" events. Although hybrid solar cells have the potential to achieve high PCE, the efficiencies currently realized remain modest (Liu *et al.,* 2018). Despite the fact that the PCE currently achieved by hybrid solar cells is relatively low, there is potential for them to reach higher levels.

The electrical structure of the inorganic material used as the electron acceptor in hybrid solar cells plays a crucial role in determining the device's performance. Ideally, an inorganic acceptor should have an optimal electrical design. Four primary categories of materials have been investigated: silicon, metal oxide nanoparticles, narrow band gap nanoparticles, and cadmium compounds, which have previously achieved a PCE of 4% (Wright & Uddin, 2012). In hybrid inorganic-organic heterojunction solar cells, organometallic halide perovskites can serve as both a hole conductor and a light absorber. The sequential deposition process, as shown in Figure 2.4, achieves a power conversion efficiency of 15% (Singh & Nagarjuna, 2014).

Although organic–inorganic tin halide perovskites have exhibited favourable semiconducting characteristics, the instability of tin in its +2 oxidation state has presented a major challenge (Noel *et al.*, 2014).

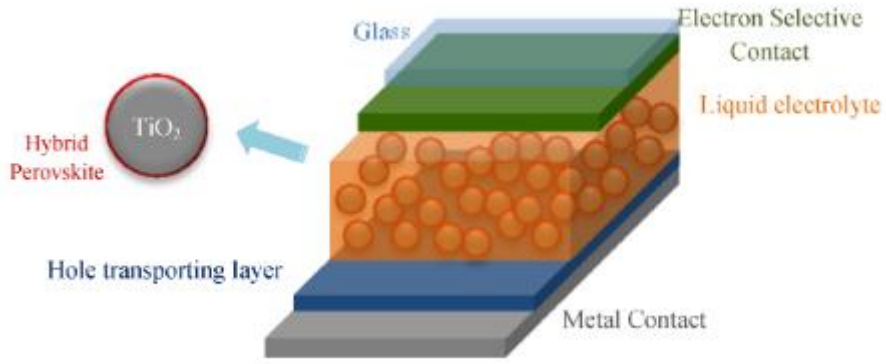

Figure 2.4: The structural design of organic-inorganic hybrid solar cells (Kandjani *et al.*, 2015)

Photovoltaics are considered a potential solution to the challenges in advancing renewable energy and achieving a clean environment due to their high-power conversion efficiency and zero emissions. However, two major obstacles for high-performance solar cells are the limited spectral absorption range and significant recombination events at the electrode/electrolyte interfaces, along with non-radiative losses and charge transport inefficiencies (Wang *et al.*, 2020; Wright & Uddin, 2012).

To leverage the cost-effective manufacturing of organic photovoltaics (OPV) while benefiting from the adjustable absorption spectra of inorganic materials, hybrid solar cells integrate both organic and inorganic components. Although these hybrid cells have the potential for higher PCE, the efficiencies achieved so far remain relatively low. The performance of the device is significantly influenced by the electrical structure of the inorganic material used as the electron acceptor. An optimal electrical structural design for the inorganic acceptor is crucial to boost the functionality of the gadget (Wright & Uddin, 2012). The materials explored encompass cadmium compounds, silicon, metal oxide nanoparticles, and narrow band gap nanoparticles. Currently, the most advanced option is cadmium sulphide (CdS) quantum dots, which achieve a practical PCE exceeding 4% (Sanglee *et al.*, 2022; Wright & Uddin, 2012).

2.7 Tandem perovskite solar cells

Perovskite-based tandem solar cells (TSCs) represent a new photovoltaic technology having the capacity to exceed the S-Q theoretical efficiency limit of single-junction silicon solar cells. By fully optimizing their optical and electrical parameters, TSCs could achieve

efficiencies of around 45% (Khan *et al.,* 2022). By employing a tandem strategy, efficiencies of up to 29% have been attained (Akhil *et al.*, 2021). Silicon solar cells possess a theoretical bandgap of 1.2 eV, which corresponds to a maximum PCE of 32% (Prasanna *et al.,* 2022). Perovskite-perovskite tandems can be formed using either physical stacking of 4-terminal (4-T) sub-cells or monolithic series integration of 2-terminal (2-T) sub-cells (Liu *et al.,* 2023). A 2-T configuration requires precise bandgap alignment to ensure current matching between the cells, while a 4-T configuration is primarily reliant on the performance of each individual sub-cell and is less sensitive to bandgap (Eg) matching. Figure 2.5 illustrates examples of Perovskite-perovskite tandem devices.

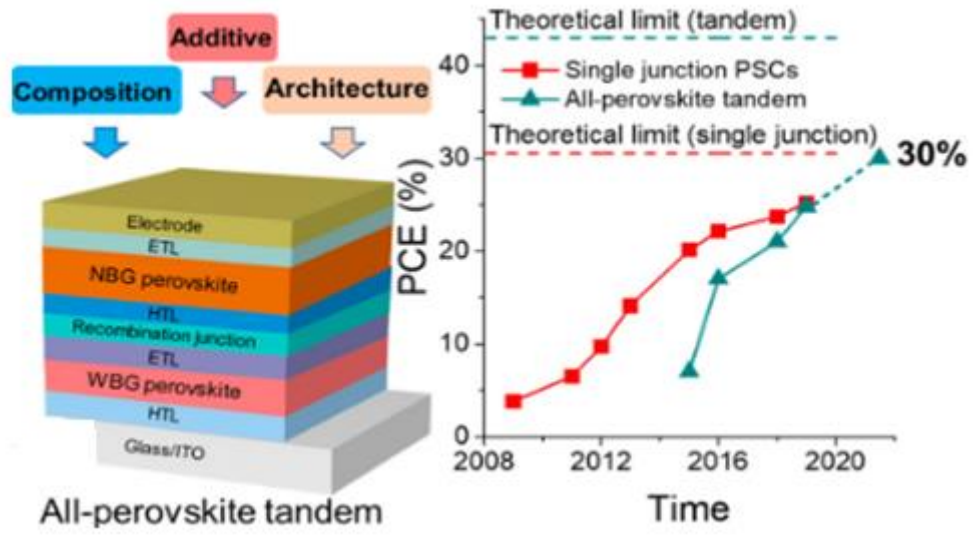

Figure 2.5: The design of perovskite cells and their PCE, comparing PSCs (indicated by the red line) with perovskite tandem solar cells (indicated by the green line) (Liu *et al.,* 2023)

Nevertheless, the 2-T setup is preferred over the 4-T because it exhibits lower parasitic absorption, greater practicality, and better economic advantages (Razzaq *et al.,* 2022). For hybrid perovskite, a 2-T structure with an optimal bandgap ratio of 1.2 to 1.8 eV could theoretically achieve a PCE of approximately 36% (Rajagopal *et al.,* 2017). Thus, enhancing 2-T perovskite tandems presents an intriguing scientific obstacle that could drive the development of new hybrid perovskite technologies and lower photovoltaic costs, thereby facilitating technology transfer (Wang *et al.,* 2021). The efficiency of tandem solar cells, which combine two layers of perovskite material, has now surpassed that of traditional solar cells made from a single layer of perovskite (Gil-Escrig *et al.,* 2022).

The best perovskite solar cells can reach a PCE of over 31%. Scientists can adjust the chemical makeup of the perovskite crystal to get it closer to the ideal bandgap (Wang *et al.,* 2021). Creating solar cells with multiple layers of perovskite materials, each with a different

energy bandgap, is a promising strategy to achieve the optimal bandgap for maximum efficiency (Akhil *et al.,* 2021). Because of its multi-layered structure, solar cells can efficiently convert sunlight into electricity. Low-energy photons excite electrons in the outer layers, while high-energy photons excite electrons in the inner layers (Sun *et al.,* 2020). Multi-junction perovskite solar cells with varying band gaps have achieved a conversion efficiency of 26% (Bacha *et al.,* 2022). In addition to silicon cells, a customizable perovskite layer can be added to a tandem cell structure to harvest more light and improve overall energy efficiency (Amri *et al.,* 2021).

2.8 All-inorganic perovskite solar cells

Owing to their remarkable all-inorganic perovskite materials have been shown to have thermal and environmental stability swiftly developed using purely inorganic cations to replace the organic cations at the A-site in the ABX_3 structure. Currently, all-inorganic perovskite solar cells (I-PSCs) have achieved efficiency levels of 19% and offer a broad spectrum of potential applications (Xiaohui *et al.,* 2020). Inorganic $CsPbI_3$ perovskites hold significant promise for tandem solar cells and various photovoltaic applications. However, $CsPbI_3$ PSCs still encounter numerous challenges, resulting in a reduced PCE in contrast to their organic-inorganic PSC equivalents (Zhong *et al.,* 2022).

Organometallic lead halide perovskites show promise as a material for solar cells because of their impressive properties. These properties include a flexible bandgap, resistance to defects, long-lasting exciton diffusion, high carrier mobility, and strong light absorption (Ouedraogo *et al.,* 2020). Organometallic lead halide perovskite solar cells have demonstrated remarkable power conversion efficiencies, with a record high of 25.2% (Ouedraogo *et al.,* 2020). The organic components of traditional perovskite solar cells are prone to environmental damage, limiting their lifespan. This has led scientists to explore all-inorganic perovskites, such as cesium lead tri-iodide, which is more chemically stable. However, cesium lead tri-iodide suffers from phase instability and the toxicity of lead (Ouedraogo *et al.,* 2020). Figure 2.6 depicts an example of device architecture for an all-inorganic perovskite solar cell.

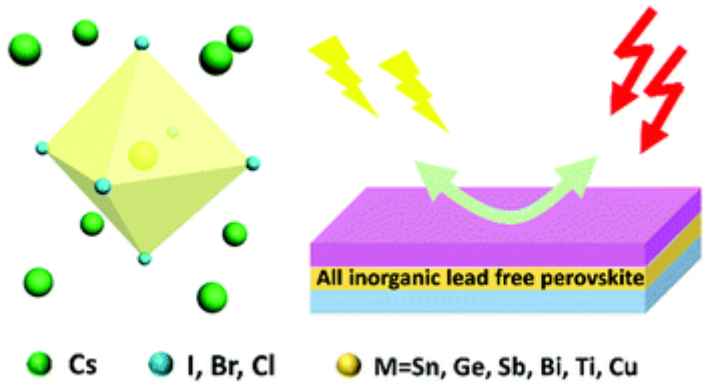

Figure 2.6: An example of a configuration for an all-inorganic perovskite solar cell (Wang *et al.,* 2019)

The hybrid organometallic tri-halide perovskite ($CH_3NH_3SnI_3$) has become a focus of significant scientific attention since its appearance in research literature (Demic *et al.,* 2017; Quarti *et al.,* 2020). This material exhibits favourable photoelectric characteristics, including a direct bandgap of 1.55 eV, a low binding energy of about 0.03 eV, and a high absorption coefficient exceeding 104 cm-1. Its solution-based processing is straightforward, and the difference between its bandgap potential and open-circuit voltage (V_{oc}) is minimal (Kong & Dai, 2022). A numerical simulation using the SCAPS-1D software was conducted to evaluate the impact of iodide $HC(NH2)^{2-}$ (SnI_3:$FASnI_3$) on doping concentration, layer thickness, and defect density in PSCs. The simulation results indicated an optimal PCE of 14.03%, with a corresponding V_{oc} of 0.92 V, J_{sc} of 22.65 mA/cm², and FF of 67.74% (Qasim, 2021).

Lakhdar and Huma (2020) used SILVACO ATLAS simulation software to report the highest PCE of 18.16% for $CH_3NH_3PbI_3$ solar cells and 9.56% for $CH_3NH_3SnI_3$ solar cells (Hima *et al.,* 2019). Aseena and his team (2021) explored the relationship between the absorber layer thickness, electron mobility, and defect density in planar perovskite solar cells with efficiencies exceeding 20%. They employed the AMPS-1D simulation tool to assess these parameters (Hima *et al.,* 2019). PSCs using gallium-doped zinc oxide (GZO) sheets have been developed, reaching a theoretical power conversion efficiency of up to 21.132% (Lakhdar & Hima, 2020; Xu *et al.,* 2019). A greater density of photo-generated excitons contributes to this phenomenon

2.9 Quantum dot solar cells

Quantum-dot-sensitized solar cells (QDSCs) offer a potential, affordable solution to traditional photovoltaic technologies like crystalline silicon and thin inorganic films. QDs can be produced using inexpensive methods, and their size can be adjusted to match specific wavelengths of light, making them a promising option for solar energy (Rühle *et al.,* 2010).

To create electron-conducting/quantum dot (QD) monolayer/hole-conducting junctions with strong light absorption, traditional dye-sensitized solar cells (DSCs) are employed as a source of nanostructures with a large microscopic surface area, redox electrolytes, and solid-state hole conductors (Markna & Rathod, 2022). QD solar cells exhibit a size-specific absorption spectrum resulting from the limited movement of electron-hole pairs within the quantum dot material (Hwang *et al.*, 2023).

A QD monolayer sensitizer is integrated into a wide-bandgap nanostructure to form QDSCs (Basit *et al.*, 2022; Rodhuan *et al.*, 2023). Theoretically, the QDSC is capable of producing up to 66% efficiency due to a unique process called multi-exciton generation (Dubey *et al.*, 2022). QDSC could be a promising third-generation solar cell technology capable of multi-exciton generation (Dubey *et al.*, 2022). The experimental efficiency of quantum dot solar cells (QDSCs) is significantly lower than theoretical predictions. One potential reason for this discrepancy is the formation of electron-hole pairs in the quasi-neutral region. To enhance QDSC efficiency, it is essential to select appropriate HTLs and ETLs that minimize recombination losses (Dubey *et al.*, 2022; Rahman, 2021). When tetrabutylammonium iodide-coated lead sulphide (PbS-TBAI) is used as the active layer and tungsten trioxide (WO_3) is used as the electron transport layer, a PCE of 15.51% is achieved (Dubey *et al.*, 2022).

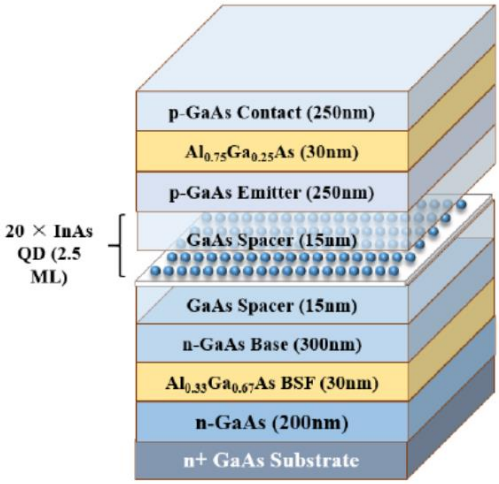

Figure 2.7: The schematic diagram of the quantum dot solar cell shows a structure composed of 20 repetitions of indium arsenide (InAs) (Lam *et al.*, 2015)

Figure 2.7 illustrates a typical quantum dot solar cell design. To improve the oxidation resistance of PbX quantum dots, their surface can be passivated with halides. This process involves binding halide ions to the Pb atoms on the surface, which decreases the quantity of locations where oxygen can attach (Siguan *et al.*, 2021). The bandgap of quantum dots (QDs) determines their absorption properties. The lowest energy states of QDs establish this bandgap.

Resonant tunnelling can enhance the efficiency of capturing photo-excited charge carriers within QDs (Du *et al.,* 2022). The Stranski-Krastanov method, a common technique for growing thin films, can be used to produce dense arrays of quantum dots (Yao *et al.,* 2022). The vertical alignment of quantum dots (QDs) is induced by strain fields originating from the underlying QD layer that penetrate the barrier material. This strong vertical coupling between QDs creates quasi-one-dimensional electronic states, resembling wires. As a result, the aligned QDs can effectively channel photo-excited electrons and holes, leading to enhanced internal quantum efficiency for carrier collection. This phenomenon facilitates efficient separation and injection of generated carriers into nearby p and n regions (Zinan *et al.,* 2021).

The size and shape of InAs islands, and therefore their quantized energy levels, can be controlled through changing the deposition technique, the thickness of the intermediate layer, and the number of repetitions of the island layer. This allows for precise control over the light absorption spectrum.

2.10 Lead colloidal quantum dot solar cells

Lead sulphide (PbS) colloidal quantum dots are highly sought-after for their potential in developing cutting-edge optoelectronic devices, including solar cells photosensing devices, and biological label (Han *et al.,* 2022). PbS colloidal quantum dots (QDs) have garnered attention as potential components in optoelectronic devices due to their adjustable bandgap, which is influenced by their size, and their adaptability through surface modification and solution-based processing (Sukharevska *et al.,* 2021). Developing a cost-effective and environmentally friendly method to produce high-quality quantum dots (QDs) in a wide range of sizes is a significant challenge. While lead sulphide (PbS) colloidal QDs offer promising potential for next-generation photovoltaic devices due to their ease of processing, low cost, and customizable optoelectronic properties, their toxicity and the need for expensive precursors remain obstacles (Tang *et al.,* 2022).

Once the material has solidified, the bulky aliphatic ligands surrounding PbS quantum dots (QDs) act as insulators, preventing efficient charge transfer and transportation between adjacent QDs (Ma *et al.,* 2022). Ligand-exchange, a process used to shorten ligands on quantum dots, can inadvertently create surface defects like vacancies and dangling bonds. These defects can reduce device efficiency through recombination. However, surface passivation methods have been developed to mitigate these issues, leading to significant improvements in the power conversion efficiency (PCE) of lead sulphide quantum dot photovoltaics (QDPVs), exceeding 10% (Yang *et al.,* 2018). Despite these advancements, the power conversion efficiency remains significantly below expectations, and surface traps pose

a substantial obstacle to the performance of PbS quantum dot photovoltaic devices. Figure 2.8 shows a lead-based colloidal quantum dot.

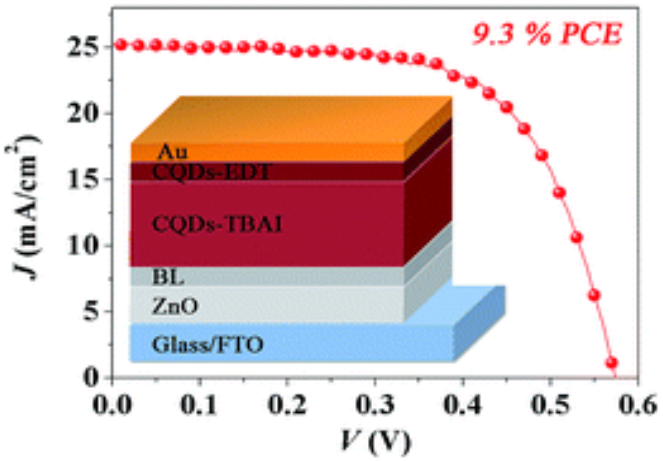

Figure 2.8: PbS colloidal quantum dot solar cell displaying J-V characteristics and PCE(Zhang & Johansson, 2017)

Design and use ligands that can enhance the interaction between the metal and the semiconductor, leading to better charge separation and collection have gained significant attention in material engineering (Zhou *et al.,* 2021). Choi et al. demonstrated that ternary PbSxSe1x quantum dots could significantly improve the performance of Schottky solar cells compared to traditional binary PbS or PbSe materials. By strategically introducing a thin oxidized layer between the PbS quantum dots and the metal contact, they were able to enhance the Schottky barrier, resulting in a more efficient and functional device (Zhou *et al.,* 2021). An inverted Schottky quantum dot solar cell was constructed using a lead sulphide quantum dot sheet sandwiched between a low level of functionality material and an elevated work function metal anode. The optimal device configuration achieved a power conversion efficiency of 3.8% and a record open-circuit voltage of 0.75 V (Deshmukh *et al.,* 2021; Liu *et al.,* 2019).

2.11 Stability of all-inorganic perovskite solar cells

All-inorganic perovskite solar cells (PSCs) have garnered significant attention because of their exceptional compatibility with tandem devices, high carrier mobility, and robust thermal stability (H. Wang *et al.,* 2020). The power conversion efficiency (PCE) of all perovskite solar cells (PSCs) has surpassed 19% due to extensive research and continuous advancements in process development. However, manufacturing PSCs for long-term applications under advanced weathering conditions is still challenging due to their relatively low phase stability. To address this, many researchers have proposed various strategies, including Interface engineering and additive engineering, and the development of all-inorganic

perovskite quantum dot solar cells, aimed at improving the long-term stability of these cells (Huirong *et al.,* 2021).

To overcome the issues caused by environmental degradation, researchers have proposed using inorganic cations like caesium (Cs^+), rubidium (Rb^+), tin (Sn^+), and potassium (K^+) to create a completely inorganic perovskite material, $CsPbX_3$ (where X is a halide) (Bernasconi *et al.,* 2019). Unlike organic-inorganic hybrid solar cells, this cation substitution aims to improve the chemical and thermal stability of the material. Currently, the most common inorganic perovskite solar cells are made with $CsPbI_3$, $CsPbI_2Br$, $CsPbIBr_2$, and $CsPbBr_3$. Of these, $CsPbI_3$ is especially good at harvesting solar energy because it has a relatively small band gap (Eg = 1.73 eV). Among all inorganic solar cells, caesium lead halide perovskite solar cells have the highest efficiency (Ouedraogo *et al.,* 2020). To enhance phase stability, substituting iodide ions with bromide ions in Cs-perovskite can produce $CsPbBr_3$. However, this material's wide band gap (Eg = 2.25 eV) limits its light absorption capabilities, which in turn reduces the cells' efficiency (Ouedraogo *et al.,* 2020).

More stability is said to exist with inorganic perovskite solar cells compared to hybrid solar cells (Ouedraogo *et al.,* 2020). In fact, some studies have found that inorganic solar cells often exhibit remarkable stability over time, even without protective encapsulation. For example, inorganic perovskite solar cells have been touted as a potential solution to the stability issues faced by hybrid PSCs, particularly their susceptibility to moisture due to their hygroscopic nature. However, it is important to note that the most common inorganic lead halide perovskite, $CsPbI_3$, is prone to significant phase instability when exposed to ambient air (Deng *et al.,* 2019; Ouedraogo *et al.,* 2020). The all-inorganic perovskite solar cells show only a slight decrease in performance in humid conditions (90–95% relative humidity, 25 °C) for over 3 months (2640 hours) without encapsulation and can tolerate exceptionally low temperatures as low as –22 °C (Liu *et al.,* 2016).

2.11.1 Perovskite efficiencies and band gap characteristics

Electrons are consistently found orbiting each atom's nucleus where they are attracted to the positively charged nucleus. The quantity of electrons an atom has dictates the number of atoms that can combine to form a molecule. Electrons that are shared among atoms move around the molecule. The electrons in the outermost shell of an atom, which orbit the nucleus, are referred to as being in its "valence band" (Yang *et al.,* 2022). When photons of light interact with the outer electrons of a semiconductor material, they excite these electrons to a higher energy state, causing them to shift from the valence band to the conduction band. This transition produces an electric current. The band gap represents the minimum energy required to promote

an electron moving from the conduction band into the valence band (Chen *et al.*, 2021). When an electron transitions to the conduction band and is no longer bound to the molecule's orbit, it becomes a charge carrier that can flow through the material. This property allows it to be used in photovoltaic cells for transporting electrical energy.

Photons of various hues in light have varying energy levels, expressed in electron volts (eV). For visible light, photon energies range from 1.75 eV (intense red) to 3.1 eV (violet). With a bandgap of 1.34 eV, an optimal photovoltaic material should be capable of converting the maximum amount of visible light into charge carriers (Chen *et al.*, 2021). Power conversion efficiency (PCE) quantifies the proportion of solar energy that a solar cell can convert into electrical energy. Research indicates that layers of materials with optimized bandgaps modified positively and negatively, play a crucial role in achieving high PCE (Jošt *et al.*, 2020). The term "S-Q limit" refers to this optimal efficiency (Zheng *et al.*, 2022). The S-Q limit implies that no single material can achieve the ideal bandgap required to reach the S-Q efficiency limit. Multi-junction (tandem) solar cells (TSCs), which consist of multiple light absorbers with distinct band gaps, have significant potential to exceed the S-Q efficiency limit of single-junction solar cells by absorbing light across a broader spectrum of wavelengths. Perovskite solar cells (PSCs) are particularly well-suited for TSCs due to their customizable band gaps, high efficiency up to 25.2%, and straightforward manufacturing process. PSCs can be effectively mixed with a variety of solar cell types, including dye-sensitized, organic, quantum dot, and narrow band gap PSCs, often using a low-temperature solution approach, resulting in high efficiencies (Li & Zhang, 2020).

Presently, technologies based on crystalline silicon dominate the photovoltaic market due to their low production costs and high reliability in both material and manufacturing processes (Tyagi *et al.*, 2013). An impressive 22.2% efficiency has been reached, while standard module efficiencies are generally around 17–18% (Huang, *et al.*, 2022). Research cells have achieved efficiencies greater than 25%, whereas the theoretical maximum efficiency for silicon solar cells is about 33% at 25 °C (Bhattacharya & John, 2019b). Therefore, with the theoretical performance ceiling of 29.4% for crystalline silicon-based solar cells, only marginal gains in performance remain possible (Zhou, Huang *et al.*, 2022). This limit is determined by accounting for Auger recombination and intrinsic losses, which encompass, among other factors, the high-energy photons' thermalization and the absorption of sub-bandgap photons by the absorber layer (Werner *et al.*, 2018). Combining both silicon-based and perovskite solar cells can yield tandem devices with the potential to surpass the performance of single-junction silicon cells that currently lead the photovoltaic market.

2.11.2 Recent progress in chemical stability of perovskite solar cells

Previous advancements elevated the record efficiency of perovskite solar cells (PSCs) from 9.7% to 20.1% which is currently aprroximately 25% (Niu *et al.,* 2015). Despite significant advancements, research into the stability issues of these solar cells remains limited, which hampers their practical use outdoors. To achieve reliable and long-lasting perovskite solar cells (PSCs) with high efficiency, it is crucial to address both perovskite degradation and device stability promptly. Without thorough stability studies, it is challenging to transition promising laboratory results to industrial and real-world applications. Recent investigations into the device's performance at elevated temperatures have shown that increasing the temperature from 300 K to 375 K reduces the power conversion efficiency (PCE) from 31.01% to 27.84% for 4-T cells and from 18.56% to 16.14% for 2-T cells (Sarker *et al.,* 2022).

Moisture and oxygen in the atmosphere can adversely affect the stability of device components throughout the assembly and testing phases. $CH_3NH_3PbI_3$, in particular, is prone to moisture, which leads to its hydrolysis and subsequent degradation of the perovskite. The following reactions are involved in this degradation process.

$$CH_3NH_3PbI_3(s) \rightleftharpoons PbI_2(s) + CH_3NH_3I\ (aq) \quad (2.1)$$

$$CH_3NH_3I\ (aq) \rightleftharpoons CH_3NH_2(aq) + HI\ (aq) \quad (2.2)$$

$$4HI\ (aq) + O_2\ (g) \rightleftharpoons 2I_2\ (s) + 2H_2O\ (l) \quad (2.3)$$

$$2HI\ (aq) \rightleftharpoons H_2\ (g) + I_2(s) \quad (2.4)$$

Thus, moisture, oxygen, and UV light are crucial factors influencing the PSC deterioration (Asghar *et al.,* 2017). In addition, the equilibrium established by reaction 2.2 leads to the coexistence of CH_3NH_3I, CH_3NH_2, and HI in the perovskite thin film. HI can then deteriorate through two main mechanisms in the following steps (Lee *et al.,* 2018). One process entails a redox reaction that occurs with the presence of oxygen 2.2, whereas the other process involves a photochemical reaction triggered by UV radiation, leading to the breakdown of HI into H_2 and I_2 2d (Heller *et al.,* 2021; Yang *et al.,* 1998). The entire process of deterioration is driven through HI consumption, according to reactions 2.3 and 2.4. Because both oxygen and moisture can lead to the degradation of organic-inorganic halide perovskite, the majority of the fabrication needs to take place in a glove box filled with inert gases, such as helium or argon (Philippe *et al.,* 2020). When devices are tested under natural lighting conditions, organic-inorganic halide perovskite often undergoes significant degradation. This

deterioration leads to an unintended decrease in efficiency, thereby restricting the practical use of perovskite solar cells (PSCs) in outdoor environments (Jones *et al.*, 2021). Several investigations have examined the influence of oxygen and humidity on the long-term performance of perovskite solar cells.

2.11.3 Perovskite solar cell configuration

PSCs present a broader variety of device structures compared to other photovoltaic technologies. These devices can be classified based on their architecture, morphology (such as mesoporous or meso-superstructure), and conductivity type, including n-type or p-type configurations (n-i-p, p-i-n, p-n, or n-p) (Mali & Hong, 2016) The structure of perovskite is classified into two primary categories: (i) normal or regular p-n type and (ii) planar, which includes either n-i-p (conventional planar) or p-i-n (inverted planar), depending on the device's electrical properties, specifically whether electrons or holes are collected at the bottom transparent conducting oxide (TCO). The traditional planar-designed perovskite device consists of two components: (a) mesoporous and (b) meso-superstructure, as illustrated in Figure 2.9.

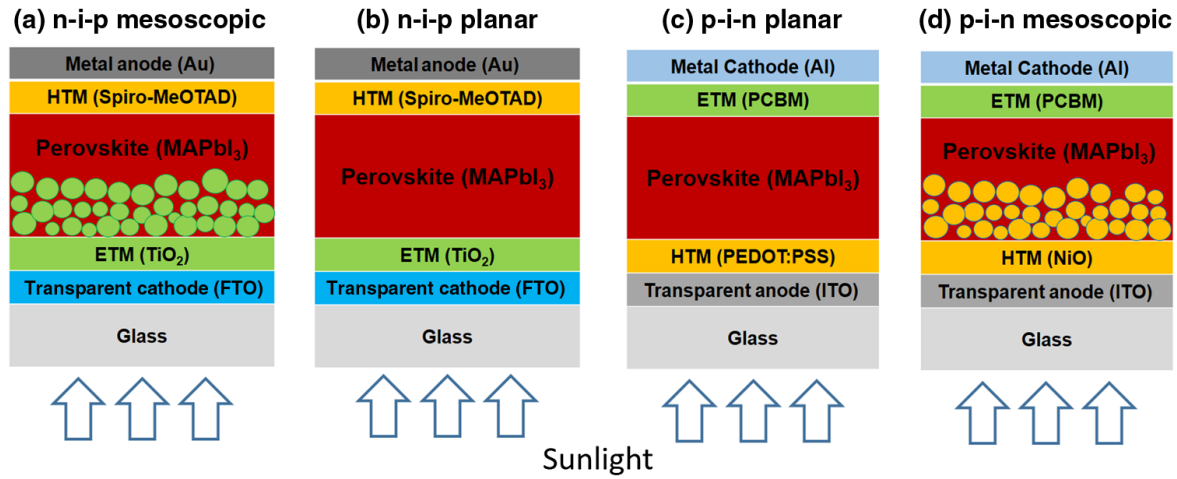

Figure 2.9: Categorization of n-i-p and p-i-n mesoscopic as well as planar shaped perovskite devices (Song *et al.*, 2016)

Through the use of layers of doped charge transfer in the device design allowed for the creation of p-i-n and n-i-p PSCs with an improved PCE of 20.3% (Li *et al.*, 2020; Yao *et al.*, 2022). HTL-free PSCs demonstrated a significant performance boost, from 5.5% to 12.8%, in both planar and mesoscopic heterojunction configurations due to improved charge extraction (Pitchaiya *et al.*, 2020). Additionally, these advancements were achieved by modifying the interface between the layers, changing the transporting and perovskite layers' thickness, and incorporating novel supporting layers (Wang & Jiang, 2021).

The effectiveness of PSC devices has not been fully investigated in various configurations, manufacturing methods, combinations of perovskite and charge-selective layers. While the most efficient absorbers contain lead, many PSC architectures still have stability issues (~13 mg m^{-2}). PSCs are also sensitive to high oxygen, moisture, UV rays, and temperatures, which hinders their commercialization (Rao *et al.,* 2021).

2.11.4 Solar device performance enhancement

The percentage of sunlight that a solar panel can convert into electricity is called power conversion efficiency. To make solar energy more affordable than fossil fuels, solar panel manufacturers need to improve their efficiency (Guangul & Chala, 2019). The highest possible efficiency that solar panels can theoretically achieve is around 30% (Bhattacharya & John, 2019a). Incorporating plasmonic nanoparticles into carbon-based perovskite cells can significantly improve their efficiency (Eswaramoorthy & Rajaram, 2022; Omrani *et al.,* 2022). In addition, when metal nanoparticles are exposed to sunlight, they scatter and bend light, which increases the amount of electricity produced in the solar cell and accelerates the creation of electrons (Hu *et al.,* 2020). Nanoparticles that can scatter light have been shown to be just as good as up-conversion materials at improving the efficiency of perovskite solar cells by 1%. By altering the size, shape, and arrangement of these nanoparticles, we might be able to boost efficiency even further (Patel *et al.,* 2018).

To increase the effectiveness of solar cells, improving light management can decrease light loss. One method to achieve this is by using transparent conducting oxide layers to minimize absorption losses and silicon oxide layers to capture more light (Azani *et al.,* 2020; Duan *et al.,* 2021). Surface gratings can enhance the internal reflection of light within a cell, leading to higher electrical and optical performance. These gratings can significantly boost the efficiency of solar cells, often exceeding 20% (Hu *et al.,* 2020). The following factors affect solar panel efficiency the cells' ability to convert sunlight, the way the cells are configured, and the amount of surface area exposed to sunlight (Kandeal *et al.,* 2020).

Enhanced PV device performance has been achieved by employing $KSnBr_3$, an inorganic material, as the photoactive layer, leading to better stability, increased charge carrier mobility, and improved PCE, positioning it as a strong contender for future solar cell technologies. The functionality of the gadget was contrasted with theoretical and empirical designs. Results showed that higher fault density in the absorber contact and lower operating temperatures negatively impacted device performance. Under ideal conditions, the solar cell achieved 19.5% PCE, FF of 14.68%, a V_{oc} of 5.32 V, and a J_{sc} of 25.55 mA/cm^{-2} (Rono *et al.,*

2022). Semiconductors, like other electrical components are sensitive to temperature changes as can be observed in Table 2.1.

Table 2.1: The influence of temperature changes on V_{oc}, J_{sc}, FF, and PCE in a PSC employing a copper thiocyanide (CuSCN) hole transport layer

Temp (K)	V_{oc} (V)	J_{sc}(mA/cm^2)	FF (%)	PCE (%)
260	1.9210	35.367021	39.69	26.96
270	1.5703	35.367897	47.72	26.51
280	1.3392	35.367246	54.97	26.04
290	1.1534	35.366813	62.58	25.53
300	1.0626	35.366642	66.53	25.00
310	0.9964	35.366514	69.41	24.46
320	0.9438	35.366119	71.61	23.90
330	0.9008	35.366236	73.23	23.33

As opposed to other solar cell technologies with similar characteristics, the PCE of $KGeBr_3$ is notably higher. While $KGeBr_3$ offers promising properties, its limited usage is primarily due to its high initial cost, reliance on intermittent solar energy, significant space requirements, and relatively small environmental impact during production, transportation, and installation (Rono *et al.,* 2022; Saikia *et al.,* 2022). The model examined how various factors affect the overall performance of a solar cell. These factors included operating temperature, the thickness of the hole and electron transport layers, and the back-contact metal work function. Additionally, the doping densities of these layers and the density of defects in the absorber layer were also investigated.

The simulation results indicated that optimizing the absorber's thickness and defect density, along with adjusting the width and doping levels of the hole transport and electron transport layers, can enhance the device's performance. It was observed that a higher defect density at the absorber contact led to poorer device performance. Nickel, platinum, and Pt metallic back contacts produced results similar to those of gold, suggesting that these more cost-effective metals could serve as viable alternatives to gold.

When a semiconductor gets hotter, its bandgap shrinks. This affects how the material behaves and can impact the performance of devices made from it, such as solar cells (Owens & Peacock, 2004; Scharber & Sariciftci, 2021). As temperature rises, the energy levels of electrons in a semiconductor widen, causing the band gap to shrink (Chen *et al.,* 2019). The open-circuit voltage of a solar cell is most sensitive to changes in its internal temperature.

2.12 Hole transport and electron transport materials

A key element in perovskite solar cells is the hole transport layer (HTL). Inverted (p-i-n) PSCs commonly utilize PSS, an organic HTL. Due to their intrinsic stability in chemicals and higher cost, inorganic HTLs are often preferred for selective contact materials. Inorganic HTLs that possess the correct energy levels as well as strong carrier mobility can improve charge transport and enhance the stability of PSCs at ambient temperatures, while also being cost-effective to produce (Wang *et al.,* 2021). Despite being expensive, unstable, and acidic, PEDOT: PSS may cause damage to the absorber (Haider *et al.,* 2019). Copper zinc tin sulphide (CZTS) is a promising material for use as a HTL in solar cells due to its low cost, easy synthesis, and high hole mobility (Haider *et al.,* 2021). A planar perovskite solar cell is composed of three primary layers sandwiched between conductive electrodes.

Table 2.2: Several HTLs used in perovskite solar cells (Pitchaiya *et al.*, 2020; Wang *et al.,* 2021b)

Organic, Inorganic, and Carbonaceous Hole-Transport Materials: Their Role in Optimizing Perovskite Solar Cell Performance
1. Inorganic HTMs: - P – type semiconductors based HTMs: CuPc, CuSCN. - Transition metal-based HTMs: - Nickel & copper based HTMs: NiO, CuI, Cu_2O, CuO, $CuCrO_2CuGaO_2$. - MoO_3, V_2O_5, VOx, WOx 2. Organic HTMs: - Small molecule-based HTMs: Pyrene, Thiophene, porphyrin, Carbazole. - Long polymer based HTMs: Spiro-OMeTAD, Fluorine doped Spiro- - OMeTAD and MoOx (interlayer in Spiro-OMeTAD), PEDOT: PSS, P3HT and PTAA. 3. Carbonaceous HTMs/electrode: Conducting Carbon, CNTs, GO, r-GO.

Table 2.2 shows that extremely effective PSCs are achieved by employing HTLs that facilitate the removal and transfer of holes from the perovskite layer to the electrodes. An efficient HTL for devices exhibiting stability over the long run is being developed by utilizing dopant-free HTLs in PSC devices, showcasing demonstrating strong operational characteristics (Niu *et al.,* 2021). Perovskite solar cells can be categorized based on the different perovskite

materials used in their HTLs. These HTLs can be classified by their molecular structure or device configuration.

Planar heterojunction perovskite solar cells usually feature a HTL, a back electrode, and an ETL. Recent studies indicate that enhancing the conductivity of the hole transport materials through doping and optimizing the absorber thickness to enhance charge collection can positively impact the efficiency of these solar cells (MaríSoucase *et al.,* 2016). A crucial element of perovskite solar cells is the use of materials that transport electrons (Saianand *et al.,* 2021). A quantitative simulation can be used to assess how various electron-transporting materials would influence the final output of a PV device. Figure 2.10 illustrates some of the common inorganic HTL materials employed in perovskite solar cells.

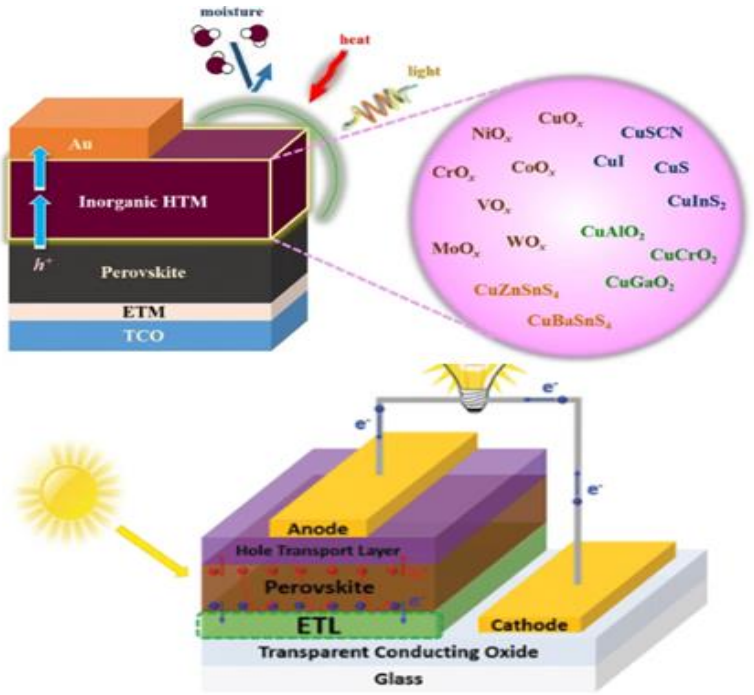

Figure 2.10: Inorganic hole-transporting layers for perovskite solar cells (Lin *et al.*, 2021)

Simulation methods can be used to optimize various photovoltaic factors, including absorber thickness and the thicknesses of other layers like the hole transport layer and electron transport layer. These optimized parameters can then be implemented experimentally (F. Liu *et al.,* 2014; MaríSoucase *et al.*, 2016). The efficiency of a device is significantly influenced by the acceptor concentration and hole mobility in the hole transport layer, as well as the trap density and work function of the back contact metal (Wang *et al.*, 2021). While these significant benefits are promising, it remains crucial to address challenges such as enhancing the hole mobility and conductivity of the HTL, improving the stability of both the perovskite material and the ETL, and finding suitable alternatives to toxic lead (Wu *et al.,* 2022). By enhancing the

efficiency of perovskite solar cells through careful design of the absorber material, selective contacts, and charge transport layers (HTL and ETL), we can significantly boost both the device's performance and its longevity (Liu *et al.,* 2014; MaríSoucase *et al.,* 2016).

The main function of HTLs in solar cells is to collect and move excitons generated by the light harvester. This separation of electrons and holes is essential for the efficient operation of PSCs (Calió *et al.,* 2016). An ideal HTL material possesses excellent photochemical and thermal stability, long-term durability energy levels in the air that align well with the perovskite layer, and inherently high hole mobility (Casas *et al.,* 2017). There are two primary types of HTLs used in perovskite solar cells (PSCs): organic and inorganic semiconductors. Inorganic HTLs, such as CuSCN, CuS, $CuInS_2$, and CuI, generally use simpler and less expensive materials than organic HTLs, such as 1-(3-methoxycarbonyl) propyl-1-phenyl [6,6]C_{61} (PCBM) and Spiro-OMeTAD. However, inorganic HTLs often require more costly deposition techniques, like sputtering, atomic layer deposition, or pulsed laser deposition (Pham *et al.,* 2020). While inorganic HTLs generally have better long-term stability due to their lack of need for dopants or additives and higher inherent hole movement, they often have a smaller variety of options compared to organic HTLs. As a result, many inorganic HTL devices exhibit lower efficiency than their organic counterparts (Pham *et al.,* 2020). Organic semiconductors used for hole transport layers in perovskite solar cells typically fall into three main groups: small molecules, polymers, and organometallic compounds (Pham *et al.,* 2020).

To enhance cell power efficiency, it's crucial to optimize the design parameters of key components. In perovskite solar cells, HTLs play a vital role in collecting and transporting holes generated from the perovskite/HTL interface to the perovskite absorber layer. Efficient charge extraction through ETLs is equally essential. While HTLs are indispensable for high-performance PSCs, they often require significant doping with additives like nanoparticles, graphene, ZnO, or polyaniline to improve charge mobility and substrate compatibility. This doping, however, can lead to stability issues, increased costs, and experimental complexities (Pham *et al.,* 2020). The combination of TiO2's excellent thermal properties, cost-effectiveness, and energy alignment makes it the most popular choice for ETLs in perovskite solar cells (Casas *et al.,* 2017). Zinc oxysulphide (ZnOS) has recently emerged as a promising alternative for electron transport materials due to its superior resistance to sulphur degradation, low toxicity, and adjustable bandgap (Korir *et al.,* 2021). The n-i-p and p-i-n solar cell architectural examples are illustrated in Figure 2.11.

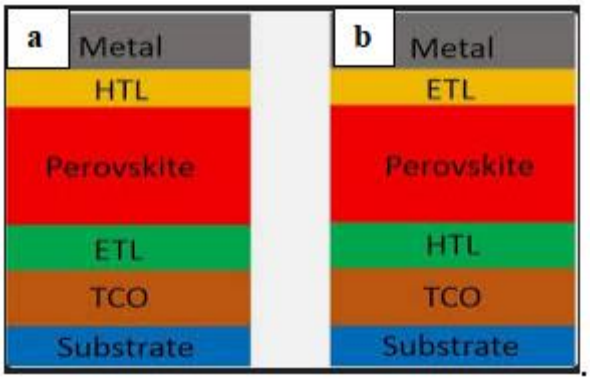

Figure 2.11: Structures of perovskite solar cells: (a) n-i-p configuration and (b) p-i-n configuration (Laalioui *et al.*, 2020)

The band gap is the energy difference between the highest energy level occupied by electrons (valence band) and the lowest energy level that electrons can occupy but is not yet filled (conduction band) (Eperon *et al.*, 2016). There are two primary configurations for perovskite solar cells: n-i-p and p-i-n. These configurations are inverted versions of each other, leading to planar solar cells with minimal hysteresis and high efficiencies. The n-i-p configuration has achieved an efficiency of 16.5%, while the p-i-n configuration has reached an efficiency of 20% (Momblona *et al.*, 2016). Figure 2.12 gives an example of a mesoscopic perovskite solar cell.

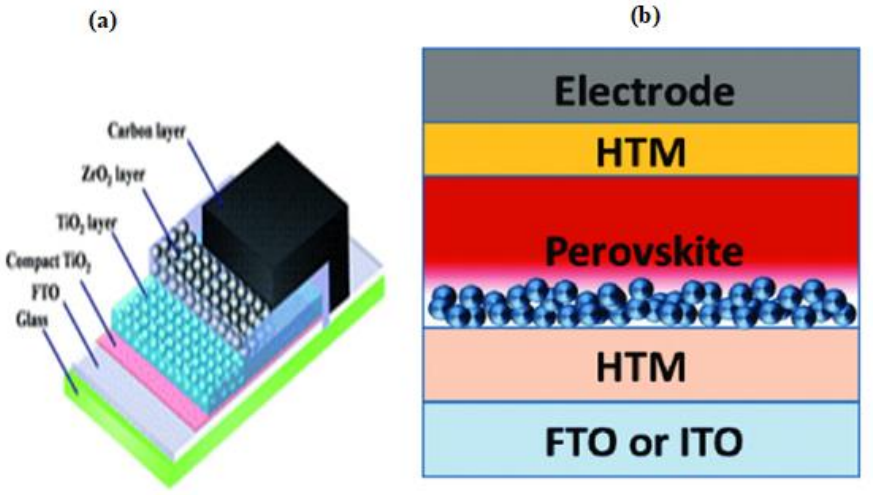

Figure 2.12: Mesoscopic perovskite solar cells (Chen & Tseng, 2017)

In order to guarantee peak efficiency, planar perovskite solar cells using a p-i-n configuration utilize layers for both electron and hole transport. These layers play a crucial role in efficiently gathering and separating the photo-generated holes and electrons, thereby boosting the overall efficiency of the solar cell (Huang *et al.*, 2016). Conversely, mesoscopic solar cells are part of third-generation solar technology. A key feature of these cells is their ability to create the absorber layer using a solution-based technique.

2.12.1 Impact of doping on ETL and HTL

Hole and electron transport materials play a key role in exciton transport. Perovskite solar cell designs often incorporate both organic and inorganic p-type semiconductor materials (Pitchaiya *et al.*, 2020). he electrical conductivity of the solar cell's layers is influenced by the doping of its photoactive material, affecting the device's performance. Optimizing the doping of the HTL and ETL enhances the device's overall efficiency by increasing the electric field at their interface (Bouazizi *et al.*, 2022; Ijaz *et al.*, 2023). Figure 2.13 illustrates the relationship between the defect density in the HTL and ETL and the various parameters that affect the efficiency of the photovoltaic device (Mandadapu *et al.*, 2017).

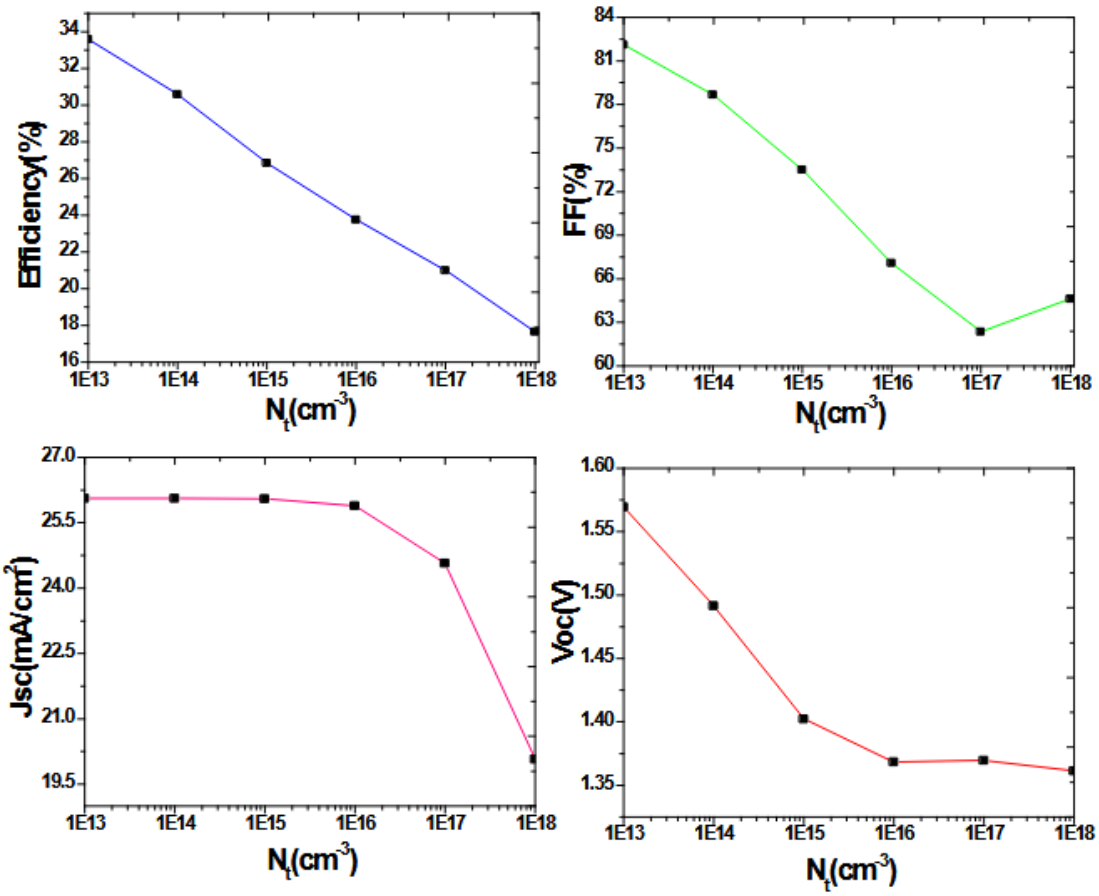

Figure 2. 13: The relationship between the concentration of defects in a photovoltaic material and its key electrical characteristics (Mandadapu *et al.*, 2017)

There are two doping techniques for HTL and ETL. One method, using minority carriers, can significantly reduce fill factor and efficiency and alter the J-V curve to an S-shape (Allen *et al.*, 2011). Another factor concerns the majority carriers, which contributes to higher efficiency and fill factor. Mild doping levels can enhance carrier transport and achieve suitable energy positioning (Mansour *et al.*, 2017). Deep-level defects in electronic devices can be minimized through careful optimization of doping processes, including self-doping. To

investigate the impact of HTL and ETL doping on device performance, doping concentrations were systematically varied from 10^{14} cm^{-3} to 10^{19} cm^{-3} (Nine *et al.*, 2019).

2.12.2 HTL and ETL free perovskite solar cells

Both HTL and ETL play a critical role in achieving efficient photovoltaic performance, but one of them has a more significant influence on the overall solar cell efficiency (Huang *et al.*, 2021). Without a HTL, the photoactive layer directly contacts the glass substrate (like ITO), hindering hole injection and reducing cell efficiency. An ideal HTL needs to have low electron affinity, high hole mobility, and energy levels corresponding with perovskite, high thermal stability, and be cost-effective (Akhil *et al.*, 2021). The TCAD Atlas tool (Technology computer-aided design) has been employed to design multiple ETL-free perovskite solar cells, with the goal of boosting device performance and decreasing production expenses (T. Wang *et al.*, 2022). Simulations of PEDOT:PSS-$CH_3NH_3PbI_3$-PCBM and CuSCN-$CH_3NH_3PbI_3$-PCBM p-i-n perovskite solar cells (PSCs) have closely matched experimental results. In ETL-free PSCs, different hole transport layers (HTLs) were directly combined with n-$CH_3NH_3PbI_3$, with CuSCN-$CH_3NH_3PbI_3$ proving to be the most effective HTL. The study explores how various factors including the back electrode material, gradient band gap, layer thickness, doping concentration, and bulk defect density affect the performance of CuSCN-$CH_3NH_3PbI_3$-based PSCs, aiming to better understand their performance characteristics (Saeed & Gelani, 2022).

Table 2.3: The efficiency of solar cells made with different layers (PCM, perovskite, PEDOT:PSS, and ITO) is highest when the perovskite layer is thickest (Shpatz Dayan & Etgar, 2022)

Cell architecture	PCE (%)
Full solar cell	~7.8
ETM free	~6.2
HTL free	~3.8

The optimization of the design is achieved through the careful alignment of the energy band and the electric field's dispersion, resulting in an improved efficiency of the CuSCN-$CH_3NH_3PbI_3$-based PSC (Tao *et al.*, 2022). HTL-free PSCs have garnered attention due to their various advantages, including reduced costs, a more straightforward manufacturing process, and the ability to prevent oxidation, which in turn improves stability and extends the device's lifespan (Shafi *et al.*, 2022). Table 2.3 provides an overview of the performance of fully

perovskite solar cells, as well as HTL-free and ETL-free configurations. This suggests that the perovskite layer is most important for light absorption and charge generation in these cells.

Recent efforts have concentrated on simplifying PSC designs by reducing the number of components. This strategy seeks to expedite PSC development by eliminating electron transport layers and leveraging advanced material combinations and solvent engineering to improve device performance and fine-tune energy level alignment at the interfaces (Huang *et al.*, 2021; Shpatz Dayan & Etgar, 2022). ETL and HTL materials facilitate charge extraction, but their removal hinders exciton extraction, leading to hysteresis and reduced cell performance (Huang *et al.*, 2021; Shpatz Dayan & Etgar, 2022).

2.12.3 Hole conductor free all-perovskite heterojunction solar cells based on tin-lead halide

In modern times, HTL-free PSCs, characterized by their simple design and production, affordable manufacturing, and remarkable durability, hold significant value (Vivo *et al.*, 2017). A highly effective and innovative HTL-free PSC structure has been developed, featuring carbon as the back electrode, WS_2 as the ETL, and a photoactive layer composed of $CH_3NH_3Pb(I_{1-x}Cl_x)_3/FA_{0.75}Cs_{0.25}Pb_{0.5}Sn_{0.5}I_3$, resulting in optimal photovoltaic performance (Rai, Pandey, & Dwivedi, 2021). This structure underwent numerical analysis using the SCAPS-1D solar cell simulator. Various parameters, including ETLs, absorber thickness, defect density, and doping concentration, were adjusted to identify the optimal values (Du *et al.*, 2016).

The device reached its highest efficiency with a carbon back contact, exhibiting an V_{oc} of 0.82 V, a J_{sc} of 31.94 mA/cm^2, a FF of 77.95%, and a PCE of 20.53% (Rai, Pandey, & Dwivedi, 2021). When gold was used as the back contact, the cell parameters; V_{oc} of 0.84 V, J_{sc} of 34.34 mA/cm^2, a fill factor of 78.54%, and PCE of 22.72% were attained (Rai, Pandey, & Dwivedi, 2021). To optimize the energy level alignment between the absorber and electron transport layer, a thin interfacial layer was incorporated, which resulted in higher power conversion efficiency (Agha & Algwari, 2022). The proposed structure has a layer of spiro-OMeTAD as the hole transport layer, a layer of $MAPbI_3$ as the absorber layer, and a layer of CdS as the electron transport layer (Bag *et al.*, 2020). Prior to introducing the interfacial layer, the perovskite solar cell's performance was enhanced by fine-tuning the thickness of the perovskite layers and the doping concentrations of the electron and hole transport layers. The maximum power conversion efficiency achieved was 18% (Agha & Algwari, 2022) using a layer thickness of 250 nm for the ETL, 400 nm for the absorber layer, and 200 nm for the HTL,

respectively. Additionally, the ETL and HTL were doped with concentrations of 10^{22} and 10^{19} cm^3, respectively (Agha & Algwari, 2022).

The inorganic-organic perovskite is garnering significant attention for its role in solar cells as a light harvester. Tin-lead halide perovskites, in particular, show great potential in mesoscopic solar cells as energy harvesters with heterojunctions, thanks to their excellent optical absorption, high carrier mobility, and impressive stability. One of the unique attributes of tin-lead halide perovskites in device applications is their dual function as both a light harvester and a hole conductor in photovoltaic panels (Aharon *et al.,* 2015). The surface photovoltage and optoelectronic properties of various perovskites show their p-type behaviour and band gap (Chang *et al.,* 2022). Tin-lead iodide perovskites are seen as the most attractive choice for low-bandgap photovoltaic materials, offering both excellent performance and reduced toxicity in perovskite solar cells (Song *et al.,* 2020). While tin-lead iodide perovskites show promise, their performance still lags behind that of pure lead-based perovskites. A crucial factor in improving the efficiency of PSCs is the HTL (Raza *et al.,* 2022). The annealing process, specifically the methylammonium to formamidinium cation ratio, can affect the band gap and stability of the layers in perovskite solar cells. Pure MAPbI3 and $FAPbI_3$ solar cells demonstrate superior stability in their photovoltaic performance across various temperatures compared to their mixed compositions (Mahapatra *et al.,* 2022).

The PSCs with a composition of $(FASnI_3)0.6(MAPbI_3)0.4$, arranged in an inverted configuration, have been fabricated using a CuI/PEDOT:PSS bilayer as the hole transport layer (Song *et al.,* 2020). The CuI/PEDOT:PSS layer exhibits a smooth surface and a strong connection with the perovskite. The introduction of CuI can influence the crystal formation process of (FASnI3)0.6(MAPbI3)0.4, leading to the development of high-quality perovskite films (Mahajan *et al.,* 2022). The combination of CuI's high mobility and the cascading energy levels within the device allows for efficient hole extraction and transportation from the perovskite material to the anode (Mahajan *et al.,* 2022). Additionally, the electrochemical impedance spectroscopy measurements revealed that the efficiency of the solar significantly impacted by the amount of CuI present, which determines its thickness. Consequently, by utilizing a double-layer CuI/PEDOT:PSS as the HTL with a CuI concentration of 10 mg/mL, the resulting PSCs based on 60% Sn perovskite achieved a higher PCE of 15.75% with minimal J-V hysteresis (Song *et al.,* 2020). The improved stability of the PSCs, which is crucial for the advancement of highly efficient PSCs, is due to the use of a double HTL consisting of CuI and PEDOT:PSS (Song *et al.,* 2020).

2.12.4 Effect of HTLs on the efficiency PSCs

HTLs play a crucial role in efficiently extracting holes from the perovskite layer and transporting them to the counter electrode. They also act as a barrier, preventing electrons from flowing back to the metal electrode Hole transport materials play a crucial role in efficiently extracting holes from the perovskite layer and transporting them to the counter electrode. They also act as a barrier, preventing electrons from flowing back to the metal electrode (Jones *et al.,* 2021). To enhance the performance and longevity of perovskite solar cells, it is crucial to focus on the design of the hole transport layer (HTL). While various organic HTLs have demonstrated promising efficiency, the influence of molecular structure on HTL performance remains unclear. Isomers, with their distinct electronic properties but similar chemical composition and molecular structures, offer a valuable opportunity to investigate the structure-property relationship of HTLs (Meng *et al.,* 2022). The impact of heteroatoms and the incorporation of double bonds into the conjugated structure on the optical, electrochemical, hydrophobic, film-forming, and photovoltaic properties of PSCs have been investigated. Molecules with double bonds exhibit higher hole mobility and improved hole extraction capability due to their enhanced planarity and intermolecular charge transfer (Xu *et al.,* 2021).

2.12.5 The metal back contact in PSCs

The use of metal back contacts in photovoltaic cells aims to create inexpensive, resistant to chemicals, simple to produce, and readily manufactured solar cells. The back contact plays a crucial role to guarantee efficient transmission of charge to the external circuit of the cell. Historically, gold has been the most popular standard back contact for PSCs, facilitating charge transfer from the HTL to the external circuit. But the exorbitant price of gold has limited the large-scale production of PSCs. Therefore, exploring alternative metal back contacts that can replace gold is essential. Table 2.4 summarizes some of the research efforts dedicated to finding suitable substitutes for gold in back contacts.

Table 2.4: Effects of altering metal back contact on Jsc, FF, and PCE (Korir *et al.*, 2021b; Vishnuwaran *et al.*, 2022).

Back contact type	Metal Work Function (eV)	V_{oc} (V)	J_{sc}	FF (%)	PCE (%)
Silver	4.26	0.9115	35.246924	35.15	11.29
Tin	4.28	0.8604	35.256642	39.28	11.92
Titanium	4.33	0.8272	35.278009	46.23	13.49
Vanadium	4.50	0.8258	35.330082	65.08	18.99
Iron	4.50	0.8258	35.330082	65.08	18.99
Tungsten	4.55	0.8433	35.341368	69.21	20.63
Molybdenum	4.60	0.8898	35.351059	70.73	22.25
Copper	4.65	0.9625	35.358882	69.69	23.72
Cobalt	5.00	1.0626	35.365407	66.53	25.00
Gold	5.10	1.0626	35.365407	66.53	25.00
Palladium	5.12	1.0626	35.365407	66.53	25.00
Nickel	5.15	1.0626	35.365407	66.53	25.00
Platinum	5.65	1.0626	35.365407	66.53	25.00

Accordingly, Table 2.5 shows that as the work function of the metal increases from 4.26 to 5.1 eV, the power conversion efficiency of the cell also improves, going from 11.29% to 25%. Gold, with a work function of 5.1 eV, seems to provide the best performance for the cell (Baptayev *et al.*, 2022). However, alternative metals can be used instead of gold that is not just costly but can also migrate through the HTL into perovskite films, leading to device degradation (Domanski *et al.*, 2016). Alternative metals like palladium (Pd) and nickel (Ni) have been explored as replacements for gold in back contacts of solar cells. These alternatives are cheaper and more accessible while offering similar performance. Studies have shown that nickel, platinum, and palladium can produce results comparable to gold. Because of their lower cost, various metals can serve as gold's replacement. Additionally, both gold and silver can interact with the halide ions in the perovskite solar cell, potentially leading to performance issues because of the combined effects of metal migration and perovskite breakdown (Guerrero *et al.*, 2016). When these devices are in use, the perovskite layer is directly exposed to light. This means that using a back contact structure, like in the p-i-n design, can help to minimize light energy that is lost as it passes through the device.

Table 2.5: The impact of modifying metal back contacts on J_{sc}, FF, and PCE (Korir *et al.*, 2021; Vishnuwaran *et al.*, 2022)

Back contact type	Metal Work Function (eV)	V_{oc} (V)	J_{sc}	FF (%)	PCE (%)
Silver	4.26	0.9115	35.246924	35.15	11.29
Tin	4.28	0.8604	35.256642	39.28	11.92
Titanium	4.33	0.8272	35.278009	46.23	13.49
Vanadium	4.50	0.8258	35.330082	65.08	18.99
Iron	4.50	0.8258	35.330082	65.08	18.99
Tungsten	4.55	0.8433	35.341368	69.21	20.63
Molybdenum	4.60	0.8898	35.351059	70.73	22.25
Copper	4.65	0.9625	35.358882	69.69	23.72
Cobalt	5.00	1.0626	35.365407	66.53	25.00
Gold	5.10	1.0626	35.365407	66.53	25.00
Palladium	5.12	1.0626	35.365407	66.53	25.00
Nickel	5.15	1.0626	35.365407	66.53	25.00
Platinum	5.65	1.0626	35.365407	66.53	25.00

Platinum, a noble metal often utilized in DSSC, could also be applied in perovskite solar cells. Despite the fact that platinum is significantly cheaper than gold, its use in PSC devices has been limited due to concerns about cost and availability. When selecting alternative metals, the main criteria include ensuring elevated PCE and robust stability throughout time conditions, alongside financial factors.

Perovskite solar cells are highly valued for their broad availability, affordability, and enhanced efficiency. As a type of fourth-generation solar cell, PSCs feature rear contacts and a layer of light-absorbing material made from either hybrid organometallic halides or inorganic perovskite materials. Additionally, these cells include an electron transport layer and a hole transport layer to facilitate charge extraction. There are several types of perovskites, such as organic-inorganic hybrid perovskites, lead-based perovskites, and all-inorganic perovskite solar cells. Due to their advantages, perovskite solar cells are gaining traction and are expected to transform the photovoltaic industry. For commercial viability, photovoltaic technologies generally need to achieve a minimum of 20 years old and less than 10% decrease in efficiency over time (Mohammed *et al.*, 2017). Efforts have concentrated regarding interface engineering, compositional engineering, and the creation of all-inorganic perovskites, and

advancements in encapsulation techniques to enhance both intrinsic and extrinsic stability, leading to considerable success (Ren *et al.*, 2021).

2.12.6 Solar cell fabrication approaches

The production of solar cells involves several different methods. The main techniques are outlined here. Both vacuum and non-vacuum methods have the potential to significantly increase the efficiency of PSCs because PSCs, DSSCs, and thin-film photovoltaics (PVs) have similar structural designs (Uhl *et al.*, 2018). Contrary to what was expected, the actual research indicates something else (Kajal *et al.*, 2018) despite having a very efficient output and a comparatively straightforward technique. There are several non-vacuum approaches for making perovskite films, including screen printing and doctor blading, which have proven effective for larger-scale production (Peng *et al.*, 2017).

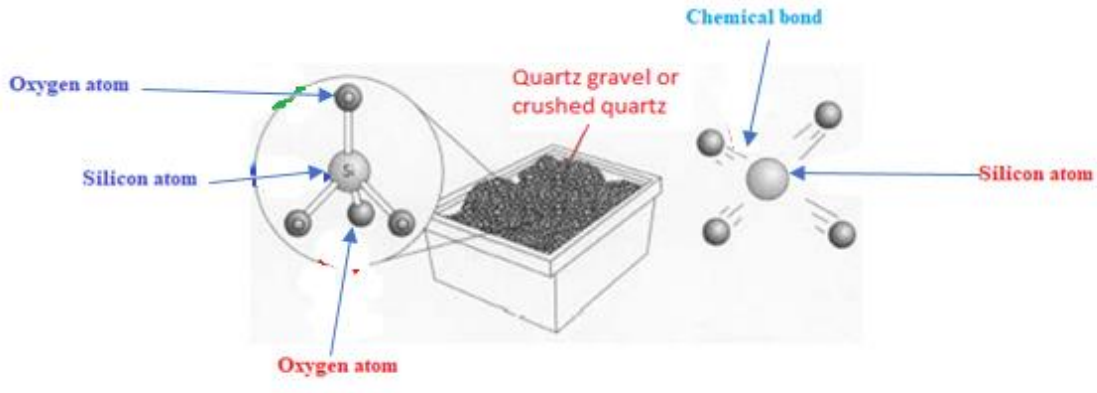

Figure 2.14: Silicon solar cells can be made using quartzite gravel as a starting material (Kumar *et al.*, 2021; Rajesh *et al.2022*)

Among vacuum-based techniques, only thermal evaporation has proven effective in producing efficient solar cells. Sputtering is seldom used due to the absence of suitable target materials or the potential harm high-energy particles pose to perovskite materials, resulting in poor stability. PSC fabrication methods can be divided into different categories, including one-step, two-step, vapour-assisted, and thermal evaporation processes (Chen *et al.*, 2021). An example of a method used to make silicon-based solar cells is shown in Figure 2.14. The phrase "solar manufacturing" is used to describe the process of manufacturing and assembling parts for the whole solar value chain, with solar PV panels holding a leading position. PV panels are made up of numerous sub-components, comprising frames, back sheets, glass, cells, and wafers

(Perez *et al.,* 2012; Recot, 2022). Silicon is the most common material used in solar cells because it makes up more than 95% of the modules available today.

Silicon, which is not pure in the state it exists in., is the main part of silicon solar cells. To make silicon dioxide from crushed quartz or quartzite stones is used in solar cells put into an electric arc furnace and heated with a carbon arc to remove the oxygen. This process makes molten silicon and carbon dioxide, as shown in Rxn 2.5.

$$SiO_2(g) + 2C(s) \longrightarrow 2CO(g) + Si(s) \qquad (2.5)$$

Before silicon can be used to make solar cells, it must be purified (Delannoy, 2012; Wei *et al.,* 2020). Thermal evaporation is the only vacuum-based method that has been successful in making solar cells with good performance. Sputtering has not been used because there might not be a suitable target for it or because the vibrant particles could damage the unstable perovskite materials. However, the SiC/SiO_2 interface can hinder the quality of the SiC/SiC surface, making it unsuitable for use as a sensor surface compared to SiO_2/SiC (Karker *et al.,* 2022).

The methods used to make perovskite solar cells can be separated into four categories: thermal evaporation, vapour-assisted, one-step, and two-step processes. One of these methods is to melt it, clean it by distillation, and after that put it into a silicon seed sample. Other methods include spin coating, thermal evaporation, and many others. Chemical cleaning is usually done in tall towers before going within the chamber of reaction. Here, ultra-pure silicon is made from filtered gas (Ishikawa *et al.,* 2020). During the manufacturing process, boron is introduced into silicon to facilitate the flow of electrons, and subsequently, phosphorous is diffused into the silicon during cell processing. This doping process, involving either phosphorous or boron, creates an excess of electrons in the silicon, enabling it to conduct electricity by reaching the conduction band (Heider *et al.,* 2019). The shiny silicon disks require an anti-reflective coating, which is commonly composed of titanium dioxide.

Usually, two layers are created, with the gap in between them serving as a barrier that keeps electrons from crossing on their own. However, photons can help the electrons overcome this barrier (Sirbu *et al.,* 2021). Typically, more electrons accumulate on the upper side of the cell, causing them to repel each other. These electrons can then flow through wires attached to the top of the cell (Yang *et al.,* 2022). Boron is employed for doping to add impurities and for crystallization to melt the mixture. Contaminants are eliminated through controlled cooling. Once the silicon bricks have solidified, they are extracted, sliced into films less than 0.2 mm thick, and these slices are used to produce solar cells (Villa, 2022). Wavering occurs in two

stages: initially, the bricks are sliced into sections, and then these sections are inserted into a wire sole. Next, a long wire containing the slurry is threaded through the bricks. Silicon carbide is used to remove the wavering from the bricks, after which they are cleaned and transferred to the adjacent cell plate (Sobayel *et al.*, 2021).

2.13 Spin-coating

Spin-coating is an effective method in order to apply uniform thin layers of highly adhesive or hydrophobic polymers to flat or axis-symmetrical substrates. This technique uses centrifugal force to spread a liquid across a solid surface, forming a consistent film. A liquid is usually deposited in the center of a circular surface and spun rapidly, resulting in even sheets with thicknesses ranging from 1 to 10 microns (Lukong *et al.*, 2022).

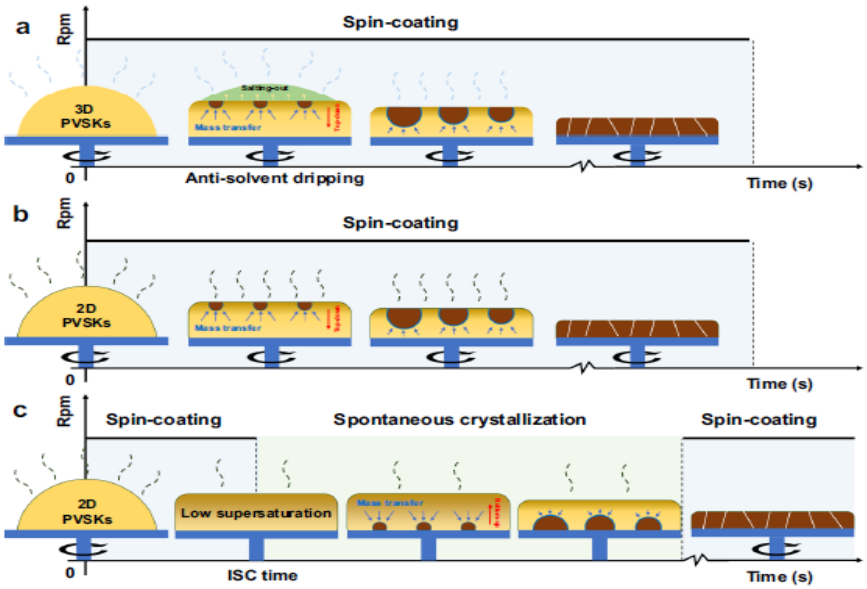

Figure 2.15: Spin coating process for preparing a self-supporting ultrathin film, (a) traditional downward crystallization using anti-solvent dripping in 3-D perovskite, (b) direct spin-coating for 2-D perovskite, and (c) ascending crystallization through intermittent steps (Yan *et al.*, 2021)

In this method, a small drop of coating material is placed at the center of the substrate, which is then rotated at a controlled high speed. During the spin-coating process, the substrate spins around an axis that must be parallel to the surface being coated (Weidner, 2022). As a result, a thin coating film develops on the surface as the coating material spreads outward and eventually moves off the substrate's edge. The final film thickness and other characteristics of the device are determined by the type of coating (including viscosity, drying rate, particle percentage, surface tension, etc.) and the spin process parameters, such as rotation speed (Buonomenna, 2016). The method of spin coating used in the fabrication of solar cell devices is illustrated in Figure 2.15. Two-dimensional lead halide perovskites (2-D perovskites) have

gained attention as stable photovoltaic materials under ambient conditions due to their distinctive layered structure.

2.14 Thermal evaporation

Thermal evaporation is a method used to apply a thin coating. The process involves heating a material in a vacuum until it vaporizes. The vapour then travels and settles onto a surface, where it cools and solidifies, forming a thin layer (Cavallari *et al.*, 2020; Zhang *et al.*, 2020). While spin-coating is often used to apply perovskite films, it's difficult to control the film thickness and create a uniform surface. Thermal evaporation, on the other hand, is a better choice for these tasks. It is more reliable and produces higher-quality films than spin-coating (Bae *et al.*, 2022). An illustration of the thermal evaporation process is shown in Figure 2.16.

2.15 Inkjet printing

Inkjet printing is a great way to make large perovskite solar cells. However, the ink often crystallizes too quickly after being printed, causing gaps and imperfections in the perovskite film. This restricts the production of perovskite using inkjet printing solar cells (Mathies *et al.*, 2018). Inkjet printing is a non-contact method that allows for quick and precise deposition of perovskite solar cells. This technique offers good control over layer formation and the J-V properties of the 0.04 cm^2 cells (Zehua Li *et al.*, 2020). Semi-transparency is a valuable property for solar cells because it opens up new possibilities in areas like tandem cells and building-integrated photovoltaics.

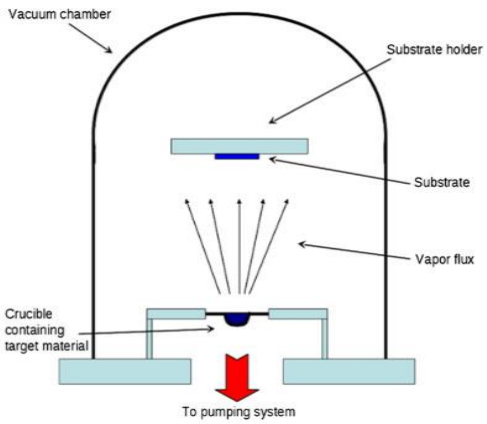

Figure 2.16: The thermal evaporation method used to create perovskite solar cells (Bashir *et al.*, 2020; Mattox & Mattox, 2003)

Figure 2.17 shows the J-V curves of inkjet-printed solar cells with the structure OMeTAD/$Cs_{0.05}MA_{0.14}FA_{0.81}PbI_{2.55}Br_{0.45}$/$C_{60}$/$TiO_2$/FTO, using different solvents. This technique has potential for large-scale production. It's also possible to design arrays of

transparent pillars made from a non-reactive photopolymerisable liquid, partially covered by perovskite, using inkjet printing. Metal halide perovskites are well-suited for use as the photoactive layer in solar cells, as they can be made thin and have the right properties. However, their chemical composition can affect their bandgap (Gao *et al.*, 2020). While highly transparent solar cells often have lower efficiency, semi-transparent perovskite solar cells can be made using inkjet printing without changing their composition or thickness (Hamukwaya *et al.*, 2022).

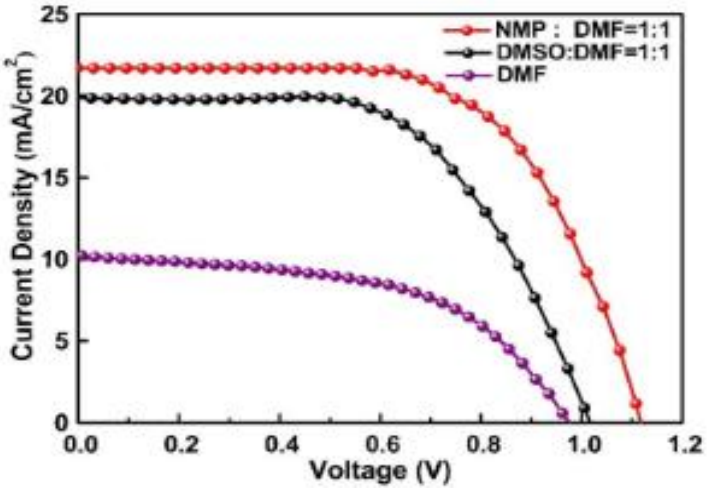

Figure 2.17: The current-voltage properties of a 0.04 cm² inkjet-printed solar cell with the structure OMeTAD/$Cs_{0.05}MA_{0.14}FA_{0.81}PbI_{2.55}Br_{0.45}$/$C_{60}$/$TiO_2$/FTO, using NMP: DMF, DMSO: DMF, and DMF solvents (Long *et al.*, 2020)

It is possible to digitally assess the solar cells' transparency and efficiency, adjusted by printing this material at specific locations and with varying array densities (Pendyala *et al.*, 2021). This innovative semi-transparent design achieves an efficiency of 11.2% and maintains an average transparency of 24%, even without the traditional upper metal contact (Pendyala *et al.*, 2021). Figure 2.16 clearly demonstrates the significant impact of solvent selection on cell performance. Cells printed in a binary mixture of N-methyl-2-pyrrolidone (NMP) and dimethyl formamide (DMF) exhibited superior operational J-V characteristics compared to those printed either in dimethyl formamide (DMF) or in a binary combination of dimethyl sulfoxide (DMSO) and dimethyl formamide alone. This suggests that the solvent composition plays a crucial role in determining the overall cell efficiency and functionality.

2.16 One step method

The one-step deposition method, which is characterized by its simplicity and affordability, has been widely adopted in the production of perovskite solar cells. By carefully controlling the perovskite precursors, it is possible to fabricate perovskite films with the desired

stoichiometric composition and free of pinholes (Ullah *et al.,* 2021). Common solvents utilized to dissolve both inorganic and organic halides, such as methylammonium/formamidinium iodide for PSC fabrication include gamma-butyrolactone (GBL), dimethylformamide (DMF), dimethyl sulfoxide (DMSO), or combinations of these solvents. To produce thick layers of phase-pure, pinhole-free perovskite, the precursor solutions are mixed and then spin-coated onto substrates followed by annealing at temperatures ranging from 100 to 150 ^{0}C (Deng *et al.,* 2020). To modify the halide anion ratio, commercially available lead chloride ($PbCl_2$) was dissolved in dimethylformamide (DMF) and mixed with methylammonium iodide (MAI) in a 3:1 molar ratio (Lee *et al.,* 2020) this represents a significant initial achievement for the one-step procedure, yielding a 10.9% power conversion efficiency. The perovskite layer is formed after spinning the solution for 30 seconds and then annealing it at 100 degrees Celsius (Wang *et al.,* 2022).

2.17 Two –step method

Unlike the one-step method, the two-step perovskite deposition process does not necessitate the complete preparation of precursors. Instead, lead halide (PbX_2, where X is chlorine, bromine, or iodine) and methylammonium/formamidinium iodide (MAI/FAI) layers are deposited separately through spin coating (Bing *et al.,* 2020; Shi & Jayatissa, 2018). Figure 2.18 illustrates an example of a two-step perovskite deposition process utilizing dimethyl sulfoxide (DMSO) as a solvent.

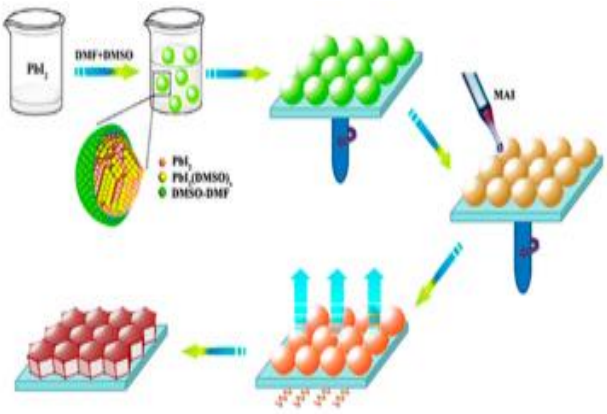

Figure 2.18: A two-step perovskite film synthesis using methylammonium iodide (MAI) and lead iodide (PbI2) with dimethyl sulfoxide (DMSO) as a solvent (Liu *et al.,* 2021)

A PbX_2 seed layer is initially formed on a substrate using either spin coating or doctor blading. Subsequently, the MAI/FAI layer is added by either spin coating with an MAI/FAI solution or immersing the PbX_2-coated substrate in the solution, often isopropanol. Following a suitable annealing process, the final perovskite films are produced (Bing *et al.,* 2020; D. Li

et al., 2021). Although the two-step method involves more complex steps, it offers greater process control as it allows for independent adjustment of parameters in each phase, leading to improved control over the appearance and quality of the perovskite films (Ge *et al.,* 2020).

2.18 Pulsed laser deposition (PLD)

In pulsed laser deposition (PLD), a high-intensity pulsed laser beam is used to vaporize a target material, which is then deposited as a thin film onto a substrate. This technique falls under the category of physical vapour deposition (PVD) (Barimah *et al.,* 2022). Compared to other methods, PLD excels in maintaining stoichiometry, adaptability, versatility, lower deposition temperatures, and the production of metastable materials. These advantages contribute to PLD's widespread use in materials research (Xu *et al.,* 2020).

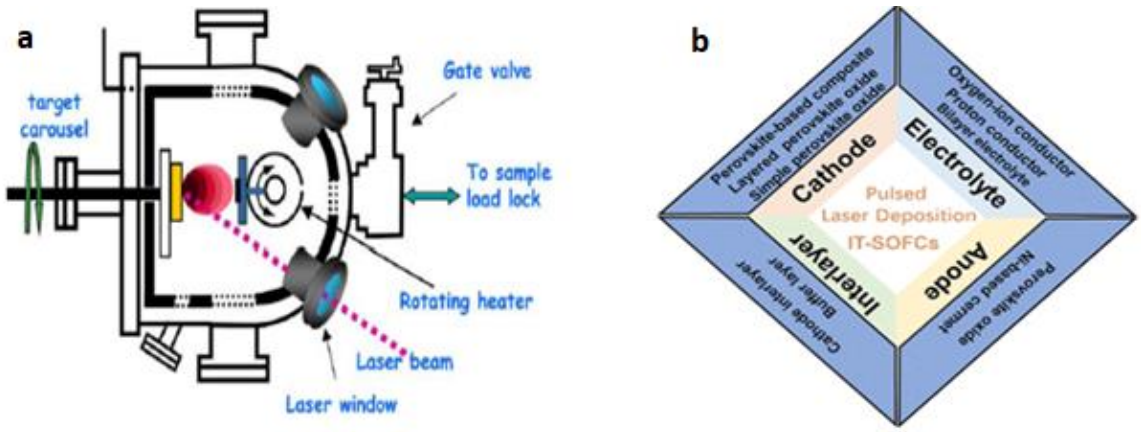

Figure 2.19: Schematic diagram of a PLD system (a) and (b) fabrication of thin films using the PLD technique (Barimah *et al.,* 2022; Blank *et al.,* 2013)

Pulsed laser deposition has been employed to fabricate thin films for various applications, including solar cells, light-emitting diodes, and solid oxide fuel cells (Barimah *et al.,* 2022). A laser beam that pulses for 10 to 50 nanoseconds is focused onto the material layer to be deposited (Zhang *et al.,* 2020). Each laser pulse vaporizes a small portion of the material with sufficient energy density (1-5 J/cm²). The substrate is placed facing the target, where it collects the plume of ablated material ejected from the target. Figure 2.19a depicts a pulsed-laser deposition system, while Figure 2.19b presents the cell structure produced by this technique.

2.19 Quantum dots

Lead halide perovskite quantum dots (PQDs), also referred to as perovskite nanocrystals, considered among the most promising classes of solar cell photovoltaic materials due to their exceptional optoelectronic properties and straightforward fabrication methods (J. Chen *et al.,* 2021). PQDs have gained significant attention due to their unique optical

properties, including tunable wavelength, narrow emission, and high photoluminescence quantum yield (PLQY) (Wang *et al.*, 2018). To prevent degradation caused by heat, oxygen, moisture, and light, the stability of PQDs needs to be improved for industrial applications like lighting and backlight devices. Unstable PQDs are susceptible to degradation by oxygen and moisture (Meena *et al.*, 2022). Crystal formation due to simple ion migration can lead to a reduction in the PLQY of PQDs. Surface coating and treatment is crucial techniques for addressing these issues (Wang *et al.*, 2018).

Semiconductor quantum dots (QDs) are recognized as superior optical gain materials compared to their bulk and quantum well counterparts. The effect of 3D quantum confinement in QDs results in distinct density of states that resembling a delta function, emission wavelengths that are tunable in size and robust optical oscillators, and promising minimal threshold and temperature-insensitive optical gains (Meena *et al.*, 2022). Figure 2.20a depicts a schematic diagram of a quantum dot preparation device, while Figure 2.20b illustrates the architecture of the cell fabricated using this approach.

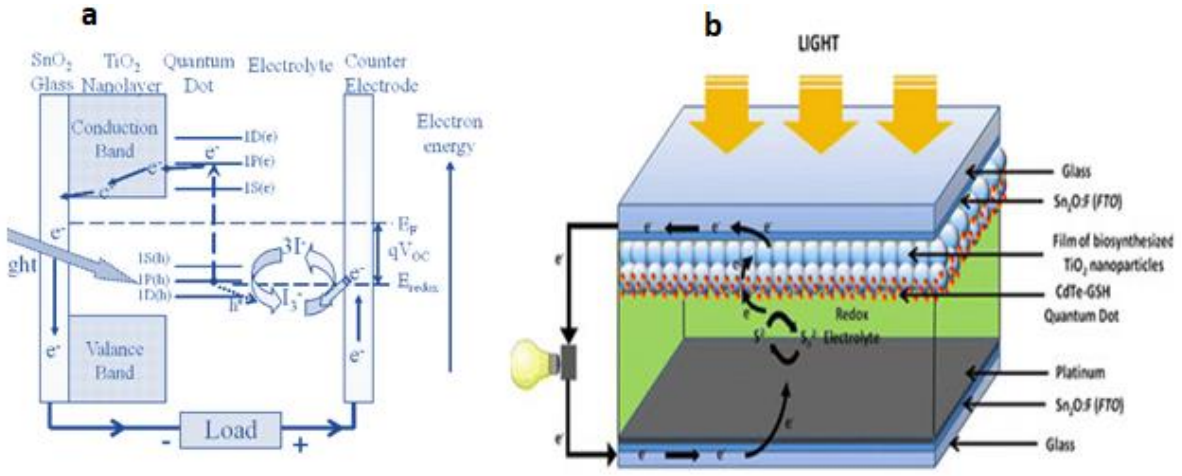

Figure 2.20: Structure and function of quantum dot-sensitized photovoltaic cells (a) and (b) manufactured cell architecture (Ilyas *et al.*, 2021)

2.20 Numerical simulation strategies

Different simulation software, including Personal Computer One-Dimensional (PC 1-D), Accelerated Mobile Pages (AMPs), COMSOL Multiphysics, Technology Computer-Aided Design (TCAD), the General-Purpose Photovoltaic Device Model (GPVDM), and SILVACO ATLAS, have been employed to optimize the electrical properties of solar cell designs (Haddout *et al.*, 2019). This review focuses on several numerical simulators that are commonly used in the study of solar cells.

2.20.1 Solar cell capacitance simulator

The SCAPS-1D solar cell simulator was designed by Professor Burgelman at Ghent University in Belgium (Belarbi *et al.*, 2020; Mandadapu *et al.*, 2018; Zyoud *et al.*, 2021). The SCAPS-1D simulator helps us understand how solar cells work by using mathematical models. These models solve three main equations that describe how electrons and holes behave in semiconductors. These equations are the Poisson equation, the continuity equation, and the equations for holes and electrons. The Poisson and continuity equations are the most important parts of the SCAPS-1D program (Ahmad *et al.*, 2022). SCAPS-1D is a popular program for simulating solar cells because it is easy to use and control. Equation 2.1 shows the Poisson expression.

$$\nabla^2\psi = \frac{q}{\varepsilon}(n - p + N_A - N_D) \quad (2.1)$$

The Poisson equation involves the electrostatic potential (ψ), the concentration of acceptors (N_A), and the concentration of donors (N_D). The continuity equations for electrons and holes are represented by equations 2.3 and 2.4.

$$\nabla . J_n - q\frac{\partial n}{\partial t} = +q \quad (2.3)$$

where R is the rate of carrier recombination and Jn is the current density of electrons.

$$\nabla . J_P + q\frac{\partial p}{\partial t} = -qR \quad (2.4)$$

Here, J_p is the current density for holes.

Furthermore, equations (2.5) and (2.6) define the Drift-diffusion current relations.

$$J_n = q_n U_n E + qD_n V_n \quad (2.5)$$

were, D_n represents the electron's diffusion coefficient.

$$J_P = qpU_p E - q\Delta_p \quad (2.6)$$

Here, D_p is the hole diffusion coefficient.

The continuity equations are given by expressions 2.7 and 2.8

$$\frac{dn}{dt} = \frac{1}{q}\frac{dJn}{dx} - (U - G) \quad (2.7)$$

$$\frac{dp}{dt} = -\frac{1}{q}\frac{dJp}{dx} - (U - G) \quad (2.8)$$

where U and G are the rates of recombination and generation.

Solar cells typically operate under steady-state conditions, meaning that their properties don't change significantly over time. Therefore, transient effects (like switching times) aren't particularly important. The concentrations of electrons and holes remain relatively constant under these conditions, as described by equations 2.9, 2.10, and 2.11.

$$\frac{dn}{dx} = \frac{dp}{dt} = 0 \quad (2.9)$$

This reorganizes the equation above such that:

$$\frac{1}{q}\frac{dJn}{dx} = U - G \quad (2.10)$$

$$\frac{1}{Q}\frac{dJp}{dx} = -(U - G) \quad (2.11)$$

The SCAPS-1D simulation provides valuable information about photovoltaic performance, including the FF, J_{sc}, V_{oc}, and PCE (Kumari *et al.*, 2022). In addition to the main photovoltaic characteristics, SCAPS-1D also calculates the recombination profiles and energy band diagrams of the solar cell. The equations for calculating the FF and V_{oc} are given by equations 2.12, 2.13, 2.14, and 2.15.

$$\mathrm{FF} = \frac{V_{MP} I_{MP}}{V_{OC} I_{SC}} \quad (2.12)$$

$$\text{Empirical Fill Factor, } \mathrm{FF} = \frac{V_{OC} - \mathrm{In}(v_{oc} + 0.72)}{V_{OC} + 1} \quad (2.13)$$

$$\text{Implied, } V_{OC} = \frac{K^T}{q} \mathrm{In}\left[\frac{(N_A + \Delta n)\Delta n}{n_i^2}\right] \quad (2.14)$$

$$V_{OC} = \frac{nKT}{q} \mathrm{In}\left(\frac{IL}{IO} + 1\right) \quad (2.15)$$

The short-circuit current density can be estimated using the formulas represented by equations 2.16 and 2.17.

$$J_{SC} = q^{G(L_n + L_P)} \quad (2.16)$$

$$J_{SC} = I_{SC} A \quad (2.17)$$

In these equations, G represents the rate at which electron-hole pairs are generated, Lp and Ln are the diffusion lengths for holes and electrons, respectively, and A is the area of the solar cell.

The SCAPS-1D software numerically solves the equations that describe how charge carriers move through semiconductor materials when they are in a steady state. This software is used to simulate p-p-n perovskite solar cells. The SCAPS-1D simulation uses a method called the Gummel iteration scheme with Newton-Raphson sub-steps to solve the equations. The calculation's first step begins with an estimate of zero for the quasi-fermi levels across the solar cell (Houimi *et al.*, 2021). Figure 2.21 shows the SCAPS panel, which is used to configure simulation devices.

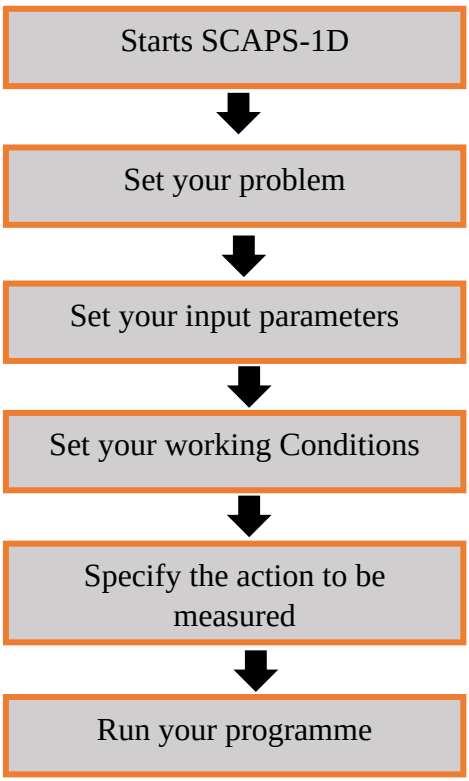

Figure 2.21: The SCAPS-1D visual interface (Thakur *et al.*, 2023)

2.20.2 SILVACO ATLAS

The ATLAS device simulator, which operates in both two- and three-dimensional modes, is grounded in physical principles. It predicts the electrical properties of particular semiconductor designs and provides insights into the internal physical processes that influence the device's operation (Bhattacharjee *et al.,* 2021). Furthermore, SILVACO offers a comprehensive suite of tools for the advancement, optimizations well as analysis of digital cell libraries, enabling Integrated Circuit (IC) design teams to explore the impact of different device models, design methodologies, and cell topologies to improve how well their state-of-charge operates (SoC) sparse optimal control systems.

A simulation of technology computer-aided design (TCAD) not only provides insight into the appearance of the reverse current-voltage curve but also helps identify the reasons behind device failure. TCAD is an effective tool for illustrating device and process adjustments, reducing manufacturing cycle times while highlighting potential performance improvements. By adjusting model parameters and coefficients, you can test theories in TCAD to understand how different physical phenomena impact the device, including wide bandgap power semiconductors (Park *et al.,* 2017). The researcher may need to identify the cause of device

failure to gain a deeper understanding of its performance (Binder *et al.*, 2003; Fichtner *et al.*, 1983; Schwarz *et al.*, 2019).

2.20.3 TCAD Silvaco simulation of epitaxial structures and wafer design

The epitaxial structures are designed using 4H-SiC, a hexagonal silicon carbide with four polytypes. Among the available silicon carbide materials, 4H-SiC is the most readily available and easiest to grow or purchase. Figure 2.22 depicts the graphical user interface of SILVACO, while Figure 2.23 outlines the ATLAS simulation methodology scheme.

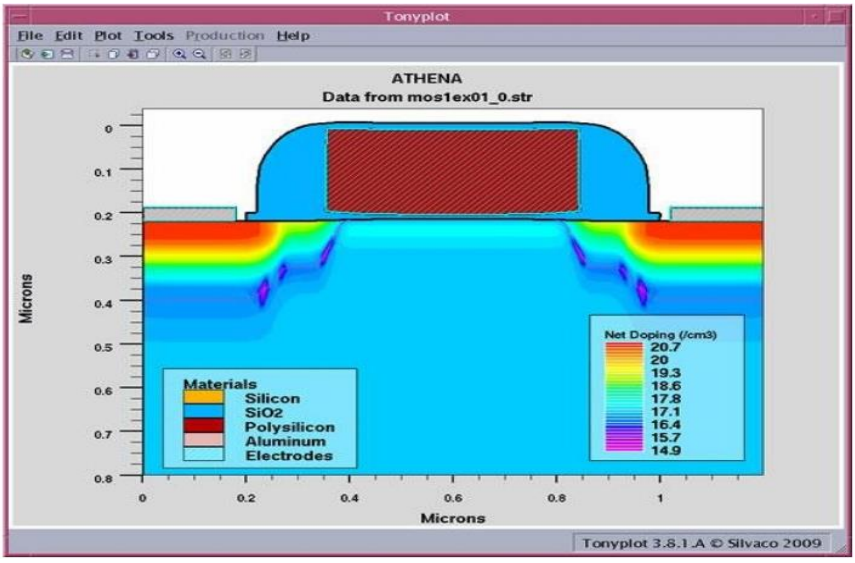

Figure 2.22: SILVACO graphical user interface used for simulating solar cells(Bhattacharjee *et al.*, 2021)

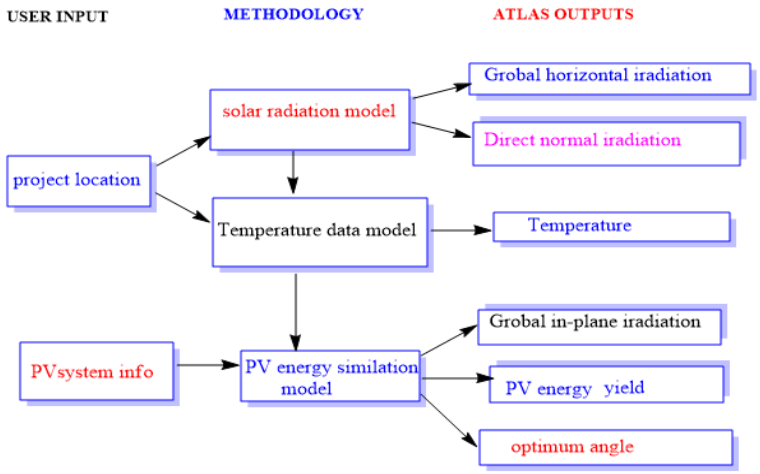

Figure 2.23: Overview of the ATLAS simulation process (Bhattacharjee *et al.*, 2021)

2.20.4 WxAMPS simulation method

A 1-D software for simulating solar cells named Widget, designed for analysing microelectronic and photonic structures (wxAMPS), was developed through a collaboration

between Nankai University in China and the University of Illinois at Urbana-Champaign (Hadjab *et al.,* 2022). This numerical simulation method follows the principles of the evaluation of Microelectronic and Photonic Structures (AMPS) physical model, incorporating tunnelling currents, improving convergence and speed, and offering enhanced visualization capabilities. The core of wxAMPS is built on an updated version of the AMPS code, with the user interface developed using the cross-platform library wxWidgets (Smucker & Gong, 2021). The performance of solar cells was evaluated through numerical analysis using the wxAMPS software. This analysis involves solving the Poisson formula, which links charge and electrostatic potential, along with the hole and electron continuity equations that describe the device's behaviour.

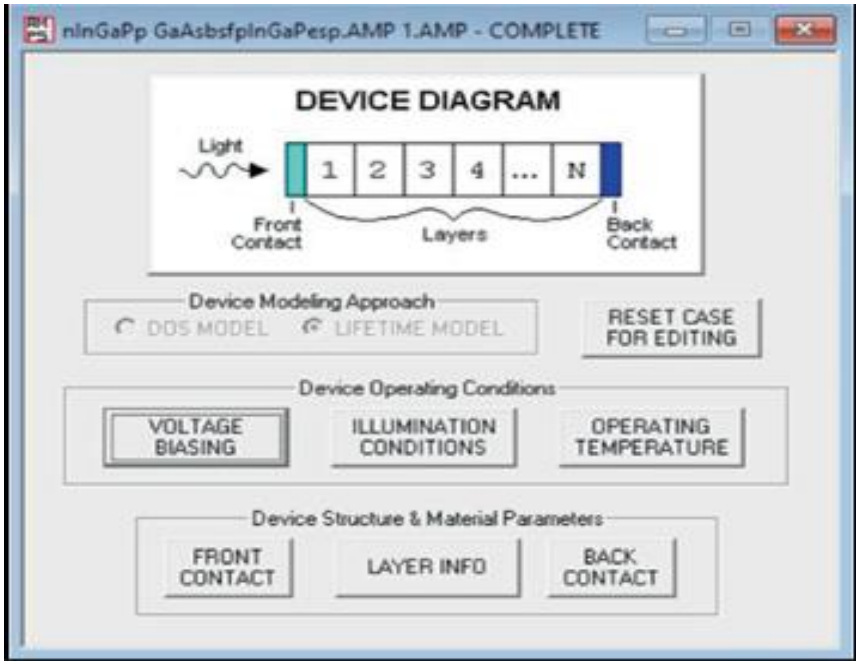

Figure 2.24: Shows its wxAMPS user interface simulation method (Hadjab *et al.,* 2022)

Figure 2.24 illustrates the graphical user interface of the wxAMPS simulation software. The simulation process in wxAMPS is conducted in three steps: initially, the ambient operating conditions, such as temperature, solar spectrum, and bias voltages, are configured, either using standard values or by adjusting the data as needed by the operator (Liu *et al.,* 2012). Secondly, the material properties for each layer of the device are inputted into the system. These properties are supplied via a database that can be modified using standard spreadsheet software, making it easy to enter data for multiple layers and to quickly adjust properties like the absorption coefficient. Once the simulation is started, the results are available in various formats, including files compatible with both directly through the graphical user interface and spreadsheet apps (Liu *et al.,* 2012).

To more accurately mimic several solar cell kinds, wxAMPS uses two different models for tunnelling: one that works well for heterojunction solar cells, and another that uses a drift-diffusion approach. These models include the important effect of trap-assisted tunnelling, which is how electrons can recombine at junctions. A new method that combines Newton-Raphson and Gummel iteration tackle has also been added to make the simulation process more reliable (Fuhrmann *et al.,* 2019). Various simulation results are compared to determine the optimal output parameters for designing high-performance practical cells (Liu *et al.,* 2011). As a result, a solar cell engineer can select the appropriate model for a specific set of materials, whether organic or inorganic.

2.21 The future outlook of perovskite solar cells

Maximizing the potential of green energy is crucial for tackling the escalating environmental issues caused by rising pollution from fossil fuels and woody biomass (Zhang *et al.,* 2022). The adoption of entirely renewable energy sources has become more significant in advancing human civilization. Among the various alternatives, including nuclear and wind power, solar power is considered of the most exciting new energy possibilities (Zhang *et al.,* 2023). Despite achieving a power conversion efficiency of 25.8%, poor stability remains a major barrier to the full commercialization of PSCs (Chowdhury *et al.,* 2023). Researchers globally have employed various approaches, including structural modifications and diverse fabrication techniques, to achieve the required stability and top-notch operation.

Aspects like great efficiency, ease of manufacturing, stability and minimal cost are crucial for the commercialization of PSCs. However, due to varying testing procedures like differences in humidity, temperature, and encapsulation methods stability results from different researchers are difficult to compare accurately (Chowdhury *et al.,* 2023). Unlike stability-related aspects such as lifetime as well as degradation rates, the PCE is a clearly defined metric that can be assessed according to established standards. It is crucial to standardize testing conditions for the stability of PSCs, paying attention to factors such as elastic modulus, heat resistance, device hysteresis, and stability under exposure of every fabrication to oxygen, moisture, and light process. Although inorganic solar cell testing methodologies are well-established, they are not commonly applied in evaluating PSC stability. To effectively advance PSC technology and meet market demands, it is essential to clearly define Research and Development (R&D) objectives (Caballero *et al.,* 2023).

The primary obstacles in creating highly efficient solar cells include selecting a durable absorber layer (such as perovskite), inadequate structural engineering device, improper band positioning at the absorber-surface contact, and carrier recombination at both the rear and front

contacts. These issues collectively impede the performance metrics of V_{oc}, J_{sc}, FF, and PCE. (Hasan Ali *et al.*, 2023). Recently, there has been increasing interest among researchers in iron disilicide ($FeSi_2$) based solar cells. This material is considered highly promising for solar cell applications due to its exceptional properties, including direct band gap energy of 0.80-0.87 eV and an optical absorption coefficient (α) exceeding 1×10^5 cm^{-1} at photon energies above 1 eV. This absorption coefficient is approximately 200 times greater than that of crystalline silicon (c-Si) (Hasan Ali *et al.*, 2023). Additionally, it exhibits strong chemical stability and is highly resistant to environmental and chemical degradation, humidity, oxidation, cosmic rays, radioactive exposure, and possesses a high thermoelectric power coefficient of approximately $k \sim 10^{-4}/K$). It also has a substantial diffusion length of around 38 μm (Hasan Ali *et al.*, 2023). The $FeSi_2$ photoactive layer is recognized as a binary, non-toxic, and widely available semiconductor material, as both iron (Fe) and silicon (Si) are environmentally friendly and abundant in the Earth's crust. Ali et al. (2023) demonstrated through numerical simulation that a solar cell design using $FeSi_2$ and PEDOT:PSS as the hole transport Layer (HTL) achieved an impressive power conversion efficiency of 39.44%. Thus, with suitable device engineering, accurate band alignment, and effective fabrication methods, it is possible to surpass the Shockley-Queisser limit for practical applications.

The advancement of 3D perovskites has significantly contributed to the growth of organic-inorganic halide perovskite solar cells in the last decade (Gangadharan & Ma, 2019). The practical application of 3D perovskite solar cells is hindered by their uncertain stability. Recent developments have focused on increasing their durability using different approaches (Grancini *et al.*, 2017). The most effective way to improve the performance of halide perovskite solar cells is by addressing their underlying chemical stability. Two-dimensional perovskites, known for their superior stability, have emerged as a potential alternative to three-dimensional perovskites (Cervantes *et al.*, 2019) (Hidalgo *et al.*, 2019).

Well-designed encapsulation methods can provide substantial protection for PSCs from damaging factors like oxygen, moisture, and UV radiation (Nazir *et al.*, 2022). To fully realize the potential of perovskite solar cells (PSCs), it is crucial to comprehend the root causes of their intrinsic instability and how to mitigate them. The degradation of PSCs is often associated with internal factors like phase segregation and compositional segregation, which are connected to changes at the interfaces between the various layers upon layers of the cells. Addressing these issues is essential for improving their performance. Moreover, increasing research focus on PSCs and exploring flexible tandem solar cell structures more rigorously could lead to significant advancements in the field (Bing *et al.*, 2022). This approach could

enhance device performance by also considering greater mechanical stability (Sun *et al.*, 2022). Examining the durability of tandem cells compared to single-junction cells, and determining if the benefits of flexible photovoltaics are unique, will be particularly important for the future commercialization of PSCs.

2.22 Conclusions

Perovskite solar cells (PSCs) have garnered significant attention due to their potential for high efficiencies and low manufacturing costs. However, their performance is still limited by factors such as device architecture, material composition, and charge carrier management. To enhance efficiency, strategies like improved light management using transparent conducting oxides and silicon oxide layers are being explored. Despite the toxicity of lead, lead-halide perovskites offer unique advantages as both light harvesters and hole conductors. Their tunable bandgap, defect tolerance, and high carrier mobility make them promising materials for solar cells. However, their long-term stability is a major concern due to the susceptibility of organic components to environmental degradation. Lead-free double perovskites (LFDPs) are emerging as a viable alternative due to their intrinsic chemical stability and environmental friendliness. While their optical, excitonic, and transport properties require further investigation, they offer a promising avenue for lead-free PSCs. Quantum-dot-sensitized solar cells (QDSCs) present another potential approach. Quantum dots (QDs) can be tailored to absorb specific wavelengths of light, and their theoretical power conversion efficiency (PCE) can be exceptionally high. However, experimental PCEs have lagged behind theoretical predictions. PbS colloidal QDs are particularly promising due to their size-dependent bandgap and tunability. The choice of hole transport layer (HTLs) and back contacts also significantly impacts device performance. Understanding the relationship between molecule shape and HTL efficiency is crucial. Metal back contacts offer potential advantages in terms of cost, chemical resistance, and processability. To improve PSC performance, researchers are focusing on compositional engineering, film deposition techniques, and energy loss mechanisms. Numerical analysis tools like SCAPS-1D, SILVACO ATLAS, and WxAMPS are valuable for simulating device behaviour and guiding optimization. Overall, while challenges remain, perovskite solar cells offer significant potential for future energy applications. Continued research and development are essential to address limitations and realize their full potential.

REFERENCES

Use APA 7th edition to correctly cite journal articles, book chapters, books and theses/dissertations as previously advised

Abate, A. (2017). Perovskite solar cells go lead free. *Joule, **1(**4), 659-664.

Agha, D. N. Q., & Algwari, Q. T. (2022). The influence of the conduction band engineering on the perovskite solar cell performance. *Results in Optics, **9*(2022), 1-7.

Aharon, S., Dymshits, A., Rotem, A., & Etgar, L. (2015). Temperature dependence of hole conductor free formamidinium lead iodide perovskite based solar cells. *Journal of Materials Chemistry A, **3*(17), 9171-9178.

Ahmad, K., Raza, W., Khan, R. A., Alsalme, A., & Kim, H. (2022). Numerical Simulation of NH3 (CH2) $2NH_3MnCl_4$ Based Pb-Free Perovskite Solar Cells Via SCAPS-1D. *Nanomaterials*, ***12***(19), 1-12.

Akhil, S., Akash, S., Pasha, A., Kulkarni, B., Jalalah, M., Alsaiari, M., Harraz, F. A., & Balakrishna, R. G. (2021). Review on perovskite silicon tandem solar cells: Status and prospects 2T, 3T and 4T for real world conditions. *Materials & Design, **211*(23), 1-38.

Albaladejo-Siguan, M., Baird, E. C., Becker-Koch, D., Li, Y., Rogach, A. L., & Vaynzof, Y. (2021). Stability of Quantum Dot Solar Cells: A Matter of (Life)Time. *Advanced Energy Materials*, ***11***(12), 1-57.

Aljaghoub, H., Abumadi, F., AlMallahi, M. N., Obaideen, K., & Alami, A. H. (2022). Solar PV cleaning techniques contribute to Sustainable Development Goals (SDGs) using Multi-criteria decision-making (MCDM): Assessment and review. *International Journal of Thermofluids*, ***16***(2022), 1-18.

Allen, J., Shu, B., Zhang, L., Das, U., & Hegedus, S. (2011). Interdigitated back contact silicon hetero-junction solar cells: The effect of doped layer defect levels and rear surface i-layer band gap on fill factor using two-dimensional simulations. 2011 37th IEEE Photovoltaic Specialists Conference, ***22***(1), 1-7.

Amri, K., Belghouthi, R., Aillerie, M., & Gharbi, R. (2021). Device optimization of a lead-free perovskite/silicon tandem solar cell with 24.4% power conversion efficiency. *Energies*, ***14***(12), 1-20.

Asghar, M., Zhang, J., Wang, H., & Lund, P. (2017). Device stability of perovskite solar cells– A review. *Renewable and Sustainable Energy Reviews*, ***77(51)***, 131-146.

Azani, M. R., Hassanpour, A., & Torres, T. (2020). Benefits, problems, and solutions of silver nanowire transparent conductive electrodes in indium tin oxide (ITO)-free flexible solar cells. *Advanced Energy Materials*, ***10***(48), 1-32.

Bacha, M., Saadoune, A., & Youcef, I. (2022). Design and numerical investigation of Perovskite/Silicon tandem solar cell. *Optical Materials*, ***131***(23), 1-61.

Bae, S.-R., Heo, D., & Kim, S. (2022). Recent progress of perovskite devices fabricated using thermal evaporation method: Perspective and outlook. *Materials Today Advances*, ***14***(2022), 1-24.

Bag, A., Radhakrishnan, R., Nekovei, R., & Jeyakumar, R. (2020). Effect of absorber layer, hole transport layer thicknesses, and its doping density on the performance of perovskite solar cells by device simulation. *Solar Energy*, ***196***(15), 177-182.

Baptayev, B., Tashenov, Y., & Balanay, M. P. (2022). Conjugated Polymers as Organic Electrodes for Photovoltaics. in *Organic Electrodes: Fundamental to Advanced Emerging Applications* Springer, ***132***(52), 137-153.

Barimah, E. K., Boontan, A., Steenson, D. P., & Jose, G. (2022). Infrared optical properties modulation of VO2 thin film fabricated by ultrafast pulsed laser deposition for thermochromic smart window applications. *Scientific Reports*, ***12***(1), 1-10.

Bashir, A., Awan, T. I., Tehseen, A., Tahir, M. B., & Ijaz, M. (2020). Interfaces and surfaces. *Chemistry of Nanomaterials*, ***16***(22), 51-87.

Basit, M. A., Ali, M. A., Masroor, Z., Tariq, Z., & Bang, J. H. (2022). Quantum dot-sensitized solar cells: a review on interfacial engineering strategies for boosting efficiency. *Journal of Industrial and Engineering Chemistry*. ***120***(2023), 1-26.

Belarbi, F., Rahal, W., Rached, D., & Adnane, M. (2020). A comparative study of different buffer layers for CZTS solar cell using Scaps-1D simulation program. *Optik*, ***216***(2020), 164743.

Bernasconi, A., Rizzo, A., Listorti, A., Mahata, A., Mosconi, E., De Angelis, F., & Malavasi, L. (2019). Synthesis, properties, and modeling of Cs1–x Rb x SnBr3 solid solution: A New mixed-cation lead-free all-inorganic perovskite system. *Chemistry of Materials*, ***31***(9), 3527-3533.

Bhattacharjee, H., Chakraborty, A., Ganguly, R., & Mitra, M. (2021). Study on Junction Temperature Management of White pcLED at High Ambient Temperature in Industrial Environment: An Indian Perspective. In *2021 Devices for Integrated Circuit (DevIC)*, IEEE, ***11***(12), 1-57.

Bhattacharya, S., & John, S. (2019a). Beyond 30% conversion efficiency in silicon solar cells: a numerical demonstration. *Scientific Reports*, ***9***(1), 1-15.

Bhattacharya, S., & John, S. (2019b). Beyond 30% Conversion Efficiency in Silicon Solar Cells: A Numerical Demonstration. *Scientific Reports*, ***9***(1), 12482.

Bibi, A., Lee, I., Nah, Y., Allam, O., Kim, H., Quan, L. N., Tang, J., Walsh, A., Jang, S. S., Sargent, E. H., & Kim, D. H. (2021). Lead-free halide double perovskites: Toward stable and sustainable optoelectronic devices. *Materials Today*, ***49***(23), 123-144.

Binder, T., Hossinger, A., & Selberherr, S. (2003). Rigorous integration of semiconductor process and device simulators. *IEEE Transactions on Computer-Aided Design of Integrated Circuits and Systems*, ***22***(9), 1204-1214.

Bing, J., Caro, L. G., Talathi, H. P., Chang, N. L., Mckenzie, D. R., & Ho-Baillie, A. W. (2022). Perovskite solar cells for building integrated photovoltaics—glazing applications. *Joule*. ***6*** (7), 1-36.

Bing, J., Huang, S., & Ho-Baillie, A. W. (2020). A review on halide perovskite film formation by sequential solution processing for solar cell applications. *Energy Technology*, ***8***(4), 1-14.

Blank, D. H., Dekkers, M., & Rijnders, G. (2013). Pulsed laser deposition in Twente: from research tool towards industrial deposition. *Journal of physics D: applied physics*, ***47***(3), 1-9.

Bouazizi, S., Tlili, W., Bouich, A., Soucase, B. M., & Omri, A. (2022). Design and efficiency enhancement of FTO/PC60BM/CsSn0. 5Ge0. 5I3/Spiro-OMeTAD/Au perovskite solar cell utilizing SCAPS-1D Simulator. *Materials Research Express*, ***9***(9), 1-13.

Buonomenna, M. (2016). Smart composite membranes for advanced wastewater treatments. In *Smart Composite Coatings and membranes.*Woodhead publishing Elsevier. ***14***(6),371-419).

Caballero, L. M. P., D'Angelo, F. N., Tschentscher, R., Gottschalk, A., Salem, A. M., Carbonell, D., Dudita-Kauffeld, M., Bruch, A., Alamaro, E., & Pasquini, L. (2023). Developing the next generation of renewable energy technologies: an overview of low-TRL EU-funded research projects. *Open Research Europe*, ***3***(8), 1-19.

Calió, L., Kazim, S., Grätzel, M., & Ahmad, S. (2016). Hole-transport materials for perovskite solar cells. *Angewandte Chemie International Edition*, ***55***(47), 14522-14545.

Cao, Q., Wang, T., Yang, J., Zhang, Y., Li, Y., Pu, X., Zhao, J., Chen, H., Li, X., & Tojiboyev, I. (2022). Environmental-Friendly Polymer for Efficient and Stable Inverted Perovskite

Solar Cells with Mitigating Lead Leakage. *Advanced Functional Materials*, ***32***(32), 1-11.

Casas, G., Cappelletti, M. Á., Cedola, A. P., Soucase, B. M., & y Blancá, E. P. (2017). Analysis of the power conversion efficiency of perovskite solar cells with different materials as Hole-Transport Layer by numerical simulations. *Superlattices and Microstructures*, ***107***(21), 136-143.

Cavallari, M. R., Pastrana, L. M., Sosa, C. D. F., Marquina, A. M. R., Izquierdo, J. E. E., Fonseca, F. J., Amorim, C. A. d., Paterno, L. G., & Kymissis, I. (2020). Organic thin-film transistors as gas sensors: a review. *Materials*, ***14***(1), 1-32.

Chang, B., Li, B., Wang, Z., Li, H., Wang, L., Pan, L., Li, Z., & Yin, L. (2022). Efficient bulk defect suppression strategy in FASnI3 perovskite for photovoltaic performance enhancement. *Advanced Functional Materials*, ***32***(12), 1-10.

Chaudhary, J., Choudhary, S., Negi, C. M. S., Gupta, S. K., & Verma, A. S. (2019). Surface morphological, optical and electrical characterization of methylammonium lead bromide perovskite (CH3NH3PbBr3) thin film. *Physica Scripta*, ***94***(10), 1-45.

Chen, C., Zheng, S., & Song, H. (2021). Photon management to reduce energy loss in perovskite solar cells. *Chemical Society Reviews*, ***50***(12), 7250-7329.

Chen, G., Chen, J., Pei, W., Lu, Y., Zhang, Q., Zhang, Q., & He, Y. (2019). Bismuth ferrite materials for solar cells: current status and prospects. *Materials Research Bulletin*, ***110***(98), 39-49.

Chen, J., Jia, D., Johansson, E. M., Hagfeldt, A., & Zhang, X. (2021). Emerging perovskite quantum dot solar cells: feasible approaches to boost performance. *Energy & Environmental Science*, ***14***(1), 224-261.

Chen, L.-C., & Tseng, Z.-L. (2017). ZnO-based electron transporting layer for perovskite solar cells. *Nanostructured Sol. Cells*, ***143***(61), 203-215.

Chen, Z., He, P., Wu, D., Chen, C., Mujahid, M., Li, Y., & Duan, Y. (2021). Processing and preparation method for high-quality opto-electronic perovskite film. *Frontiers in Materials*, ***8***(4), 1-13.

Chen, Z., Su, Q., Qin, Z., & Chen, S. (2021). Effect and mechanism of encapsulation on aging characteristics of quantum-dot light-emitting diodes. *Nano Research*, ***14(7)***, 320-327.

Cheng, D., Yang, Z., & Liang, Y. (2022). Preparation and Energy Storage Performance of Perovskite Luminescent Materials by an Electrochemiluminescence Method. *Adsorption Science & Technology*, ***4(9)***, 1-27..

Chowdhury, T. A., Zafar, M. A. B., Islam, M. S.-U., Shahinuzzaman, M., Islam, M. A., & Khandaker, M. U. (2023). Stability of perovskite solar cells: issues and prospects. *RSC Advances*, ***13***(3), 1787-1810.

Delannoy, Y. (2012). Purification of silicon for photovoltaic applications. *Journal of Crystal Growth*, ***360****(32)*, 61-67.

Demic, S., Ozcivan, A. N., Can, M., Ozbek, C., & Karakaya, M. (2017). Recent progresses in perovskite solar cells. *Nanostructured Solar Cells*, ***110***(78), 277-304.

Deng, J., Li, J., Yang, Z., & Wang, M. (2019). All-inorganic lead halide perovskites: a promising choice for photovoltaics and detectors. *Journal of Materials Chemistry C*, ***7***(40), 12415-12440.

Deng, W., Li, F., Li, J., Wang, M., Hu, Y., & Liu, M. (2020). Anti-solvent free fabrication of FA-Based perovskite at low temperature towards to high performance flexible perovskite solar cells. *Nano Energy*, ***70***(20), 1-45.

Deshmukh, M. A., Park, S.-J., Hedau, B. S., & Ha, T.-J. (2021). Recent progress in solar cells based on carbon nanomaterials. *Solar Energy*, ***220***(55), 953-990.

Domanski, K., Correa-Baena, J.-P., Mine, N., Nazeeruddin, M. K., Abate, A., Saliba, M., Tress, W., Hagfeldt, A., & Grätzel, M. (2016). Not All That Glitters Is Gold: Metal-Migration-Induced Degradation in Perovskite Solar Cells. *ACS Nano*, ***10***(6), 6306-6314.

Du, H.-J., Wang, W.-C., & Zhu, J.-Z. (2016). Device simulation of lead-free CH3NH3SnI3 perovskite solar cells with high efficiency. *Chinese Physics B*, *25*(10), 1-9.

Du, P., Egaña-Ugrinovic, D., Essig, R., & Sholapurkar, M. (2022). Doped Semiconductor Devices for sub-MeV Dark Matter Detection. *arXiv preprint arXiv:* ***30***(12), 1-25..

Duan, W., Bittkau, K., Lambertz, A., Qiu, K., Yao, Z., Steuter, P., Qiu, D., Rau, U., & Ding, K. (2021). Improved Infrared Light Management with Transparent Conductive Oxide/Amorphous Silicon Back Reflector in High-Efficiency Silicon Heterojunction Solar Cells. *Solar RRL*, ***5***(3), 1-7.

Dubey, P., Pandey, B., & Dwivedi, D. (2022). Contribution towards the selection of electron and hole transport layers for the development of highly efficient PbS colloidal quantum dot solar cell. *Optik*, ***266***(32), 1-18.

Elseman, A. M., Xu, C., Yao, Y., Elisabeth, M., Niu, L., Malavasi, L., & Song, Q. L. (2020). Electron Transport Materials: Evolution and Case Study for High-Efficiency Perovskite Solar Cells. *Solar Rrl*, ***4***(7), 1-22.

Eperon, G. E., Leijtens, T., Bush, K. A., Prasanna, R., Green, T., Wang, J. T.-W., McMeekin, D. P., Volonakis, G., Milot, R. L., & May, R. (2016). Perovskite-perovskite tandem photovoltaics with optimized band gaps. *Science*, ***354***(6314), 861-865.

Eswaramoorthy, N., & Rajaram, K. (2022). Planar perovskite solar cells: Plasmonic nanoparticles-modified ZnO as an electron transport layer for enhancing the device performance and stability at ambient conditions. *International Journal of Energy Research*. ***25***(10), 1-17.

Fang, Z., Zeng, Q., Zuo, C., Zhang, L., Xiao, H., Cheng, M., Hao, F., Bao, Q., Zhang, L., & Yuan, Y. (2021). Perovskite-based tandem solar cells. *Science Bulletin*, ***66***(6), 621-636.

Fichtner, W., Rose, D. J., & Bank, R. E. (1983). Semiconductor device simulation. *SIAM Journal on Scientific and Statistical Computing*, ***4***(3), 391-415.

Fu, Q., Tang, X., Huang, B., Hu, T., Tan, L., Chen, L., & Chen, Y. (2018). Recent progress on the long-term stability of perovskite solar cells. *Advanced Science*, ***5***(5), 1-17.

Fuhrmann, J., Guhlke, C., Linke, A., Merdon, C., & Müller, R. (2019). Models and numerical methods for electrolyte flows. In *Topics in Applied Analysis and Optimisation*. Springer. ***4***(3), 183-209)

Gangadharan, D. T., & Ma, D. (2019). Searching for stability at lower dimensions: current trends and future prospects of layered perovskite solar cells. *Energy & Environmental Science*, ***12***(10), 2860-2889.

Gao, T., Yang, Q., Guo, X., Huang, Y., Zhang, Z., Wang, Z., Liao, M., Shou, C., Zeng, Y., & Yan, B. (2019). An industrially viable TOPCon structure with both ultra-thin SiOx and n+-poly-Si processed by PECVD for p-type c-Si solar cells. *Solar Energy Materials and Solar Cells*, ***200(15)***, 1-19.

Gao, W., Chen, C., Ran, C., Zheng, H., Dong, H., Xia, Y., Chen, Y., & Huang, W. (2020). A-Site Cation Engineering of Metal Halide Perovskites: Version 3.0 of Efficient Tin-Based Lead-Free Perovskite Solar Cells. *Advanced Functional Materials*, *30*(34), 1-29.

Ge, C., Xue, Y., Li, L., Tang, B., & Hu, H. (2020). Recent progress in 2D/3D multidimensional metal halide perovskites solar cells. *Frontiers in Materials*, ***7***(3), 1-9.

Ghosh, S., Shankar, H., & Kar, P. (2022). Recent developments of lead-free halide double perovskites: a new superstar in the optoelectronic field [10.1039/D2MA00071G]. *Materials Advances*, ***3***(9), 3742-3765.

Gil-Escrig, L., Hu, S., Zanoni, K. P., Paliwal, A., Hernández-Fenollosa, M. A., Roldán-Carmona, C., Sessolo, M., Wakamiya, A., & Bolink, H. J. (2022).

Perovskite/Perovskite Tandem Solar Cells in the Substrate Configuration with Potential for Bifacial Operation. *ACS Materials Letters*, ***4****(76)*, 2638-2644.

Grancini, G., Roldán-Carmona, C., Zimmermann, I., Mosconi, E., Lee, X., Martineau, D., Narbey, S., Oswald, F., De Angelis, F., & Graetzel, M. (2017). One-Year stable perovskite solar cells by 2D/3D interface engineering. *Nature Communications*, ***8***(1), 1-8.

Green, M. A., Ho-Baillie, A., & Snaith, H. J. (2014). The emergence of perovskite solar cells. *Nature Photonics*, ***8***(7), 506-514.

Guangul, F. M., & Chala, G. T. (2019). Solar energy as renewable energy source: SWOT analysis. In 2019 4th MEC international conference on big data and smart city (ICBDSC),IEEE, ***2***(1), 1-5.

Guerrero, A., You, J., Aranda, C., Kang, Y. S., Garcia-Belmonte, G., Zhou, H., Bisquert, J., & Yang, Y. (2016). Interfacial Degradation of Planar Lead Halide Perovskite Solar Cells. *ACS Nano*, ***10***(1), 218-224.

Haddout, A., Raidou, A., & Fahoume, M. (2019). A review on the numerical modeling of CdS/CZTS-based solar cells. *Applied physics A*, ***125***(2), 1-16.

Hadjab, M., Wagner, J.-M., Bouzid, F., Boudour, S., Hadj Larbi, A., Bennacer, H., Ziane, M. I., Saeed, M., Abid, H., & Berrah, S. (2022). A numerical optimization study of CdS and Mg0. 125Zn0. 875O buffer layers in CIGS-based solar cells using wx AMPS-1D package. *International Journal of Modelling and Simulation*, ***42***(2), 179-191.

Haider, S. Z., Anwar, H., & Wang, M. (2019). Theoretical device engineering for high-performance perovskite solar cells using CuSCN as hole transport material boost the efficiency above 25%. *Physica Status Solidi (a)*, ***216***(11),1-12.

Haider, S. Z., Anwar, H., & Wang, M. (2021). Remarkable performance optimization of inverted pin architecture perovskite solar cell with CZTS as hole transport material. *Physica B: Condensed Matter*, *620*(2021), 41-70.

Hamukwaya, S. L., Hao, H., Zhao, Z., Dong, J., Zhong, T., Xing, J., Hao, L., & Mashingaidze, M. M. (2022). A Review of Recent Developments in Preparation Methods for Large-Area Perovskite Solar Cells. *Coatings*, ***12***(2), 1-39.

Han, M., Karatum, O., & Nizamoglu, S. (2022). Optoelectronic Neural Interfaces Based on Quantum Dots. *ACS Applied Materials & Interfaces*, ***14***(18), 20468-20490.

Hasan Ali, M., Saiful Islam, A. T. M., Haque, M. D., Ferdous Rahman, M., Khalid Hossain, M., Sultana, N., & Touhidul Islam, A. Z. M. (2023). Numerical analysis of FeSi2 based

solar cell with PEDOT:PSS hole transport layer. *Materials Today Communications*, ***34****(2)*, 1-7.

Heider, Y., Willmes, P., Huch, V., Zimmer, M., & Scheschkewitz, D. (2019). Boron and Phosphorus Containing Heterosiliconoids: Stable p-and n-Doped Unsaturated Silicon Clusters. *Journal of the American Chemical Society*, ***141***(49), 19498-19504.

Heller, J., Pascher, T. F., Muß, D., van der Linde, C., Beyer, M. K., & Ončák, M. (2021). Photochemistry and UV/vis spectroscopy of hydrated vanadium cations, V+(H 2 O) n, n= 1–41, a model system for photochemical hydrogen evolution. *Physical Chemistry Chemical Physics*, ***23***(39), 22251-22262.

Hidalgo, J., Castro-Méndez, A. F., & Correa-Baena, J. P. (2019). Imaging and mapping characterization tools for perovskite solar cells. *Advanced Energy Materials*, ***9***(30), 1-30.

Hima, A., Lakhdar, N., Benhaoua, B., Saadoune, A., Kemerchou, I., & Rogti, F. (2019). An optimized perovskite solar cell designs for high conversion efficiency. *Superlattices and Microstructures*, ***129***(23), 240-246.

Houimi, A., Gezgin, S. Y., Mercimek, B., & Kılıç, H. Ş. (2021). Numerical analysis of CZTS/n-Si solar cells using SCAPS-1D. A comparative study between experimental and calculated outputs. *Optical Materials*, ***121****(2021)*, 111544.

Hu, T., Dai, K., Zhang, J., & Chen, S. (2020). Noble-metal-free Ni2P modified step-scheme SnNb2O6/CdS-diethylenetriamine for photocatalytic hydrogen production under broadband light irradiation. *Applied Catalysis B: Environmental*, ***269***(384), 1-44.

Huang, L., Hu, Z., Xu, J., Sun, X., Du, Y., Ni, J., Cai, H., Li, J., & Zhang, J. (2016). Efficient planar perovskite solar cells without a high temperature processed titanium dioxide electron transport layer. *Solar Energy Materials and Solar Cells*, ***149****(56)*, 1-8.

Huang, L., Huang, J., Peng, R., & Ge, Z. (2021). Efficient Electron Transport Layer-Free Perovskite Solar Cells Enabled by Discontinuous Polar Molecular Films: A Story of New Materials and Old Ideas? *ACS Sustainable Chemistry & Engineering*, ***9***(2), 936-943.

Huirong, P., Molang, C., Shuang, M., Xiaoqiang, S., Xuepeng, L., & Songyuan, D. (2021). Fabrication and stability of all-inorganic perovskite solar cells. *Progress in Chemistry*, ***33***(1), 1-36.

Husainat, A., Ali, W., Cofie, P., Attia, J., Fuller, J., & Darwish, A. (2020). Simulation and analysis method of different back metals contact of CH3NH3PbI3 perovskite solar cell

along with electron transport layer TiO2 using MBMT-MAPLE/PLD. *American Journal of Optics and Photonics*, ***8***(1), 6-26.

Hwang, D.-K., Jo, H. J., Kim, D.-H., Lee, E. J., & Chang, R. P. (2023). Hybrid dual-stage flow-synthesis of eco-friendly ZnCuInSSe quantum dots for solar cells: Improvement in efficiency using inorganic ligand exchange. *Journal of Power Sources*, ***555****(19)*, 232344.

Ibn-Mohammed, T., Koh, S., Reaney, I., Acquaye, A., Schileo, G., Mustapha, K., & Greenough, R. (2017). Perovskite solar cells: An integrated hybrid lifecycle assessment and review in comparison with other photovoltaic technologies. *Renewable and Sustainable Energy Reviews*, ***80***(2017), 1321-1344.

Ijaz, S., Raza, E., Ahmad, Z., Zubair, M., Mehmood, M. Q., Mehmood, H., Massoud, Y., & Rehman, M. M. (2023). Numerical simulation to optimize the efficiency of HTM-free perovskite solar cells by ETM engineering. *Solar Energy*, ***250***(34), 108-118.

Ilyas, M., Waris, A., Khan, A. U., Zamel, D., Yar, L., Baset, A., Muhaymin, A., Khan, S., Ali, A., & Ahmad, A. (2021). Biological synthesis of titanium dioxide nanoparticles from plants and microorganisms and their potential biomedical applications. *Inorganic Chemistry Communications*, ***133****(25)*, 1-8.

Ishikawa, R., Ueno, K., & Shirai, H. (2020). Improved efficiency of methylammonium-free perovskite thin film solar cells by fluorinated ammonium iodide treatment. *Organic Electronics*, ***78****(74)*, 1-6.

Jain, M., Bhumla, P., Kumar, M., & Bhattacharya, S. (2022). Lead-Free Alloyed Double Perovskites: An Emerging Class of Materials for Optoelectronic Applications. *The Journal of Physical Chemistry C*, ***126***(15), 6753-6760.

Jones, D. M., An, Y., Hidalgo, J., Evans, C., Vagott, J. N., & Correa-Baena, J.-P. (2021). Polymers and interfacial modifiers for durable perovskite solar cells: a review. *Journal of Materials Chemistry C*, ***9***(37), 12509-12522.

Jošt, M., Lipovšek, B., Glažar, B., Al-Ashouri, A., Brecl, K., Matič, G., Magomedov, A., Getautis, V., Topič, M., & Albrecht, S. (2020). Perovskite solar cells go outdoors: field testing and temperature effects on energy yield. *Advanced Energy Materials*, ***10***(25), 1-14.

Kajal, P., Ghosh, K., & Powar, S. (2018). Manufacturing techniques of perovskite solar cells. *Applications of Solar Energy*, 341-364.

Kandeal, A., Thakur, A. K., Elkadeem, M., Elmorshedy, M. F., Ullah, Z., Sathyamurthy, R., & Sharshir, S. W. (2020). Photovoltaics performance improvement using different cooling methodologies: A state-of-art review. *Journal of Cleaner Production*, ***273***(195), 12-72.

Kandjani, S. A., Mirershadi, S., & Nikniaz, A. (2015). Inorganic–organic perovskite solar cells. *Solar Cells-New Approaches and Reviews*, ***10****(6)*, 1-8.

Karker, O., Zekentes, K., Bouchard, A., Gélard, I., Mescot, X., Stambouli, V., & Bano, E. (2022). Modelling and Development of 4H-SiC Nanowire/Nanoribbon Biosensing FET Structures. *Materials Science Forum*, ***1062***(675), 608-612.

Ke, W., Fang, G., Liu, Q., Xiong, L., Qin, P., Tao, H., Wang, J., Lei, H., Li, B., Wan, J., Yang, G., & Yan, Y. (2015). Low-Temperature Solution-Processed Tin Oxide as an Alternative Electron Transporting Layer for Efficient Perovskite Solar Cells. *Journal of the American Chemical Society*, ***137***(21), 6730-6733.

Ke, W., & Kanatzidis, M. G. (2019). Prospects for low-toxicity lead-free perovskite solar cells. *Nature Communications*, ***10***(1), 1-4.

Khan, F., Rezgui, B. D., Khan, M. T., & Al-Sulaiman, F. (2022). Perovskite-based tandem solar cells: Device architecture, stability, and economic perspectives. *Renewable and Sustainable Energy Reviews*, ***165***(24), 61-85.

Khirade, P. P., & Raut, A. V. (2022). Perovskite Structured Materials: Synthesis, Structure, Physical Properties and Applications. In *Recent Advances in Multifunctional Perovskite Materials*. *IntechOpen*. ***130***(62), 670-733.

Kong, F., & Dai, S. (2022). The dyes used in dye-sensitized solar cells. *Dye-sensitized Solar Cells*, ***7****(5)*, 1-39.

Kong, L., Yuan, Z., Sun, N., Ding, J., Liu, S., Zhang, S., Lv, Z., Xu, W., Liu, G., & Liu, X. (2023). Advances in flexible hydrogels for light-thermal-electricity energy conversion and storage. *Journal of Energy Storage*, ***60****(25)*, 1-18.

Korir, B. K., Kibet, J. K., & Ngari, S. M. (2021). Computational Simulation of a Highly Efficient Hole Transport-Free Dye-Sensitized Solar Cell Based on Titanium Oxide (TiO_2) and Zinc Oxysulfide (ZnOS) Electron Transport Layers. *Journal of Electronic Materials*, ***50***(12), 7259-7274.

Kumar, N., Phani, M. K., Chamoli, P., Manoj, M., Sharma, A., Ahmed, W., Srivastava, A. K., & Kumar, S. (2021). Nanomaterials for advanced photovoltaic cells. *Emerging Nanotechnologies for Renewable Energy*, ***33***(65), 239-258.

Kumari, P., Punia, U., Sharma, D., Srivastava, A., & Srivastava, S. K. (2022). Enhanced Photovoltaic Performance of PEDOT: PSS/Si Heterojunction Solar Cell with ZnO BSF Layer: A Simulation Study using SCAPS-1D. *Silicon*, ***15***(84), 2099–2112.

Kung, P.-K., Li, M.-H., Lin, P.-Y., Jhang, J.-Y., Pantaler, M., Lupascu, D. C., Grancini, G., & Chen, P. (2020a). Lead-Free Double Perovskites for Perovskite Solar Cells .*Solar RRL*, ***4***(2), 1-6.

Kung, P.-K., Li, M.-H., Lin, P.-Y., Jhang, J.-Y., Pantaler, M., Lupascu, D. C., Grancini, G., & Chen, P. (2020b). Lead-free double perovskites for perovskite solar cells. *Solar RRL*, ***4***(2), 1-9.

Laalioui, S., Alaoui, K. B., Dads, H. A., El Assali, K., Ikken, B., & Outzourhit, A. (2020). Progress in perovskite based solar cells: scientific and engineering state of the art. *Reviews on Advanced Materials Science*, ***59***(1), 10-25.

Lakhdar, N., & Hima, A. (2020). Electron transport material effect on performance of perovskite solar cells based on CH3NH3GeI3. *Optical Materials*, ***99****(20)*, 1-7.

Lal, N. N., Dkhissi, Y., Li, W., Hou, Q., Cheng, Y. B., & Bach, U. (2017). Perovskite tandem solar cells. *Advanced Energy Materials*, ***7***(18), 1602761.

Lam, P. M., Wu, J., Hatch, S., Kim, D., Tang, M., Liu, H., Wilson, J., & Allison, R. (2015). Effect of rapid thermal annealing on InAs/GaAs quantum dot solar cells. *IET Optoelectronics*, ***9***(2), 65-68.

Lee, S., Jeong, D., Kim, C., Lee, C., Kang, H., Woo, H. Y., & Kim, B. J. (2020). Eco-friendly polymer solar cells: advances in green-solvent processing and material design. *Acs Nano*, ***14***(11), 14493-14527.

Lee, Y. I., Jeon, N. J., Kim, B. J., Shim, H., Yang, T. Y., Seok, S. I., Seo, J., & Im, S. G. (2018). A low-temperature thin-film encapsulation for enhanced stability of a highly efficient perovskite solar cell. *Advanced Energy Materials*, ***8***(9), 1701928.

Li, D., Zhang, D., Lim, K. S., Hu, Y., Rong, Y., Mei, A., Park, N. G., & Han, H. (2021). A review on scaling up perovskite solar cells. *Advanced Functional Materials*, ***31***(12), 1-27.

Li, H., & Zhang, W. (2020). Perovskite tandem solar cells: from fundamentals to commercial deployment. *Chemical Reviews*, ***120***(18), 9835-9950.

Li, M. H., Shao, J. Y., Jiang, Y., Qiu, F. Z., Wang, S., Zhang, J., Han, G., Tang, J., Wang, F., & Wei, Z. (2021). Electrical Loss Management by Molecularly Manipulating Dopant-free Poly (3-hexylthiophene) towards 16.93% CsPbI2Br Solar Cells. *Angewandte Chemie*, ***133***(30), 16524-16529.

Li, W., Wang, Z., Deschler, F., Gao, S., Friend, R. H., & Cheetham, A. K. (2017). Chemically diverse and multifunctional hybrid organic–inorganic perovskites. *Nature Reviews Materials*, ***2***(3), 1-18.

Li, Y., Meng, L., Yang, Y. M., Xu, G., Hong, Z., Chen, Q., You, J., Li, G., Yang, Y., & Li, Y. (2016). High-efficiency robust perovskite solar cells on ultrathin flexible substrates. *Nature communications*, ***7***(1), 1-10.

Li, Z., Klein, T. R., Kim, D. H., Yang, M., Berry, J. J., Van Hest, M. F., & Zhu, K. (2018). Scalable fabrication of perovskite solar cells. *Nature Reviews Materials*, ***3***(4), 1-20.

Li, Z., Li, P., Chen, G., Cheng, Y., Pi, X., Yu, X., Yang, D., Han, L., Zhang, Y., & Song, Y. (2020). Ink Engineering Of Inkjet Printing Perovskite. *ACS Applied Materials & Interfaces*, ***12***(35), 39082-39091.

Li, Z., Park, J., Park, H., Lee, J., Kang, Y., Ahn, T. K., Kim, B.-G., & Park, H. J. (2020). Graded heterojunction of perovskite/dopant-free polymeric hole-transport layer for efficient and stable metal halide perovskite devices. *Nano Energy*, ***78***(23), 1-9.

Lin, L., Jones, T. W., Yang, T. C. J., Duffy, N. W., Li, J., Zhao, L., Chi, B., Wang, X., & Wilson, G. J. (2021). Inorganic electron transport materials in perovskite solar cells. *Advanced Functional Materials*, ***31***(5), 1-24.

Liu, D., Gangishetty, M. K., & Kelly, T. L. (2014). Effect of CH 3 NH 3 PbI 3 thickness on device efficiency in planar heterojunction perovskite solar cells. *Journal of Materials Chemistry A*, ***2***(46), 19873-19881.

Liu, D., Kim, K., Kim, J., Gong, J., Chang, T.-H., & Ma, Z. (2019). Novel Materials-Based Flexible Solar Cells. *Inorganic Flexible Optoelectronics: Materials and Applications*. ***12***(46), 873-881.

Liu, F., Zhu, J., Wei, J., Li, Y., Lv, M., Yang, S., Zhang, B., Yao, J., & Dai, S. (2014). Numerical simulation: toward the design of high-efficiency planar perovskite solar cells. *Applied Physics Letters*, ***104***(25), 1-5.

Liu, H., Zhang, Z., Zuo, W., Roy, R., Li, M., Byranvand, M. M., & Saliba, M. (2023). Pure Tin Halide Perovskite Solar Cells: Focusing on Preparation and Strategies. *Advanced Energy Materials*, ***13***(3), 1-9.

Liu, L., Xiao, H., Jin, K., Xiao, Z., Du, X., Yan, K., Hao, F., Bao, Q., Yi, C., & Liu, F. (2023). 4-Terminal Inorganic Perovskite/Organic Tandem Solar Cells Offer 22% Efficiency. *Nano-Micro Letters*, ***15***(1), 1-23.

Liu, P., Han, N., Wang, W., Ran, R., Zhou, W., & Shao, Z. (2021). High-quality ruddlesden–popper perovskite film formation for high-performance perovskite solar cells. *Advanced Materials*, ***33***(10), 1-12.

Liu, X., Du, X., Wang, J., Duan, C., Tang, X., Heumueller, T., Liu, G., Li, Y., Wang, Z., & Wang, J. (2018). Efficient Organic Solar Cells with Extremely High Open-Circuit Voltages and Low Voltage Losses by Suppressing Nonradiative Recombination Losses. *Advanced Energy Materials*, ***8***(26), 1-16.

Liu, X., Wu, T., Luo, X., Wang, H., Furue, M., Bessho, T., Zhang, Y., Nakazaki, J., Segawa, H., & Han, L. (2022). Lead-Free Perovskite Solar Cells with Over 10% Efficiency and Size 1 cm2 Enabled by Solvent–Crystallization Regulation in a Two-Step Deposition Method. *ACS Energy Letters*, ***7***(1), 425-431.

Liu, Y.-Y., Wang, Y., Walsh, T. R., Yi, L.-X., Zhang, R., Spencer, J., Doi, Y., Tian, G., Dong, B., & Huang, X. (2016). Emergence of plasmid-mediated colistin resistance mechanism MCR-1 in animals and human beings in China: a microbiological and molecular biological study. *The Lancet Infectious Diseases*, ***16***(2), 161-168.

Liu, Y., Heinzel, D., & Rockett, A. (2011). A new solar cell simulator: WxAMPS. 2011 37th IEEE Photovoltaic Specialists Conference, **17**(9), 625-631.

Liu, Y., Sun, Y., & Rockett, A. (2012). A new simulation software of solar cells—wxAMPS. *Solar Energy Materials and Solar Cells*, ***98****(78)*, 124-128.

Liu, Z., Sofia, S. E., Laine, H. S., Woodhouse, M., Wieghold, S., Peters, I. M., & Buonassisi, T. (2020). Revisiting thin silicon for photovoltaics: a technoeconomic perspective. *Energy & Environmental Science*, ***13***(1), 12-23.

Long, Z., Li, Q., Wei, T., Zhang, G., & Ren, Z. (2020). Historical development and prospects of photocatalysts for pollutant removal in water. *Journal of Hazardous Materials*, ***395***(33), 630-686

Lukong, V. T., Ukoba, K., & Jen, T.-C. (2022). Review of self-cleaning TiO2 thin films deposited with spin coating. *The International Journal of Advanced Manufacturing Technology*, ***5***(1), 1-22.

Ma, S., Yuan, G., Zhang, Y., Yang, N., Li, Y., & Chen, Q. (2022). Development of encapsulation strategies towards the commercialization of perovskite solar cells. *Energy & Environmental Science*, ***15***(1), 13-55.

Mahajan, P., Padha, B., Verma, S., Gupta, V., Datt, R., Tsoi, W. C., Satapathi, S., & Arya, S. (2022). Review of current progress in hole-transporting materials for perovskite solar cells. *Journal of Energy Chemistry*, ***68***(33), 330-386.

Mahapatra, A., Kumar, S., Kumar, P., & Pradhan, B. (2022). Recent progress in perovskite solar cells: challenges from efficiency to stability. *Materials Today Chemistry*, ***23****(11)*, 1-6.

Mali, S. S., & Hong, C. K. (2016). pin/nip type planar hybrid structure of highly efficient perovskite solar cells towards improved air stability: synthetic strategies and the role of p-type hole transport layer (HTL) and n-type electron transport layer (ETL) metal oxides. *Nanoscale*, ***8***(20), 10528-10540.

Mandadapu, U., Vedanayakam, S. V., & Thyagarajan, K. (2017). Simulation and analysis of lead based perovskite solar cell using SCAPS-1D. *Indian J. Sci. Technol.*, ***10***(11), 65-72.

Mandadapu, U., Vedanayakam, S. V., Thyagarajan, K., & Babu, B. (2018). Optimisation of high efficiency tin halide perovskite solar cells using SCAPS-1D. *Int. J. Simul. Process. Model.*, ***13***(3), 221-227.

Mani, M. S., Joshi, M. B., Shetty, R. R., DSouza, V. L., Swathi, M., Kabekkodu, S. P., & Dsouza, H. S. (2020). Lead exposure induces metabolic reprogramming in rat models. *Toxicology Letters*, ***335****(45)*, 11-27.

Mansour, A. E., Said, M. M., Dey, S., Hu, H., Zhang, S., Munir, R., Zhang, Y., Moudgil, K., Barlow, S., & Marder, S. R. (2017). Facile Doping and Work-Function Modification of Few-Layer Graphene Using Molecular Oxidants and Reductants. *Advanced Functional Materials*, ***27***(7), 1-13.

Marinova, N., Valero, S., & Delgado, J. L. (2017). Organic and perovskite solar cells: Working principles, materials and interfaces. *Journal of Colloid and Interface Science*, ***488****(124)*, 373-389.

MaríSoucase, B., Pradas, I. G., & Adhikari, K. R. (2016). Numerical simulations on perovskite photovoltaic devices. *Perovskite materials: synthesis, characterisation, properties, and applications*, ***445***(15), 444-447.

Markna, J., & Rathod, P. K. (2022). Review on the efficiency of quantum dot sensitized solar cell: Insights into photoanodes and QD sensitizers. *Dyes and Pigments*, ***199***,

(24), 73-89.

Mathies, F., Eggers, H., Richards, B. S., Hernandez-Sosa, G., Lemmer, U., & Paetzold, U. W. (2018). Inkjet-printed triple cation perovskite solar cells. *ACS Applied Energy Materials*, ***1(***5), 1834-1839.

Mattox, D. M., & Mattox, V. (2003). Vacuum coating technology. *Springer*, ***7***(1), 1-31.

Meena, M. L., Gupta, K. K., Dutta, S., Kumar, R., Singh, R. K., Lu, C.-H., Lin, S. D., & Som, S. (2022). Short review on the instability and potential solutions for perovskite quantum dots. *Current Research in Green and Sustainable Chemistry*, ***9***(6), 1-21.

Meng, D., Xue, J., Zhao, Y., Zhang, E., Zheng, R., & Yang, Y. (2022). Configurable Organic Charge Carriers toward Stable Perovskite Photovoltaics. *Chemical Reviews*, ***122***(18), 14954-14986.

Min, H., Lee, D. Y., Kim, J., Kim, G., Lee, K. S., Kim, J., Paik, M. J., Kim, Y. K., Kim, K. S., & Kim, M. G. (2021). Perovskite solar cells with atomically coherent interlayers on SnO2 electrodes. *Nature*, ***598***(7881), 444-450.

Mohammadnia, A., Rezania, A., Ziapour, B. M., Sedaghati, F., & Rosendahl, L. (2020). Hybrid energy harvesting system to maximize power generation from solar energy. *Energy Conversion and Management*, ***205***(2020), 112352.

Momblona, C., Gil-Escrig, L., Bandiello, E., Hutter, E. M., Sessolo, M., Lederer, K., Blochwitz-Nimoth, J., & Bolink, H. J. (2016). Efficient vacuum deposited pin and nip perovskite solar cells employing doped charge transport layers. *Energy & Environmental Science*, ***9***(11), 3456-3463.

Nazir, G., Lee, S. Y., Lee, J. H., Rehman, A., Lee, J. K., Seok, S. I., & Park, S. J. (2022). Stabilization of Perovskite Solar Cells: Recent Developments and Future Perspectives. *Advanced Materials*, ***34***(50), 1-45.

Nine, K. B., Hossain, M. F., & Mahmood, S. A. (2019). Analysis of stable, environment friendly and highly efficient perovskite solar cell. TENCON 2019-2019 IEEE Region 10 Conference (TENCON), **29**(411), 456-463.

Niu, G., Guo, X., & Wang, L. (2015). Review of recent progress in chemical stability of perovskite solar cells. *Journal of Materials Chemistry A*, ***3***(17), 8970-8980.

Niu, T., Zhu, W., Zhang, Y., Xue, Q., Jiao, X., Wang, Z., Xie, Y.-M., Li, P., Chen, R., & Huang, F. (2021). DA-π-AD-type dopant-free hole transport material for low-cost, efficient, and stable perovskite solar cells. *Joule*, ***5***(1), 249-269.

Noel, N. K., Stranks, S. D., Abate, A., Wehrenfennig, C., Guarnera, S., Haghighirad, A.-A., Sadhanala, A., Eperon, G. E., Pathak, S. K., & Johnston, M. B. (2014). Lead-free organic–inorganic tin halide perovskites for photovoltaic applications. *Energy & Environmental Science*, ***7***(9), 3061-3068.

Noel, N. K., Stranks, S. D., Abate, A., Wehrenfennig, C., Guarnera, S., Haghighirad, A.-A., Sadhanala, A., Eperon, G. E., Pathak, S. K., Johnston, M. B., Petrozza, A., Herz, L. M., & Snaith, H. J. (2014). Lead-free organic–inorganic tin halide perovskites for

photovoltaic applications [10.1039/C4EE01076K]. *Energy & Environmental Science*, ***7***(9), 3061-3068.

Omrani, M., Keshavarzi, R., Abdi-Jalebi, M., & Gao, P. (2022). Impacts of plasmonic nanoparticles incorporation and interface energy alignment for highly efficient carbon-based perovskite solar cells. *Scientific Reports*, ***12***(1), 1-10.

Ortiz-Cervantes, C., Carmona-Monroy, P., & Solis-Ibarra, D. (2019). Two-dimensional halide perovskites in solar cells: 2D or not 2D? *ChemSusChem*, ***12***(8), 1560-1575.

Ouedraogo, N. A. N., Chen, Y., Xiao, Y. Y., Meng, Q., Han, C. B., Yan, H., & Zhang, Y. (2020). Stability of all-inorganic perovskite solar cells. *Nano Energy*, ***67***(12), 1-49.

Owens, A., & Peacock, A. (2004). Compound semiconductor radiation detectors. *Nuclear Instruments and Methods in Physics Research Section A: Accelerators, Spectrometers, Detectors and Associated Equipment*, ***531***(1-2), 18-37.

Park, Y., Zechner, C., Oh, Y., Kim, H., Martin-Bragado, I., Bazizi, E., & Benistant, F. (2017). Dopant diffusion in Si, SiGe and Ge: TCAD model parameters determined with density functional theory. 2017 IEEE International Electron Devices Meeting (IEDM), ***2***(8), 97-99

Patel, S. B., Patel, A. H., & Gohel, J. V. (2018). A novel and cost effective CZTS hole transport material applied in perovskite solar cells. *CrystEngComm*, ***20***(47), 7677-7687.

Pendyala, N. K., Magdassi, S., & Etgar, L. (2021). Fabrication of perovskite solar cells with digital control of transparency by inkjet printing. *ACS Applied Materials & Interfaces*, ***13***(26), 30524-30532.

Peng, X., Yuan, J., Shen, S., Gao, M., Chesman, A. S., Yin, H., Cheng, J., Zhang, Q., & Angmo, D. (2017). Perovskite and organic solar cells fabricated by inkjet printing: progress and prospects. *Advanced Functional Materials*, ***27***(41), 1-27.

Perez, M. J., Fthenakis, V., Kim, H. C., & Pereira, A. O. (2012). Façade–integrated photovoltaics: a life cycle and performance assessment case study. *Progress in Photovoltaics: Research and Applications*, ***20***(8), 975-990.

Pham, H. D., Yang, T. C. J., Jain, S. M., Wilson, G. J., & Sonar, P. (2020). Development of dopant-free organic hole transporting materials for perovskite solar cells. *Advanced Energy Materials*, ***10***(13), 1-23.

Philippe, B., Man, G. J., & Rensmo, H. (2020). Photoelectron spectroscopy investigations of halide perovskite materials used in solar cells. In *Characterization Techniques for Perovskite Solar Cell Materials* . Elsevier ***45***(2020), 109-137

Pitchaiya, S., Natarajan, M., Santhanam, A., Asokan, V., Yuvapragasam, A., Ramakrishnan, V. M., Palanisamy, S. E., Sundaram, S., & Velauthapillai, D. (2020). A review on the classification of organic/inorganic/carbonaceous hole transporting materials for perovskite solar cell application. *Arabian Journal of Chemistry*, ***13***(1), 2526-2557.

Prasanna, J. L., Goel, E., Kumar, A., Laref, A., Santhosh, C., Ranjan, P., & Kumar, A. (2022). Bandgap graded perovskite solar cell for above 30% efficiency. *Optik*, ***269****(92)*, 1-91.

Quarti, C., Katan, C., & Even, J. (2020). Physical properties of bulk, defective, 2D and 0D metal halide perovskite semiconductors from a symmetry perspective. *Journal of Physics: Materials*, ***3***(4),1-16.

Rahman, M. A. (2021). Design and simulation of a high-performance Cd-free Cu 2 SnSe 3 solar cells with SnS electron-blocking hole transport layer and TiO 2 electron transport layer by SCAPS-1D. *SN Applied Sciences*, ***3***(2), 1-15.

Rai, S., Pandey, B., & Dwivedi, D. (2021). Designing hole conductor free tin–lead halide based all-perovskite heterojunction solar cell by numerical simulation. *Journal of Physics and Chemistry of Solids*, ***156***(2021), 1-8.

Rai, S., Pandey, B., Garg, A., & Dwivedi, D. (2021). Hole transporting layer optimization for an efficient lead-free double perovskite solar cell by numerical simulation. *Optical Materials*, ***121***(2021), 1-11.

Rajagopal, A., Yang, Z., Jo, S. B., Braly, I. L., Liang, P. W., Hillhouse, H. W., & Jen, A. K. Y. (2017). Highly efficient perovskite–perovskite tandem solar cells reaching 80% of the theoretical limit in photovoltage. *Advanced Materials*, ***29***(34), 1-10.

Rao, M. K., Sangeetha, D., Selvakumar, M., Sudhakar, Y., & Mahesha, M. (2021). Review on persistent challenges of perovskite solar cells' stability. *Solar Energy*, ***218****(90)*, 469-491.

Raza, E., Ahmad, Z., Asif, M., Aziz, F., Riaz, K., Mehmood, M. Q., Bhadra, J., & Al-Thani, N. J. (2022). Numerical modeling and performance optimization of carbon-based hole transport layer free perovskite solar cells. *Optical Materials*, ***125***(12), 220-375.

Razzaq, A., Allen, T. G., Liu, W., Liu, Z., & De Wolf, S. (2022). Silicon heterojunction solar cells: Techno-economic assessment and opportunities. *Joule*, ***6***(3), 514-542.

Ren, M., Qian, X., Chen, Y., Wang, T., & Zhao, Y. (2021). Potential lead toxicity and leakage issues on lead halide perovskite photovoltaics. *Journal of Hazardous Materials*, ***18***(14), 1-8.

Rodhuan, M. B., Kahar, R. A., Yazid, H. N. M., Rapi, A. N. M., Baharin, N. H., & Burhan, N. (2023). Size dependency of CdSe for light harvesting in quantum dots solar cell using

COMSOL Multiphysics. *International Journal of Application on Sciences, Technology and Engineering*, ***1***(1), 234-242.

Rono, N., Merad, A. E., Kibet, J. K., Martincigh, B. S., & Nyamori, V. O. (2022). Simulation of the photovoltaic performance of a perovskite solar cell based on methylammonium lead iodide. *Optical and Quantum Electronics*, ***54***(5), 1-15.

Roy, P., Ghosh, A., Barclay, F., Khare, A., & Cuce, E. (2022). Perovskite solar cells: A review of the recent advances. *Coatings*, ***12***(8), 1089.

Roy, P., Sinha, N. K., Tiwari, S., & Khare, A. (2020). A review on perovskite solar cells: Evolution of architecture, fabrication techniques, commercialization issues and status. *Solar Energy*, ***198***(76), 665-688.

Rühle, S., Shalom, M., & Zaban, A. (2010). Quantum-dot-sensitized solar cells. *ChemPhysChem*, ***11***(11), 2290-2304.

Saeed, F., & Gelani, H. E. (2022). Unravelling the effect of defect density, grain boundary and gradient doping in an efficient lead-free formamidinium perovskite solar cell. *Optical Materials*, ***124***(2022), 111952.

Saianand, G., Sonar, P., Wilson, G. J., Gopalan, A.-I., Roy, V. A., Unni, G. E., Reza, K. M., Bahrami, B., Venkatramanan, K., & Qiao, Q. (2021). Current advancements on charge selective contact interfacial layers and electrodes in flexible hybrid perovskite photovoltaics. *Journal of Energy Chemistry*, ***54***(23), 151-173.

Said Al Ghaithi, A. O. (2020). fabrication and characterization of perovskite structures for solar cell applications. *Physics_Theses*, ***8***(4), 1-5.

Saikia, D., Alam, M., Bera, J., Betal, A., Gandhi, A. N., & Sahu, S. (2022). A First-principles study on ABBr3 (A= Cs, Rb, K, Na; B= Ge, Sn) halide perovskites for photovoltaic applications. *arXiv preprint arXiv:2205.01384*. ***5***(12), 1-10.

Sanglee, K., Nukunudompanich, M., Part, F., Zafiu, C., Bello, G., Ehmoser, E.-K., & Chuangchote, S. (2022). The current state of the art in internal additive materials and quantum dots for improving efficiency and stability against humidity in perovskite solar cells. *Heliyon*, ***8***(12), 1-10.

Sarker, S., Islam, M. T., Rauf, A., Al Jame, H., Ahsan, S., Islam, M. S., Jani, M. R., Nishat, S. S., Shorowordi, K. M., & Ahmed, S. (2022). A simulation based incremental study of stable perovskite-on-perovskite tandem solar device utilizing non-toxic tin and germanium perovskite. *Materials Today Communications*, ***32***(2022), 1-52.

Scharber, M. C., & Sariciftci, N. S. (2021). Low band gap conjugated semiconducting polymers. *Advanced Materials Technologies*, ***6***(4), 1-9.

Schwarz, M., Senz, V., Dannenberg, A., Feiler, W., Heuck, F., Friedrich, T., Sorger, C., & Franz, J. R. B. (2019 March). Simulation methodology for active semiconductor devices in MEMS. 2019 20th International Conference on Thermal, Mechanical and Multi-Physics Simulation and Experiments in Microelectronics and Microsystems (EuroSimE), ***6***(12), 1-10.

Shafi, M. A., Ullah, H., Ullah, S., Khan, L., Bibi, S., & Soucase, B. M. (2022). Numerical Simulation of Lead-Free Sn-Based Perovskite Solar Cell by Using SCAPS-1D. *Engineering Proceedings*, ***12***(1), 1-5.

Shi, Z., & Jayatissa, A. H. (2018). Perovskites-based solar cells: A review of recent progress, materials and processing methods. *Materials*, ***11***(5), 1-34.

Shpatz Dayan, A., & Etgar, L. (2022). Study of Electron Transport Layer-Free and Hole Transport Layer-Free Inverted Perovskite Solar Cells .*Solar RRL*, ***6***(1), 1-9.

Singh, N., Agarwal, A., & Agarwal, M. (2021). Performance evaluation of lead–free double-perovskite solar cell. *Optical Materials*, ***114***(111), 110-964.

Singh, S. P., & Nagarjuna, P. (2014). Organometal halide perovskites as useful materials in sensitized solar cells. *Dalton Transactions*, ***43***(14), 5247-5251.

Sirbu, D., Balogun, F. H., Milot, R. L., & Docampo, P. (2021). Layered perovskites in solar cells: structure, optoelectronic properties, and device design. *Advanced Energy Materials*, ***11***(24), 1-26.

Smucker, J., & Gong, J. (2021). A comparative study on the band diagrams and efficiencies of silicon and perovskite solar cells using wxAMPS and AMPS-1D. *Solar Energy*, ***228***(54), 187-199.

Sobayel, M., Chowdhury, M., Hossain, T., Alkhammash, H., Islam, S., Shahiduzzaman, M., Akhtaruzzaman, M., Techato, K., & Rashid, M. (2021). Efficiency enhancement of CIGS solar cell by cubic silicon carbide as prospective buffer layer. *Solar Energy*, ***224***(98), 271-278.

Song, J., Hu, W., Li, Z., Wang, X.-F., & Tian, W. (2020). A double hole-transport layer strategy toward efficient mixed tin-lead iodide perovskite solar cell. *Solar Energy Materials and Solar Cells*, ***207***(74), 1-35.

Song, Z., Watthage, S. C., Phillips, A. B., & Heben, M. J. (2016). Pathways toward high-performance perovskite solar cells: review of recent advances in organo-metal halide perovskites for photovoltaic applications. *Journal of Photonics for Energy*, ***6***(2), 022001-022001.

Su, P., Liu, Y., Zhang, J., Chen, C., Yang, B., Zhang, C., & Zhao, X. (2020). Pb-based perovskite solar cells and the underlying pollution behind clean energy: Dynamic leaching of toxic substances from discarded perovskite solar cells. *The Journal of Physical Chemistry Letters*, ***11***(8), 2812-2817.

Sukharevska, N., Bederak, D., Goossens, V. M., Momand, J., Duim, H., Dirin, D. N., Kovalenko, M. V., Kooi, B. J., & Loi, M. A. (2021). Scalable PbS Quantum Dot Solar Cell Production by Blade Coating from Stable Inks. *ACS Applied Materials & Interfaces*, ***13***(4), 5195-5207.

Sun, H., Deng, K., Xiong, J., & Li, L. (2020). Graded bandgap perovskite with intrinsic n–p homojunction expands photon harvesting range and enables all transport layer-free perovskite solar cells. *Advanced Energy Materials*, ***10***(8), 1-9.

Sun, Y., Ma, R., Kan, Y., Liu, T., Zhou, K., Liu, P., Fang, J., Chen, Y., Ye, L., & Ma, C. (2022). Simultaneously Enhanced Efficiency and Mechanical Durability in Ternary Solar Cells Enabled by Low-Cost Incompletely Separated Fullerenes. *Macromolecular Rapid Communications*, ***43***(22), 1-7..

Tang, H., Xu, Y., Hu, X., Hu, Q., Chen, T., Jiang, W., Wang, L., & Jiang, W. (2021). Lead-Free Halide Double Perovskite Nanocrystals for Light-Emitting Applications: Strategies for Boosting Efficiency and Stability .*Advanced Science*, ***8***(7), 1-23.

Tang, Y., Zhao, Y., & Liu, H. (2022). Room-Temperature Semiconductor Gas Sensors: Challenges and Opportunities. *ACS sensors*, ***7***(12), 3582-3597.

Tao, W., Xiao, G.-J., Sun, R., Luo, L.-B., & Yi, M.-X. (2022). High efficiency ETM-free perovskite cell composed of CuSCN and increasing gradient CH3NH3PbI3. *Chinese Physics B*, ***31***(1), 1-13.

Turkevych, I., Kazaoui, S., Belich, N. A., Grishko, A. Y., Fateev, S. A., Petrov, A. A., Urano, T., Aramaki, S., Kosar, S., & Kondo, M. (2019). Strategic advantages of reactive polyiodide melts for scalable perovskite photovoltaics. *Nature Nanotechnology*, ***14***(1), 57-63.

Thakur, N., Kumar, P., Neffati, R., & Sharma, P. (2023). Design and simulation of chalcogenide perovskite BaZr (S, Se) 3 compositions for photovoltaic applications. *Physica Scripta*, *98*(6), 065921.

Tyagi, V., Rahim, N. A., Rahim, N., Jeyraj, A., & Selvaraj, L. (2013). Progress in solar PV technology: Research and achievement. *Renewable and Sustainable Energy Reviews*, ***20***(5), 443-461.

Uhl, A. R., Rajagopal, A., Clark, J. A., Murray, A., Feurer, T., Buecheler, S., Jen, A. K. Y., & Hillhouse, H. W. (2018). Solution-processed low-bandgap CuIn (S, Se) 2 absorbers for high-efficiency single-junction and monolithic chalcopyrite-perovskite tandem solar cells. *Advanced Energy Materials*, ***8***(27), 1-8.

Ullah, S., Wang, J., Yang, P., Liu, L., Li, Y., Rehman, A.-U., Yang, S.-E., Xia, T., Guo, H., & Chen, Y. (2021). Evaporation Deposition Strategies for All-Inorganic CsPb (I1–x Br x) 3 Perovskite Solar Cells: Recent Advances and Perspectives. *Solar RRL*, ***5***(8), 1-24.

Villa, F. F. (2022). Silicon Properties and Crystal Growth. In *Silicon Sensors and Actuators* :*The Feynman Roadmap*.Cham: Springer International Publishing. ***70***(50) 3-33.

Vishnuwaran, M., Ramachandran, K., Anand, D., & Ragavendran, V. (2022). Using low-cost materials for highly efficient eco-friendly formamidinium tin iodide based solar cell with copper oxide as hole transport material and titanium oxide as electron transport material with different metal contacts. *Ceramics International*, ***48***(19), 29314-29321.

Vivo, P., Salunke, J. K., & Priimagi, A. (2017). Hole-transporting materials for printable perovskite solar cells. *Materials*, ***10***(9),1-45.

Wang, H., Li, H., Cai, W., Zhang, P., Cao, S., Chen, Z., & Zang, Z. (2020). Challenges and strategies relating to device function layers and their integration toward high-performance inorganic perovskite solar cells. *Nanoscale*, ***12***(27), 14369-14404.

Wang, H. C., Bao, Z., Tsai, H. Y., Tang, A. C., & Liu, R. S. (2018). Perovskite quantum dots and their application in light-emitting diodes. *Small*, ***14***(1),1-23.

Wang, J., Zhang, J., Zhou, Y., Liu, H., Xue, Q., Li, X., Chueh, C.-C., Yip, H.-L., Zhu, Z., & Jen, A. K. Y. (2020). Highly efficient all-inorganic perovskite solar cells with suppressed non-radiative recombination by a Lewis base. *Nature Communications*, ***11***(1), 1-9.

Wang, M., Fei, C., Uddin, M. A., & Huang, J. (2022). Influence of voids on the thermal and light stability of perovskite solar cells. *Science Advances*, ***8***(38), 1-7.

Wang, M., Wang, W., Ma, B., Shen, W., Liu, L., Cao, K., Chen, S., & Huang, W. (2021). Lead-Free Perovskite Materials for Solar Cells. *Nano-Micro Letters*, ***13***(1), 1-37.

Wang, T., Xiao, G.-J., Sun, R., Luo, L.-B., & Yi, M.-X. (2022). High efficiency ETM-free perovskite cell composed of CuSCN and increasing gradient CH3NH3PbI3. *Chinese Physics B*, ***31***(1),1-13.

Wang, X., Zhang, T., Lou, Y., & Zhao, Y. (2019). All-inorganic lead-free perovskites for optoelectronic applications . *Materials Chemistry Frontiers*, ***3***(3), 365-375.

Wang, Y., Gu, S., Liu, G., Zhang, L., Liu, Z., Lin, R., Xiao, K., Luo, X., Shi, J., Du, J., Meng, F., Li, L., Liu, Z., & Tan, H. (2021). Cross-linked hole transport layers for high-efficiency perovskite tandem solar cells. *Science China Chemistry*, ***64***(11), 2025-2034.

Wang, Z., & Jiang, Y. (2021). Advances in perovskite solar cells: Film morphology control and interface engineering. *Journal of Cleaner Production*, ***317***(176), 1-28.

Wei, K., Yang, S., Wan, X., Ma, W., Wu, J., & Lei, Y. (2020). Review of silicon recovery and purification from saw silicon powder. *Jom*, ***72***(7), 2633-2647.

Weidner, D. E. (2022). Numerical modeling of the spray/spin coating of the interior of metal beverage cans: complete three-dimensional simulation. *Journal of Coatings Technology and Research*, ***19***(1), 97-109.

Werner, J., Niesen, B., & Ballif, C. (2018). Perovskite/silicon tandem solar cells: marriage of convenience or true love story?–An overview. *Advanced Materials Interfaces*, ***5***(1),1-19.

Wright, M., & Uddin, A. (2012). Organic—inorganic hybrid solar cells: A comparative review. *Solar energy materials and solar cells*, ***107***(77), 87-111.

Wu, C., Zhang, Q., Liu, Y., Luo, W., Guo, X., Huang, Z., Ting, H., Sun, W., Zhong, X., & Wei, S. (2018). The dawn of lead-free perovskite solar cell: highly stable double perovskite Cs2AgBiBr6 film. *Advanced Science*, ***5***(3),1-8.

Wu, H., Li, Z., Zhang, F., Kang, C., & Li, Y. (2022). Ionic Liquids for Efficient and Stable Perovskite Solar Cells. *Advanced Materials Interfaces*, ***9***(32), 1-25.

Xiaohui, M., Liqun, Y., Shijian, Z., Qilin, D., Cong, C., & Hongwei, S. (2020). All-inorganic perovskite solar cells: status and future. *Progress in Chemistry*, ***32***(10), 1-8.

Xu, G., Xue, R., Stuard, S. J., Ade, H., Zhang, C., Yao, J., Li, Y., & Li, Y. (2021). Reducing energy disorder of hole transport layer by charge transfer complex for high performance p–i–n perovskite solar cells. *Advanced Materials*, ***33***(13), 1-10.

Xu, M., Yu, J., Song, Y., Ran, R., Wang, W., & Shao, Z. (2020). Advances in ceramic thin films fabricated by pulsed laser deposition for intermediate-temperature solid oxide fuel cells. *Energy & Fuels*, ***34***(9), 10568-10582.

Xu, Y., Xie, L., Zhang, X., Chen, X., Qi, G.-J., Tian, Q., & Xiong, H. (2019). Pc-darts: Partial channel connections for memory-efficient architecture search. *arXiv preprint arXiv*,***19***(13), 97-109.

Yan, H., Wang, B., Yan, X., Guan, Q., Chen, H., Shu, Z., Wen, D., & Cai, Y. (2022). Efficient passivation of surface defects by lewis base in lead-free tin-based perovskite solar cells. *Materials Today Energy*, ***27***(127), 10-103.

Yan, Y., Yang, Y., Liang, M., Abdellah, M., Pullerits, T., Zheng, K., & Liang, Z. (2021). Implementing an intermittent spin-coating strategy to enable bottom-up crystallization in layered halide perovskites. *Nature Communications*, ***12***(1), 1-11.

Yang, J., Lee, J., Lee, J., & Yi, W. (2018). Suppressed interfacial charge recombination of PbS quantum dot photovoltaics by graphene incorporated into ZnO nanoparticles. *ACS applied materials & interfaces*, ***10***(30), 25311-25320.

Yang, Q., Yang, S., Xi, T., Li, H., Yi, J., & Zhong, J. (2022). Gradient doping simulation of perovskite solar cells with CH3NH3Sn1− xPbxI3 as the absorber layer. *Current Applied Physics*, ***44***(5), 55-62.

Yang, Y., Hoang, M. T., Bhardwaj, A., Wilhelm, M., Mathur, S., & Wang, H. (2022). Perovskite Solar Cells Based Self-Charging Power Packs_ Fundamentals, Applications and Challenges. *Nano Energy*, ***94***(32). 1-10.

Yang, Y., Wyatt, I., Travis, D., & Bahorsky, M. (1998). Decolorization of Dyes Using UV/H 2 O 2 Photochemical Oxidation. *Textile Chemist & Colorist*, ***30***(4)1-5.

Yao, Y., Cheng, C., Zhang, C., Hu, H., Wang, K., & De Wolf, S. (2022). Organic Hole-Transport Layers for Efficient, Stable, and Scalable Inverted Perovskite Solar Cells. *Advanced materials*, ***34***(44),1-31.

Yao, Z., Jiang, C., Wang, X., Chen, H., Wang, H., Qin, L., & Zhang, Z. (2022). Recent Developments of Quantum Dot Materials for High Speed and Ultrafast Lasers. *Nanomaterials*, ***12***(7), 1-33.

Ye, S., Sun, W., Li, Y., Yan, W., Peng, H., Bian, Z., Liu, Z., & Huang, C. (2015). CuSCN-based inverted planar perovskite solar cell with an average PCE of 15.6%. *Nano letters*, ***15***(6), 3723-3728.

Zhang, H., Kinnear, C., & Mulvaney, P. (2020). Fabrication of Single-Nanocrystal Arrays. *Advanced Materials*, ***32***(18), 1-19.

Zhang, H., Yu, Z., Zhu, C., Yang, R., Yan, B., & Jiang, G. (2023). Green or not? Environmental challenges from photovoltaic technology. *Environmental Pollution*, ***320***(128), 121-266.

Zhang, L., Wang, Z., Zhou, H., Li, X., Liu, Q., Wang, P., & Yuan, A. (2022). Synergistic Coupling of Li6.4La3Zr1.4Ta0.6O12 and Fluoroethylene Carbonate Boosts Electrochemical Performances of Poly(Ethylene Oxide)-Based All-Solid-State Lithium Batteries .*ChemElectroChem*, ***9***(17), 1-8.

Zhang, X., & Johansson, E. M. (2017). Reduction of charge recombination in PbS colloidal quantum dot solar cells at the quantum dot/ZnO interface by inserting a MgZnO buffer layer. *Journal of Materials Chemistry A*, ***5***(1), 303-310.

Zhang, X., Turiansky, M. E., & Van de Walle, C. G. (2021). All-inorganic halide perovskites as candidates for efficient solar cells. *Cell Reports Physical Science*, ***2***(10),1-11.

Zhang, Z., Zhang, Q., Wang, Q., Su, H., Fu, Y., & Xu, J. (2020). Investigation on the material removal behavior of single crystal diamond by infrared nanosecond pulsed laser ablation. *Optics & Laser Technology*, ***126****(74)*, 1-6.

Zheng, L., Xuan, Y., Wang, J., Bao, S., Liu, X., & Zhang, K. (2022). Inverted perovskite/silicon V-shaped tandem solar cells with 27.6% efficiency via self-assembled monolayer-modified nickel oxide layer. *Journal of Materials Chemistry A*, ***10***(13), 7251-7262.

Zhong, H., Li, W., Huang, Y., Cao, D., Zhang, C., Bao, H., Guo, Z., Wan, L., Zhang, X., & Zhang, X. (2022). All-Inorganic Perovskite Solar Cells with Tetrabutylammonium Acetate as the Buffer Layer between the SnO2 Electron Transport Film and CsPbI3. *ACS Applied Materials & Interfaces*, ***14***(4), 5183-5193.

Zhou, J., Huang, Q., Ding, Y., Hou, G., & Zhao, Y. (2022). Passivating contacts for high-efficiency silicon-based solar cells: From single-junction to tandem architecture. *Nano Energy*, ***92****(15)*, 1-12.

Zhou, J., Su, X., Huang, Q., Zhang, B., Yang, J., Zhao, Y., & Hou, G. (2022). Recent advancements in poly-Si/SiOx passivating contacts for high-efficiency silicon solar cells: technology review and perspectives. *Journal of Materials Chemistry A*, ***10***(4), 20147-20173.

Zhou, R., Xu, J., Luo, P., Hu, L., Pan, X., Xu, J., Jiang, Y., & Wang, L. (2021). Near-Infrared Photoactive Semiconductor Quantum Dots for Solar Cells. *Advanced Energy Materials*, ***11***(40), 1-33.

Zyoud, S. H., Zyoud, A. H., Ahmed, N. M., Prasad, A. R., Khan, S. N., Abdelkader, A. F., & Shahwan, M. (2021). Numerical modeling of high conversion efficiency FTO/ZnO/CdS/CZTS/MO thin film-based solar cells: Using SCAPS-1D software. *Crystals*, ***11***(12), 1-21.

CHAPTER THREE

NUMERICAL OPTIMIZATION OF INTERFACE ENGINEERING PARAMETERS FOR A HIGHLY EFFICIENT HTL-FREE PEROVSKITE SOLAR CELL

Abstract

The global shift towards decarbonizing energy systems has increasingly favoured renewable energy sources, particularly solar energy, known for its reliability, abundance, and sustainability. Nonetheless, photovoltaic technology encounters notable challenges in scalability, durability, and stability. These issues can be addressed through careful optimization of solar cell architecture, which can reduce production costs while improving performance and durability. This study presents a thorough investigation of a novel high-performance perovskite solar cell (PSC) that operates without a hole transport layer (HTL), showcasing the arrangement ITO/$PC_{61}BM$/$CH_3NH_3SnI_3$/Pt. The research, conducted through device simulations, focuses on enhancing Electron Transport Efficiency, metal back contacts, front contact materials, and buffer layers. Emphasis is placed on enhancing device efficiency by incorporating various buffer layers, such as cadmium sulphide (CdS), into the solar cell model. By fine-tuning the electron transport layers and adjusting the densities of perovskite acceptors and donors, improved device performance was achieved. Additionally, Mott-Schottky (MS) capacitance analysis provided valuable insights into the interface properties and charge carrier dynamics in a solar cell. Maximizing the number of back contacts is also crucial for effective charge extraction and minimizing recombination losses. Using the advanced SCAPS-1D simulation platform, the study evaluates the impact of design strategies on key photovoltaic parameters, including open-circuit voltage (V_{oc}), power conversion efficiency (PCE), short-circuit current density (J_{sc}), and fill factor (FF). The HTL-free device demonstrated impressive performance with a PCE of 38.11%, J_{sc} of 35.32 mA/cm², FF of 88.67%, and V_{oc} of 1.2168 V. This research highlights the potential of HTL-free PSCs for achieving high solar energy efficiency while reducing costs, marking a significant step in the direction of scalable solar cell modules with better performance and affordability.

3.1. Introduction

The search for high performance solar cells has recently received considerable momentum in the photovoltaic technology. In recent years, HTL-free perovskite solar cells have become a compelling area of innovation in solar cell design and production (Benjamin K. Korir *et al.*, 2021a; Zhou & Pang, 2020). This development is driven by the observation that perovskite materials possess extended diffusion lengths, allowing for efficient charge transfer and exhibiting ambipolar characteristics (Li *et al.*, 2015); as a result, they are capable of functioning efficiently as materials for transfer and separation of charges, eliminating the requirement for an HTL. Additionally, materials such as poly(3,4-ethylenedioxythiophene) polystyrene sulfonate (PEDOT) and spiro-OMeTAD, which are often used in making HTLs, are costly in perovskite solar cell production. This drives the necessity for devices that do not require HTL (Meng *et al.*, 2024; Nair *et al.*, 2020; Yan *et al.*, 2022). As a result, there has been significant progress in developing HTL-free perovskite solar cells, which do away with the requirement for a hole transport layer (Ouedraogo *et al.*, 2022a). This strategy streamlines both the design and production of devices, cuts costs, and improves the stability of perovskite solar cells. Different types of HTL-free perovskite solar cells are currently being explored, including those that use metals with low work-function like gold and silver or carbon-based alternatives with materials such as graphite or carbon nanotubes as hole-collecting electrodes (Principe *et al.*, 2022).

This study aims to enhance interface engineering techniques for Perovskite solar cells (PSCs) without HTLs to tackle issues such as stability under severe weather conditions, scalability, and cost-effectiveness. Although there have been improvements in performance metrics like PCE, a significant research void remains concerning the HTL-free PSC's durability and dependability designs. The investigation presents encouraging outcomes, but there are still uncertainties about how these devices will perform over time and in real-world circumstances. Without a comprehensive understanding of the stability and processes of degradation challenges of HTL-free PSCs, the practical feasibility and this technology's economic scalability could be at risk. Thus, this research not only offers potential for major advances in renewable energy but also underscores the role of computational techniques in revolutionizing device engineering and materials science for renewable energy solutions.

To attain peak efficiency in HTL-free perovskite solar cells, it is essential to meticulously fine-tune multiple cell components, including the ETL (Ijaz *et al.*, 2024; Qaid *et al.*, 2024). This process requires significant time and resources, increasing the intricacy of developing the device. Although HTL-free perovskite solar cells (PSCs) present an

encouraging option due to their simplified design and potential for enhanced stability, they face challenges in sustaining high efficiency, managing interface issues, and preventing degradation. Striking a balance among these factors is essential to fully realize their potential in photovoltaic technology.

Conventional solar cells made of silicon face several challenges, comprising high production expenses, limited efficiency, and cumbersome design, which hinder their broad adoption and scalability in renewable energy systems (Buonomenna, 2023; Singh *et al.*, 2024). In contrast, third-generation perovskite solar cells among them HTL-free variants, offer a compelling solution to these issues. HTL-free perovskite solar cells promise higher efficiency, lower production costs, and less complicated fabrication techniques, making them more viable for widespread adoption and commercialization. By removing the need for expensive and complex hole transport layers and their associated deposition processes, HTL-free perovskite solar cells not only improve performance but also advance the cost-effectiveness and efficiency of solar energy methods aiding their incorporation into conventional energy systems.

Interface engineering plays a crucial role in semiconductor devices. Variations in semiconductor materials' band gaps can substantially affect device performance, leading to imbalances in carrier concentrations, mobility, and current flow within the material (Choi *et al.*, 2024; Zhou *et al.*, 2023). These variations may arise from flaws or trapped conditions, which can disrupt charge carrier recombination and potentially reduce the device's lifespan. To improve device performance, several approaches can be utilized. Material engineering focuses on minimizing differences in band gaps during production, whereas strain engineering seeks to modify the band arrangement to reduce non-uniformities.

Defect engineering aims to neutralize or eliminate flaws in device materials, while managing temperature and the effects of bandgap variations by running devices at lower temperatures (Abbas *et al.*, 2024). Furthermore, refining device design and employing sophisticated characterisation methods are essential for addressing and precisely assessing band gaps not matching up.

Responding to variations between energy band diagrams in the band gap is crucial for boosting the dependability and effectiveness of semiconductor devices. By Combining temperature, strain, fault, and material engineering regulation, device design optimization, and advanced characterization techniques, it is possible to reduce the impact of band gap discrepancies and improve overall device performance. Methylammonium tin iodide ($CH_3NH_3SnI_3$), used as the perovskite light absorber layer, demonstrates a wide absorption spectrum that covers both visible and near-infrared (NIR) regions, ranging approximately from

350 nm to 900 nm (Angmo *et al.,* 2017). Its main function is to act as the main absorber of light, producing charge carriers by transforming absorbed photons into excitons.

Without a HTL, efficient hole transport from the perovskite layer to the ITO anode is crucial for device functionality. Optimizing the material's composition and thickness of the perovskite layer is necessary in order to achieve sufficient absorbance of light while preserving effective charge transport properties (Abou *et al.,* 2024; Ahamed *et al.,* 2023). Doping the perovskite with suitable elements can improve its ability to conduct, making hole extraction more efficient. Optimizing the interfaces between the perovskite and adjacent layers can boost charge collection efficiency and reduce recombination losses. Additionally, nanostructured back contacts can expand the surface area, thereby enhancing charge acquisition (Roy *et al.,* 2023).

Managing surface roughness effectively can enhance light trapping and minimize reflection, which in turn optimizes overall efficiency (Cui *et al.,* 2023). The device architecture plays a crucial role in influencing performance. Investigating tandem or multi-junction cell configurations can increase light absorption, while incorporating interlayers between the perovskite and the back contact can improve charge transport and minimize interfacial losses (Anirudh *et al.,* 2023a; Kumar *et al.,* 2023). Enhancing the manufacturing procedure using deposition methods like sputtering, evaporation, or chemical vapor deposition can create a uniform and well-tuned back contact layer. Fine-tuning annealing processes can improve crystallinity and electrical characteristics. Comprehensive electrical measurements provide insights into processes for charge extraction and transport, but stability assessments gauge long-term durability. Modelling using computation assists in predicting the performance of various back contact structures and materials, directing optimization through experimentation (Saiki & Gomes, 2024; Shen *et al.,* 2023).

It is essential to recognize that improving HTL-free perovskite solar cells' back contact typically requires iterative methods, integrating various strategies to attain maximum performance (Huang *et al.,* 2023a). A crucial part of this optimization process involves conducting systematic experiments, thoroughly analysing the results, and continuously refining the approach based on the findings. Platinum (Pt) is favoured as the back contact material in PSCs because of its stability and compatibility, especially when interfaced with layers like the HTL or other elements in the device (Chowdhury *et al.,* 2023a; Mohammad & Mahjabeen, 2023). This stability guarantees reliable and enduring performance, which is essential for the practical application of these solar cells.

Conversely, optimizing the interface between the MAI ($CH_3NH_3SnI_3$) layer and the electrodes becomes crucial for reducing recombination and enhancing charge extraction, particularly when there's not an HTL (Chang *et al.,* 2023). Addressing these challenges involves strategies like passivation of defects with halide anions such as iodide or bromide and doping with elements like Cs or Rb to adjust band gaps and improve charge transport (Shen *et al.,* 2023), regulating grain size and morphology to reduce defect sites, along with adjusting electrode work functions to enhance charge extraction and lower recombination, are key strategies. Overcoming these challenges requires sophisticated approaches to defect management, material and interface engineering, and reliable encapsulation in perovskite solar cells without HTL based on MAI. The pursuit of defect-tolerant materials, new low-temperature processing methods, and inventive apparatus designs offers potential for improving efficiency and aiding commercialization. These efforts are essential for advancing technology for solar cells based on MAI in the future.

In semiconductor technology, the idea of ideal concentrations of donors and acceptors involves adjusting the concentrations of acceptor and donor dopant atoms introduced into a substance used in semiconductors to control its electrical properties (Azhar *et al.,* 2023). These densities greatly influence the performance of semiconductor equipment such as transistors and diodes. Acceptor dopants add positively charged holes to the semiconductor, while donor dopants contribute negatively charged electrons (Klein *et al.,* 2023). Controlling the concentrations of acceptors and donors allows for precise adjustment of the number of charge carriers in the semiconductor. Optimal densities ensure that the semiconductor exhibits the intended electrical properties, including conductivity, resistivity, and carrier mobility (Hossain *et al.,* 2023). This is crucial for designing semiconductor devices with precise accomplishment characteristics. Dopant densities also affect the semiconductor's bandgap, which determines its ability to both emit and absorb light. Increasing the dopant density can boost carrier concentration, but it may also reduce carrier mobility due to increased scattering (Khan *et al.,* 2024). This balance affects the overall conductivity and speed of semiconductor devices. Moreover, achieving optimal dopant densities while managing the depth of junctions presents a significant difficulty in optimising interface engineering characteristics. Deeper junctions can increase capacitance and slow down device performance, while shallower junctions may lead to leakage currents and reliability problems (Khan *et al.,* 2024). Maintaining consistent dopant distributions across large semiconductor wafers and addressing process variations are significant challenges. Dopant densities can be sensitive to temperature changes, which affects device performance under various operating conditions. To ensure reliable electrical

characteristics despite temperature fluctuations, careful management of concentrations of dopants is essential. Maximizing concentrations of dopants also requires extra processing steps and materials, which increases manufacturing costs. Additionally, conformity with the base semiconductor material and combining it with other parts of the device needs to be considered to ensure the device's reliability and output.

Accordingly, precisely adjusting densities of dopants can greatly enhance gadget efficiency and speed by optimizing the balance between carrier concentration and mobility (Khan *et al.,* 2024). This is crucial for achieving top performance in applications such as memory components and microprocessors. Proper management of dopant concentration can reduce power usage by enhancing conductivity and limiting leakage currents. For semiconductor devices with low power, carefully engineered dopant profiles are essential for maximizing performance while conserving energy. Ideal dopant levels also enhance the dependability and durability of semiconductor electronics by decreasing degradation factors like impacts of hot carriers, electromigration, and oxide degradation (Khan *et al.,* 2024). In summary, reaching ideal densities of acceptors and donors in semiconductor materials requires carefully balancing various trade-offs and overcoming several challenges. Accurate control of dopant levels is crucial for creating semiconductor apparatuses having the necessary electrical characteristics and functionality attributes, and dependability.

The impressive functionality of the suggested cell design is credited with the careful optimization of phenomena related to interface engineering. This includes precisely tuned interfaces between layers, efficient charge transport enabled by each component, favourable energy level alignments that enhance charge gathering and separation, and possibly unique material properties or structures within the layers that are active. Furthermore, careful design elements such as thickness control, interface optimization, as well as apparatus design are crucial for maximizing the cell's photovoltaic performance. A deeper exploration of these aspects could provide valuable insights into the mechanisms behind the exceptional efficiency observed, potentially developing photovoltaic technologies with great performance. Nevertheless, this study relies on simulations of the device’s photovoltaic properties; its findings are significant and could guide experimentalists in developing a functional actual solar cell module with possibility of commercialization and scaling.

3.2. Device simulation

The SCAPS program is widely utilized for simulating the performance of solar cells, particularly in modelling various types such as both single- and multiple-junction cells under different environments (Salah *et al.,* 2024; Shakoor *et al.,* 2023). SCAPS-1D specifically

focuses on simulating the behaviour of solar cells along a single dimension, typically their depth or thickness (Samajdar, *et al.*, 2023). Engineers and scholars use this program to predict and analyse the electrical characteristics and performance parameters of solar cells. It takes into account various factors such as material characteristics, gadget design, and operational conditions like light intensity and temperature that affect solar cell efficiency.

SCAPS is a crucial software instrument for simulating the complex solar cell behaviours, particularly those that use perovskite materials. Its importance is rooted in its ability to model and examine the electrical properties of different solar panels, such as perovskite-based ones. By utilizing input parameters and equations that define cell behaviour, SCAPS enables investigators to replicate and forecast these cells' electrical properties. A deep grasp of the interactions between Poisson's equation, continuity equations, and the application of SCAPS allows researchers to enhance the functionality and appearance of perovskite solar cells.

Poisson's equation plays a vital role in semiconductor physics and the modelling of electronic devices (Masut, 2023). It clarifies the relationship in a material between its charge density and the resulting electric potential. In the context of solar cells, including those using perovskite materials, Poisson's equation is crucial for analysing the movement of charge carriers such as electrons and holes, as well as for knowing how the electric field is distributed within the semiconductor layers.

After establishing the cell structure, several factors and the cell's overall performance are determined by applying differential equations (Ahmad *et al.*, 2023). While the continuity, transport, and carrier lifespan equations are provided by 3.2, 3.3, and 3.4, the Poisson equation is written as 3.1.

$$\frac{\partial^2\varphi}{\partial^2 x} = \frac{dE}{dx} = -\frac{\rho}{\varepsilon_s} = -\frac{q}{\varepsilon_s}\left[p - n + N_D(x) - N_A(x) \pm N_{def}(x)\right] \quad (3.1)$$

$$\frac{\partial n,p}{\partial t} = \frac{1\partial J_n}{q\partial x} + (G_n - R_n) + \frac{1\partial J_p}{q\partial x} + \left(G_p - R_p\right) \quad (3.2)$$

$$J_{n,p} = nq\mu_n E + qD_n\frac{\partial n}{\partial x} + pq\mu_p E + qD_p\frac{\partial p}{\partial x} \quad (3.3)$$

$$\tau = \frac{1}{\sigma * Nt * Vth} \quad (3.4)$$

Several significant characteristics and variables are utilized to characterize the behaviour and properties of the materials involved in semiconductor physics and solar cells. where σ is the

material's electrical conductivity, Nt The number of charge carriers or the density of states Vth stands for thermal voltage, and E stands for the electric field. The letters p and q stand for the elementary charge. n represents the free electron and hole densities. Doping densities are denoted by the symbols N_A for acceptors and N_D for donors. They indicate the concentration of impurities supplied to the semiconductor to change its electrical characteristics. The charge carrier concentration gradient, shown by dn, p/dx, indicates how these carriers' concentration varies spatially within the material.

3.3. The layout of the suggested cell

The suggested solar cell structure consists of a glass substrate covered with a transparent conductive oxide (TCO), which acts as the n-type semiconductor for the ETL, a perovskite absorber layer, and a metal (Pt) back contact. Figure 3.1a illustrates the arrangement of the cell and whereas Figure 3.1b gives the energy level diagram. In a standard PSC, changes in materials and configuration can impact its exciton properties as well the band structure.

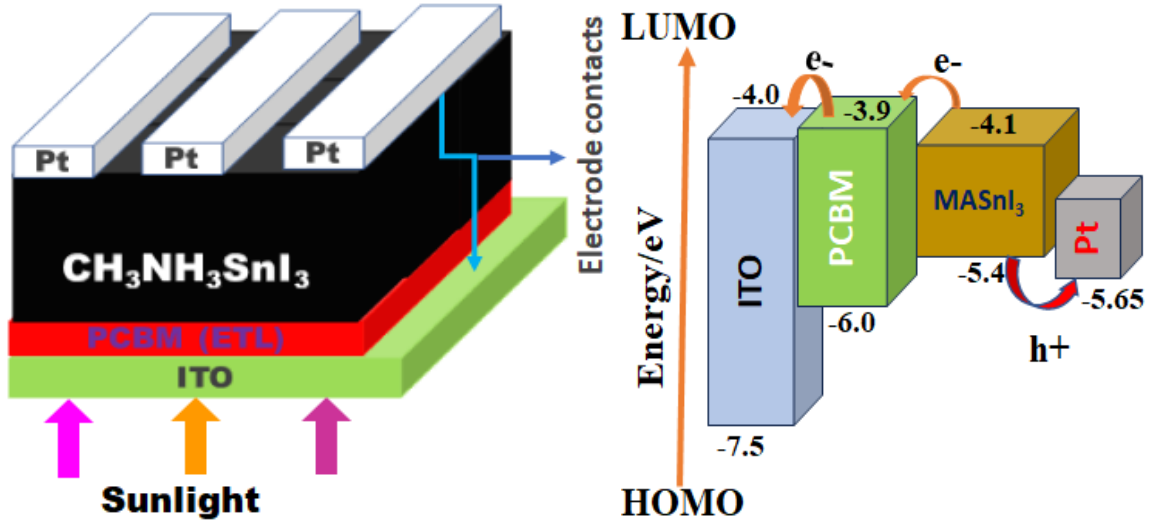

Figure 3.1: Architecture of the perovskite solar cell without HTL and its band alignment diagram

The inclusion or exclusion of layers such as the HTL considerably affects the behaviour of excitons within the device. In the model configuration, the band structure generally provides a more direct pathway for the extraction of electrons because of the close proximity of the ETL (Singh & Agarwal, 2023). As shown in Figure 3.1, ITO and PC61BM have the highest energy levels, which restrict electron and hole movement and thus help maintain their energy. The model cell's basic input parameters are listed in Table 3.1.

Platinum, chosen for its elevated work function and cost-effectiveness, accustomed to enhance functionality. Previous research indicates that performance improves with higher work

functions (Kanoun *et al.*, 2019). Indium tin oxide (ITO) is a transparent conductor with a broad bandgap of around 3.7 eV, resulting in minimal absorption of visible light (Taniguchi *et al.*, 2024). Its main role is to act as a transparent anode, allowing light to pass through to the active layer. PC61BM, an organic electron acceptor material, shows considerable ultraviolet (UV) and near-ultraviolet (NUV) absorption regions, specifically below around 500 nm (Taffelli, 2023). It is essential for capturing UV and NUV light, which helps facilitate the extraction of electrons from the perovskite layer (Chenna *et al.*, 2023). Careful selection of materials for each layer, taking into account factors such as band gaps, compatibility, charge carrier mobilities, and absorption coefficients, is essential for achieving optimal device performance and enhancing the PCE of solar cell modules.

Table 3.1: Basic input parameters of each layer

Parameters	**$CH_3NH_3SnI_3$** (Sunny *et al.*, 2021a)	**PC61BM** (Korir *et al.*, 2021)	**ITO** (Das *et al.*, 2023)
Thickness (nm)	1600	10	90
Band gap (eV)	1.3	2.1	3.5
Electron affinity (eV)	4.1	3.9	4
Dielectric permittivity	8.2	3.90	9
CB effective density of states (cm^{-3})	1.0×10^{18}	2.2×10^{19}	2.2×10^{18}
VB effective density of states (cm^{-3})	1.0×10^{18}	2.2×10^{19}	1.8×10^{19}
Electron mobility ($cm^2\ V^{-1}s^{-1}$)	1.6	0.2	20
Hole mobility ($cm^2\ V^{-1}s^{-1}$)	1.6	0.2	10
Donor concentration N_D (cm^{-3})	0	0.001	1.1×10^{21}
Acceptor concentration N_A (cm^{-3})	1.0×10^{15}	0.002	0
Defect density (cm^{-3})	1.0×10^{11}	1.0×10^{11}	N/A

In the suggested solar cell design, various strata perform crucial roles in light capture, charge carrier generation, and charge transfer. The substrate at the base is generally made of ITO, which serves as a transparent conductive electrode. ITO facilitates transmission of light while efficiently conducting electrons, thereby reducing current loss. Its combination of transparency and conductivity makes it an ideal choice with relation to the bottom electrode. PC61BM is chosen as the ETL for this device due to its thermal stability, processing simplicity, and enhanced light absorption (Hrostea *et al.*, 2018).

3.4 Results and discussion

3.4.1 The band diagram of the model cell

A band diagram shows the energy levels of charge carriers in a device in a visual manner (Meng *et al.*, 2022). With a perovskite solar cell, for example, it shows the alignment between the conduction and valence bands throughout different layers such as the ETL, perovskite absorber layer, and HTL (Manjunath *et al.*, 2022; Singh *et al.*, 2020). A perovskite solar cell without a HTL bypasses the necessity of an HTL to collect holes created by the perovskite layer's absorption of light. Rather, the holes proceed straight to a metal electrode, like silver or gold. This method simplifies the manufacturing process, reduces costs, and enhances the stability of the perovskite solar cell.

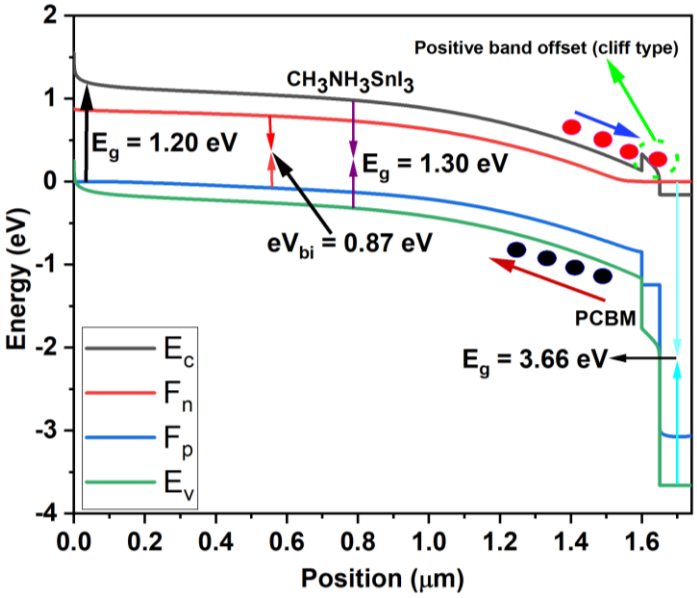

Figure 3.2: Energy band diagram of a solar cell structure without HTL

Figure 3.2 illustrates the energy levels within perovskite, metal, and ETL layers, as well as the direction of charge carrier movement. In this setup, the ETL and perovskite layers create a type-II heterojunction. Here, the conduction band of the ETL is positioned lower than that of the perovskite, promoting electron movement from the perovskite to the ETL. Conversely, the valence band of the ETL is situated higher than that of the perovskite, facilitating the transfer of holes in the reverse direction (Ouedraogo *et al.*, 2022b).

A Mott-Schottky (MS) contact exists between the perovskite and metal layers, forming a possible obstacle whose height is determined by the metal's operational mechanism and the electron affinity of the perovskite (Lin *et al.*, 2018; Luo *et al.*, 2021). Introducing dopants into the perovskite layer or incorporating a tiny layer of interlayer can lower this obstacle, thereby enhancing the holes being transferred from the perovskite to the metal electrode (Abdi-Jalebi

et al., 2019; Lin *et al.,* 2022). Additionally, the band diagram illustrates cliffs and bends at the interfaces between layers. Discontinuities represent sudden changes in energy levels, whereas gradations indicate gradual transitions. These characteristics affect the movement of charges and their recombination.

An optimal band diagram would feature no abrupt energy level changes and instead display smooth transitions, promoting effective charge separation and collection (Al-Ghiffari *et al.,* 2022). Essential mechanisms of recombination arise when the band configurations display abrupt changes at the interface. Figure 3.2 demonstrates that the band placement within the proposed solar cell varies slightly with different band positions. The diagram indicates that the energy gap decreases with increasing distance. The results indicate that the intrinsic voltage gap is roughly +1.30 eV while at 300 K, the built-in potential (V_{ib}) is +0.87 V in an equilibrium state and AM 1.5 G. The non-uniformity in the band gap may be attributed to cliffs at various interfaces within the cell structure and variations in band bending.

The layer of perovskites exhibits a slope in its energy levels and band structure changing throughout its thickness, which can be achieved through doping or varying works of art. This gradient establishes a built-in electric field that directs charge carriers towards their respective electrodes (Xu *et al.,* 2023). However, a gradual bending at the contact of the metal electrode indicates smoother changes in energy levels, which may lower the possible obstacle and improve hole injection. In Figure 3.2, the band diagram shows that $CH_3NH_3SnI_3$ and PC61BM form a heterojunction of type-II featuring valence and conduction bands positioned less than those of the perovskite layer. Nevertheless, a notable energy level discontinuity at their interface suggests potential challenges for charge transfer and an increased likelihood of recombination.

3.4.2 Absorption characteristics of the layers in the HTL-Free model cell

In PSCs without HTLs, understanding the absorption properties of the materials used is crucial for optimizing device performance. Figure 3.3 illustrates the absorption coefficient as a function of photon energy for ITO, PC61BM, and $CH_3NH_3SnI_3$ layers. The data reveal that the photoactive absorber, $CH_3NH_3SnI_3$, has a high coefficient of absorption ($>1.5\times10^5$ cm^{-1}), surpassing that of the electron transport layer, highlighting its superior absorption of light capabilities. This makes it a promising candidate for use as the perovskite material in high performance solar cells. Furthermore, ITO and PC61BM, being the ETL materials, exhibit the lowest light absorption, which allows most photons to be taken up by the layer of perovskite, maximizing the generation of hole-electron pairs.

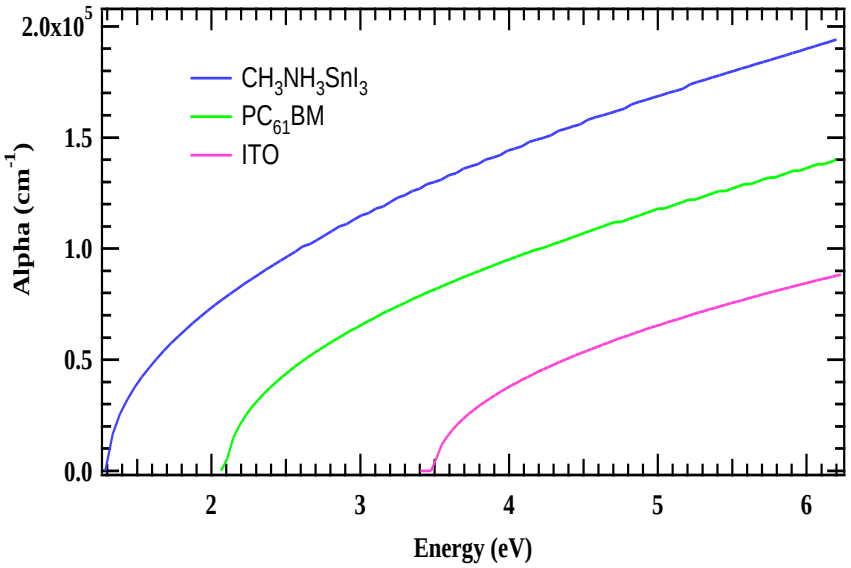

Figure 3.3: Absorption characteristics of the layers of the model solar cell

3.4.3 Mott-Schottky capacitance analysis

The MS capacitance investigation is a valuable technique for investigating the electrical properties of semiconductor electronics, especially PSCs without HTLs (Rehman *et al.*, 2023). This method provides essential insights into different parameters by examining the relationship between the measured capacitance and the applied voltage. One crucial factor revealed is the width of the depletion layer, an area near the electrode where mobile charge carriers are reduced under reverse bias conditions (Huang *et al.*, 2023b; Yu *et al.*, 2023). The width of the depletion layer has a major impact on mobility of carriers and recombination. Moreover, the doping density, which indicates the level of contaminants in the perovskite strata, is crucial for determining both conductivity and the built-in potential (Attia *et al.*, 2023).

Figure 3.4a illustrates the capacitance-voltage properties of the suggested perovskite solar cell without HTL across various temperatures. At lower temperatures, capacitance increases with rising voltage, whereas at higher temperatures, capacitance decreases as voltage increases. In contrast, Figure 3.4b displays Mott-Schottky (MS) curves at various temperatures show a decline with increasing temperature. The built-in potential (V_{ib}) at 300, 340, 360, and 400 K was measured as 0.86, 0.79, 0.75 V, and 0.70 V, respectively (cf. Figure 3.4b). This indicates that the prototype cell is able to maintain about 81% of its power at 400 K, due to its higher V_{ib} at 300 K. It is evident that V_{ib} decreases with elevated temperature.

The voltage differential between the perovskite and the electrode is represented by the built-in potential when the circuit is open, which is a critical factor for the efficiency of the device. Additionally, the defect density, which reflects the presence of trap states within the

perovskite, affects the longevity of charge carriers and the extent of non-radiative recombination (Amit Kumar *et al.*, 2023; Z. Wang *et al.*, 2023). Applying MS analysis to perovskite solar cells without HTL presents distinct challenges because of the lack of a HTL (Chowdhury *et al.*, 2023b). The primary the build-up of capacitance at the perovskite/electrode contact can mask the capacitance of the diminishing layer, especially when doping densities are low (Moseley, 2023). Thus, choosing the appropriate measurement frequency and voltage range is essential for accurately isolating the desired capacitance component.

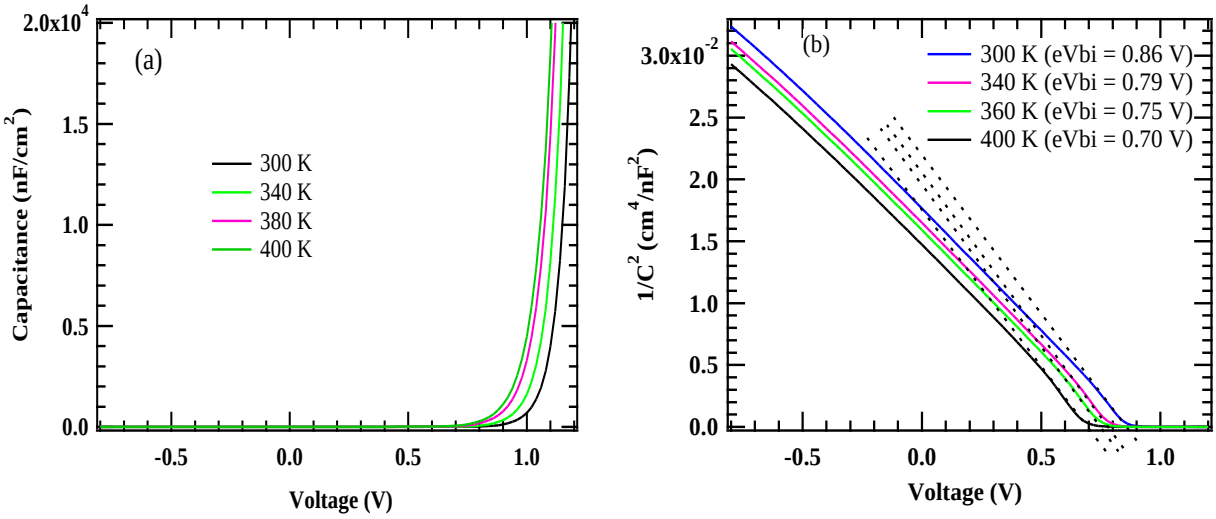

Figure 3.4: Capacitance – voltage characteristics (a) and (b) Mott-Schottky capacitance analysis

Additionally, the accuracy of the estimation of depletion may be affected low doping densities and in thin perovskite layers, which could lead to incorrect determination of parameters like doping density (Kuddus, *et al.*, 2023). Moreover, hysteresis effects often seen in perovskite solar cells, caused through procedures for trap filling and de-trapping, require the use of polarization is initiated by positive bias and slow scan speeds. In spite of these challenges, many studies have successfully employed MS analysis to obtain valuable information about HTL-free perovskite solar cells (Chowdhury *et al.*, 2023b). For example, it has played a crucial role in calculating the inherent potential, providing proof of effective extraction and separation of charge carriers. Additionally, analysing capacitance at various frequencies has revealed important information regarding the electrode/perovskite interaction, including the formation of Schottky barriers and recombination across interfaces (Li *et al.*, 2022).

Variations in voltage impact Fermi level, energy levels, and eventually the concentration of charge carriers, which in turn affects the capacitance of the solar cell. Temperature has a substantial effect on the dielectric properties of materials, leading to

increased capacitance. The Mott-Schottky analysis of how temperature affects solar cell performance is connected to equation 3.5 (Gelderman *et al.*, 2007).

$$\frac{1}{C^2} = \frac{1}{S^2.\varepsilon.\ q} \times \frac{1}{N_A} \times \left(V - V_{ib} - \frac{k_B T}{q}\right) \quad (3.5)$$

In this context, C represents capacitance, S denotes surface area, q is the elementary charge, and ε refers to space permittivity. Additionally, NA indicates V_{bi}, the acceptor density, is the flat band potential (built-in voltage), k_B is the Boltzmann constant, and T stands for temperature in Kelvins.

Analysing the relationship between measured parameters and device performance has enabled MS analysis to inform the design and optimization of HTL-free PSCs, with the goal of enhancing both efficiency and stability (Ouedraogo *et al.*, 2022b). Using MS analysis on PSCs without HTL requires careful attention to their unique structure and behaviour. When used effectively, this analysis provides crucial insights into their electrical properties, supporting the ongoing development and optimization of these innovative solar cells. Capacitance plays a key role in determining the performance of solar cells, particularly perovskite ones (Zouhair *et al.*, 2022).

3.4.4 Conductance characteristics

While perovskite solar cells with HTLs typically demonstrate superior conductance (KV *et al.*, 2023), HTL-free solar cells can show varying conductance levels depending on the materials and structures used, and may lack the optimized charge transport mechanisms found in devices with HTLs. Figure 3.5 illustrates the conductance properties of HTL-free perovskite solar cells across different voltages and temperatures. The figure reveals that conductance stays steady from 0.2 V up to 0.8 V (forward bias), after which it increases sharply. Additionally, the data shows that conductance is greater at lower temperatures but decreases as the temperature rises.

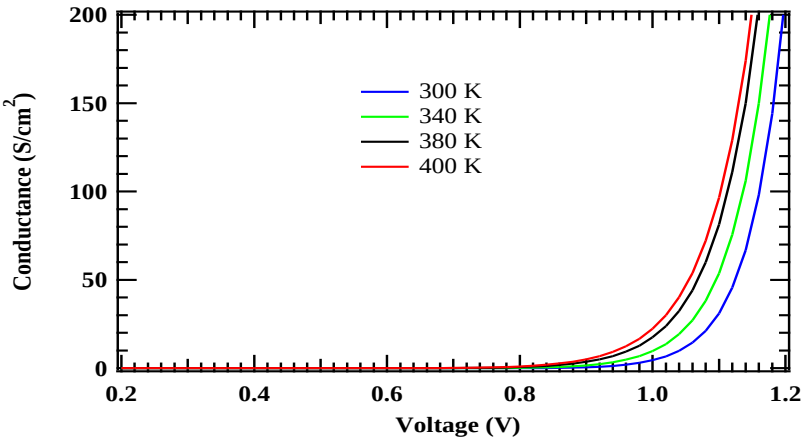

Figure 3.5: Conductance characteristics of the model HTL-Free perovskite solar cell structure

In terms Perovskite solar cells' dependability and effectiveness with HTLs generally perform better due to the enhanced charge transport provided by the HTL. On the other hand, HTL-free solar cells might be more advantageous in terms of cost and simplicity (Iqbal *et al.*, 2023) but might miss out on the enhanced charge transport mechanisms that are characteristic of HTL-incorporated configurations. Ultimately, the decision to use a solar cell without an HTL versus a perovskite solar cell with HTL integration depends regarding the particular application, budget constraints, and the coveted balance between complexity, stability, and efficiency. Every artwork offers distinct benefits and compromises, necessitating a customized strategy determined by the priorities and intended use (Bandari *et al.*, 2023; Smith *et al.*, 2023).

3.4.5 Impedance analysis

Within the field of perovskite solar cells, the charge-extracting layers play a crucial role, fundamentally influencing the device's performance. The HTL is particularly important as it facilitates the movement of positively charged holes from the perovskite layer to the electrode. This process significantly affects both the efficiency and stability of the solar cell (Zhu *et al.*, 2023). Additionally, the model cell device's impedance spectrum known as Nyquist plots, were examined. These plots, depicting the imaginary part of impedance versus the real part, are illustrated in Figure 3.6.

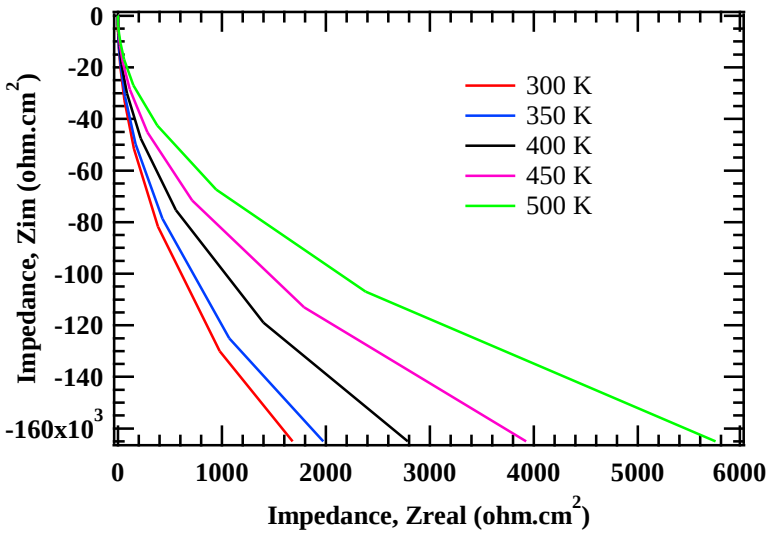

Figure 3.6: Effect of temperature on impedance characteristics

Figure 3.6 clearly shows that impedance is lower at lower temperatures but rises significantly with increasing temperature. Elevated temperatures degrade cell performance by raising impedance and enhancing exciton recombination at interfaces. Additionally, when the temperature rises, the radii of the Nyquist plots shrink due to a rise in junction resistance (Korir *et al.,* 2021b). However, the reduction in the radii of the plots with increasing temperature is minimal, indicating that the model of solar cells exhibits good tolerance for temperature. Nonetheless, the plots display characteristics of Warburg-type impedance (Aleksandrova, 2023).

3.4.6 Optimization of back contacts

Enhancing the effectiveness and performance of the back contact in HTL-free perovskite solar cells requires careful consideration of various factors. Key among these is the choice of back contact materials. Metals like gold, silver, and aluminium are potential candidates because of their compatibility with the perovskite layer and conductivity. However, their effectiveness is influenced by the composition and quality of the other layers in the cell structure (Zhang *et al.,* 2022b). To optimize the interface between the perovskite layer and the back contact, it is crucial to reduce defects and improve charge carrier extraction. This can be accomplished by applying surface treatments and incorporating passivation layers, which help minimize recombination losses and enhance the efficiency of charge extraction.

Platinum possesses little resistance, facilitating effective charge extraction from the perovskite layer (Anoop & Ahipa, 2023). This characteristic is crucial for optimizing the device's overall efficiency by reducing energy dissipation during the charge transfer process. Additionally, Pt is compatible with various layers in the solar cell structure, promoting robust

electrical connections and thus improving the device's overall performance (Yang *et al.*, 2023). However, it is important to recognize that the price of Pt can present noteworthy challenges, especially in large-scale production.

Table 3.2: Summary of Optimization Strategies for HTL-Free Solar Cells Using Different Back Contacts

Metal	Work function (eV)	V_{oc} (V)	J_{sc} (mA/cm^2)	FF (%)	PCE (%)
Pt	5.65	1.2168	35.32	88.66	38.11
Ni	5.15	0.9178	35.02	83.80	26.94
Pd	5.12	0.9034	35.00	83.57	26.43
Au	5.10	0.8899	34.99	83.38	25.96
Mo	4.6	0.3977	34.69	72.54	10.01
Fe	4.5	0.3977	34.69	72.54	10.01
Al	4.2	0.0337	33.09	30.77	0.34

Table 3.2 clearly shows that Pt is the optimal the model cell's back contact, given its excellent electrical properties. Having a 5.65 eV work function, platinum provides an ideal electron barrier height at the rear contact interface, making it possible to forgo the need for HTL in perovskite-based solar cell designs (Al Ahmed *et al.*, 2023; Noorasid *et al.*, 2023). The metal back contact Pt achieves a high- PCE of 38.11%, while silver exhibits the lowest performance with a remarkably low 0.34% PCE. Additionally, Fe and Mo show poor performance with a PCE of 10.01% each. The data in Table 3.2 highlights that the metal electrode's operational mechanism significantly affects the way a solar cell module function. However, other factors like cost, stability as well as toxicity of the metal back contacts should also be considered in the device design.

3.4.7 J-V characteristics

The J-V attribute, or current-voltage curve, depicts the relationship between the current output of a solar cell and the applied voltage (Morales & Acevedo, 2023). The J-V characteristic is a crucial measure of a solar cell's functionality, determining its power generation capability. Figure 3.7 illustrates the typical J-V curves for solar cells both with and without an HTL component, showcasing the respective execution. The curve begins at the origin, where both voltage and current are zero, and rises as the voltage increases, leading to a corresponding increase in the present till it reaches the maximum power point (MPP) (Katche *et al.*, 2023).

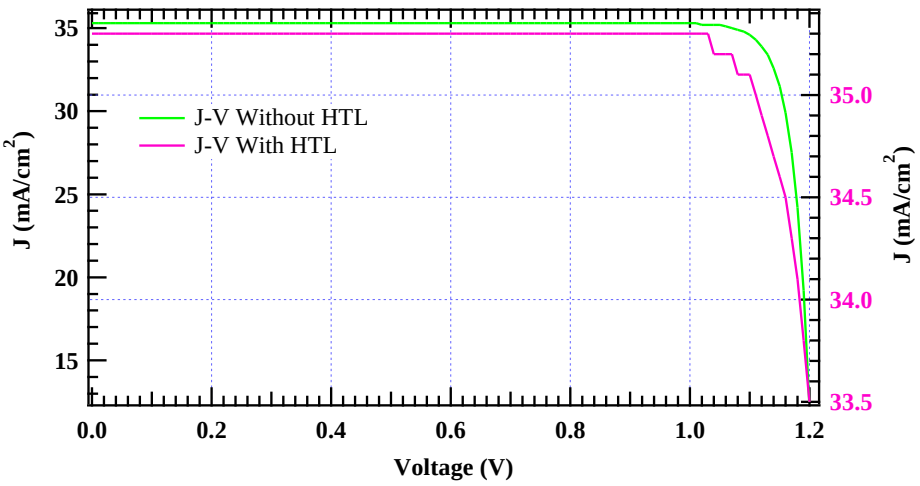

Figure 3.7: J-V characteristics of the proposed HTL-free solar cell module with and without interface

The J-V characteristic curve features the open-circuit voltage (V_{oc}), which represents the voltage at no current, indicating the peak voltage the solar cell can achieve. In Figure 3.7, the short-circuit current density (J_{sc}) is shown as the current when the voltage is zero, reflecting the highest current the cell can produce. For the proposed cell, the maximum J_{sc} is approximately 35.3 mA/cm². J_{sc} remains steady from V_{oc} = 0.0 V up to V_{oc} = 1.0 V, after which it drops to 12.1 mA/cm² at V_{oc} = 1.2 V for the device without a HTL. In contrast, for the traditional device structure with HTL, J_{sc} stays constant at 35.3 mA/cm² until it decreases to 33.3 mA/cm² at V_{oc} is equal to 1.0 V. This indicates that the conventional cell maintains higher current across the range of V_{oc}, in spite of issues like higher cost and complex fabrication. Additionally, the fill factor (FF) of the curve measures the degree of squareness, assessing whether the cell efficiently converts power across different voltages or loses potential output.

The cell's FF depicted within the graph is approximately 84%. The curve's maximum power point (MPP) indicates the point at which the cell achieves its highest power output. According to the graph, the MPP falls within the range of 0.0 V and 35.3 mA/cm². The J-V characteristics of a solar cell can be affected by various factors, including the type of cell, temperature, and the intensity of incident light. The J-V curve shown represents an HTL-free solar cell, a newer type that could possibly offer higher efficiency compared to traditional cells. However, the production process is more intricate, in spite of the potential for improved performance.

3.4.8 Quantum efficiency of the model solar cell

Attaining elevated QE is crucial for the performance of solar cells, as it immediately influences their ability to transform incoming light into a stream of electricity. An elevated QE

means that a greater percentage of incident photons is effectively converted into electrons, thereby boosting the overall power output of the cell (Jung *et al.*, 2023). This is particularly important for improving the efficiency of energy conversion of solar cells, making them more practical for real-world applications. Figure 3.8 illustrates the QE of a solar cell without an HTL and one with an HTL layer using PEDOT:PSS, demonstrating its efficiency in changing the light of different wavelengths into the current of electricity. A higher QE signifies greater effectiveness in converting electricity from light.

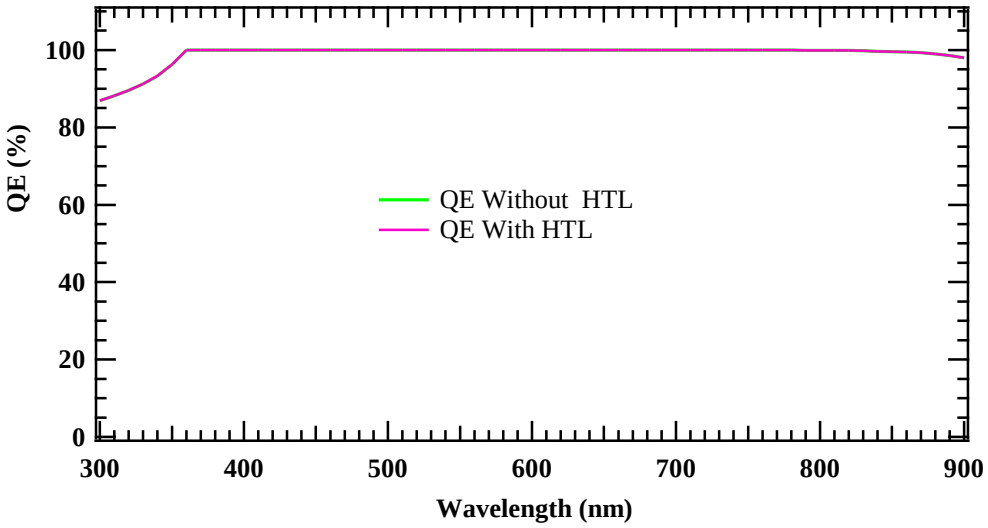

Figure 3.8: QE characteristics for the proposed cell HTL-free solar cell

Figure 3.8 reveals that both types of solar cells achieve remarkably high QE across a broad wavelength range, roughly spanning between 300 and 900 nm. This is beneficial as it indicates the cells' ability to effectively convert a wide spectrum of sunlight into electrical energy. At its peak, this particular model of solar cell achieves a QE of nearly 100%, signifying its capacity to convert up to 100% of the incident electricity from light, even when using longer wavelengths. Despite this, the HTL-free device as well as the traditional solar cell demonstrates similar QE characteristics.

Beyond 800 nm is when the QE starts to decline, indicating that the solar cell struggles to effectively absorb wavelengths of light. Despite this, the QE characteristics of the solar cell without HTL are remarkable, featuring a high QE peak and strong capability when transforming a broad range of photons in sunlight that become electricity. This highlights the possibility that these cells could be highly productive in solar energy harvesting. Numerous elements, such as the QE of a solar cell can be influenced by the material qualities, cell thickness, and fabrication quality. While QE can provide insights into the theoretical efficiency of a cell, actual efficiency is often reduced as a result of reflection and recombination losses

issues. The decrease after 800 nm in QE, longer-wavelength photons are less prevalent efficiently absorbed, can reduce the total efficiency of the solar cell by limiting its ability to capture the full sun spectrum. This drop in QE highlights the importance of engineering strategies to increase the solar cells' range of absorption. These tactics could include the use of multi-junction or tandem cell architectures, or the incorporation of spectral converters to enhance execution and expand relevance across various surrounding circumstances (Karduri & Ananth, 2023).

3.5 Influence of defect density on perovskite performance

The perovskite layer is highlighted in the solar cell without HTL specifically explores the influence the fault density. While $MASnI_3$-based perovskites offer benefits like high absorption coefficients and tunable bandgaps, their vulnerability to defects remains a considerable challenge (Shah *et al.,* 2023). MAI perovskites encounter further challenges, such as the existence at the band margins, deep trap states, which significantly hinder the capture of both electrons and holes due to their large cross-sections (Xiao *et al.,* 2023). This issue highlights the critical need for efficient hole extraction in design architectures without HTL. Additionally, the sensitivity to moisture presents a risk by perhaps increasing defect formation, which in turn exacerbates recombination losses (Abhinav Kumar *et al.,* 2023). To address these challenges, effective encapsulation techniques have become essential.

Figure 3.9a shows that as the trap density, or defect density in the perovskite material increases, the J_{sc} remains stable in between 10^{11} cm^{-3} and 10^{14} cm^{-3} but begins to decline between 10^{15} cm^{-3} and 10^{17} cm^{-3}. This decrease happens as a result of the traps capture charge carriers, stopping them in their tracks contributing to the flow of current in the solar cell. The ideal density of defects for perovskite was found between 10^{11} cm^{-3} and 10^{14} cm^{-3}, where the highest J_{sc} value was 34.84 mA/cm^2. Conversely, as shown in Figure 3.9b, the V_{oc} of the model cell shrinks as the defect density increases. This happens because defects in the perovskite material act as sites for electron and hole recombination. This recombination reduces the quantity of charge carriers that the solar cell can collect, so lowering the output's voltage and current. Higher defect density accelerates electron-hole recombination, hindering their capacity to produce current efficiently, which results in a reduced V_{oc}.

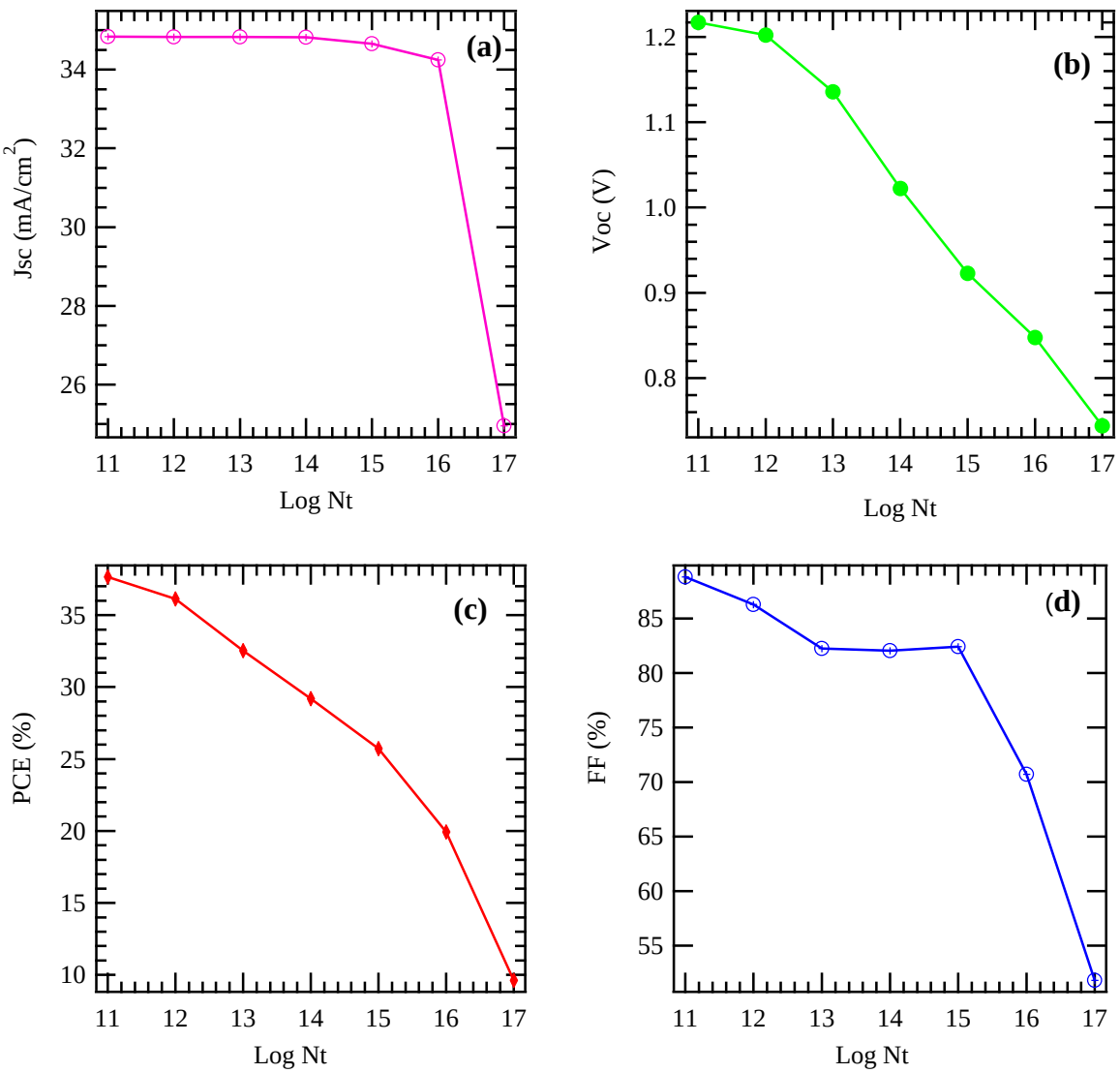

Figure 3.9: The influence of defect density of the absorber on electrical parameters of the model cell

The ideal defect density, at which the highest V_{oc} of 1.2172V was achieved, was determined to be 10^{11} cm^{-3}. Figure 3.9c clearly shows that increasing defect density from 10^{11} cm^{-3} to 10^{17} cm^{-3} causes PCE to drop. In the MAI layer, defect density promotes non-radiative recombination, which stops charge carriers in their tracks before they reach the electrodes. Additionally, it lowers the inherent capacity, resulting in a reduced V_{oc} and a decreased FF. The ideal density of defects, yielding the highest PCE (38.48%) and FF (88.79%), was found at 10^{11} cm^{-3}. Figure 3.9d illustrates a decrease in FF as defect density increases, indicating that as trap density rises, the FF diminishes. This relationship occurs because defects trap charge carriers, reducing the quantity of carriers able to add to the existing. The perovskite's ideal defect density, where the maximum FF (89.79%) was observed, is 10^{11} cm^{-3}.

3.5.1 The impact of acceptor density on the absorber

Within the perovskite solar cell, the device's execution is heavily dependent regarding the acceptor density. These elements play a key role in facilitating charge movement, especially for positive holes, which depend on the HTL to help transport them toward the electrode (Murugan *et al.*, 2022). When opting for PSCs without an HTL, it is essential to replace traditional HTL materials with alternatives. These replacements fulfil comparable roles but have different characteristics. In such configurations, the ETL frequently acts as a barrier to holes. Therefore, the density of acceptors at the perovskite layer's interaction with the ETL/HTL junction is crucial (Wang *et al.*, 2023).

A higher acceptor density in this region is advantageous as it enhances effective excision of holes and reduces recombination losses. Conversely, when an HTL is used in perovskite solar cells, the density of acceptors in this stratum plays a crucial role in facilitating hole transport (Huang *et al.*, 2022). An optimally adjusted acceptor density within the HTL guarantees efficient removal from the layer of perovskite and facilitates seamless transport of charge to the electrode (Zhang *et al.*, 2023). Achieving the right balance is crucial for optimal performance. A low acceptor density can lead to inefficient charge extraction and increased recombination rates, ultimately decreasing the efficiency of the gadget (Ding *et al.*, 2022). On the other hand, an excessively high density can lead to negative effects, like enhanced charge trapping or interface recombination.

The effect density of acceptors on perovskite solar panels varies depending on the device architecture, materials, and interfacial properties used. However, fine-tuning acceptor densities in both configurations is essential for achieving high efficiency in perovskite solar cells. Figure 3.10a provides valuable insights into the model solar cell's behaviour, highlighting a significant connection between acceptor density and J_{sc}. It shows that J_{sc} remains constant as acceptor density rises from 10^{12} cm^{-3} to 10^{16} cm^{-3}, suggesting that lower acceptor densities could enhance performance. The optimal acceptor density for achieving the highest J_{sc} is 10^{14} cm^{-3}. However, as the acceptor density continues to increase, J_{sc} decreases, reaching 32.5 mA/cm^2 at an acceptor density of 10^{19} cm^{-3}. Higher acceptor densities can lead to reduced carrier mobility within the perovskite material, causing scattering of electrons and holes and impeding their movement. This disruption affects their effective passage via the apparatus, resulting in the noted decrease in J_{sc}. Acceptor density optimal for the perovskite is 10^{17} cm^{-3}, where 34.87 mA/cm^2 is the maximum J_{sc}.

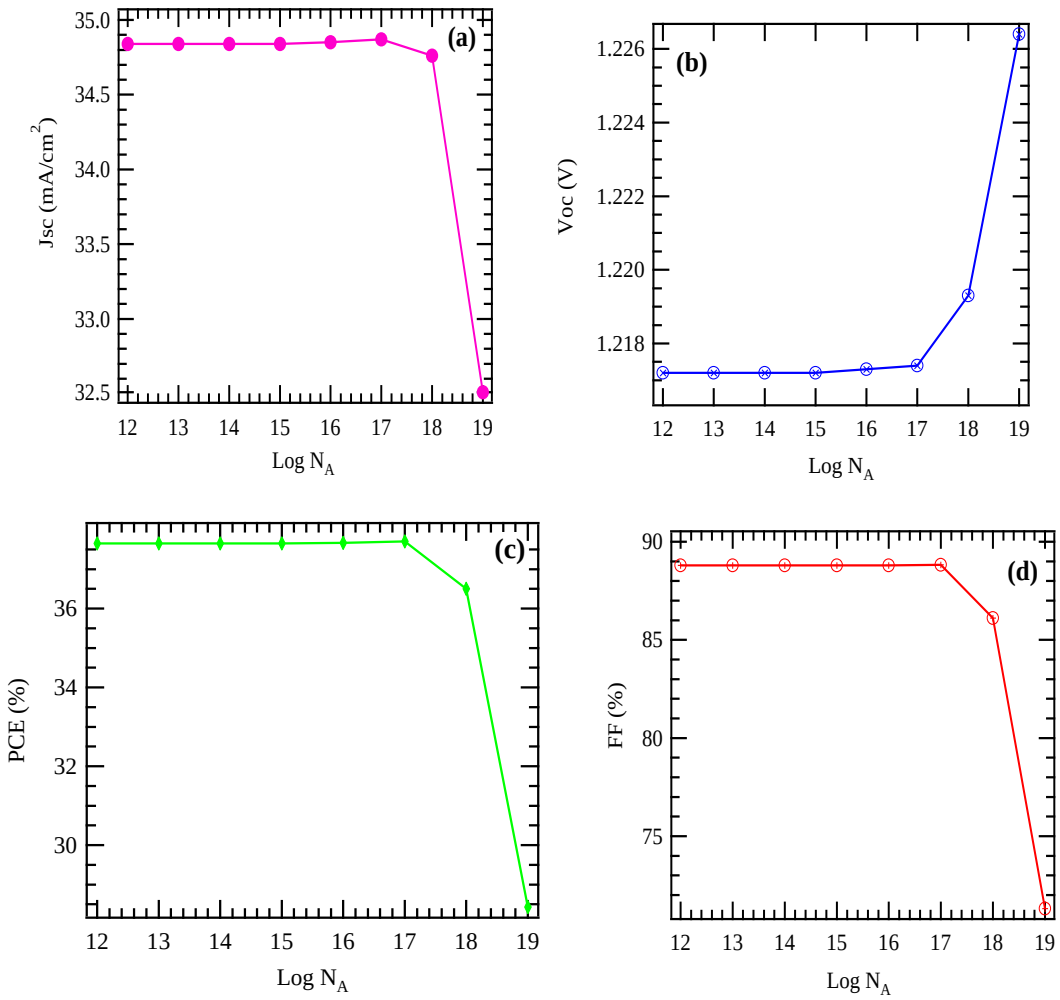

Figure 3.10: The influence of acceptor density of the absorber on electrical parameters of the model cell

Figure 3.10b shows that V_{oc} remains relatively stable as acceptor density increased from 10^{12} to 10^{16} cm^{-3}, then gradually increases, reaching the optimal value of 1.2264 V with an acceptor density of 10^{19} cm^{-3}. Figure 3.10c reveals that PCE remains fairly constant as acceptor density rises from 10^{10} to 10^{14} cm^{-3}, but then begins to decline as density increases to 10^{21} cm^{-3}. This trend can be given credit for the complex interactions between energy transmission throughout the system, charge carrier movement, and recombination rates. It is possible that defects affect charge carrier dynamics, maybe enhancing certain characteristics of the device's performance. The optimal acceptor density is between 10^{12} cm^{-3} and 10^{17} cm^{-3}, where the maximum PCE is 38.43%. Beyond this range, PCE drops precipitously to around 29.5%.

Figure 3.10d shows that the ideal density of acceptors for achieving the best FF in solar cells solar cells is approximately 10^{12} cm^{-3}, with an FF of around 88.79%. The effect of acceptor density on FF is influenced by several factors. The recombination factor, of the density of acceptors impacts the speed at which holes and electrons recombine inside the apparatus. There

will not be any if the acceptor density is too low to effectively capture electrons, leading to non-productive recombination in the perovskite layer. Conversely, a very high acceptor density at the interface of the electron transport layer and the perovskite layer causes recombination losses which also adversely affect FF. Another important consideration is shunt resistance, which measures current leakage through the solar cell outside of the intended external circuit path. Elevated resistance of shunt is beneficial for achieving a high FF. Additionally, high shunt resistance is correlated with optimal acceptor density for FF suggesting a favourable equilibrium between decreased current leakage and effective charge transport.

3.5.2 Influence of donor density

Density of electron donors describes the number of components concentrated within a material that contribute electrons (Saifina *et al.,* 2023). Within the framework of PSCs without HTLs, this term in particular refers to the level of doping within the ETL (Chowdhury *et al.*, 2023b). Increasing the donor density involves adding more electrons to the ETL, which affects its electronic properties as well as conductivity. In PSCs without HTLs, raising the donor density has multiple important effects. It can enhance electron extraction from the electrode to the perovskite layer, possibly boosting the PCE as well as the J_{SC}. However, too much doping may lead due to recombination losses that are not radiative, and which could negate the benefits gained.

Moreover, donor density influences the built-in potential at the interface between the perovskite layer and the ETL, which in turn affects the V_{oc} (Guo *et al.*, 2022). Adjusting the doping level is essential for fine-tuning the built-in potential, which enhances the efficiency of charge separation and collection (Zhang *et al.,* 2022a). However, doping presents its own set of challenges. It can introduce defect states at the interface, which may promote charge carrier recombination and potentially hinder device performance (Nowsherwan *et al.,* 2023). Therefore, choosing the appropriate dopant, controlling the doping level, and employing engineering of important interfaces are crucial to minimizing these negative effects (Zhao *et al.*,2022). Figure 3.11 illustrates how varying donor density affects HTL-free solar cells with different thicknesses. The results show that the ideal density of donors is 10^{19} cm^{-3}, achieving a PCE of 37.98% and a strong fill factor (FF) of 89.31%. The simulation was performed with the density of acceptors of the perovskite material held unchanging at 0.00 cm^{-3}.

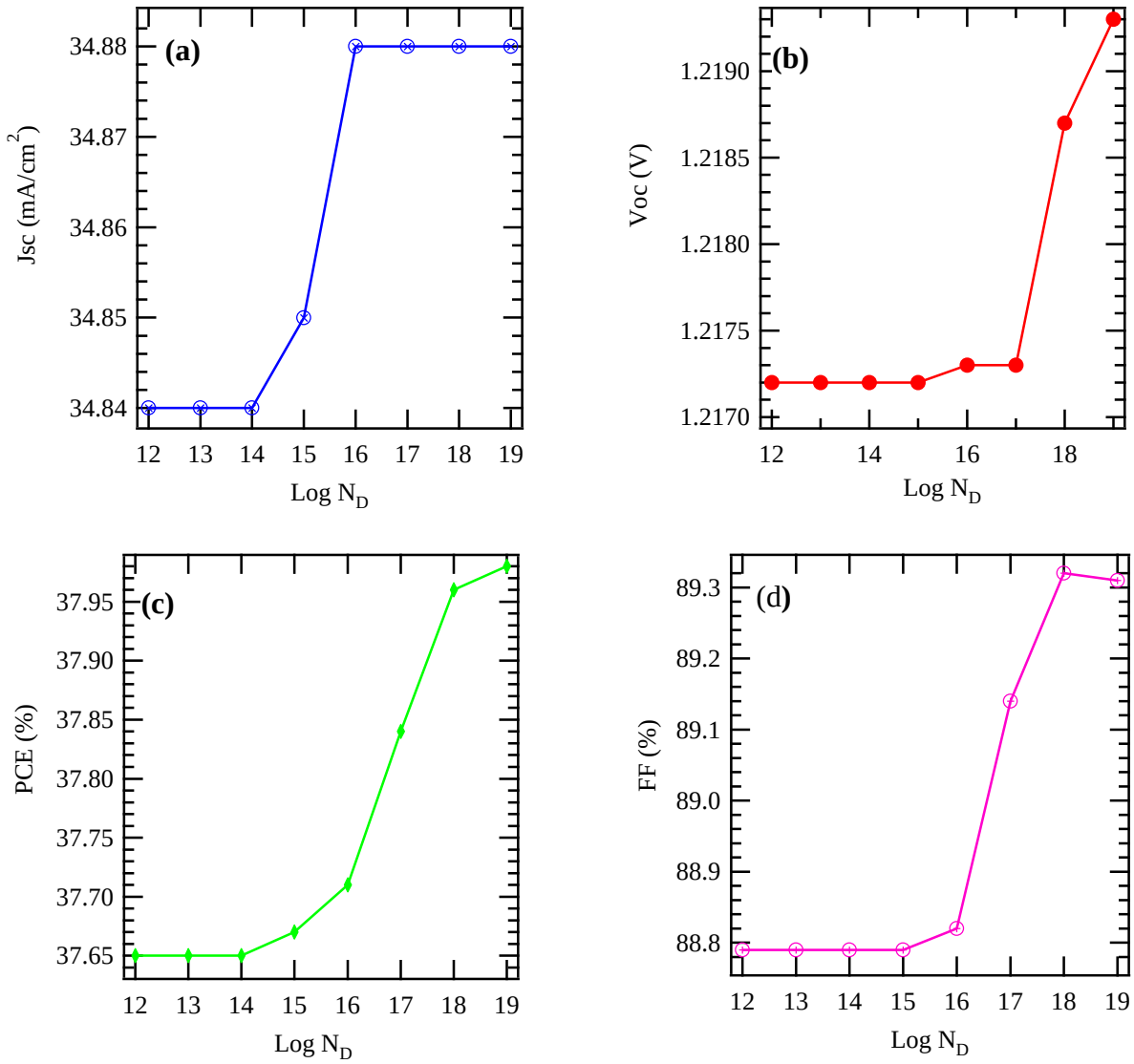

Figure 3.11: The effect of the absorber's donor density on the electrical characteristics of the model cell

In Figure 3.11a, it is observed that the J_{sc} stays relatively stable before rising as the donor density increases. The perovskite reaches its peak J_{sc} of 34.88 mA/cm² at a donor density of 10^{19}cm^{-3}. Figure 3.11b illustrates that the V_{oc} slightly decreases with increasing donor density, indicating that higher donor densities could improve the V_{oc} of this specific perovskite material. The ideal density of donors for achieving the highest V_{oc} of 1.2193 V is also 10^{19} cm^{-3}. Figure 3.11c demonstrates the relationship between the perovskite's donor density and PCE. An increase in donor density initially boosts PCE, suggesting that a higher donor concentration enhances the efficiency of the solar cell. However, PCE starts to decrease once donor density exceeds a certain level. The highest PCE of 37.98% is achieved at a donor density of 10^{19}cm^{-3}. Finally, Figure 3.11d shows the effect of donor density on the FF of the perovskite model

cell. At first, the FF does not change but increases with higher donor density. The ideal donor density for the maximum FF of 89.32% is 10^{18} cm^{-3}.

3.6 Device optimization at interfaces

The tactics presented encompass a range of elements, from choosing materials to refining fabrication methods, all geared towards enhancing interface quality, conductivity, and transparency of the device. By improving these characteristics, the device achieves more efficient charge extraction, minimized recombination losses, and greater defence of the delicate perovskite layer. Additionally, incorporating advanced techniques like nano-structuring or using alternative materials such as graphene offers opportunities to boost performance while tackling challenges such as flexibility and stability (Al-Fartoos *et al.*, 2023; Li *et al.*, 2023). In summary, this thorough approach emphasizes the intricate and interdisciplinary efforts required to optimize HTL-free perovskite solar cells' interfacial layers. It illustrates the necessity of integrating multiple scientific fields to make significant progress in solar cell technology. The fundamental criteria of entry for optimizing the interface within the model cell are detailed in Table 3.3.

Table 3.3: The parameters for the suggested interface and front contact configuration

	CdS (Mamta *et al.*, 2021)	**ZnO** (Mamta *et al.*, 2021**)**	**ZnSe** (Salah *et al.*, 2019)	**TiO_2** (Tiwari & Belwal, 2024**)**	**AZO** (Yadav & Kumar, 2022**)**	**FTO** (Deswal *et al.*, 2024; Tiwari & Belwal, 2024**)**	**ITO** (Das *et al.*, 2023)
Thickness (nm)	2500	200	50	100	40	50	90
Bandgap (eV)	2.4	3.3	2.81	3.2	3.37	3.5	3.5
Electron affinity (Ev)	4.2	4.4	4.09	4.0	4.4	4.0	4
Dielectric permittivity (relative)	10	9	8.6	9.0	9	9.0	9
CB effective density of states	2.2×10^{18}	2.2×10^{18}	2.2×10^{18}	1×10^{19}	$1.\times10^{19}$	9.2×10^{18}	2.2×10^{18}
VB effective density of states.	1.8×10^{19}	1.8×10^{19}	1.9×10^{19}	1×10^{19}	$1.\times10^{19}$	$1.\times10^{19}$	1.8×10^{19}
Electron mobility (cm^2/Vs)	100	100	400	2.0	100	2×10^{1}	20
Hole mobility (cm^2/Vs)	25	25	110	1.0	25	1×10^{1}	10
Donor density	1.0×10^{17}	1.0×10^{18}	1.0×10^{21}	1×10^{16}	1×10^{14}	1×10^{19}	1.0×10^{21}
Acceptor density (cm^{-3})	0.0	0.0	0.0	0	0	0	0
Defect density (cm^{-3})			1.0×10^{14}	0	1.0×10^{14}	0	0

3.6.1 Optimization of different ETL materials

ETLs are essential for facilitating the extraction and the transfer of the perovskite layer's electrons to the electrode, greatly influencing the total efficiency of solar cells (Manjunath *et al.,* 2022). When exploring the improvement of HTL-free perovskite solar cells using ETL materials, multiple key factors must be considered. Firstly, material selection is of paramount importance. Various compounds, metal oxides, such as tin oxide (SnO_2), zinc oxide (ZnO), and titanium dioxide (TiO_2), are widely utilized due to their excellent electron mobility and stability (Gouthaman & Thomas, 2023). Another important consideration is the perovskite layer's and the ETL's energy band alignment. Matching the energy levels of both the perovskite layer and the ETL are necessary for efficient charge extraction. In order to improve adherence and maximize the transmission of charge at the perovskite layer/ETL contact, interface engineering methods such as surface treatments or the incorporation of interlayers are utilized (Zhang *et al.,* 2022).

Furthermore, the efficiency of charge extraction is greatly influenced by the ETL's ideal thickness and morphology (Elnaggar *et al.,* 2023). Changes in these factors directly affect the solar cell's performance and stability. Methods designed to enhance electron flow inside the ETL, including doping or adding specific substances, are investigated to improve electron transport characteristics (Abidin *et al.,* 2023; Du *et al.,* 2023). For commercial success, it is crucial that ETL materials demonstrate long-term stability and durability across various environmental conditions. To evaluate the characteristics and functionality of ETL materials inside the solar cell architecture, a range of characterization methods, such as Impedance spectroscopy, scanning electron microscopy, and X-ray diffraction (XRD) are utilized (Rasheed *et al.,* 2023).

Figure 3.12a shows the impact of optimizing different ETLs in an HTL-free model solar cell, with varying Voc values. ZnO proves to be the most effective ETL, achieving the highest V_{oc} of 2.7219V, while WO_3 has the least amount of V_{oc} at 1.2162V. Figure 3.12b details the ETL materials' optimization in HTL-free solar cells, indicating different J_{sc} values. WO_3 stands out with the highest J_{sc} of 35.33 mA/cm², in contrast, ZnO has the J_{sc} lowest at 35.07 mA/cm². Figure 3.12c highlights the results of optimizing different ETL materials, showing varied FF values. PC61BM and TiO_2 are identified as the most effective ETLs, providing the ideal FF being 88.66%, while at 10.97%, ZnO has the lowest FF. Lastly, Figure 3.12d presents the optimization outcomes for ETL materials, revealing different PCE values. PC61BM emerges as the best ETL with ZnO has the lowest PCE at 10.47%, whereas ideal PCE is 38.11%.

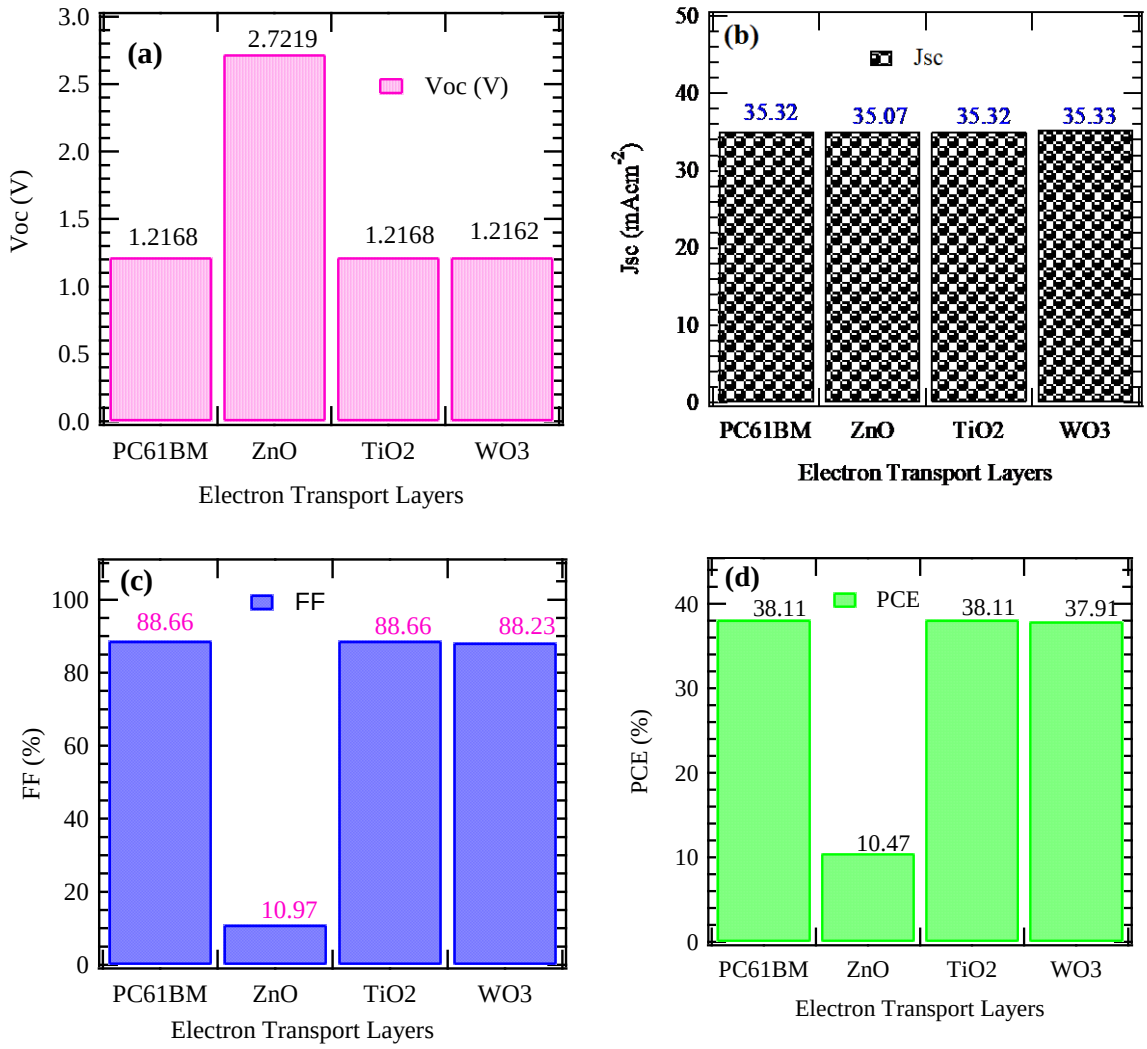

Figure 3.12: The effect of optimizing the ETL on the electrical characteristics of the model cell structure

Recent progress in materials for ETL and methods for perovskite solar cells without HTL has shown promising improvements. Nonetheless, challenges remain, such as issues related to toxicity of the material, scalability, and consistency throughout the fabrication process (Chowdhury *et al.*, 2023b). Optimizing ETL materials involves a multidisciplinary strategy that includes examining gadget construction, material qualities, and functionality assessment. This field represents a dynamic area of current research focused on improving the efficiency, stability, and commercial viability of perovskite solar cells (Bansal *et al.*, 2023; Chowdhury *et al.*, 2023b).

Figure 3.12 illustrates that the features of photovoltaic such as V_{oc}, J_{sc}, FF, and PCE of gadgets using different ETL resources such as $PC_{61}BM$, ZnO, TiO_2, and WO_3 vary due to the distinct characteristics of these substances and their effects on gadget performance. The V_{oc} is

primarily determined by how well the energy levels align between the ETL and the photoactive layer. PC61BM and TiO_2 show similar V_{oc} values, suggesting they have similar degree of energy alignments utilizing the layer of photoactivity. WO_3 also has a similar V_{oc}, indicating a close energy level alignment, though minor differences might originate from variations in the electronic architecture. Zinc Oxide, however, has a significantly greater V_{oc}, suggesting a dissimilar energy level correspondence with the photoactive layer that results in a higher V_{oc}. The J_{sc} depends on how well light is absorbed and how efficiently charge carriers are generated inside the layer that is active. PC61BM, WO_3, and TiO_2 have similar J_{sc} values, indicating similar light absorption and charge carrier generation efficiencies. Conversely, ZnO shows a slightly lower J_{sc}, which may be due to reduced comparison of the efficiency of light absorption or charge carrier generation to the other ETLs tested.

The fill factor reflects the quality of a device in terms of charge carrier retrieval and minimizing losses. High FF values in PC61BM, WO_3, and TiO_2 indicate effective charge carrier collection and minimal losses in the system. In contrast, ZnO shows a much reduced FF, suggesting increased power losses, likely due to less efficient charge carrier retrieval or higher recombination rates. The PCE is a comprehensive FF, J_{sc}, and V_{oc} all have an impact on this device performance parameter. PC61BM and TiO_2 achieve the highest PCE values, thanks to their high V_{oc}, J_{sc}, and FF. WO_3 has a little lower PCE, which may be because of slightly lower V_{oc} and J_{sc} compared to PC61BM and TiO_2. ZnO has the lowest PCE, mainly because of its much lower FF, even though its V_{oc} and J_{sc} are similar to those of other ETLs. Overall, the differences in solar properties across different devices with many ETL resources result from changes in the device's losses, light absorption, charge carrier generation and collecting efficiency, and energy level alignment. Thus, PC61BM emerges as the most effective ETL content in this.

3.6.2 Optimization of various front contacts for the HTL-free model cell

Boosting the effectiveness as well as stability of perovskite solar cells free of HTL is largely contingent upon refining the front point of contact inside the apparatus (Ma *et al.*, 2022a). This contact is essential for efficient charge extraction, minimizing losses, and protecting the perovskite layer. Optimization techniques often use materials like indium tin oxide (ITO) and fluorine-doped tin oxide (FTO) because of their excellent conductivity and transparency (Habis *et al.*, 2022).

TCOs, including FTO and ITO, as well as newer alternatives, provide both electrical conductivity and optical transparency, facilitating efficient light transmission (Zhang *et al.*, 2023). Enhancing the deposition techniques, adjusting thickness, as well as optimizing surface

modification can increase both the conductivity and transparency of these materials, leading to better light transmission and more effective charge extraction (Subudhi & Punetha, 2023). Modifying the interaction forming the front contact and perovskite layer is essential. Methods for instance, surface passivation employing interfacial layers like PEDOT:PSS, or surface functionalization are effective in minimizing defects, improving charge extraction, and increasing device stability (Mohammad & Mahjabeen, 2023).

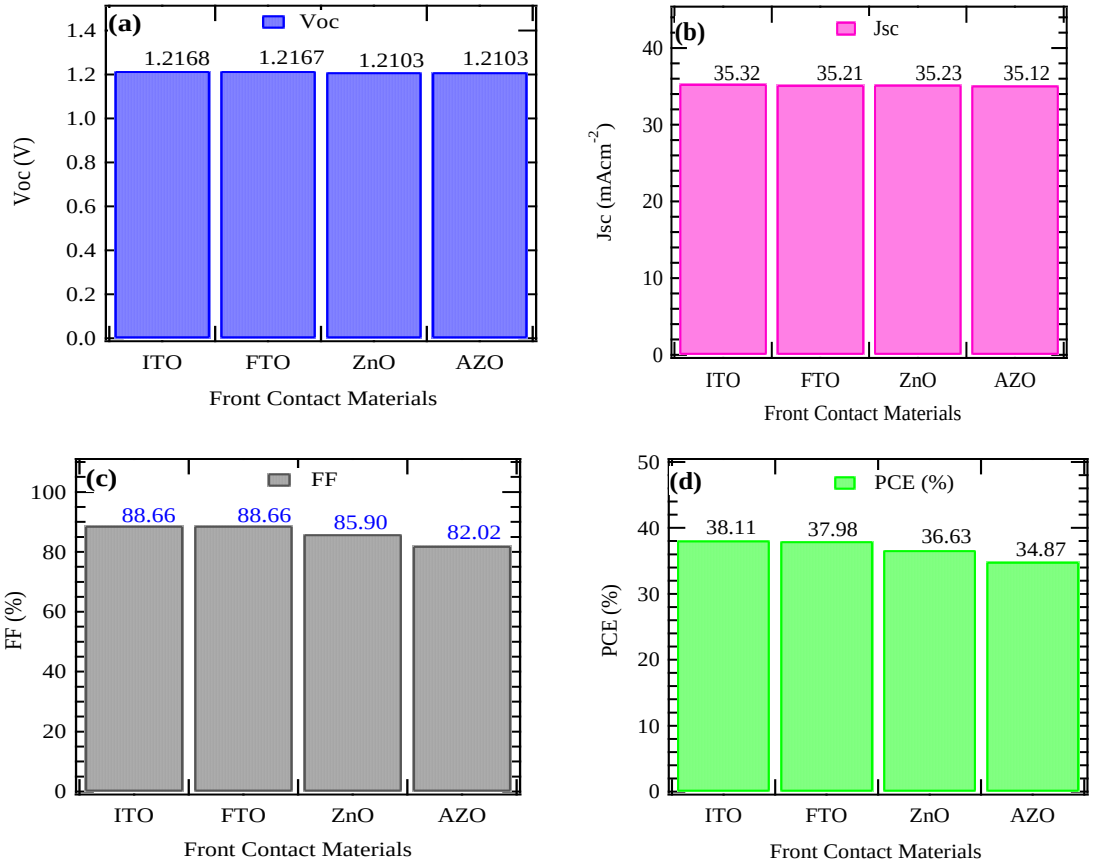

Figure 3.13: Improving various front contact materials on HTL-free solar cell

Utilizing surfaces that are rough or nanostructured on the front touch increases the surface area in use, thereby improving light absorption and trapping inside the gadget. This can be achieved through techniques such as nanoimprint lithography or nanoparticle deposition (Capitaine *et al.*, 2023). Investigating materials like Carbon nanotubes or graphene for front contacts might offer enhanced conductivity, flexibility, and stability, all as though preserving transparency (Sayem *et al.*, 2022).

Figure 3.13 compares the effectiveness of various front contact materials within the proposed device structure. The V_{oc} values shown in Figure 3.13a are similar across all materials, varying from about 1.2103 V to 1.2168 V, suggesting that the material selected for

the front contact has little effect on Voc. Likewise, the J_{sc} values in Figure 3.13b are also quite consistent, varying from 35.12 to 35.32 mA/cm², indicating that the front contact material does not have a significant impact on J_{sc}. However, Figure 3.13c reveals some variation in the FF, which measures the effectiveness of the solar cell in producing power from sunlight. ITO shows the greatest FF of 88.66%, while AZO has the lowest at 82.02%, indicating variations in how effectively the materials reduce losses within the solar cell. In terms of PCE, depicted in Figure 3.13d, values range from 34.87% to 38.11%, with ITO-based cells achieving the highest efficiency and AZO-based cells the lowest. Overall, while V_{oc} and J_{sc} remain fairly constant variances in FF and PCE across various front contact materials highlight the significant impact of material choice on solar cell performance, with ITO proving to be the most effective. This underscores the importance of selecting the right material to enhance gadget effectiveness.

Applying light-trapping or anti-reflection coatings to the front contact minimizes loss of reflection and improves light absorption, thereby increasing the overall efficiency of the cell (Wang *et al.,* 2023). Maintaining the front contact's resistance to environmental elements such as oxygen and moisture is essential for ensuring long-term stability (Ma *et al.,* 2022b). Encapsulation techniques protect the entire device, including the front contact, from deterioration. Using computational tools and simulations helps forecast the outcome of various materials and structures in front contact, guiding their optimization. Additionally, refining the fabrication process, including deposition techniques and post-treatment procedures, plays a crucial role in enhancing the quality and properties of the front contact (Wang *et al.,* 2023). Each of these approaches combines engineering, physics of devices, and material science to meet the performance standards for HTL-free PSCs. Therefore, In HTL-free PSCs, maximizing the front contact is crucial as it directly influences the devices' effectiveness and dependability. This enhancement requires a comprehensive strategy that explores device physics, engineering, and material science.

3.6.3 Effect of buffer layers on device performance

Enhanced transport of electrons can lead to better photo-carrier gathering, resulting in improved device performance metrics (Al-Mousoi *et al.,* 2022). It can minimize recombination and enhance transport charges. Figure 3.14 displays the effects of using ZnSe, TiO_2, and CdS buffers on a PSC with PEDOT: PSS acting as the HTL. The PCEs for all three buffers were similar, around 40.22%. However, while the PCE was high with these buffers, the FF dropped significantly to about 51%. This differs from the data in Figure 3.13, where the FF remained high at approximately 88.6%, and the PCE was about 38.11%. In general, the choice of buffer did not substantially affect the cell’s electrical performance.

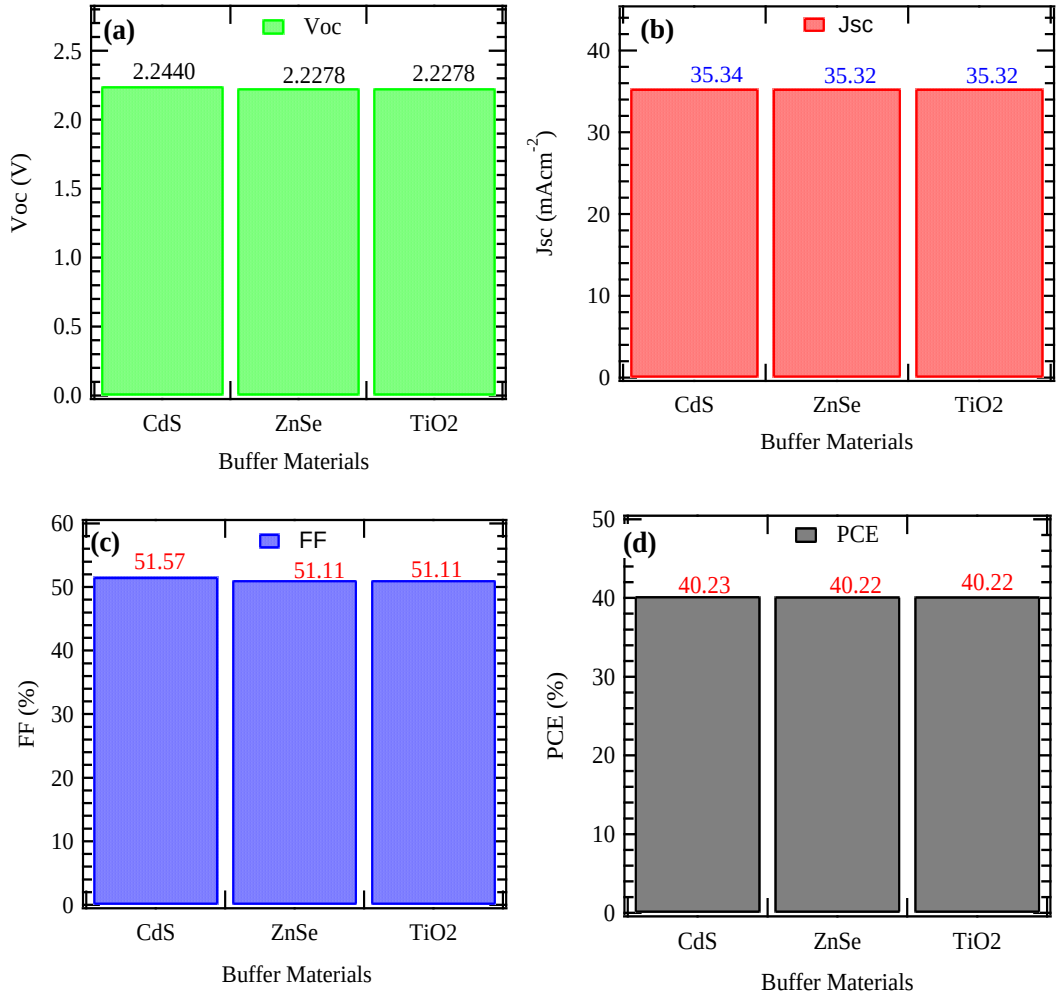

Figure 3.14: Effect of the buffer layer on a complete perovskite solar cell featuring a PEDOT: PSS hole transport layer

The data shown in Figure 3.14 indicate that PEDOT: PSS serving in the HTL produce similar outcomes throughout a range of performance measurements. Figure 3.14a reveals that the V_{oc} values are alike for these materials, demonstrating their effectiveness in promoting charge isolation as well as reducing recombination at the perovskite/HTL interface. Likewise, Figure 3.14b shows comparable J_{sc} for ZnSe, TiO_2, and CdS, reflecting similar capabilities in light absorption and electron injection into the perovskite layer. The FF, as illustrated in Figure 3.14c, remains stable across the tested materials, indicating effective transfer and collecting of charges with low resistive losses. Additionally, Figure 3.14d shows that the PCE of solar cells with these buffer layers is almost identical, suggesting consistent improvements in device functionality. These findings imply that ZnSe, TiO_2, and CdS are effective in enhancing the performance of perovskite solar cells when used with PEDOT: PSS HTL. The choice of buffer materials may be influenced by elements like manufacturing simplicity, cost, and compatibility

with additional layers. Reducing losses and maximizing charge extraction can greatly boost the total efficiency of the cell. The introduction of a buffer layer aims to improve transfer charge, lessen recombination, and enhance stability; however, its effectiveness may vary depending on the HTL used (Lin *et al.*, 2022; Y. Zhang *et al.*, 2022), leading to varying impacts on the dynamics of charge injection and extraction.

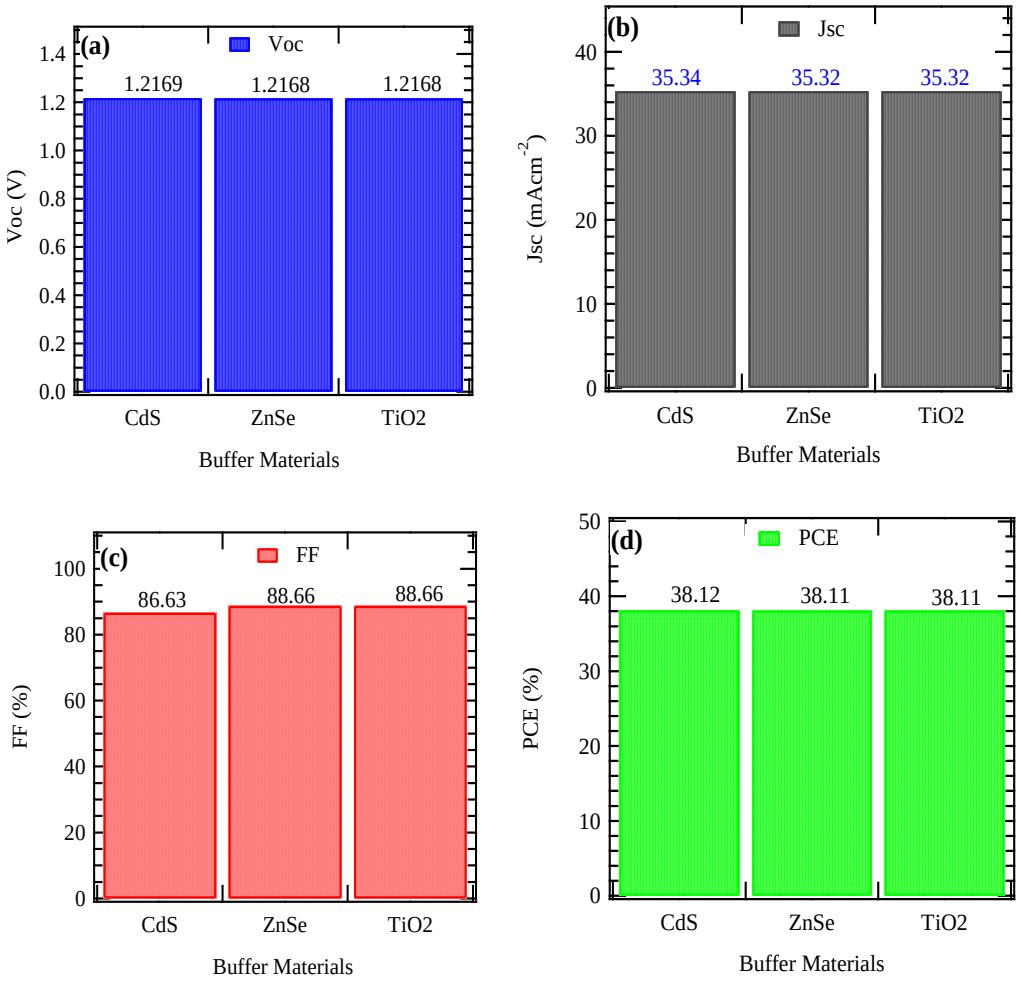

Figure 3.15: Effect of buffer materials on perovskite solar cells without a hole transport layer

Figure 3.15 shows the effect of the buffer layers of CdS, ZnSe, and TiO_2 on the performance of the perovskite solar cell without HTL. These layers of buffers are vital for improving electron extraction, reducing recombination, and enhancing the overall efficiency of the device. The performance metrics, comprising PCE, FF, J_{sc}, and V_{oc}, are comparable across CdS, ZnSe, and TiO_2, as depicted in Figures 3.15a, b, c, and d, suggesting comparable efficiency in charge separation, light absorption, as well as energy conversion. This implies that decision among ZnSe, TiO_2, and CdS for buffer materials are guided by factors such as cost, accessibility, and suitability with processing. However, TiO_2 shows reduced FF values than CdS and ZnSe, indicating potential challenges in reducing energy loss in the gadget.

Consequently, CdS and ZnSe, nevertheless are encouraging choices for perovskite solar cells without HTL, TiO_2 might be less efficient.

In general, the results emphasize that CdS, ZnSe, and TiO_2 buffers perform similarly, allowing for flexible material selection to optimize device performance. The PCEs achieved with these buffers in the solar cells without HTL include nearly identical, suggesting that the choice of buffer does not significantly affect the electrical properties of the solar cell. The device structure for evaluating these buffer layers seen in the model cell without HTL is shown in Figure 3.16.

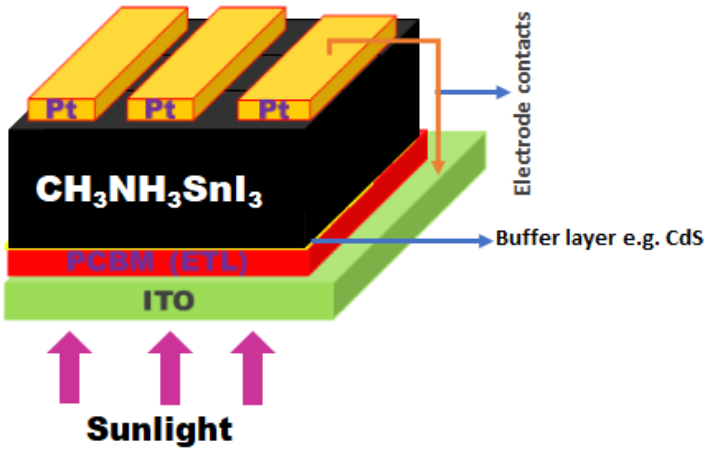

Figure 3.16: HTL-free cell architecture incorporating a buffer layer

The hole transport layer plays a vital role in solar cells made of organic materials by facilitating efficient transport of charges. When evaluating the impact of including buffer layers in solar cells with and without HTLs, several important factors need to be considered. Adding a buffer layer improves charge extraction, reduces charge recombination between surfaces, and enhances the stability of the device. Metal substrates like CdS or ZnSe are frequently used as buffer layers to improve electron transport and lower barriers to charge carrier extraction (Anirudh Kumar *et al.*, 2023b). Thus, buffer layers can modify interface energy levels by decreasing energy losses from charge recombination, which may impact the V_{oc} (Ouedraogo *et al.*, 2022b).

3.8 Comparative study

This study compares the HTL-free devices' performance with modules of experimental perovskite solar cells based on tin documented shown in Table 3.4. The results reveal variations in cell layouts between experimental as well as simulated data. The proposed solar cell model demonstrates superior electrical parameters, achieving a PCE of 38.11%, exceeding the S-Q threshold. This achievement represents a significant advancement in solar cell technology,

suggesting enhanced possibility of converting energy efficiency. However, as indicated in Table 4, the performance of tin-based PSCs remains relatively low. To improve performance, both theoretical and experimental approaches need further development. The subpar performance of the experimentally fabricated tin-based devices may be due to their limited stability when exposed to harsh environmental conditions such as moisture, light, and heat.

Table 3.4: Instances of a perovskite solar cell without HTL configurations and the corresponding PCEs

Device structure	**Type**	**J_{sc} (mA/cm^2)**	**V_{oc} (V)**	**FF (%)**	**PCE (%)**	**Ref.**
ITO/SnO_2/$MAPbI_3$/carbon	Expt.	22.77	1.02	0.61	14.17	(Iqbal *et al.,* 2023)
ITO/SnO_2/ ZnO/Perovskite/carbon	Expt.	23.26	1.12	62.96	16.39	(Wei *et al.,* 2023)
FTO/TiO_2/Cs_x $(FA_{0.4}MA_{0.6})_{1-x}PbI_{2.8}Br_{0.2}$/C	Simul.	22.54	1.13	79.75	20.43	(Raza *et al.,* 2022)
ITO/PEDOT:PSS/ $MA_{0.8}HA_{0.2}SnI_3$/PCBM /Al	Exp.	0.38	14.1	49	2.6	(Tsarev *et al.,* 2018)
ITO/PEDOT:PSS/$MASnI_3$/C_{60}/Ag	Exp.	0.45	11.82	0.4	2.14	(Fujihara *et al.,* 2017)
FTO/ZnO/WS_2/$CH_3NH_3PbI_3$/Au	Simul.	24.60	1.20	26.25	26.25	(Chakraborty *et al.,* 2022)
FTO/TiO_2/$CH_3NH_3SnI_3$/Ni/glass.	Simul.	31.93	0.98	84.34	26.33	(Sunny *et al.,* 2021b)
FTO/TiO_2/$CH_3NH_3SnI_3$/Ni/glass.	Simul.	31.93	0.98	84.34	26.33	(Sunny *et al.,* 2021b)
FTO/TiO_2-Li-TiO_2/perovskite/Au	Simul.	22.265	1.387	85.53	26.72	(Danladi *et al.,* 2023)
ITO/PC61BM/$CH_3NH_3SnI_3$/Pt	Simul.	35.32	1.2168	88.66	38.11	This study

The cell configuration ITO/PC61BM/$CH_3NH_3SnI_3$/Pt (from this study) exhibits more efficiency in comparison to other gadgets. HTLs can occasionally erect obstacles that hinder

the effective passage of holes from the electrode to the perovskite layer. Within the suggested design, the direct interaction between the layer of perovskite and the Pt electrode may improve hole transport effectiveness, thereby enhancing overall current generation. Additionally, both ITO and PC61BM have beneficial bandgaps and energy level alignments for effective charge extraction. High work function ITO and appropriate bandgap support efficient injection of holes from the layer of perovskites to the electrode, while PC61BM low efficiency of work and suitable bandgap facilitate effective electron extraction from the perovskite layer to the electrode.

The exceptional PCE attained by the suggested cell's simulation marks a notable advance in performance of photovoltaic devices. However, practical implementation requires additional validation from experiments prior to these results can be applied in actual life settings. While simulations provide valuable theoretical insights into potential high-performance designs, experimental studies yield concrete results, though they may not capture all the details. Despite the promising simulation results, it's crucial to evaluate the viability in practice of translating these configurations into real-world applications. Key factors such as scalability, cost-effectiveness, long-term stability, and manufacturability must be thoroughly assessed before these configurations can be deemed suitable for use in commercial manufacturing.

3.7 Conclusions

This document has shed light on how various parameters related to interface engineering, including front and back contact, and buffer layer incorporation can be optimized in solar cells devoid of HTL to enhance device performance. The best performance for the proposed cell was achieved with platinum as the back contact and indium tin oxide (ITO) as the front contact, resulting in electrical outputs of J_{sc} (35.32 mA/cm²), PCE (38.11%), FF (88.67%), and V_{oc} (1.2168 V). The full cell, incorporating PEDOT:PSS as the HTL, showed impressive results but with a reduced FF. For this configuration, the optimal performance was PCE (40.22%), J_{sc} (35.32 mA/cm²), FF (51.11%), and V_{oc} (2.277 V). Mott-Schottky capacitance investigation provided insights into charge carrier depletion zones and trap densities, which helped refine perovskite/ETL interface. The analysis by MS indicated a Vib of 0.86 V at 300 K, decreasing to 0.70 V at 400 K. At this elevated temperature, the model cell retained about 81% of its power, demonstrating strong high-temperature tolerance. The Vib value from the MS plots was consistent with the band diagram of the PSC without HTL at 300 K (+0.87 V). The ideal density of acceptors was 10^{14} cm^{-3}, leading to a PCE of 38.43%, while the optimal donor density was 10^{19} cm^{-3}, resulting in a PCE of 38.56%. The addition of various

buffers like ZnS, TiO_2, and CdS did not significantly affect the HTL-free solar cell's electrical specifications. Removing the HTL from PSCs simplifies the manufacturing process, potentially reducing production costs and enhancing the feasibility of large-scale production. Thus, this study highlights HTL-free PSCs' promise for high-performance and streamlined solar cells. Nevertheless, based on simulations, the findings are promising and could guide experimentalists in developing scalable and commercially viable solar cell modules.

REFERENCES

Abbas, W., Ibrahim, M. S., Waseem, M., Lu, C., Lee, H. H., Fazal, S., Loo, K., & Pramanick, A. (2024). Defect and texture engineering of relaxor thin films for High-Power energy storage applications. *Chemical Engineering Journal*, ***482***(15), 1-19..

Abdi-Jalebi, M., Ibrahim Dar, M., Senanayak, S. P., Sadhanala, A., Andaji-Garmaroudi, Z., Pazos-Outón, L. M., Richter, J. M., Pearson, A. J., Sirringhaus, H., & Grätzel, M. (2019). Charge extraction via graded doping of hole transport layers gives highly luminescent and stable metal halide perovskite devices. *Science Advances.*, ***5***(2), 1-9.

Abidin, N. A. Z., Arith, F., Noorasid, N. S., Sarkawi, H., Mustafa, A. N., Safie, N., Shah, A. M., Azam, M., Chelvanathan, P., & Amin, N. (2023). Dopant engineering for ZnO electron transport layer towards efficient perovskite solar cells. *RSC Advances.*, ***13***(48), 33797-33819.

Abou, B. C., Kokora, A. F., Meledje, D., Aka, B., & Soucase, B. M. (2024). Optimization of Tin-Doped Hybrid Perovskite Solar Cells. *Open Journal of Applied Sciences*, ***14***(3), 687-706.

Ahamed, T., Rahaman, I., Karmakar, S., Halim, M. A., & Sarkar, P. K. (2023). Thickness optimization and the effect of different hole transport materials on methylammonium tin iodide ($CH_3NH_3SnI_3$)-based perovskite solar cell. *Emergent Mater.*, ***6***(1), 175-183.

Al-Fartoos, M. M. R., Roy, A., Mallick, T. K., & Tahir, A. A. (2023). Advancing Thermoelectric Materials: A Comprehensive Review Exploring the Significance of One-Dimensional Nano Structuring. *Nanomaterials*, ***13***(13), 2011.

Al-Ghiffari, A. D., Ludin, N. A., Davies, M. L., Yunus, R. M., & Suait, M. S. (2022). Systematic review of molybdenum disulfide for solar cell applications: Properties, mechanism and application. *Mater. Today Commun.*, ***32***(2022), 104078-104083.

Al-Mousoi, A. K., Mohammed, M. K., Pandey, R., Madan, J., Dastan, D., Ravi, G., & Sakthivel, P. (2022). Simulation and analysis of lead-free perovskite solar cells incorporating cerium oxide as electron transporting layer. *RSC Advances.*, ***12***(50), 32365.-

Al Ahmed, S. R., Rahaman, M., Sunny, A., Rahman, S., Islam, M. S., Taha, T. A. E.-M., Alrowaili, Z., & Mian, M. S. (2023). Enhancing the efficiency of Cu_2Te thin-film solar cell with WS_2 buffer layer: A simulation study. *Opt. Laser Technol.*, ***159***(2023), 1-42.

Aleksandrova, M. P. (2023). Study of lead-free perovskite photoconverting structures by impedance spectroscopy. *Energy*, ***273***(15),1-7.

Angmo, D., Gao, M., & Vak, D. (2017). Organic-Inorganic Hybrid Perovskite Solar Cells with Scalable and Roll-to-Roll Compatible Printing/Coating Processes. *Printable Solar Cells*, ***44***(32), 313-362.

Anoop, K., & Ahipa, T. (2023). Recent advancements in the hole transporting layers of perovskite solar cells. *Sol. Energy*, ***263***(2023*)*,1-37.

Attia, A., Fatima, M., Khan, M., Hussain, S., Seliem, A. F., Mohammed, A. Y., & Ibrahim, M. M. (2023). Revolutionizing perovskite solar cells: Enhancing current density through Zr doping in $MAPbBr_3$ to engineer shifted band gap edges near the electron transport layer. *Optical Materials.*, ***145***(2023), 1-7.

Azhar, M., Nowsherwan, G. A., Iqbal, M. A., Ikram, S., Butt, A. F., Khan, M., Ahmad, N., Hussain, S. S., Raza, M. A., & Choi, J. R. (2023). Morphological, photoluminescence, and electrical measurements of rare-earth metal-doped cadmium sulfide thin films. *ACS omega*, ***8***(39), 36321-36332.

Bandari, R., Moallemi, E. A., Szetey, K., Flanagan-Smith, C., Hadjikakou, M., Marcos-Martinez, R., Kharrazi, A., Trogrlić, R. Š., & Bryan, B. A. (2023). Participatory Modeling for Analyzing Interactions Between High-Priority Sustainable Development Goals to Promote Local Sustainability. *Earth's Future*, ***11***(12), 1-22.

Bansal, N. K., Mishra, S., Dixit, H., Porwal, S., Singh, P., & Singh, T. (2023). Machine learning in perovskite solar cells: Recent developments and future perspectives. *Energy Technol.*, ***11***(12), 1-28.

Buonomenna, M. G. (2023). Inorganic thin-film solar cells: challenges at the terawatt-scale. *Symmetry*, ***15***(9), 1718.

Capitaine, A., Bochet-Modaresialam, M., Poungsripong, P., Badie, C., Heresanu, V., Margeat, O., Santinacci, L., Grosso, D., Garnett, E., & Sciacca, B. (2023). Nanoparticle Imprint Lithography: From Nanoscale Metrology to Printable Metallic Grids. *ACS nano*. ***17***(10), 9361–9373.

Chakraborty, D., Somay, S., & Pandey, S. K. (2022). Numerical analysis of a novel HTL-free perovskite solar cell with gradient doping and a WS_2 interlayer. *Micro and Nanostructures*, ***163****(*2023*),* 1-14.

Chang, X., Zhong, J.-X., Yang, G., Tan, Y., Gong, L., Ni, X., Ji, Y., Li, Y., Zhang, G., & Zheng, Y. (2023). Targeted passivation and optimized interfacial carrier dynamics improving the efficiency and stability of hole transport layer-free narrow-bandgap perovskite solar cells. *Science Bulletin.* ***68***(12), 1271-1282.

Chenna, P., Gandi, S., Pookatt, S., & Parne, S. R. (2023). Perovskite white light emitting diodes: A review. *Mater. Today Electron*, ***36***(5), 271-282.

Choi, A. R., Lim, D. H., Shin, S.-Y., Kang, H. J., Kim, D., Kim, J.-Y., Ahn, Y., Ryu, S. W., & Oh, I.-K. (2024). Review of Material Properties of Oxide Semiconductor Thin Films Grown by Atomic Layer Deposition for Next-Generation 3D Dynamic Random-Access Memory Devices. *Chemistry of Materials*, ***68***(12), 194–2219.

Chowdhury, T. A., Zafar, M. A. B., Islam, M. S.-U., Shahinuzzaman, M., Islam, M. A., & Khandaker, M. U. (2023b). Stability of perovskite solar cells: issues and prospects. *RSC advances*, ***13***(3), 1787-1810.

Cui, Z., Wei, L., Hao, X., Li, S., Zhang, W., Xu, B., Li, Y., & Li, W. (2023). Controllable fabrication and adjustment of optical anti-reflectance micro-nano structures on NiTi alloy surface made by nanosecond laser circular scanning. *Opt. Laser Technol.*. ***163***(32), 1-37.

Danladi, E., Jubu, P. R., Tighezza, A. M., Hossain, I., Tasie, N. N., Abdulmalik, M. O., Egbugha, A. C., Awoji, M. O., Kashif, M., & Onoja, E. D. (2023). Highly efficient, hole transport layer (HTL)-free perovskite solar cell based on lithium-doped electron transport layer by device simulation. *Emergent Materials*, ***6***(6), 1779-1795.

Das, T., Rana, N. K., & Guchhait, A. (2023). Structural optimization of inverted $CsPbI_2Br$ perovskite solar cells for enhanced performance via SCAPS-1D simulation. *Physica Scripta.* **98** (2023) 1-28

de Castro Saiki, L. E., & Gomes, G. F. (2024). Understanding and mitigating delamination in composite materials: A comprehensive review. *Mechanics of Advanced Materials and Structures*, ***17***(18), 1-21.

Deswal, V., Kaushik, S., Kundara, R., & Baghel, S. (2024). Numerical simulation of highly efficient Cs2AgInBr6-based double perovskite solar cell using SCAPS 1-D. *Materials Science and Engineering: B*, ***299***(2024), 1-41.

Ding, C., Wang, D., Liu, D., Li, H., Li, Y., Hayase, S., Sogabe, T., Masuda, T., Zhou, Y., & Yao, Y. (2022). Over 15% Efficiency PbS Quantum-Dot Solar Cells by Synergistic Effects of Three Interface Engineering: Reducing Nonradiative Recombination and Balancing Charge Carrier Extraction. *Advaneced Energy Materials*, ***12***(35), 1-16.

Du, B., He, K., Tian, G., Che, X., & Song, L. (2023). Robust electron transport layer of SnO_2 for efficient perovskite solar cells: Recent advances and perspectives. *Journal of Materials Chemistry.C.* ***11***(2023), 13625-13646

Elnaggar, M. M., Mumyatov, A. V., Emelianov, N. A., Gutsev, L. G., Ozerova, V. V., Fedyanin, I. V., Nelyubina, Y. V., Troyanov, S. I., Ramachandran, B. R., & Troshin, P. A. (2023). What defines the perovskite solar cell efficiency and stability: fullerene-based ETL structure or film morphology? *Sustain. Energy Fuels.*, ***7***(16), 3893-3901.

Fujihara, T., Terakawa, S., Matsushima, T., Qin, C., Yahiro, M., & Adachi, C. (2017). Fabrication of high coverage MASnI 3 perovskite films for stable, planar heterojunction solar cells. *Journal of Materials Chemistry C*, ***5***(5), 1121-1127.

Gelderman, K., Lee, L., & Donne, S. W. (2007). Flat-Band Potential of a Semiconductor: Using the Mott–Schottky Equation. *Chem. Educ.*, ***84***(4), 1-4.

Gouthaman, S., & Thomas, K. J. (2023). Metal Oxide Nanostructures as an Electron Transport Layer for Dye-Sensitized Solar Cells. In *Optical Properties of Metal Oxide Nanostructures* . Springer. ***89***(26), 223-262.

Guo, Z., Jena, A. K., Kim, G. M., & Miyasaka, T. (2022). The high open-circuit voltage of perovskite solar cells: a review. *Energy & Environmental Science*. ***15*****(**2022), 3171-3222

Habis, C., Zaraket, J., & Aillerie, M. (2022). Transparent Conductive Oxides. Part I. General Review of Structural, Electrical and Optical Properties of TCOs Related to the Growth Techniques, Materials and Dopants. *Defect and Diffusion Forum*, ***417***(67), 243-256.

Hossain, M. K., Toki, G. I., Kuddus, A., Rubel, M., Hossain, M., Bencherif, H., Rahman, M. F., Islam, M. R., & Mushtaq, M. (2023). An extensive study on multiple ETL and HTL layers to design and simulation of high-performance lead-free $CsSnCl_3$-based perovskite solar cells. *Sci. Rep.*, ***13***(1), 1-24.

Hossain, M. K., Toki, G. I., Samajdar, D., Mushtaq, M., Rubel, M., Pandey, R., Madan, J., Mohammed, M. K., Islam, M. R., & Rahman, M. F. (2023). Deep Insights into the Coupled Optoelectronic and Photovoltaic Analysis of Lead-Free CsSnI3 Perovskite-Based Solar Cell Using DFT Calculations and SCAPS-1D Simulations. *ACS Omega*. ***8***(25) 22466−22485

Hossain, N., Mobarak, M. H., Mimona, M. A., Islam, M. A., Hossain, A., Zohur, F. T., & Chowdhury, M. A. (2023). Advances and significances of nanoparticles in semiconductor applications–A review. *Results Eng.* ***19***(2023) 1-17 .

Hrostea, L., Girtan, M., Mallet, R., & Leontie, L. (2018). Optical and morphological properties of P3HT and P3HT: PCBM thin films used in photovoltaic applications. *IOP Conference Series: Materials Science and Engineering.*, ***374***(1), 1-17.

Huang, J., Wang, H., Jia, C., Tang, Y., Yang, H., Chen, C., Gou, K., Zhou, Y., Zhang, D., & Liu, S. (2023a). Advances in crystallization regulation and defect suppression strategies for all-inorganic $CsPbX_3$ perovskite solar cells. *Progress in Materials Science. **141***(45), 23973-23981.

Huang, J., Wang, H., Jia, C., Tang, Y., Yang, H., Chen, C., Gou, K., Zhou, Y., Zhang, D., & Liu, S. (2023b). Advances in Crystallization Regulation and Defect Suppression Strategies for All-inorganic CsPbX3 Perovskite Solar Cells. *Progress in Materials Science*, ***145***(2024), 1-6.

Huang, Q., Jing, J., Zhang, K., Chen, Y., Song, A., Liu, Z., & Huang, F. (2022). Simultaneous improvement of efficiency and stability of inverted organic solar cell via composite hole transport layer. *Journal of Materials Chemistry A.*, ***10***(45), 23973-23981.

Ijaz, S., Raza, E., Ahmad, Z., Mehmood, H., Zubair, M., Mehmood, M. Q., & Massoud, Y. (2024). A numerical approach to optimize the performance of HTL-free carbon electrode-based perovskite solar cells using organic ETLs. *Heliyon*. ***10***(7), 1-19

Iqbal, S., Yin, X., Wang, B., Zhang, J., Nisar, M. Z., Zhang, J., & Que, W. (2023). Fully Printed HTL-Free $MAPbI_3$ perovskite solar cells with carbon electrodes. *Coatings*, ***13***(8), 1338-1343.

Jung, S.-K., Park, N.-G., & Lee, J.-W. (2023). Light management in perovskite solar cells. *Mater. Today Energy*, ***37***(296), 338-343.

. Kanoun, A.-A., Kanoun, M. B., Merad, A. E., & Goumri-Said, S. J. S. E. (2019). Toward development of high-performance perovskite solar cells based on $CH_3NH_3GeI_3$ using computational approach. *Sol. Energy*, ***182***(23), 237-244.

Karduri, R. K. R., & Ananth, C. (2023). Advancements in photovoltaic materials for sustainable energy generation. *IJARET*, ***7***(1), 2456-5717.

Katche, M. L., Makokha, A. B., Zachary, S. O., & Adaramola, M. S. (2023). A comprehensive review of maximum power point tracking (mppt) techniques used in solar pv systems. *Energies*, ***16***(5), 1-23.

Khan, A. H. H., Ullah, H., Li, L., Basit, A., Boughanbour, K., Khan, S., & Khan, A. D. (2024). Exploring the efficiency and transparency in toxic and non-toxic perovskite solar cells by using SCAPS-1D. *Optoelectron. Reports*, ***1***(1) 1-20.

Klein, A., Albe, K., Bein, N., Clemens, O., Creutz, K. A., Erhart, P., Frericks, M., Ghorbani, E., Hofmann, J. P., & Huang, B. (2023). The Fermi energy as common parameter to describe charge compensation mechanisms: A path to Fermi level engineering of oxide electroceramics. *J. Electroceramics*, ***51***(3), 147-177.

Korir, B. K., Kibet, J. K., & Ngari, S. M. (2021a). Computational simulation of a highly efficient hole transport-free dye-sensitized solar cell based on titanium oxide (TiO_2) and zinc oxysulfide (ZnOS) electron transport layers. *J. Electron. Mater.*, ***50***(12), 7259-7274.

Korir, B. K., Kibet, J. K., & Ngari, S. M. (2021b). Computational Simulation of a Highly Efficient Hole Transport-Free Dye-Sensitized Solar Cell Based on Titanium Oxide (TiO2) and Zinc Oxysulfide (ZnOS) Electron Transport Layers. *Journal of Electronic Materials*, ***50***(12), 7259-7274.

Korir, B. K., Kibet, J. K., & Ngari, S. M. (2021). Simulated performance of a novel solid-state dye-sensitized solar cell based on phenyl-C61-butyric acid methyl ester (PC61BM) electron transport layer. *Optical and Quantum Electronics*, ***53***(7), 368-375.

Kumar, A., Ganesan, H., Saini, V., Almujibah, H., Petrounias, P., Jeyan, J. M. L., Sharma, S., & Agrawal, A. (2023). An assessment of photovoltaic module degradation for life expectancy: A comprehensive review. *Engineering Failure Analysis.* ***156***(23), 1-7.

Kumar, A., Gupta, S. K., Dhamaniya, B. P., Pathak, S. K., & Karak, S. (2023). Understanding the origin of defect states, their nature, and effects on metal halide perovskite solar cells. *Mater. Today Energy*, ***37***(960), 7259-7274.

Kumar, A., Kumar, D., Jain, N., Kumar, M., Ghodake, G., Kumar, S., Sharma, R. K., Holovsky, J., Saji, V. S., & Sharma, S. K. (2023a). Enhanced efficiency and stability of electron transport layer in perovskite tandem solar cells: Challenges and future perspectives. *Sol. Energy*, ***266***(2023) 1-44.

Kumar, P., Thokala, S., Singh, S. P., & Singh, R. (2023). Research progress and challenges in extending the infra-red absorption of perovskite tandem solar cells. *Nano Energy*, ***121***(2024) 1-16..

KV, G. M., George, J., & Balachandran, M. (2023). Polymer-nanocarbon composites: a promising strategy for enhanced performance of organic solar cells. *Emergent Mater.*, ***7***(2024)1-17.

Li, D., Dong, X., Cheng, P., Song, L., Wu, Z., Chen, Y., & Huang, W. (2022). Metal halide perovskite/electrode contacts in charge-transporting-layer-free devices. *Advanced Science.9*(36),1-34 .

Li, F., Ma, C., Wang, H., Hu, W., Yu, W., Sheikh, A. D., & Wu, T. (2015). Ambipolar solution-processed hybrid perovskite phototransistors. *Nature Communications.*, ***6***(1), 1-8.

Li, S., Dong, R., Li, Y., Lu, X., Qian, J., Wu, F., Wu, C., & Bai, Y. (2023). Advances in free-standing electrodes for sodium ion batteries. *Materials. Today*. ***72***(2024), 87-96.

Lin, C.-H., Li, T.-Y., Cheng, B., Liu, C., Yang, C.-W., Ke, J.-J., Wei, T.-C., Li, L.-J., Fratalocchi, A., & He, J.-H. (2018). Metal contact and carrier transport in single crystalline CH3NH3PbBr3 perovskite. *Nano Energy*, ***53***(78), 817-827.

Lin, C., Liu, G., Xi, X., Wang, L., Wang, Q., Sun, Q., Li, M., Zhu, B., Lara, D. P. d., & Zai, H. (2022). The Investigation of the Influence of a Cu2O Buffer Layer on Hole Transport Layers in MAPbI3-Based Perovskite Solar Cells. *Materials*, ***15***(22), 1-34.

Lin, C. H., Hu, L., Guan, X., Kim, J., Huang, C. Y., Huang, J. K., Singh, S., & Wu, T. (2022). Electrode engineering in halide perovskite electronics: plenty of room at the interfaces. *Advanced Materials.. ,* ***34***(18), 1-29.

Luo, D., Li, X., Dumont, A., Yu, H., & Lu, Z. H. (2021). Recent progress on perovskite surfaces and interfaces in optoelectronic devices. *Advanced Materials..*, ***33***(30), 1-24.

Ma, S., Yuan, G., Zhang, Y., Yang, N., Li, Y., & Chen, Q. (2022a). Development of encapsulation strategies towards the commercialization of perovskite solar cells. *Energy & Environmental Science*, ***15***(1), 13-55.

Ma, S., Yuan, G., Zhang, Y., Yang, N., Li, Y., & Chen, Q. (2022b). Development of encapsulation strategies towards the commercialization of perovskite solar cells. *Energy Environmental Science.*, ***15***(1), 13-55.

Mamta, Maurya, K. K., & Singh, V. N. (2021). Enhancing the performance of an Sb2Se3-based solar cell by dual buffer layer. *Sustainability*, ***13***(21), 1-33.

Manjunath, V., Bimli, S., Shaikh, P. A., Ogale, S. B., & Devan, R. S. (2022). Understanding the role of inorganic carrier transport layer materials and interfaces in emerging perovskite solar cells. *Journal of Materials Chemistry C.*, ***10***(42), 15725-15780.

Masut, R. A. (2023). Poisson's equation in semiconductors: impact of charge depletion on Hall effect measurements. *Canadian Journal of Physics.*, ***101***(3), 141-149.

Meng, D., Xue, J., Zhao, Y., Zhang, E., Zheng, R., & Yang, Y. (2022). Configurable organic charge carriers toward stable perovskite photovoltaics. *Chemical Reviews.*, ***122***(18), 14954-14986.

Meng, F., Wang, D., Chang, J., Li, J., & Wang, G. (2024). Application of Carbon Materials in Conductive Electrodes for Perovskite Solar Cells. *Solar RRL*. ***8***(6), 1-14.

Mohammad, A., & Mahjabeen, F. (2023). Promises and challenges of perovskite solar cells: a comprehensive review. *BULLET: Jurnal Multidisiplin Ilmu*, ***2***(5), 1147-1157.

Morales-Acevedo, A. (2023). Fundamentals of solar cell physics revisited: Common pitfalls when reporting calculated and measured photocurrent density, open-circuit voltage, and efficiency of solar cells. *Sol. Energy*, ***262(15),***1-28.

Moseley, O. (2023). *Development and Characterisation of Halide Perovskite Visible Light and X-Ray Detection Devices* University of Cambridge. ***22(5),***1-7.

Murugan, P., Hu, T., Hu, X., & Chen, Y. (2022). Advancements in organic small molecule hole-transporting materials for perovskite solar cells: past and future. *Journal of Materials Chemistry A.*, ***10***(10), 5044-5081.

Nair, S., Patel, S. B., & Gohel, J. V. (2020). Recent trends in efficiency-stability improvement in perovskite solar cells. *Mater. Today Energy*, ***17***(8), 262-277.

Noorasid, N. S., Arith, F., Mustafa, A. N., Chelvanathan, P., Hossain, M. I., Azam, M. A., & Amin, N. (2023). Improved performance of lead-free Perovskite solar cell incorporated with TiO_2 ETL and CuI HTL using SCAPs. Applied Physics A: Materials Science & Processing, ***129***(2), 132-145.

Nowsherwan, G. A., Nowsherwan, N., Anwar, N., Ahmed, M., Usman, Y., Amin, F., Nowsherwan, N., Ikram, S., Irfan, S., & Umar, M. (2023). Performance evaluation of modified zinc-phthalocyanine groups as an active material in dye-sensitized solar cells. *Energies*, ***16***(23), 1-17.

Ouedraogo, N. A. N., Odunmbaku, G. O., Guo, B., Chen, S., Lin, X., Shumilova, T., & Sun, K. (2022a). Oxidation of spiro-OMeTAD in high-efficiency perovskite solar cells. *ACS Applied Materials & Interfaces. Interfaces.*, ***14***(30), 34303-34327.

Ouedraogo, N. A. N., Odunmbaku, G. O., Guo, B., Chen, S., Lin, X., Shumilova, T., & Sun, K. (2022b). Oxidation of spiro-OMeTAD in high-efficiency perovskite solar cells. *ACS Applied Materials & Interfaces*, ***14***(30), 34303-34327.

Principe, J., Duarte, V. C., & Andrade, L. (2022). Inverted perovskite solar cells: The emergence of a highly stable and efficient architecture. *Energy Technol.*, ***10***(4), 1.45.

Qaid, S. M., Shaker, A., Jayan, K. D., Alkadi, M., Ahmed, A. A. A., & Zein, W. (2024). Design and numerical simulation of B-γ CsSnI3-based perovskite solar cells: Conventional versus inverted configurations. *Sol. Energy*, ***268***(23), 17.

Rasheed, S., Latif, H., Masood, M. F. U. D., Sattar, A., Shabbir, S. A., Razaq, A., Fareed, A., Usama, M., & Ali, S. (2023). Comparative study of 2D/3D hybrid perovskite solar cell containing different modified carbon nanomaterials based electron transport layers (ETL). *Optics Materials*, ***144***(2023), 1-64.

Raza, E., Ahmad, Z., Asif, M., Aziz, F., Riaz, K., Mehmood, M. Q., Bhadra, J., & Al-Thani, N. J. (2022). Numerical modeling and performance optimization of carbon-based hole transport layer free perovskite solar cells. *Optical Materials,****125***(2022), 1-8.

Rehman, U. u., Almousa, N., Sahar, K. u., Ashfaq, A., Mahmood, K., Shokralla, E. A., Al-Buriahi, M. S., Alrowaili, Z. A., Capangpangan, R. Y., & Alguno, A. C. (2023). Optimizing the efficiency of lead-free Cs_2TiI_6-based double halide perovskite solar cells using SCAPS-1D. *Energy Technol.*, ***11***(9), 1-11.

Roy, A., Patil, D., Yarlagadda, P. K., & Chatterjee, K. (2023). Cooperative stiffening of flexible high aspect ratio nanostructures impart mechanobactericidal activity to soft substrates. *J. Colloid Interface Sci.*, ***652****(120)*, 2127-2138.

Saifina, A. F., Kartashov, S. V., Stash, A. I., Tsirelson, V. G., & Fayzullin, R. R. (2023). Unified picture of interatomic interactions, structures, and chemical reactions by means of electrostatic and kinetic force density fields: Appel's salt and its ion pairs. *Cryst. Growth Des*, ***23***(4), 3002-3018.

Salah, M. M., Hassan, K. M., Abouelatta, M., & Shaker, A. (2019). A comparative study of different ETMs in perovskite solar cell with inorganic copper iodide as HTM. *Optik*, ***178***(65), 958-963.

Salah, M. M., Saeed, A., Mousa, M., Abouelatta, M., Zekry, A., Shaker, A., Amer, F. Z., & Mubarak, R. I. (2024). Numerical analysis of carbon-based perovskite tandem solar cells: Pathways towards high efficiency and stability. *Renew. Sustain. Energy Rev.*, ***189***(13), 1-41.

Sayem, A. S. M., Lalbakhsh, A., Esselle, K. P., Buckley, J. L., O'Flynn, B., & Simorangkir, R. B. (2022). Flexible transparent antennas: Advancements, challenges, and prospects. *IEEE Open Journal of Antennas and Propagation,****3***(3), 1-25.

Shah, N., Shah, A., Leung, P., Khan, S., Sun, K., Zhu, X., & Liao, Q. (2023). A Review of Third Generation Solar Cells. *Processes*, ***11***(6), 1-58.

Shakoor, A., Nowsherwan, G. A., Aamir, M. F., Ali, A., Rehman, S. U., Alam, W., Yasir, M., Arif, K., Ahmad, M., & Yousaf, J. (2023). Performance evaluation of solar cells by different simulating softwares. In *Solar PV Panels-Recent Advances and Future Prospects*. IntechOpen, ***311***(6), 2127-2138.

Shen, S. C., Khare, E., Lee, N. A., Saad, M. K., Kaplan, D. L., & Buehler, M. J. (2023). Computational Design and Manufacturing of Sustainable Materials through First-Principles and Materiomics. *Chemical Reviews.*, ***123***(5), 2242-2275.

Shen, X., Kang, K., Yu, Z., Jeong, W. H., Choi, H., Park, S. H., Stranks, S. D., Snaith, H. J., Friend, R. H., & Lee, B. R. (2023). Passivation strategies for mitigating defect challenges in halide perovskite light-emitting diodes. *Joule*, ***7***(2), 272-308.

Singh, N. K., & Agarwal, A. (2023). Numerical Investigation of Electron/Hole Transport Layer for Enhancement of Ecofriendly Tin-Ge Based Perovskite Solar Cell. *Energy Sources, Part A: Recovery, Utilization, and Environmental Effects*, ***45***(1), 3087-3106.

Singh, N. K., Agarwal, A., Kanumuri, T., & Varshney, T. (2020). A Study of an Inorganic-Organic HTM on the Implementation of Lead based PSC Device. 2020 IEEE Students Conference on Engineering & Systems (SCES), ***1***(6), 1-18.

Singh, N. K., Agarwal, A., Singh, A. K., & Singh, S. N. (2024). Design and performance evaluation of eco-friendly $FASnI_3/CsSn_{0.5}Ge_{0.5}I_3$ based perovskite solar cell with distinct charge transport layer: A computational modeling. *Sol. Energy*, ***268(2024)***, 1-56.

Smith, A. C., Harrison, P. A., Leach, N. J., Godfray, H. C. J., Hall, J. W., Jones, S. M., Gall, S. S., & Obersteiner, M. (2023). Sustainable pathways towards climate and biodiversity goals in the UK: the importance of managing land-use synergies and trade-offs. *Sustainability Science,****18***(1), 521-538.

Subudhi, P., & Punetha, D. (2023). Progress, challenges, and perspectives on polymer substrates for emerging flexible solar cells: A holistic panoramic review. *Progress in Photovoltaics: Research and Applications, **31***(8), 753-789.

Sunny, A., Rahman, S., Khatun, M., & Ahmed, S. R. A. (2021a). Numerical study of high performance HTL-free $CH_3NH_3SnI_3$-based perovskite solar cell by SCAPS-1D. *AIP Adv.*, ***11***(6) 1-17.

Sunny, A., Rahman, S., Khatun, M., & Ahmed, S. R. A. (2021b). Numerical study of high performance HTL-free CH3NH3SnI3-based perovskite solar cell by SCAPS-1D. *AIP Advances*, ***11***(6) 1-17.

Taniguchi, Y., Nishinaka, H., Shimazoe, K., Kawaharamura, T., Kanegae, K., & Yoshimoto, M. (2024). Visible-light absorption of indium oxide thin films via Bi^{3+} doping for visible-light-responsive photocatalysis. *Mater. Chem. Phys.*, ***315***(96) 128961-128977.

Tiwari, C., & Belwal, N. (2024). Numerical analysis of Ag/Cu2O/TiO2/FTO based solar cell with Ch3Nh3PbI3 interfacial layer using SCAPS 1D. AIP Conference Proceedings, ***2978***(1) 1-7.

Tsarev, S., Boldyreva, A. G., Luchkin, S. Y., Elshobaki, M., Afanasov, M. I., Stevenson, K. J., & Troshin, P. A. (2018). Hydrazinium-assisted stabilisation of methylammonium tin iodide for lead-free perovskite solar cells. *Journal of Materials Chemistry A*, ***6***(43), 21389-21395.

Wang, J., Zhu, R., Liu, Y., & Zhang, L. (2023). Understanding melt pool characteristics in laser powder bed fusion: An overview of single-and multi-track melt pools for process optimization. *Adv. Powder Mater.*, ***2***(4), 1-37.

Wang, S., Cui, H., Jin, S., Pi, X., He, H., Shou, C., Yang, D., & Wang, L. (2023). Anti-reflection effect of high refractive index polyurethane with different light trapping structures on solar cells. *Heliyon*, ***9***(9) 1-23.

Wang, T., Deng, W., Cao, J., & Yan, F. (2023). Recent progress on heterojunction engineering in perovskite solar cells. *Advanced Energy Materials.*, ***13***(33), 1-35.

Wang, Z., Zhang, P., Wei, W., & Li, W. (2023). Beneficial effects of tensile strain on charge carrier lifetime in metal halide perovskites containing halogen vacancies. *Journal of Materials Chemistry C.*, ***11***(41), 14097-14107.

Wei, Q., Cheng, Y., Gao, Y., Wang, N., Hou, X., Zan, L., Duan, Y., Fu, F., Yang, D., & Liu, S. (2023). Boosted ultraviolet irradiation and environmental stability of hole transport layer-free perovskite solar cells. *Sol. RRL*, ***8***(3), 1-8.

Xiao, S., Qian, W., & Yang, S. (2023). Interfaced structures between halide perovskites: From basics to construction to optoelectronic applications. *Adv. Energy Mater.*, ***13***(33), 1-28.

Xu, F., Zhang, M., Li, Z., Yang, X., & Zhu, R. (2023). Challenges and perspectives toward future wide-bandgap mixed-halide perovskite photovoltaics. *Advanced Energy Materials.*, ***13***(13), 1-14.

Yadav, C., & Kumar, S. (2022). Numerical Simulation for Optimization of Ultra-thin n-type AZO and TiO2 Based Textured p-type c-Si Heterojunction Solar Cells. *Silicon*, ***14***(8), 4291-4299.

Yan, J., Savenije, T. J., Mazzarella, L., & Isabella, O. (2022). Progress and challenges on scaling up of perovskite solar cell technology. *Sustain. Energy Fuels*, ***6(***12), 243-266.

Yang, Y., Xiao, Y., Xu, B., & Hou, J. (2023). Cross-linkable cathode interlayer for inverted organic solar cells with enhanced efficiency and stability. *Advanced Energy Materials*, ***13***(30), 1-13.

Yu, L., Zhang, Q., Bian, Z., Zuo, G., van Eersel, H., Bobbert, P. A., Coehoorn, R., Liu, F., & Zhou, G. (2023). Schottky-contact formation between metal electrodes and molecularly doped disordered organic semiconductors. *Physical Review Applied.*, ***19***(2), 1-23.

Zhang, C., Wei, K., Hu, J., Cai, X., Du, G., Deng, J., Luo, Z., Zhang, X., Wang, Y., & Yang, L. (2023). A review on organic hole transport materials for perovskite solar cells: Structure, composition and reliability. *Mater.Today*. ***67***(2023), 518-547.

Zhang, D., Yu, W., Zhang, L., & Hao, X. (2023). Progress in the Synthesis and Application of Transparent Conducting Film of AZO (ZnO: Al). *Materials*, ***16***(16), 1-19.

Zhang, H., Zhang, X., Li, Y., Huang, G., Du, W., Shi, J., Wang, B., Li, S., Jiang, T., & Zhang, J. (2022a). Interfacial molecular doping at donor and acceptor interface in bilayer organic solar cells. *Sol. RRL*, ***6***(6), 1-6.

Zhang, H., Zhang, X., Li, Y., Huang, G., Du, W., Shi, J., Wang, B., Li, S., Jiang, T., & Zhang, J. (2022b). Interfacial Molecular Doping at Donor and Acceptor Interface in Bilayer Organic Solar Cells. *Solar RRL*, ***6*(**6), 1-8.

Zhang, T., He, Q., Yu, J., Chen, A., Zhang, Z., & Pan, J. (2022). Recent progress in improving strategies of inorganic electron transport layers for perovskite solar cells. *Nano Energy*, ***15*(**6), 1-18.

Zhang, Y., Yang, Y., Mbumba, M. T., Akram, M. W., Rop, E. K., Bai, L., & Guli, M. (2022). Research progress of buffer layer and encapsulation layer prepared by atomic layer deposition to improve the stability of perovskite solar cells. *Sol. RRL*, ***6***(12), 1-15.

Zhao, C., Zhang, H., Krishna, A., Xu, J., & Yao, J. Interface engineering for highly efficient and stable perovskite solar cells. *Advanced Optical Materials.*, ***12*(**7), 1-16.

. Zhou, X., Yan, Y., Zhang, F., Li, M., Zhao, J., Hu, R., Geng, A., Xu, D., & Li, X. (2023). Efficiency and stability improvement of non-fullerene organic solar cells with binary anode buffer layer. *Journal of Materials Science: Materials in Electronics*, ***34***(18), 1-15.

Zhou, Z., & Pang, S. (2020). Highly efficient inverted hole-transport-layer-free perovskite solar cells.Journal of Materials Chemistry A, ***8***(2), 503-512.

Zhu, H., Teale, S., Lintangpradipto, M. N., Mahesh, S., Chen, B., McGehee, M. D., Sargent, E. H., & Bakr, O. M. (2023). Long-term operating stability in perovskite photovoltaics. *Nat. Rev. Mater.*, ***8***(9), 569-586.

Zouhair, S., Luo, B., Bogachuk, D., Martineau, D., Wagner, L., Chahboun, A., Glunz, S. W., & Hinsch, A. (2022). Fill factor assessment in hole selective layer free carbon electrode-based perovskite solar cells with 15.5% certified power conversion efficiency. *Sol. RRL*, ***6***(2), 1-10.

CHAPTER FOUR

PERFORMANCE OPTIMIZATION OF A NOVEL PEROVSKITE SOLAR CELL WITH POWER CONVERSION EFFICIENCY EXCEEDING 37% BASED ON METHYLAMMONIUM TIN IODIDE

Abstract

The pursuit of highly efficient lead-free solar cells is vital for sustainable energy production due to diminishing fossil fuel supplies and the detrimental effects of climate change. Lead-containing perovskite solar cells (PSCs) bring significant environmental and health risks, coupled with challenges related to thermal stability and durability. This study investigates a novel lead-free solar cell design with the structure ITO/PC61BM/$CH_3NH_3SnI_3$/PEDOT: PSS/Mo, focusing on improving light absorption, device efficiency, and performance under varying temperatures. The optimal thickness of the light-absorbing layer, $CH_3NH_3SnI_3$, was determined to be 1000 nm for achieving maximum quantum efficiency (QE). The cell's temperature tolerance was assessed through Mott-Schottky (MS) capacitance analysis, showing that it retains about 95% of its power at 400 K, demonstrating excellent thermal stability and robust performance. The solar cell also displays strong electrical characteristics, including a short-circuit current density (J_{sc}) of 34.84 mA/cm², an open-circuit voltage (V_{oc}) of 1.5226 V, a fill factor (FF) of 71.04%, and an impressive power conversion efficiency (PCE) of 37.66% at 300 K. The effects of buffer layers such as CdS, ZnS, ZnSe, and V_2O_5 on the cell's electrical performance were extensively analysed. The study also explored the impacts of parasitic resistances and doping on the cell's operational performance. This research provides significant insights into solar energy harvesting, offering potential solutions for sustainable energy generation and supporting efforts to decarbonize the environment and mitigate climate change.

4.1 Introduction

As the global economy and population continue to grow, there is an increasing need for sustainable and environmentally-friendly energy solutions. The extensive reliance on conventional fossil fuels has led to considerable environmental harm and depletion of resources. Securing renewable and clean energy sources is a critical objective of the 21st century, essential for addressing climate change and ensuring energy security. Solar energy stands out as a highly dependable, cost-effective, and resilient energy source due to its eco-friendly characteristics and lack of geographical constraints (Lee *et al.,* 2023). The burning of fossil fuels, including coal, oil, and natural gas, is the primary driver of the serious air pollution issues that the world is experiencing today (Chen *et al.,* 2023). Thus, generating electricity

from renewable sources can help protect the environment, and widespread adoption of these technologies is essential.

Photovoltaic (PV) technology has become a key solution for electricity generation in this context (Baigorri *et al.,* 2023). The demand for a dependable and proven technology to convert renewable energy into electricity is growing and needs to be maintained. Undoubtedly, solar energy is the most abundant, clean, and easily controllable renewable energy source available (Obaideen *et al.,* 2023). As a result, this study aims to fill the gap in current solar technologies by offering a more effective and eco-friendlier alternative to lead-based solar cells.

In recent years, PSCs have garnered considerable attention due to their strong performance, minimal hysteresis, and the ability to be fabricated at low temperatures (Chowdhury *et al.,* 2023). The primary aim is to improve the PCE and expedite the commercialization and scaling up of solar cell technologies. The choice of interface materials influences the performance of PSCs by affecting charge-selective contacts, charge accumulation, transport, transfer/recombination, band alignment, and electrical stability. In a typical PSC, an electron-selective contact and a hole-selective contact are positioned between the perovskite film to create the interfaces with the heterojunction solar cells (HSCs) and the electron-selective contact (ESC), respectively (Zheng *et al.,* 2019). The performance of PSCs, including factors like photovoltaic action, V_{oc}, device stability, and hysteresis, is determined by the choice of contacts and their interfaces. When these elements are effectively integrated into the solar cell design, they could enhance durability, improve material utilization, and potentially increase efficiency compared to traditional device configurations.

Advancements in solar cell technology offer the potential for affordable and highly efficient photovoltaic systems and could pave the way for effective and sustainable energy generation methods. As a result, achieving practical and economically feasible solar energy solutions is becoming more attainable through innovative approaches. To enhance the development of renewable solar technologies, it is crucial to focus on the durability of PSCs through practical design and materials processing, ultimately supporting the widespread adoption of photovoltaic technologies.

In the last ten years, significant research has focused on PSCs to boost their contribution to renewable energy. However, their commercial potential remains hindered primarily by issues related to operational stability (Duan *et al.,* 2023) employing polymers for encapsulation, UV filtering, charge transport layers, and interfacial layers offers a promising approach to improve stability and boost the performance of solar cells (Ganesh *et al.,* 2023). Polymers can

be incorporated into perovskite solar cells as additives to alter the nucleation and crystallization processes within the perovskite films (Yang *et al.,* 2023). To enhance carrier separation efficiency and reduce recombination, polymers can be utilized as interface layers, as well as materials for hole transport and electron transfer (Ghosh *et al.,* 2023).

In organic solar cells, polymers are commonly used as buffer layers and donor layers, and additional polymer-based nanostructures are incorporated in binary or ternary devices to enhance the overall performance of the solar cell (Duan *et al.,* 2023). Perovskite materials offer extended lifetimes, enhanced charge-carrier mobilities, and exceptional light absorption, which contribute to high device efficiencies and the possibility of creating cost-effective, scalable technologies for industry use (Soultati *et al.,* 2023). The scientific community has long encountered difficulties in developing solar cells that are affordable, straightforward to manufacture, efficient, and adaptable. However, progress in perovskite solar cell technology presents a promising outlook for achieving scalable and effective solar cells.

Perovskite solar cells have made significant strides in stability, scalability, and rapidly improving power conversion efficiencies. Nonetheless, two critical challenges hindering commercialization are their limited stability and the need to prove their scalability (Fu & Jen, 2023). The photovoltaic community has made impressive progress in rapidly enhancing the power conversion efficiency of solution-processed organometallic hybrid halide perovskite solar cells (Wright *et al.,* 2023); this advancement has broadened their application to other electronic devices such as light-emitting diodes, photodetectors, and batteries. Over the past decade, perovskite solar cells have gained substantial attention, with their power conversion efficiency showing significant improvement. Currently, the highest efficiency for a single-junction device is around 25%, comparable to the established and widely used silicon solar cell technology (Mohammad & Mahjabeen, 2023).

Despite these advancements, the short lifespan and instability of perovskite solar cells remain significant challenges that need to be urgently resolved to promote their commercialization. To address these durability and stability concerns, it is crucial to employ high-performance barrier and encapsulation materials, along with developing more stable perovskite materials and optimizing device design. Using polymer-based encapsulation techniques can help balance device longevity with processing costs (Li *et al.,* 2023). Perovskite solar cells have substantial potential for commercialization in photovoltaic technology due to their high-power conversion efficiency, low cost, ease of solution processing, and capability for large-area fabrication. To fully optimize device performance, effective interface and additive engineering are crucial.

A cutting-edge lead-free solar cell achieves high performance through a complex interplay of semiconductor materials, their inherent properties, and the behaviour of excitons when exposed to light. The bandgap energy of a semiconductor dictates the range of light wavelengths it can absorb effectively. In solar cells, having the right bandgap is crucial for capturing light across the entire solar spectrum (Li *et al.,* 2024). Lead-free perovskites, such as those based on tin or bismuth, along with various metal chalcogenides, provide a range of bandgaps. High carrier mobilities, which indicate the speed at which charge carriers move in an electric field, are crucial for effective charge collection. This characteristic is important for efficiently transporting electrons and holes to the respective contacts in a solar cell. Additionally, the rate of electron and hole recombination affects the overall efficiency of the cell (Chauhan *et al.,* 2023). Reducing recombination rates is crucial for maintaining high concentrations of charge carriers and minimizing the loss of excitons before they are collected. Lead-free solar cells face challenges such as achieving power conversion efficiencies comparable to those of lead-based cells, ensuring long-term stability, enabling scalable production, and using eco-friendly and cost-effective materials. Numerical simulations play a key role in optimizing material selection, device design, and manufacturing processes by providing insights into carrier physics within the cell. Researchers focus on improving carrier mobility, reducing recombination rates, and enhancing absorption through adjustments in material properties, interface engineering, and device architecture to ultimately boost solar cell performance.

While considerable advancements have been made in the design and testing of perovskite solar cells, there has been limited progress in exploring the full potential of solar cell modules. Traditional solar cell designs use various materials to improve stability, which could potentially enhance their overall durability (Song *et al.,* 2023). Optimal material selection can reduce energy losses, especially recombination losses typically found in conventional solar cells. Additionally, well-designed device architectures can improve solar cell efficiency by enhancing light absorption and charge carrier transport. This flexibility in material choices during fabrication fosters the exploration of innovative materials for better performance. However, perovskite solar cells are often impacted by environmental factors like moisture, oxygen, and light exposure (Li *et al.,* 2023). To protect against progressive weathering conditions like moisture, oxygen, and heat, solar cell modules can be made more resilient by positioning the more sensitive layers closer to the substrate and enhancing encapsulation. This approach improves the durability of the modules against environmental factors.

They can enhance charge transport and minimize recombination losses, potentially leading to greater efficiencies. The adaptability of perovskite solar cells makes them ideal for various applications, including wearable technologies and building-integrated photovoltaics (BIPV) (Li *et al.,* 2023). In certain instances, traditional designs use fewer cost-effective materials, reducing production costs while maintaining cell performance. These architectures also allow for simpler integration of tandem or multi-junction cells, which can capture a broader range of the sunlight spectrum, thereby enhancing overall efficiency (Ašmontas & Mujahid, 2023). For example, some configurations are particularly effective at capturing light, optimizing photon utilization, and minimizing optical losses. These solar cell modules frequently incorporate a broader range of advanced or innovative materials, leading to enhancements in both design and efficiency.

Traditional architectures often streamline manufacturing processes, leading to substantial reductions in production costs and making large-scale production more achievable. The benefits of these designs depend on the specific configurations and materials used in the solar cell. Researchers and manufacturers consistently investigate and improve these structures to enhance both performance and cost-efficiency in solar energy harvesting. Techniques that allow for solution processing, such as spin coating, dip coating, and spray coating, can be employed to create perovskite solar cells from commonly available compounds like lead iodide and organic halides (Amrillah *et al.,* 2023). Since the precursor materials for making solar cell absorbers dissolve readily in common organic solvents, it is feasible to use high-volume production methods like roll-to-roll (R2R) or sheet-to-sheet processing (Chen *et al.,* 2023). The core element of a perovskite solar cell is a metal halide hybrid perovskite, usually situated between an ETL and a HTL (Subudhi & Punetha, 2023). The layers serve to transfer excitons generated by light exposure and to absorb incoming light.

Methyl ammonium lead iodide is a widely used organic-inorganic perovskite material renowned for its exceptional photophysical and electrical characteristics (Priyadarshini *et al.,* 2023). It features a long charge carrier diffusion length, low exciton binding energy, a high absorption coefficient, and the ability to easily adjust the bandgap using straightforward solution-processing methods (Khan *et al.,* 2023). Lead toxicity and stability are two issues that need to be resolved before PSC is commercialized. Many effective techniques have been developed to stabilize lead-based PSC devices; still, the toxic element lead must be replaced with a harmless material, such tin. PSCs based on tin have the potential to oxidize from Sn2+ to Sn4+. (Zeng *et al.,* 2023), Despite this, they are nevertheless superior to their lead-based counterparts in that they have lower optical band gaps and higher charge mobility. Sn4+ acts

as a p-dopant within the perovskite through a process called "self-doping," which raises the concentration of holes that could seriously disrupt charge carrier recombination in solar cells (Bandara *et al.,* 2022).

The better PV qualities and possible applicability for large-scale deposition techniques of the next generation of solar cells, or PSCs, have garnered a lot of attention (Chowdhury *et al.,* 2023). Notwithstanding their noteworthy advancements in development, non-radiative recombination losses persist as an obstacle to their progress. Two crucial factors to minimize non-radiative recombination losses are the perovskite layer's defect density and the adjustment of the thickness of the different layers. Typical influences on PV device efficiency include temperature, oxygen concentrations, humidity, and lighting. To enhance the PCEs of large-area PSC devices, numerous researchers have created significant innovations. The first technique modifies the chemical composition of the perovskite by means of increased charge generation, bandgap engineering, solvent engineering, interfacial engineering, and bandgap correction (Jaffri *et al.,* 2023).

The unique characteristics and purposes of each material used in the model cell design must be taken into account. For a device to function properly, each layer's characteristics regarding stability, band gap energy, absorption coefficients, and charge mobility must be considered. Transparent conducting oxide (TCO) ITO provides excellent electron mobility in the range of 10 - 40 $cm^2/V{\cdot}s$ in the current cell construction. It is a very transparent electrode that maximizes light reaching the photoactive layer (PAL) due to its low absorption in the visible spectrum (Kumar *et al.,* 2023). ITO is transparent and has an efficient band gap of 3.7–4.3 eV for carrying electricity. Its resistance to moisture and chemical stability further increases its dependability in solar cell applications (Cho *et al.,* 2024). Conversely, PC61BM serves as a moderately mobile organic electron acceptor, often operating in the range of 10^{-3} to 10^{-2} $cm^2/V{\cdot}s$ (Khelifi & Luscombe, 2024). Since transporting electrons rather than absorbing light is its main function, it has a low absorption coefficient.

PC61BM has a bandgap of roughly 1.8 eV (Uddin & Afrin, 2024). A tin-based perovskite with high electron and hole charge mobility is $CH_3NH_3SnI_3$ (Ahamed *et al.,* 2023). It is an effective light absorber because of its high absorption coefficients, which exceed 10^7 cm^{-1} throughout the visible spectrum. Its 1.3 eV band gap makes it perfect for solar absorption. In contrast, PEDOT: PSS is a conductive polymer that exhibits high hole mobility, usually between 0.1 and 1 $cm^2/V{\cdot}s$ (Li & Liu, 2022). By changing its thickness, one can alter its mild absorption in the visible spectrum. PEDOT: PSS's function as an HTL is made easier by its bandgap, which spans 1.6 to 1.8 eV (Cho *et al.,* 2023). When utilized as the back contact,

molybdenum has extraordinarily high electron mobility often surpassing 100 $cm^2/V \cdot s$ (Zhou *et al.,* 2024). Because of its great reflectivity, it has no effect on how much light is absorbed by the solar cell. Since Mo is a metal, it has a continuous electrical structure but no bandgap. Because of its strong stability and ability to withstand corrosion, molybdenum is a dependable material for the back electrode. By combining these materials, a strong and effective solar cell design is produced, opening up a new avenue for the development of scalable and environmentally friendly solar energy equipment.

Overall, this work fills several knowledge gaps by determining the ideal thickness of the light-absorbing layer for maximum photon absorption, looking at interface characteristics, and investigating the role of different buffer layers in charge separation and transport. It also presents a novel lead-free solar cell design that greatly increases light harvesting and efficiency, marking a significant step in sustainable energy technology. Overall, by examining interface properties, figuring out the optimal thickness of the light-absorbing layer for optimum photon absorption, and delving into the function of several buffer layers in charge separation and transport, this work closes a number of knowledge gaps. A major advancement in sustainable energy technology is also demonstrated by the innovative lead-free solar cell design it offers, which significantly boosts light harvesting and efficiency. This solar cell construction has a lot of practical applications because of its remarkable electrical output parameters and integration potential. All things considered, this work offers a high-performing, lead-free alternative for solar energy harvesting and offers insightful information on material optimization, additive manufacturing, and interface engineering, improving PV efficiency and adding to the field of renewable energy.

The current design uses advanced materials to boost photon-to-electricity conversion efficiency and improve light absorption, marking a significant development in solar technology. The overall performance of the device is improved by minimizing optical losses within the cell through the careful selection and placement of material layers. The study also highlights the important role that interface passivation and engineering play in maximizing the operational performance of solar cells, as demonstrated by the remarkable electrical output metrics. The results of this study, albeit being based on theoretical simulation, are crucial in paving the way for the creation of a real solar cell with remarkable stability and operating efficiency.

4.2 Device simulation

Development of the Solar Cell Capacitance Simulator (SCAPS-1D) at the Department of Electronics and Information Systems (ELIS) of the University of Gent, Belgium (Ebon *et*

al., 2023; Hunde & Woldeyohannes, 2023), has been used to model the suggested solar cell's performance. The computer-based device simulator is ideal for examining hetero- and homo-junctions, multiple junctions, and photovoltaic devices with Schottky barriers. With amazing accuracy, the instrument has been calibrated using experimental data. To guarantee that the data produced is reliable, the current simulation is optimized for absorber thickness while also being calibrated against real values found in the literature. In addition, to replicate real-world conditions, the simulation was run at 1.5 AM with one sun and a power distribution of 1000 mW/cm^2 at 300 K. The Poisson's and the continuity equations for electrons and holes form the foundation for the software's simulation and functionality. Numerical techniques used in PSCs to solve the equations for semiconductor devices are the Gummel and Newton-Raphson iterative equations. The Gummel method increases stability by decoupling the equations, while the Newton-Raphson method provides faster convergence by solving them simultaneously (Butcher, 2000), as expressed by equation 4.1.

$$x_n + 1 = x_n - \frac{f(x_n)}{f\prime(x_n)} \qquad (4.1)$$

where, x_n is the current approximation, x_{n+1} is the next approximation, $f(x_n)$ is the value of the function at x_n , $f'(x_n)$ is the value of the derivative of the function at x_n .

The performance of solar cells is optimized by a number of factors, such as thickness, absorber layer defect density, and doping concentrations (N_D and N_A) of ETLs and HTLs, respectively. Consequently, resolving equations related to semiconductor device physics, such the continuity equation, and taking into consideration carrier generation, recombination, diffusion, and drift under external electric fields are necessary to comprehend carrier behaviour.

Chapter 3 page 87 covers the continuity and Poisson's equations, providing an in-depth explanation of their role in modelling charge carrier dynamics and electrostatic potential distribution in PSCs. The equations are mathematically derived and used to illustrate how electron and hole transport occurs, as well as their interactions with electric fields within the device. This discussion forms the basis for later analyses and simulations of PSC performance, highlighting the importance of these equations in optimizing the cell's overall efficiency.

Band energy ideas are equivalent to the Lowest Unoccupied Molecular Orbital (LUMO) and the Highest Occupied Molecular Orbital (HOMO) levels in the context of PSCs. Understanding the energy states involved in electron bonding and how solar cell devices function depends on these levels. This alignment lies between the acceptor material's LUMO

level, which is the lowest energy level of its empty molecular orbitals, and the donor material's HOMO level, which is the highest energy level of its occupied molecular orbitals. The efficiency of charge transfer between materials is determined by the energy offsets between these levels, which are important. Effective charge transfer influences exciton separation and charge transport, both of which are vital for the operation of optoelectronic devices. Proper band alignment is necessary for these processes.

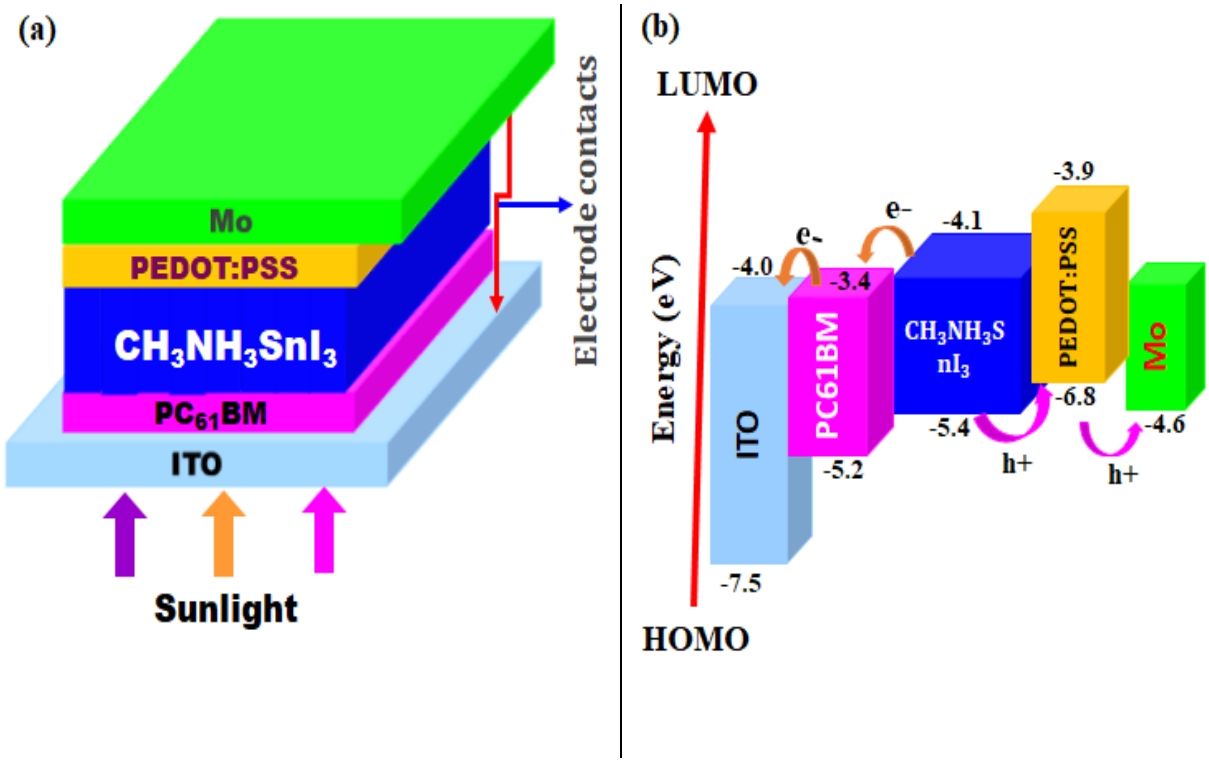

Figure 4.1: The suggested architecture of the solar cell (a) and (b) the band alignment

Figure 4.1a shows the suggested cell arrangement for this study. The semiconductor materials used to build solar cells have the ability to carry electricity under particular circumstances. The energy levels of the electrons in the semiconductor and the electrodes are displayed by a solar cell's band alignment. Light energy may be converted into electrical energy by the solar cell thanks to the energy level disparities between the bands. Figure 4.1b shows the band energy of a single material, where energy is represented by the vertical axis and distance by the horizontal axis. The energy gap (Eg), which is essential for comprehending the material's inherent properties, is depicted in this diagram along with the valence and conduction bands.

The band diagram displays the relative positions of the HOMO and LUMO levels for the donor and acceptor materials as well as how the valence and conduction bands of certain materials align when they come into contact. It draws attention to any energy offsets that affect charge transfer, which is crucial for comprehending the dynamics of charge transfer and the

device's overall performance. The band alignment diagram illustrates how the many layers that compose the solar cell's structure have distinct energies and how holes and electrons travel in opposite directions (cf. Figure 4.1b). Because the HTL is primarily involved in receiving and transmitting holes from the valence band of the perovskite material, its energy is higher on the band exciton chart than that of the ETL. In contrast, the ETL typically maintains lower energy levels that correspond with the conduction band of the perovskite material. The suggested solar cell's device structure consists of several layers, including a glass coated with transparent conductive oxide (ITO) substrate, an n-type semiconductor serving as the ETL, an absorber layer made of perovskites, a p-type semiconductor serving as the HTL, and a metal or carbon back contact.

The efficient mobility among carriers of charges both holes and electrons in the solar cell is greatly aided by this alignment of energy levels. This thus improves the device's overall efficiency in turning sunlight into electrical energy. It is evident from Figure 4.1b that PEDOT: PSS has the maximum energy as well as prevents holes and electrons from hopping, hence preserving energy. Band energy is concerned with the particular energy levels found in a material, with particular attention to the valence and conduction bands. The conduction band (CB) has higher energy levels where electrons can flow freely and contribute to electrical conduction, whereas the valence band (VB) contains the largest range of energies where electrons are normally found. The bandgap (Eg) is the term used to describe the energy difference between the valence band and the conduction band. When assessing a material's optical absorption and electrical conductivity, its bandgap is crucial.

4.3 Device basic input parameters

Solar cell architecture's input parameter may vary depending on the specific cell design; materials used, and desired output.

Table 4.1: The fundamental input parameters of the suggested cell architecture

Parameters	PEDOT:PSS (Hima *et al.*, 2019)	$CH_3NH_3SnI_3$ (Azmi *et al.*, 2022)	PC61BM (Goje *et al.*, 2023)	ITO (Baig *et al.*, 2019)
Thickness (nm)	50	1000	50	90
Band gap Eg/Ev	1.8	1.3	2.1	3.500
Electron affinity x/eV	3.4	4.1	3.9	4.000
Dielectric permittivity	3	8.2	3.90	9.000
CB effective density of states/cm^{-3}	2.2×10^{18}	1×10^{18}	2.2×10^{19}	2.2×10^{18}
VB effective density of states /cm^{-3}	1.8×10^{19}	1×10^{18}	2.2×10^{19}	1.8×10^{19}
Electron mobility/ cm^2/ V.s	1×10^{2}	1.6	1×10^{7}	2×10^{1}
Hole mobilitycm^2/V.s	4	1.6	1×10^{7}	1×10^{1}
Donor concentration N_D/cm^{-3}	0	0	0.001	1×10^{21}
Acceptor concentration N_A/cm^{-3}	2×10^{19}	1×10^{15}	0.002	0
Defect density/cm^{-3}	1×10^{14}	1×10^{11}	0	0

Complicated interplay among all parameters and other factors affects the overall efficiency and performance of the solar cell, by examining how variations in these parameters impact the behaviour of the cell, simulation tools and models may aid in improving the design of the cell for better performance. Table 4.1 lists the fundamental variables used in this investigation.

4.4 Results and discussion

4.4.1 The absorption model of the cell structure

Electron-hole pairs are produced when the semiconductor absorbs photons. The optical characteristics and bandgap of the material determine the process efficiency and absorption spectrum (Hanna *et al.*, 2023). Through a variety of processes, carriers can recombine, which can impact the overall performance of the solar cell. For solar cells to function well, charge carriers must be efficiently gathered at the electrodes prior to recombination. Each of the fundamental parts of PSCs has unique characteristics related to light absorption. The most crucial element is the perovskite absorber layer (PAL), which typically produces electron-hole pairs by absorbing light. Perovskite materials are able to absorb a broad variety of light wavelengths, spanning from the visible to the near-infrared portions of the electromagnetic spectrum. Transport layers facilitate the passage of electrons and holes toward electrodes, increasing charge extraction and decreasing recombination losses.

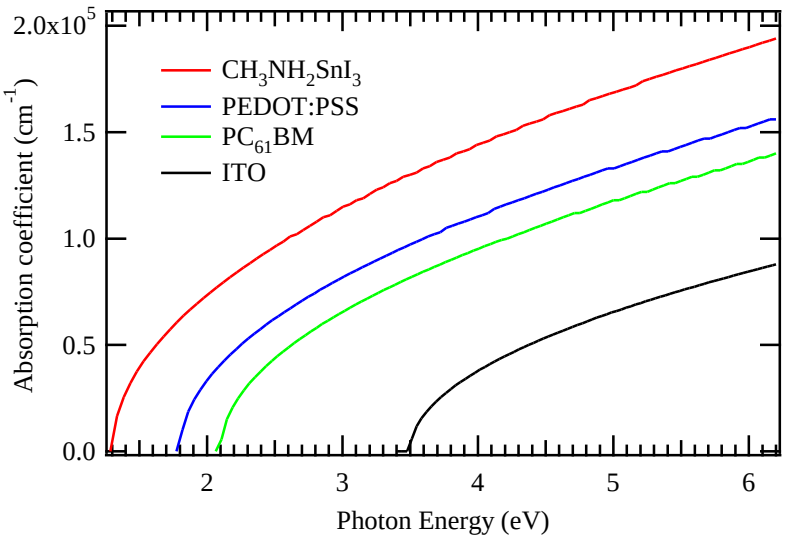

Figure 4.2: SCAPS absorption model for the cell structure

The absorption of light at various wavelengths and photon energies throughout the layers of the suggested solar cell architecture is shown in Figure 4.2. As a result, the absorption coefficients of the layers PC61BM, ITO, $CH_3NH_3SnI_3$, and PEDOT: PSS vary, affecting their ability to absorb photons. Throughout the whole wavelength range, PC61BM and PEDOT: PSS

follow $CH_3NH_3SnI_3$ as the layers with the highest absorption coefficients at ~ 2.0 ×,10-5cm^{-1}. The photons that are absorbed are excited into the conduction band of the semiconductor. The absorption coefficients basically tell us how well a given wavelength of light can enter the solar device before it is absorbed. Wavelengths that are less energetic than the band gap energies cannot excite an electron from the valence band to the conduction band. Surprisingly, the ITO layer has a lower absorption capacity than the other layers.

Composite layer absorption balances out the perovskite layer's absorption, guaranteeing effective charge extraction without absorbing a large amount of light. While reducing light absorption, electrodes made of TCO and metal contacts gather and move charge carriers out of the cell (Michel *et al.,* 2023). High efficiency depends on the absorption characteristics of each component. Compared to other materials, the perovskite layer's broad absorption spectrum is particularly useful since it allows for the capture of more sunlight. In the end, scientists have worked to improve efficiency and stability, reduce energy losses in non-active layers, and increase light absorption in each layer. Optimizing absorbance and performance of a solar cell can be achieved using simple techniques such as adjusting band gaps and materials in each layer.

4.4.2 The impact of HTL on the cell performance

PEDOT: PSS HTL is preferred for usage in PSCs due to its outstanding film-forming capabilities, strong electrical conductivity, and exceptional transparency. Hole transport from the perovskite layer to the anode is greatly enhanced by it due to its high conductivity and appropriate energy level alignment with the valence band of $CH_3NH_3SnI_3$, which lowers recombination losses (Imani *et al.,* 2023). The performance of PSCs with and without this HTL must be compared in order to comprehend the influence of PEDOT: PSS. The use of PEDOT:PSS provides an effective route for the extraction of holes from the $CH_3NH_3SnI_3$ perovskite layer to the Mo electrode (Ali *et al.,* 2023). At the perovskite/HTL interface, the work function of PEDOT:PSS (~5.0 eV) effectively coordinates with the valence band of $CH_3NH_3SnI_3$ (~5.4 eV), facilitating effective hole transport and reducing recombination losses. Higher PCE, V_{oc}, J_{sc}, and FF result from this as opposed to devices without the HTL. On the other hand, holes from the perovskite layer must be removed straight to the Mo electrode in the absence of the PEDOT: PSS layer. Because of the poor alignment of energy levels, this direct contact frequently leads to ineffective hole extraction and higher recombination losses. As a result, devices lacking the HTL show reduced PCE, V_{oc}, J_{sc}, and FF.

We investigated and published a high-performance hole transport layer-free (HTL-free) PSC with the arrangement ITO/PC61BM/ $CH_3NH_3SnI_3$/Pt in our most recent study. Through

the optimization of crucial elements such buffer layers, materials for front and back contacts made of metal, and electron transport materials, we were able to attain outstanding outcomes. The results of the SCAPS-1D simulation were as follows: PCE = 38.11%, J_{sc} = 35.32 mA/cm², FF = 88.67%, and V_{oc} = 1.2168 V. Furthermore, Mott-Schottky capacitance study contributed significantly to the improvement of charge extraction and decrease in recombination losses by offering insightful information about charge carrier behaviour and interface characteristics. The results show how promising HTL-free PSCs can be in providing highly efficient and economically viable solar energy solutions, opening the door for more accessible and scalable solar cell technologies. However, even though the electrical results of this kind of device (HTL-free) are remarkable, further theoretical and experimental research is necessary to determine its stability.

4.4.3 The influence of photoactive layer thickness on QE and J-V Characteristics

The creation of highly efficient solar cell devices depends on optimizing solar cell properties like FF, PCE, J_{sc}, and V_{oc}. The photoactive layer, or perovskite, is a crucial element in PSC modelling and simulation. The SCAPS-1D device simulator is used to investigate how altering the thickness of the perovskite layer affects the properties of the solar cell. A solar cell's QE is determined by how well light photons are converted to electrons. For a variety of reasons, including the fact that a thicker cell can absorb more light due to its increased material content, which raises the possibility of absorbing photons, the thickness of the cell is important to this process. However, some photons may pass through without interacting if the material is sufficiently thin, which would lower the device's efficiency (Nazir *et al.*, 2023). However, because charge carriers must travel a greater distance to reach the electrode terminals, larger cells have difficulties collecting the generated electron-hole pairs. This separation may result in increased recombination losses and decreased operating efficiency of the device. Accordingly, thicker cells may have larger optical losses due to light trapping in the material, which increases the re-absorption of electrons and holes and ultimately lowers the device's overall efficiency.

The variation of QE with wavelength over different photoactive layer thicknesses, from 200 to 1000 nm, is illustrated in Figure 4.3a. This shows that QE rises with increasing photoactive layer thickness, indicating improved photon absorption, especially at longer wavelengths. This increase is attributed to improved electron-hole pair production in the photoactive material. The curves converge at a thickness of 1000 nm, indicating a QE saturation limit, and then attain their maximum QE. As a result, Figure 4.3a calculates that 1000 nm is the ideal thickness for the suggested solar cell construction to achieve maximum

performance. Low QE is the result of the absorber's thinner thickness. For example, at 200 nm thickness, the device's QE is significantly reduced across the whole wavelength range. Light wavelength is shown by the x-axis and ranges from 300 to 900 nm, or ultraviolet (UV), violet, blue, and near-infrared light, respectively. The device's performance can be better understood by analysing its efficiency at various wavelengths, which helps with application-specific tuning. Applications where such photon energy predominates for solar cell or photodetector applications may be guided by high efficiency at specific wavelengths.

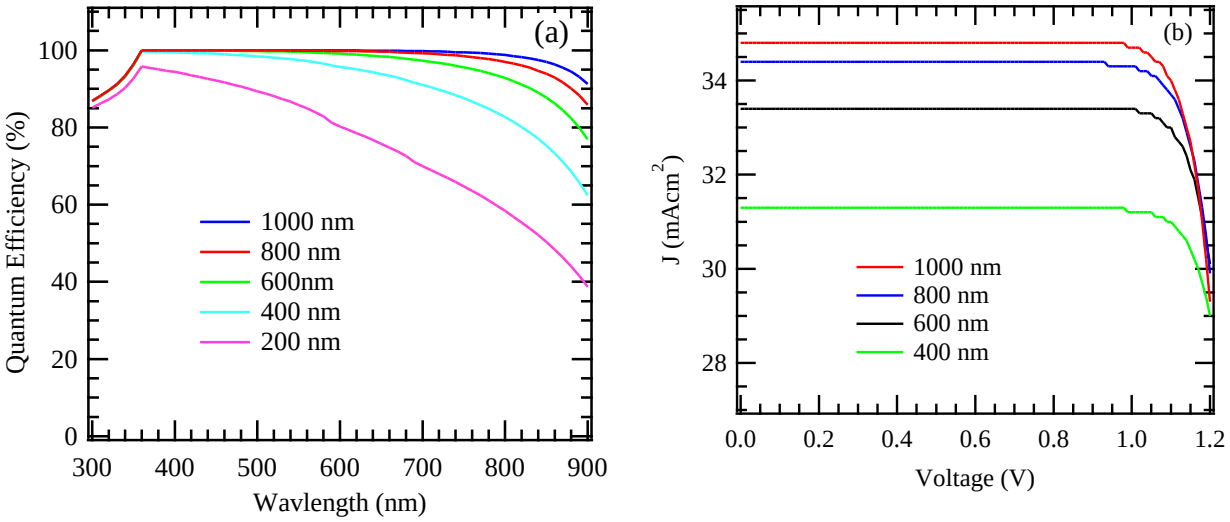

Figure 4.3: The impact of thickness on the proposed solar cell architecture's J-V characteristics (b) and quantum efficiency (a)

A distinct trend showing an increase in voltage (V) with absorber layer thickness is shown in Figure 4.3b. This happens because a thicker layer generates a higher V and higher current density by providing a longer path for the produced carriers to traverse before recombination can occur. For all layer thicknesses, Figure 4.3b demonstrates that the J_{sc} levels off at around 0.4 V. Furthermore, over the whole voltage range, the thicker layers, measuring 1000 nm and 800 nm, have larger J_{sc} values than the thinner layers, measuring 600 nm and 400 nm. It is significant to remember that other factors, such the characteristics of the material and the design of the device, are also very important in deciding how well the solar cell performs.

One crucial electrical result that the thickness of the perovskite layer might affect is voltage (These *et al.*, 2024). Consequently, one aspect of the bigger issue in solar cell engineering and design is optimizing the perovskite layer's thickness. The perovskite layer needs to be just thick enough to absorb light without creating defects or preventing charge transfer in order to transform light into energy efficiently. Recombination losses are more likely

in thicker perovskite layers due to the longer distance charge carriers must travel to reach the electrodes.

Exciton recombination prevents excitons from contributing to voltage output, which lowers the Voc. Furthermore, while a thicker layer of perovskite facilitates higher photon absorption and produces more electron-hole pairs, an overly thick layer runs the danger of absorbing the majority of input light, preventing it from reaching important underlying layers like electron and hole transport layers (Noh *et al.,* 2023). This restriction may have a negative impact on V_{oc}. Changing the thicknesses also affects the transport properties and charge carrier mobility in the perovskite layer; the best thicknesses promote effective charge transfer to the electrodes, which raises V_{oc}. Furthermore, more flaws or grain boundaries may be present in larger layers, which would trap charge carriers and encourage charge recombination, lowering the value of V_{oc}. According to Figure 3b, 1000 nm is the ideal thickness for the suggested solar cell's maximum performance. A thickness of less than 1000 nm causes a decrease in cell performance. Because of the device's shortened diffusion length, exciton recombination is the likely cause of this. Improved PCE is the outcome of increased electron-hole pair generation within the perovskite, which is linked to the increase in J_{sc} as the photoactive thickness increases. A PSC's ability to function as a whole, particularly in terms of its photoactive layer, depends on how thick each layer is made.

4.4.4 Effect of buffer layers on electrical output

In PSCs, buffer layers are essential to overall performance, as they have a direct impact on many operational parameters such as stability, efficiency, and other metrics (Duan *et al.,* 2023). This layer's thickness is very important since it affects a number of crucial aspects of the device's operation. First, for effective charge transfer and collection, the buffer layer's thickness is essential. Recombination losses are minimized through effective charge transport, which is ensured by an ideally thick buffer layer. The performance of the cell could be compromised by an excessively thin layer that can cause faults or fail to properly inhibit recombination. Conversely, an overly thick buffer layer may make it more difficult for charge carriers to reach the electrodes, which would lower the J_{sc} and increase series resistance. The thickness of the buffer layer also affects the morphology and quality of the interface between the charge transport layers and the perovskite.

Poor contact and increased recombination rates could arise from thin buffer layers' insufficient ability to smooth the interface. On the other hand, while thicker layers may raise recombination rates by providing obstacles to charge extraction, they can also enhance coverage and smoothness at the interface. The buffer layer thickness affects all photovoltaic

performance measures, including V_{oc}, J_{sc}, FF, and PCE. By inhibiting recombination and promoting effective charge separation, an ideal thickness contributes to the maintenance of a high V_{oc}. On the other hand, overly thick layers can lower J_{sc} by impeding charge transmission and raising resistance. When the buffer layer thickness is tuned, the FF which is affected by series resistance is likewise maximized, supporting a high PCE. The buffer layer must protect the perovskite layer from the environment while maintaining stability and durability; this need must be balanced with the necessity for effective charge transmission.

Table 4.2: The impact of adding different buffer materials on the suggested solar cell's electrical results

Buffer	**V_{oc} (V)**	**J_{sc} (mA/cm^2)**	**FF (%)**	**PCE (%)**	**References**
CdS	1.4414	34.85	72.48	36.41	(Mamta *et al.*, 2021)
ZnS	1.2555	34.80	65.63	28.68	(Tobbeche *et al.*, 2019)
ZnSe	1.5216	34.84	71.04	37.65	(Biswas *et al.*, 2023)
V_2O_5	1.5028	34.84	71.68	37.63	(Al Mahmud *et al.*, 2023)

Sufficient thickness can both prevent the perovskite from degrading and increase the mechanical stability of the apparatus, possibly prolonging its useful life (Li *et al.*, 2024). The buffer layer thickness adjustment is further complicated by material considerations. The appropriate thickness varies depending on the material conductivity. Variations in film quality and uniformity can also impact the required thickness when using different deposition processes like spin-coating or sputtering. To sum up, charge transfer, interface quality, performance metrics, stability, and other conflicting aspects must all be balanced in PSCs by adjusting the buffer layer thickness. An excessively thick buffer layer can hinder charge transfer and lower efficiency, whereas an excessively thin buffer layer can result in inadequate coverage and more recombination. For PSCs to function better and last longer, the buffer layer thickness must be carefully optimized in addition to choosing the right material.

The performance characteristics of solar cells using different buffer layers, such as V_2O_5 (vanadium (V) oxide), ZnS (zinc sulphide), ZnSe (zinc selenium), and CdS (cadmium sulphide), are shown in Table 4.2. Because of its appropriate band gap and advantageous electrical characteristics, CdS is a widely used material for solar cells. In the model cell

architecture, it provides a V_{oc} of 1.4414 V and a J_{sc} of 34.85 mA/cm². Additionally modest at 72.48% is the FF, which results in an impressive PCE of 36.41%. Because of this combination, CdS functions as a dependable buffer layer for effective solar cell operation. Conversely, ZnS exhibits a nearly equal J_{sc} of 34.80 mA/cm² to CdS, but a lower V_{oc} of 1.2555 V. On the other hand, the FF is much lower at 65.63%, which means that the PCE is lowered to 28.68%. The lower FF indicates possible problems that could have a detrimental effect on overall efficiency, such as increased series resistance or reduced shunt resistance. ZnSe has the highest J_{sc} of 34.84 mA/cm² and the highest V_{oc} of all the buffer layers under study, at 1.5216 V. Not to mention, the FF is excellent at 71.04%, which leads to a comparatively high PCE of 37.65%. This indicates that ZnSe performs exceptionally well, positioning it as a leading candidate for extremely efficient solar cells. With a somewhat higher FF of 71.68%, a V_{oc} of 1.5028 V, and a J_{sc} of 34.84 mA/cm², V_2O_5 exhibits strong performance. This yields a high PCE of 37.63%, which is almost identical to that of ZnSe. This suggests that V_2O_5 can be used to generate high performance solar cells quite well. With the lowest V_{oc} is ZnS. Since J_{sc} values are fairly comparable for all buffer layers, choosing a buffer layer has little effect on J_{sc}. V_2O_5 has a little greater FF value than CdS and ZnSe. ZnSe and V_2O_5 attain the highest PCE and a much lower FF, respectively, indicating that they are the most efficient buffer layers for the current model cell. ZnS is less efficient than CdS because of its lower FF, which lowers PCE. CdS likewise exhibits minor efficiency.

4.4.5 Influence of temperature on the electrical characteristics of the cell

The amount of electricity that a solar cell device generates is significantly influenced by temperature. Solar cells generally lose efficiency with increasing temperature. This mostly occurs because greater temperatures can increase the rate at which electrons and holes recombine, decreasing the voltage the cell generates (Mohammed *et al.*, 2023). As a result, the cell's capacity to transform light photons into electrical energy is diminished. In general, rising temperatures can hinder solar cell performance, which reduces the amount of electricity they can produce effectively.

J_{sc} appears to stay constant as the cell temperature rises, as seen in Figure 4.4a. The distinctive behaviour can be explained by the fact that the processes of creation and recombination cancel each other out, independent of temperature changes. As seen in Figure 4.4b, V_{oc}, on the other hand, shows a rapid increase between 280 and 400 K, finally decreasing from 1.77 V at 340 K to about 1.26 V at 400 K. Solar cells have temperature sensitivity, just like other semiconductor devices. The efficiency of solar cells tends to decrease with temperature. The temperature increase causes the cell's internal resistance to increase, which

lowers voltage output and ultimately reduces the solar cell's overall operational efficiency. Temperature fluctuations have a substantial impact on perovskite solar cells' performance, affecting the FF and PCE in different ways. Because the perovskite material's electrical properties alter with temperature, the FF is especially susceptible to temperature fluctuations. In general, the FF of PSCs tends to decrease with increasing temperature.

High temperatures have the potential to accelerate charge carrier recombination in the perovskite layer, which would decrease the efficiency of charge collecting and eventually lower the FF value. Temperature variations also have an effect on exciton mobility in the perovskite material, which affects charge carrier mobility and, in turn, the FF. In a similar vein, temperature changes have a big effect on PSCs' PCE. Because of higher charge recombination rates, a decline in V_{oc}, and a corresponding decrease in FF, higher temperatures frequently result in lower PCE. As shown in Figure 4.4b, there is an ideal temperature range where efficiency peaks before declining. This ideal temperature range, however, changes according to the PSC's particular composition and technical layout. The absorber material ($CH_3NH_3SnI_3$) in the suggested solar cell architecture has a high limit of flaw tolerance and exceptional temperature stability.

When the voltage across a solar cell is zero, which occurs when the cell is short-circuited, the current density that flows is known as J_{sc} (Perez *et al.,* 2024). The device's photogenerated current is measured by J_{sc}. Understanding the fundamental physics of the photogeneration and collecting processes inside the solar cell can help to explain why J_{sc} stays constant. First, the number of photogenerated charge carriers in the solar cell, such as electrons and holes, directly correlates with J_{sc}. When photons with energy matching or exceeding the absorber material's bandgap are introduced into the cell, electron-hole pairs are produced (Chee, 2023). The p-n junction's or heterojunction's inherent electric field then divides these pairs, collecting the current. The creation rate of these electron-hole pairs stays constant if the solar cell is exposed to a constant amount of light. As a result, J_{sc} does not change because it is closely correlated with both the efficiency of charge carrier separation and the quantity of photons absorbed.

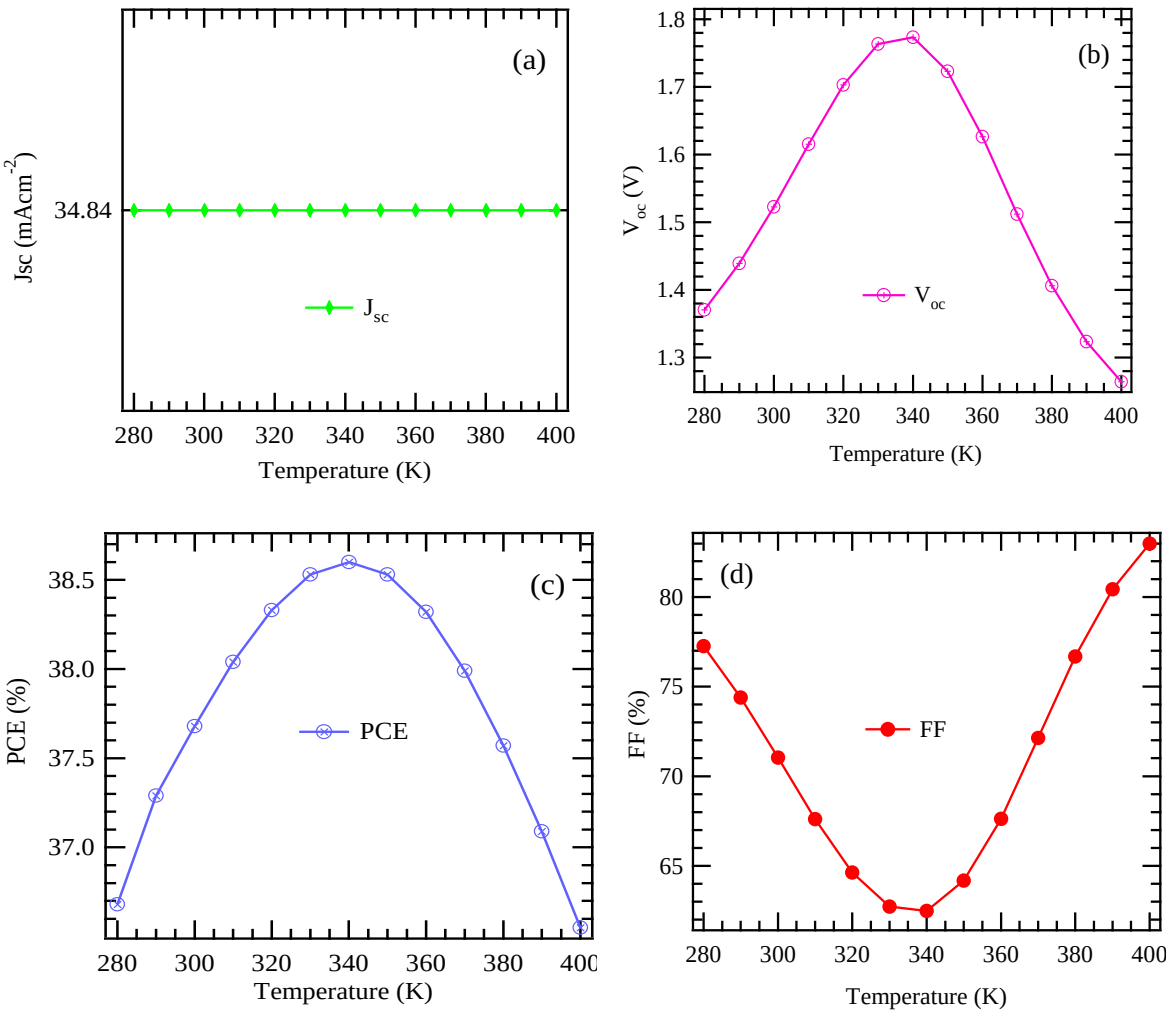

Figure 4.4: Temperature effects on the electrical outcomes of the model cell structure (a) J_{sc}, (b) V_{oc}, (c) PCE and (d) FF

The FF and PCE values change as the temperature rises from 280 to 400 K, as shown in Figures 4.4c and d. As seen in Figure 4d, the FF increases from 61% to 83.5% between 280 and 340 K, then falls to roughly 61% at 400 K. In contrast, because of improved exciton transport, the PCE rises from 280 K and reaches an ideal value of about 38.7% at 340 K. PCE thereafter declines gradually to 400 K, where it reaches a value of roughly 36.6%. On the other hand, by decreasing carrier mobility, lower temperatures reduce J_{sc}, however, this can occasionally be compensated by a decrease in recombination losses. Yet, because of greater non-radiative recombination and shortened carrier lifetimes, higher temperatures usually result in a drop in V_{oc}. Despite the fact that better charge extraction and reduced series resistance at lower temperatures may initially result in a minor rise in V_{oc}, this effect eventually decreases at higher temperatures due to higher recombination rates. To put it simply, while higher temperatures may momentarily increase J_{sc} by improving carrier mobility, this advantage may

be offset by an increase in recombination rates. Due to an increase in non-radiative recombination processes, V_{oc} often drops as temperatures rise.

The current is solely driven by these photogenerated carriers under short-circuit situations, when there is no voltage across the solar cell and the external circuit has no effect. Instead of being dependent on the external voltage, the photogeneration process is mostly dependent on the light intensity and the material qualities of the solar cell (Soonmin *et al.,* 2023). J_{sc} thus stays constant. From a physics perspective, equation 4.2 gives the rate at which electron-hole pairs form in a solar cell.

$$G = \frac{P_{in.(I-R)}.\eta_{abs}}{h_V} \quad (4.2)$$

where P_{in} is the incident light power density, R is the reflectance of the solar cell surface, η_{abs} is the absorption efficiency of the solar cell material, and h_V is the energy of the incident photons. If the absorption efficiency, reflectance, and other material properties such as the density of incident light remain constant, then so does the generation rate. At short-circuit conditions, the created electron-hole pairs are effectively separated and collected by the built-in electric field in the solar cell's depletion area, resulting in a continuous current flow (Rehman *et al.,* 2023). Mathematically, the short-circuit current density can be expressed by equation 4.3.

$$J_{sc} = q.G.L_{eff} \quad (4.3)$$

The elementary charge is denoted by q, the generation rate by G, and the effective length over which carriers are gathered by L_{eff}. G is constant in the presence of constant light, and J_{sc} is constant since the effective length, L, is dictated by the geometry of the cell and the characteristics of the material. As a result of stable photogeneration and charge carrier accumulation within the solar cell under continuous illumination, a stable short-circuit current density is produced, as indicated by the constant J_{sc} in the Figure.

The V_{oc} of a solar cell decreases with increasing temperature. The bandgap energy of the semiconductor material changes, which is the main cause of this shift. Since intrinsic resistance rises with temperature, increased temperature energizes electrons and reduces voltage output. Surprisingly, as temperatures rise, solar cell devices' J_{sc} frequently sees a little increase even as voltage drops. But typically, this increase is insufficient to counteract the voltage drop, which leads to a fall in power output overall. Elevated temperatures may also have an adverse effect on the longevity of solar panels by gradually reducing their performance over time. Extended exposure to elevated temperatures can lead to material degradation, which could have an impact on the solar cell structure's overall longevity. Sensible engineering at

interfaces typically advances designs that include structures and materials that efficiently drain heat in order to minimize these impacts and maximize solar panel performance. In addition, temperature variations are controlled by cooling methods and monitoring systems, guaranteeing more reliable gadget performance.

The rise in V_{oc} seen in the model cell when the temperature increased from 280 to 340 K can be ascribed to many causes associated with the characteristics of the perovskite material and the physics of the device. Trap-assisted recombination and non-radiative recombination, which includes defects, predominate at lower temperatures. Increased temperature causes thermal energy to assist in releasing carriers from trap states, which lowers non-radiative recombination rates and raises the V_{oc}. Higher temperatures may also result in better charge carrier movement. Furthering the increase in V_{oc}, this enhanced mobility permits more effective charge extraction and lowers recombination losses. Furthermore, the perovskite material's trap states can be thermally activated as temperature rises, reducing their influence on recombination processes and raising the V_{oc}.

As temperature rises, the density of defect states in the perovskite material may also decrease, reducing recombination losses and increasing V_{oc}. An additional variable is the temperature-dependent shift in the perovskite material's bandgap. The quasi-Fermi level splitting, which determines V_{oc}, may be affected in a way that causes V_{oc} to increase within a specific temperature range, despite the fact that semiconductor bandgaps normally drop with rising temperature. Finally, if the perovskite material contains dopants, higher temperatures may improve their activation, enhancing the material's conductivity and charge transport capabilities and raising V_{oc}. Overall, decreased non-radiative recombination, increased charge carrier mobility, and other temperature-dependent characteristics of the perovskite material are responsible for the rise in V_{oc} with temperature from 280 to 340K.

4.4.6 The band alignment diagram of the model cell

The process of turning light into electricity requires the use of a solar cell band diagram, which shows the electron energy levels inside the apparatus. Different energy bands in the diagram are essential for this conversion in semiconductor-based solar cells. The two main states shown in the diagram are usually the semiconductor sections of the p-type (positively doped) and n-type (negatively doped), divided by a junction (Wang *et al.,* 2016). Doping has created excess positively charged "holes" in the p-type semiconductor. Compared to the conduction band, the valence band is positioned closer to the Fermi level in this instance. The conduction band of an n-type semiconductor, on the other hand, is positioned closer to the Fermi level than the valence band because it contains an excess of negatively charged electrons

due to doping. A depletion layer with no free charge carriers and an electric field owing to varying charge concentration develops at the intersection of these zones. Electrons in the semiconductor are excited by photons striking the solar cell, resulting in the creation of electron-hole pairs.

Interface defects are a result of the mismatch in the lattice between two interfaces shown in Figure 4.5. These defects ultimately lead to exciton recombination. The two forms of band structures that are seen at the interface, where charge carrier recombination is most likely to happen, are cliff and spike. The presence of a cliff structure at the interface is thought to be the cause of band bending in the conduction band. To achieve optimal device performance, there must to be a positive (spike-like) band offset at the p-n-junction. Figure 5 shows that the negative cliff offset in the suggested cell structure occurs at 0.17 eV, suggesting improved device performance with appropriate band alignment. This can be explained by the fact that the absorber layer's recombination activation energy (Ea) has a significant impact on the functionality of the device.

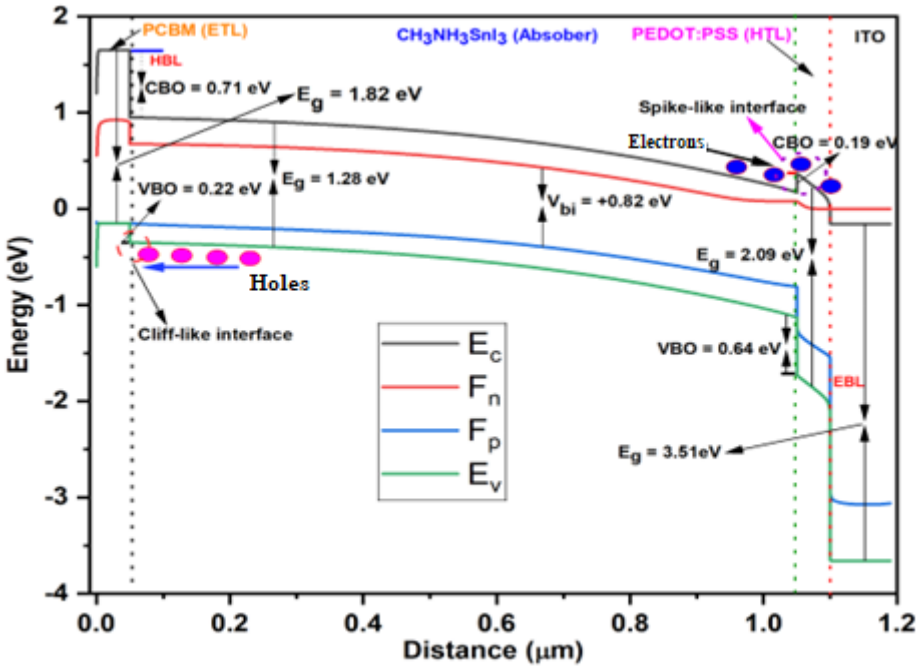

Figure 4.5: The band diagram of the proposed solar cell device

When excitons holes and electrons are connected to an external circuit, the electric field in the depletion area drives them in opposite directions, creating current flow. The mechanism by which absorbed photon energy transfers electrons from the valence to the conduction band, allowing them to contribute to the electrical current, is illustrated clearly by the band diagram. Figure 5 illustrates how, depending on the band position, the proposed solar cell exhibits a small variation in band alignment. Due to band bending at interfaces, the diagram shows a trend

where the gap shrinks as distance rises. The band diagram illustrates that the intrinsic voltage gap is roughly + 0.82 eV. The non-uniformity of the band gap could be explained by band bending at various cell structural contacts.

The energy levels of the different materials in a solar cell are shown in Figure 4.5, where the built-in voltage (Vbi) is one of the most important observations. The potential difference, or V_{bi}, between the conduction band (CB) of an n-type semiconductor and the valence band (VB) of a p-type semiconductor at thermal equilibrium is shown in Figure 4.5 as +0.82 eV at 300 K. When the flow of electrons within a material reaches a steady state, thermal equilibrium a state obtained when a material stabilizes at a constant temperature occurs. The material's lattice vibrations become more intense as temperature rises. This increased lattice vibration may cause the semiconductor's bandgap (Eg), or the energy difference between its valence and conduction bands, to decrease. The energy difference between the Fermi levels (Fp and Fn) of the p-type and n-type materials, respectively, is lessened with a decrease in the bandgap.

As a result, this decrease in the energy difference between the Fermi levels leads to a decrease in the solar cell architecture's Vbi. The hole blocking layer (HBL) at 3.5 eV at the given energy level is identified as the PEDOT:PSS HOMO level. The valence band (VB) edge of $CH_3NH_3SnI_3$ is 1.82 eV, whereas the conduction band (CB) edge is 2.09 eV. The electron blocking layer (EBL) at -1.27 eV is assigned to the LUMO level in PCBM. The configuration and transitions between these energy states are what drive the solar cell's activity, and temperature changes impact the Vbi and, in turn, the cell's total efficiency.

Between PEDOT:PSS and $CH_3NH_3SnI_3$, there is a spike contact. With a conduction band offset (CBO) of +0.19 eV, this spike is distinguished by a barrier that prevents electrons from moving from the absorber into the HTL. The obstruction of electron transport caused by such a spike may result in recombination losses, which can be harmful. The interaction between $CH_3NH_3SnI_3$ and the PCBM is a cliff after that. This creates a drop for holes traveling originating from the absorber to the ETL because the valence band offset (VBO) is -0.22 eV. Another reason cliffs can be troublesome is that they can lead to the accumulation of holes at the interface, which would speed up recombination. The energy difference between the valence band edges of two materials at their contact is known as the valence band offset (VBO). There is a slight barrier for holes between PC61BM (ETL) and $CH_3NH_3SnI_3$ (absorber), as indicated by the VBO of 0.22 eV. The VBO of $CH_3NH_3SnI_3$ (absorber) and PEDOT:PSS (HTL) is 0.64 eV, indicating a larger hole barrier. The energy differential between two materials' conduction band edges at their interface is indicated by the symbol CBO. The CBO of 0.71 eV between PC61BM (ETL) and $CH_3NH_3SnI_3$ (absorber) indicates a substantial electron barrier in this

instance. A lower electron barrier is indicated by the CBO of 0.19 eV between PEDOT PSS (HTL) and $CH_3NH_3SnI_3$ (absorber).

4.4.7 The effect of optimizing ETL on the electrical output of the model cell

Comparing the performance of perovskite solar cells to that of a model cell has allowed researchers to examine the effects of five distinct ETLs. PC61BM, CdS, ZnS, ZnSe, and V2O5 are among the ETLs; each was selected based on its distinct qualities that influence power and stability in the device. Because of its excellent electron mobility and compatibility with perovskite materials, PC61BM is a popular ETL used in perovskite solar cells. PC61BM reduces recombination losses, promotes effective electron transport, and improves overall device performance by creating a homogeneous interface. Another significant ETL with strong electrical conductivity and high electron affinity is CdS. It contributes to increased photovoltaic efficiency by optimizing electron extraction and transport inside the structure of the solar cell. Because of their large bandgaps and stability, zinc and zinc selenium (ZnS and ZnSe) are important ETLs that improve charge separation and decrease interfacial recombination.

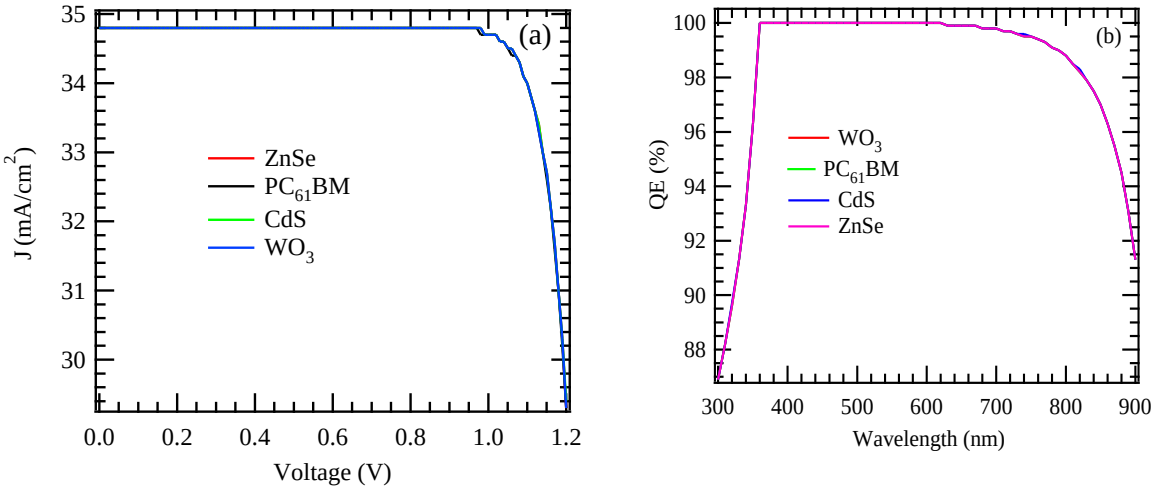

Figure 4.6: Impact of ETL on the J-V characteristics (a) and the QE characteristics (b)

For perovskite solar cells to continue operating at high efficiency and longevity, these characteristics are necessary. High electron affinity and optical transparency are displayed by V_2O_5, which also assists to sustain the stability of the solar cell interface while facilitating effective electron extraction. Its incorporation contributes to increased device longevity and overall performance. This study intends to shed light on the various contributions that these various ETLs have made to improving the performance of perovskite solar cells by analysing and contrasting their respective performances. Combining various ETLs provides a tactical method for optimizing device efficiency overall and balancing electron transport dynamics. With this method, the discussion of each ETL is incorporated into a unified story, highlighting

their unique contributions to the stability and performance of perovskite solar cells. The performance of several ETLs in the model solar cell is shown in Figure 4.6a, based on their current density-voltage (J-V) characteristics. In this investigation, the materials ZnSe, PC61BM, CdS, and WO_3 are compared. First, all ETLs share comparable J-V properties. This implies that both materials have similar beginning current generating capacities. The maximum power point, which maximizes the product of voltage and current density, is another crucial location. This point is crucial for figuring out the solar cell's efficiency.

The voltage, which denotes the greatest voltage the cell can generate in the absence of an external load, varies slightly throughout the various ETLs. It is where the current density decreases to zero. With minor voltage fluctuations, the curve for PC61BM indicates performance comparable to other ETLs. Similar features and equivalent performance to PC61BM are also displayed by CdS and WO_3. ZnSe performs similarly to the other ETLs, with just slight variations in the curve's shape. PC61BM, however, stands out as a superior ETL material for a number of reasons. Its high electron mobility makes it easier to extract electrons efficiently and lowers recombination losses, both of which are essential for increasing the efficiency of solar cells. Furthermore, PC61BM can be used with a variety of solar cell layouts due to its great compatibility with perovskite layers and other organic materials. Its usefulness and appeal are further enhanced by its scalability for large-area applications due to its ease of processing, especially with solution-based approaches.

Conversely, Figure 4.6b illustrates the QE properties of PSCs with four distinct interfacial materials: WO3, PC61BM, CdS, and ZnSe. As can be seen from Table 4.3 superior current density and noticeably better FF, ZnSe performs the best. In comparison to ZnSe, WO_3 and CdS show moderate performance with comparable trends, but lower J_{sc} and FF. The lowest performance, PC61BM, points to potential issues with charge transmission or collection. The results highlight how important it is to use the right interfacial materials for perovskite solar cells in order to maximize their efficiency. These materials can minimize recombination losses and greatly improve charge extraction. PC61BM has poorer performance, but it can be made to work better in perovskite solar cells by experimenting with different device topologies, doping, blending, surface passivation, and hybrid interface layers, among other techniques.

All of the ETL materials had comparable V_{oc}, J_{sc}, and FF values, with only minor variations in PCE, as Table 4.3 demonstrates. PCE values of 37.69% are slightly higher for ZnSe and WO_3 than for PC61BM and CdS. Because of their marginally higher efficiencies and similar V_{oc}, J_{sc}, and FF values, ZnSe and WO_3 seem to be the better options; nevertheless,

PEDOT:PSS has superior absorption and charge transport capabilities, which are essential for reliable cell performance. a great ETL option for the model cell structure as a result.

Table 4.3: Effect of different ETLs on the electrical parameters of the proposed solar cell structure

ETL material	**V_{oc} (V)**	**Jsc (mA/cm^2)**	**FF (%)**	**PCE (%)**
PC61BM	1.5220	34.84	71.04	37.66
CdS	1.5230	34.84	71.04	37.69
ZnSe	1.5225	34.84	71.06	37.69
WO_3	1.5224	34.84	71.06	37.69

4.4.8 The effect of optimizing HTL on electrical output

The J-V characteristics for copper antimony sulphide ($CuSbS_2$), PEDOT: PSS, and copper iron tin sulphide (CFTS), the three HTLs utilized in the model cell construction, are shown in Figure 4.7a. The curves' positions and shapes indicate how well the solar cells' charge transfer and collection processes are working. PEDOT: PSS has superior hole extraction and transport characteristics as evidenced by a higher rise in current density (J) when compared to the other HTLs. A greater J and overall better cell function are the outcomes of this modification.

PEDOT: PSS is consequently a better HTL since it raises the efficiency of the solar cell by improving charge carrier mobility, lowering recombination losses, and improving the quality of the interface between the active layer and the electrode. The optimization of HTLs is demonstrated in Figure 4.7b, which compares the QE for three HTLs ($CuSbS_2$, CFTS, and PEDOT: PSS) at various wavelengths. While all three HTLs function well in the visible light spectrum, PEDOT: PSS shows a continuously strong QE over the whole wavelength range, even at longer wavelengths when $CuSbS_2$ and CFTS's QE begins to somewhat decline. This suggests that PEDOT: PSS performs better overall in devices by having reduced recombination losses due to its superior charge transport characteristics and energy band alignment with the active layer.

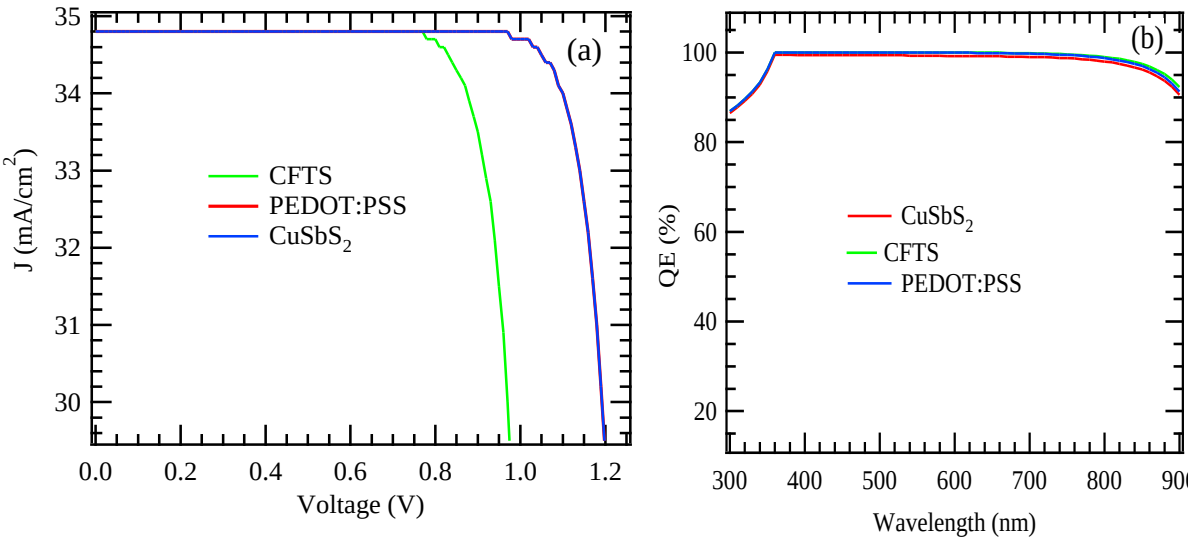

Figure 4.7: The impact of HTL on the J-V characteristics (a) and the QE characteristics (b)

Table 4.4 presents the electrical results of different HTL optimizations of the suggested cell configuration. The table shows that while CFTS and $CuSbS_2$ and PEDOT:PSS have similar V_{oc} and J_{sc} values, PEDOT:PSS obtains a higher PCE of 37.66%. This suggests that PEDOT:PSS is a more efficient option for the HTL in the cell architecture since it converts sunlight into energy more efficiently.

Table 4.4: A comparison of the electrical properties of the proposed solar cell construction with different HTLs

HTL material	V_{oc} (V)	J_{sc} (mA/cm^2)	FF (%)	PCE (%)
PEDOT: PSS	1.5220	34.84	71.04	37.66
CFTS	1.0611	34.83	81.99	30.30
$CuSbS_2$	1.5220	34.84	71.04	37.66

4.4.9 Capacitance-voltage characteristics of the cell

The capacitance of perovskite solar cells, a measurement of their ability to store charge, can be greatly affected by changes in voltage. Capacitance and the electrical characteristics of the materials are intimately related in PSCs. Variations in voltage have an impact on energy levels, which in turn influence the Fermi level and, ultimately, the concentration of charge carriers, which in turn influences the capacitance of the solar cell. Temperature significantly affects a material's dielectric properties, which raises capacitance. Equation 4.4 provides the results of a MS analysis of temperature and how it impacts performance of solar cells (Gelderman *et al.*, 2007).

$$\frac{1}{C^2} = \frac{1}{S^2.\varepsilon.\ q} \times \frac{1}{N_A} \times \left(V - V_{ib} - \frac{k_B T}{q}\right) \qquad (4.4)$$

In this case, the variables N_A corresponds to acceptor density, V_{bi} for flat band potential (built-in voltage), K_B for the Boltzmann constant, T for temperature in Kelvins, and S, q, ε, and capacitance, respectively.

Figure 4.8 makes it clear that capacitance is not affected by low bias (< 0.5 V) and is affected by high bias (> 0.5 V). The V_{bi} is obtained from the MS plots by the tangent intersecting at the voltage axis. The built-in voltage (V_{ib}) at 300 K is + 0.82 eV, as shown in Figure 4.8, and this value is in line with the value found from the band diagram shown in Figure 4.8 at the same temperature. This highlights the resilience of the band alignment in the solar cell design suggested by this research. However, when the temperature increases from 300 to 500 K, the V_{ib} drops from + 0.82 to + 0.53 eV, suggesting increased exciton recombination at elevated temperatures. This phenomenon is explained by the temperature-dependent increase in series resistance. The high V_{bi} value of the suggested cell architecture allows it to maintain 95% of its efficiency at 400 K; but, at 500 K, strong recombination losses at high temperatures results in V_{bi} dropping to about 65%.

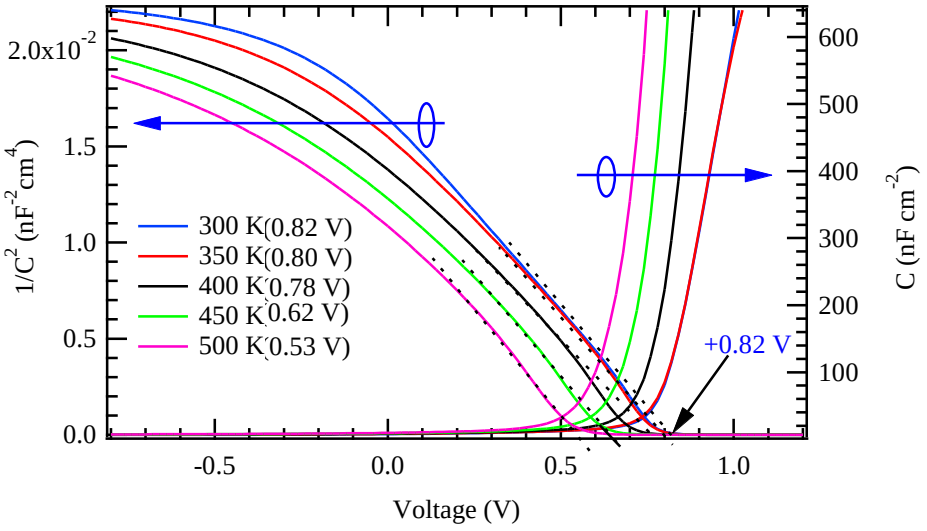

Figure 4.8: The impact of voltage on capacitance and MS analysis

The intrinsic potential difference between the p-type and n-type regions of a p-n junction at equilibrium that results from charge carrier migration is denoted by V_{bi} in Figure 4.8. Initially, diffusion of majority carriers across the junction forms a charged region on each side until equilibrium forms a depletion region, defining the V_{bi}. Temperature affects this voltage by changing the carrier concentration and depletion region width. Band alignment within the junction also plays a crucial role in influencing current flow. These ideas help to explain the electrical behaviour of the p-n junction that is shown, as well as the performance mechanisms of a model cell device.

Voltage variations affect the motion of charge carriers as well as the density and distribution of charges. Changes in voltage have a direct impact on charge carrier separation and transport as well as the internal electric field. The dielectric characteristics of the materials can also be altered by voltage shifts, and this has an impact on how charge is distributed and stored within the solar cell architecture. Optimizing PSC performance improves efficiency, stability, and the general functioning of the solar cell device. It is crucial to comprehend and manage these elements.

4.4.10 Generation and recombination characteristics of the proposed solar cell

Understanding the underlying concepts of generation and recombination is crucial to comprehending the features of a proposed solar cell. Photon absorption is the first step in the production of charge carriers in a solar cell. Photon energy must be at least as high as the bandgap energy (Eg) of the material used to make the solar cell in order for electron-hole pairs to form (Sabri *et al.,* 2023). Greater generation rates are produced by materials with greater absorption coefficients (α) because they absorb photons more effectively (Arunachalam & Sivaperuman, 2024) according to equation 4.5.

$$G = \alpha \,.\, \phi \qquad (4.5)$$

where ϕ represents the photon flux.

For materials having a direct bandgap, the recombination of electrons and holes results in the emission of a photon. Another electron or hole receives the energy from recombination. Defect states within the bandgap facilitate the Shockley-Read-Hall (SRH) recombination, which is significant in defective materials (Vedel *et al.,* 2023). Equation 4.6 provides information on the SRH recombination rate.

$$R_{SRH} = \frac{nP - n_i^2}{\tau_p\,[n + n_i] + \tau_n\,(P + n_i)} \qquad (4.6)$$

Here, τ_p and τ_n are carrier lifetimes, and n_i is the intrinsic carrier concentration. Equation 4.7 states that in an equilibrium, the rates of generation and recombination are identical.

$$G = R \qquad (4.7)$$

Conditions that are out of balance are brought about by illumination, which speeds up the production rate and produces more electron-hole pairs. V_{oc} is impacted by recombination, whereas charge carrier production contributes to photocurrent. Reduced carriers available for current due to high recombination rates lower V_{oc}. QE gauges how well absorbed photons transform into charge carriers. Because there are fewer carriers available for collection, a high

recombination rate reduces QE. SRH recombination events can be decreased via surface recombination through passivating dangling bonds and reducing defects (Min *et al.*, 2024).

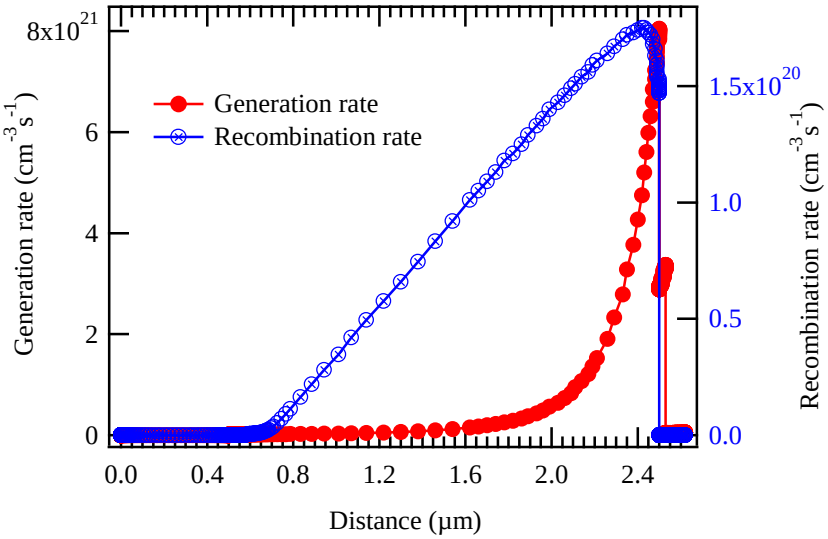

Figure 4.9: Generation –recombination characteristics

The process of the suggested solar cell device is depicted in Figure 4.9, emphasizing a number of critical phases intended to effectively convert solar energy into electrical energy. It displays the rates of recombination and carrier production brought on by optical excitation. Within the light-harvesting layer of the model cell architecture, light enters the device from the ETL side, where exciton production and recombination rates are lower than on the HTL side. Therefore, Figure 4.9 makes it clear that the generation rate outpaces the recombination rate, improving cell operational performance and producing reliable electrical results. Greater surface area improves light absorption without appreciably raising recombination, which improves the device architecture's operating efficiency. Optimizing the production and recombination processes are essential for a solar cell to function efficiently. Device efficiency is increased by maximizing electron-hole pair formation through material and structural design and reducing recombination through defect management and passivation. Therefore, by comprehending these traits, specific enhancements that result in increased effectiveness and enhanced device functionality can be made. Note the discrepancies between the right and left axes of Figure 4.9 in order to clearly observe this occurrence.

4.4.11 The effect of series resistance on electrical parameters

A perovskite solar cell's series resistance (Rs) significantly influences both its electrical properties and the device structure's overall performance. These materials have inherent resistance, contact resistance, and resistance resulting from the movement of charge carriers

inside the device. They come from several sources. The efficiency of a solar cell in converting photon energy into electrical power is measured by the FF, and Rs lowers this value.

Higher series resistance lowers FF by lowering the useful output voltage through voltage drops across the resistance (Uddin *et al.*, 2024). Furthermore, the solar cell device's V_{oc} decreases as a result of series resistance. A cell's ability to conduct current can be hampered by excessive series resistance, which lowers the J_{sc}. Rs has a major impact on the PSC's total PCE. Usually, higher series resistance leads to lower power conversion efficiency because of voltage and current losses (Saha & Panda, 2023). Many techniques are employed to counteract the effects of Rs and improve PSC performance, including refining device architectures, enhancing contacts and interfaces, using materials with reduced resistance, and adopting fabrication techniques that reduce resistive losses (Ahmed *et al.,* 2024). Enhancing PSC performance and, thus, increasing its competitiveness as sustainable renewable energy technologies in the near future, requires an understanding of and reduction in series resistance.

In this work, the series resistance (RS) was varied from 0 to 10 Ω cm^2, while the shunt resistance (RSH) was maintained at a standard value of 1.0 × 103 Ω cm^2, which is frequently utilized in the production of commercial solar cells. As seen in Figure 4.10a above, V_{oc} is unaffected by an increase in Rs, but J_{sc} is essentially constant on increasing Rs between 0 and 7 Ω cm^2 but declines to 34.84 mA/cm^2 at 8 Ω cm^2 and stays constant up to 10 Ω cm^2. As Rs increases, Figure 10c indicates that the PCE decreases from 39.9% to around 27.02%, yet the FF consistently decreases from 71.5% to 50.94 as Rs increases. As a result, FF is a crucial statistic for determining RS. Variations in RS have a substantial impact on the solar device's PV performance, as Figure 4.10 illustrates. Interface barriers, the material's resistance to light absorption, metal-based electrodes, and the interlayers that gather excitons are the sources of RS.

In Figure 4.10b, V_{oc} does not change while other factors or circumstances do. Numerous fundamental physics concepts can be used to explain this phenomenon. First, the difference between the quasi-Fermi levels of electrons and holes, which is impacted by the semiconductor's bandgap, temperature, and carrier recombination dynamics, is the main factor determining V_{oc}. V_{oc} will also stay consistent if the perovskite material's bandgap energy stays constant. The recombination processes are also quite important. V_{oc} will not change much if the recombination rates and mechanisms stay the same. This is possible if the interfaces with other materials, the perovskite layer's quality, and the defect density are all constant. V_{oc} is also influenced by photo-generated charge carrier concentration. A stable V_{oc} is produced when the rate of electron-hole pair creation is constant under constant light intensity. Another element

affecting V_{oc} is temperature. The thermal energy contribution to carrier dynamics stays constant, maintaining V_{oc} constant, provided that the temperature is constant during measurement.

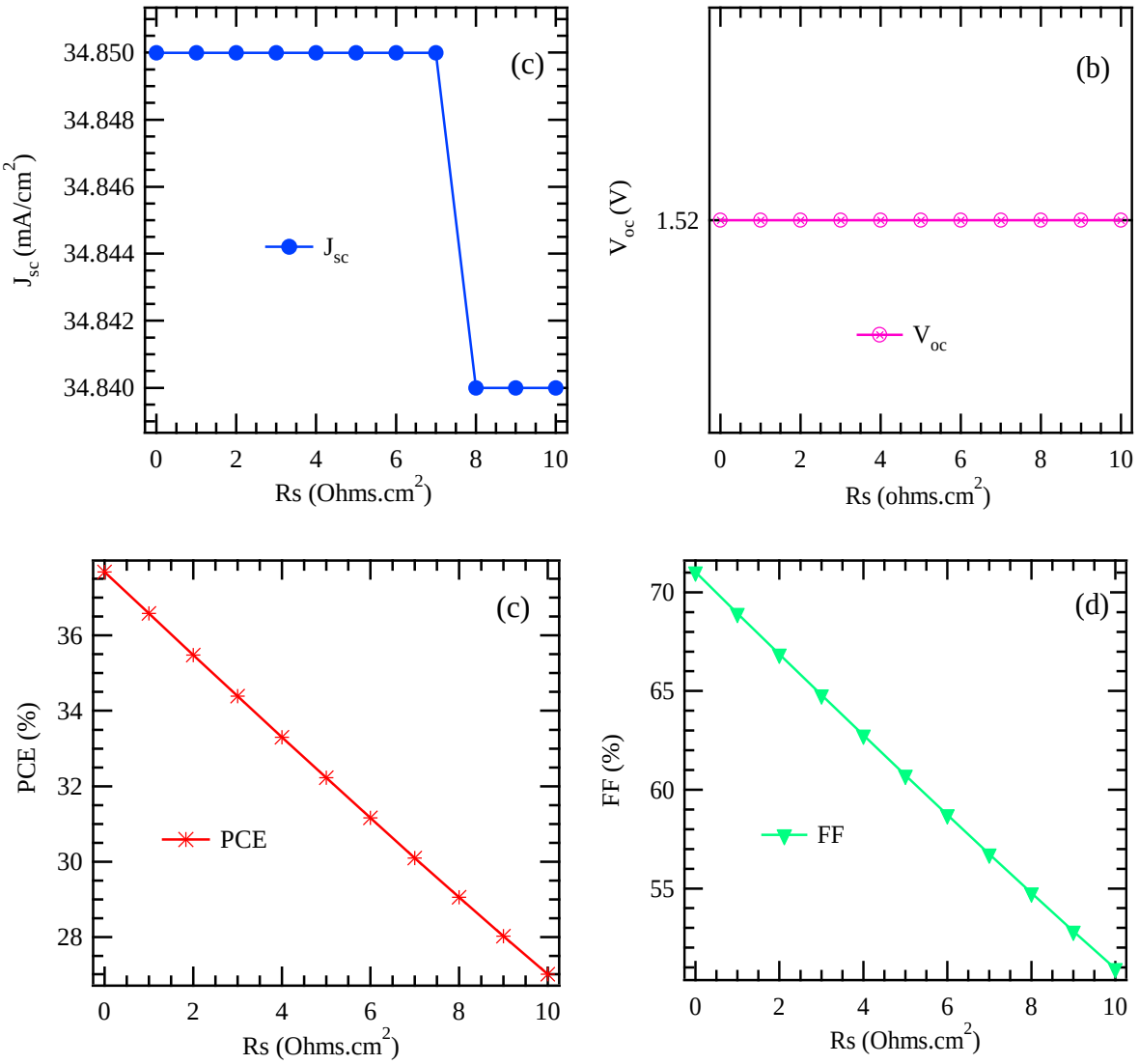

Figure 4.10: Effect of series resistance on the model cell's electrical parameters: (a) J_{sc}, (b) V_{oc}, (c) PCE, and (d) FF

The quasi-Fermi level splitting for electrons and holes under illumination is represented by the V_{oc}. The splitting stays constant, producing a constant V_{oc}, if both the material's characteristics and the external environment (such as temperature and light intensity) are stable. The electrical properties, including V_{oc}, will also be consistent across various measurements or devices if the perovskite material and the other layers in the solar cell structure are homogeneous and consistent across the device. Consequently, in the circumstances or devices under comparison, the constant V_{oc} in Figure 4.10b implies that the variables influencing it,

such as the bandgap, recombination rates, carrier concentration, and temperature, are stable and uniform.

4.4.12 The effect of shunt resistance on electrical parameters

The performance of a perovskite solar cell is largely determined by its shunt resistance (RSH). It is a crucial electrical characteristic that affects the operational stability and efficiency of the cell. In the PCE of the solar cell architecture, RSH is essential. Elevated RSH diminishes current leakage, averting power outages and preserving elevated PCE. On the other hand, a smaller RSH causes a higher leakage current, which reduces the performance of the cell. RSH has a direct impact on the solar cell's FF. Significantly; a greater RSH improves the FF, which gauges the cell's capacity to power a connected load. RSH also affects the solar cell structure's V_{oc}.

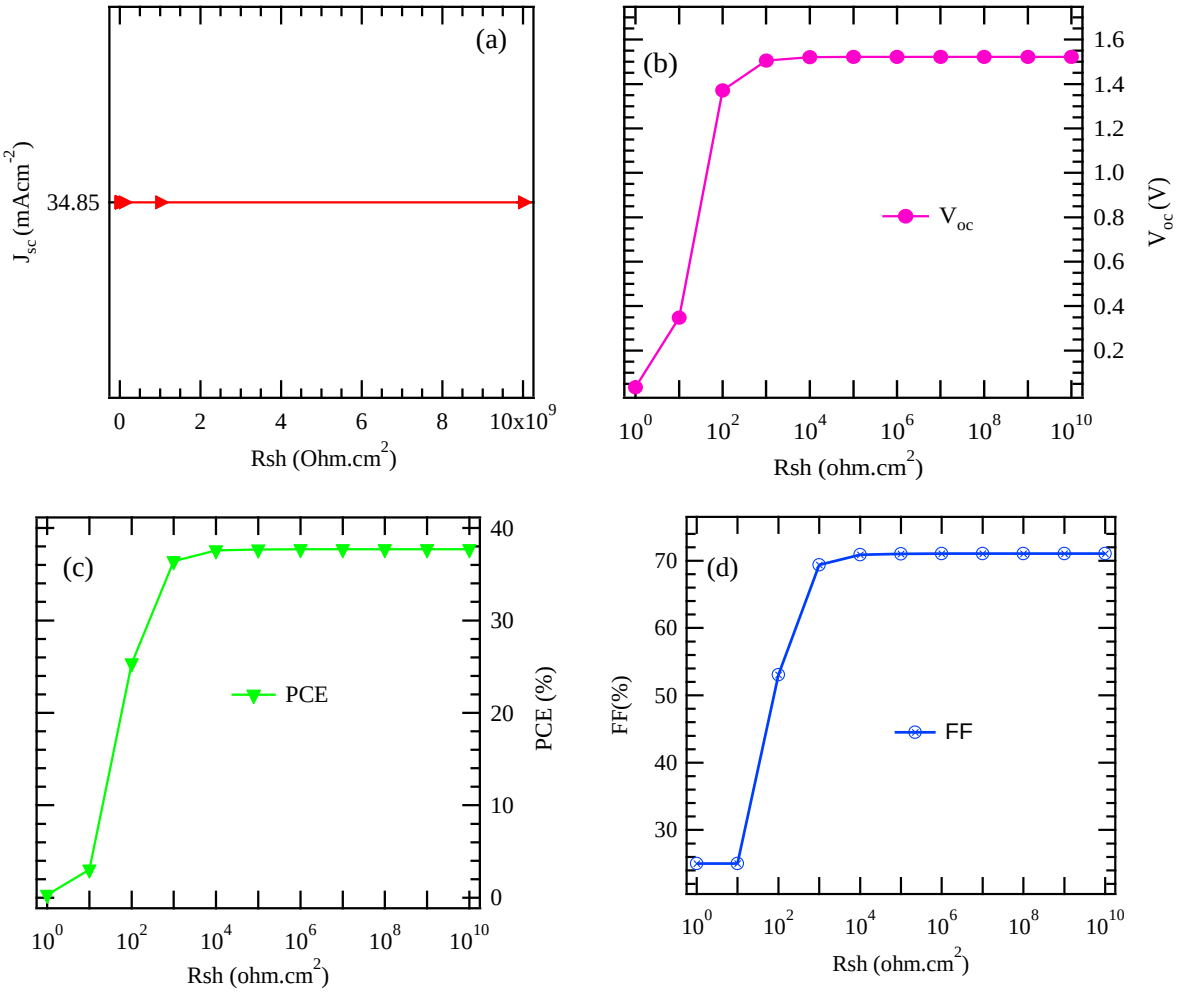

Figure 4.11: Impact of shunt resistance on electrical output (a) J_{sc}, (b) V_{oc}, (c) PCE and (d) FF

Increasing RSH usually results in an overall improvement in the PCE of the solar cell, as Figure 4.11a illustrates. A solar cell device that strives for high efficiency would therefore want a higher RSH value. Notably, as Figure 4.11a shows, RSH has very little effect on J_{sc}. With increasing RSH, J_{sc} in this type device fluctuates slightly, but stays mostly constant when RSH rises from 100 Ω cm^2 to 1010 Ω cm^2. Conversely, as the shunt resistance rises, the V_{oc} at which the device runs essentially stays the same (Figure 4.11b). As the R_{SH} increases, the V_{oc} increases from 0.035 V to 1.5 V before levelling off. Raising RSH causes the exciton loss to be reduced, which raises Voc. The PV device's PCE rises noticeably when the RSH is increased, from 0.9% to 38%, after which it essentially stays constant, as shown in Figure 4.11c.

Figure 4.11d shows that FF first stays constant between 100 and 101 cm^2, after which it climbs gradually to reach an ideal value of almost 71% at 1010 cm^2. Therefore, while designing and producing solar cells for commercial use, an increase in RSH is necessary to achieve optimal photoelectric conversion in the solar cell devices, but a prudent decrease in RS is also necessary.

Higher RSH generally improves voltage performance by decreasing leakage current and increasing Voc. RSH has an impact on PSC stability and dependability. The performance of the cell gradually deteriorates due to issues like hot spots and localized increased current flow caused by lower RSH. PSC hysteresis behaviour is influenced by RSH. In the end, reduced RSH may intensify hysteresis effects, leading to changes in the J-V properties of the cell under various operating circumstances. The proper balance of shunt resistance and other electrical factors must be determined by engineers when designing materials and device constructions to maximize PSC performance.

4.4.13 The impact of changing electron affinity on cell performance

The electron affinity (EA) of the materials used in PSCs is a crucial factor in the overall performance and efficiency of these devices. PSCs are usually made up of layers, with the ETL and HTL sandwiched between the perovskite layer. In the perovskite layer, electrons are activated by photon absorption. To create an electric current, excited electrons must flow through the material efficiently. The perovskite's higher EA can improve electron extraction, which will raise the solar cell's efficiency. For this reason, precise energy band alignment between the ETL and the perovskite layer is crucial. Electrons from the perovskite layer can travel more easily into the ETL when their electron affinities match, which lowers energy losses and improves device performance.

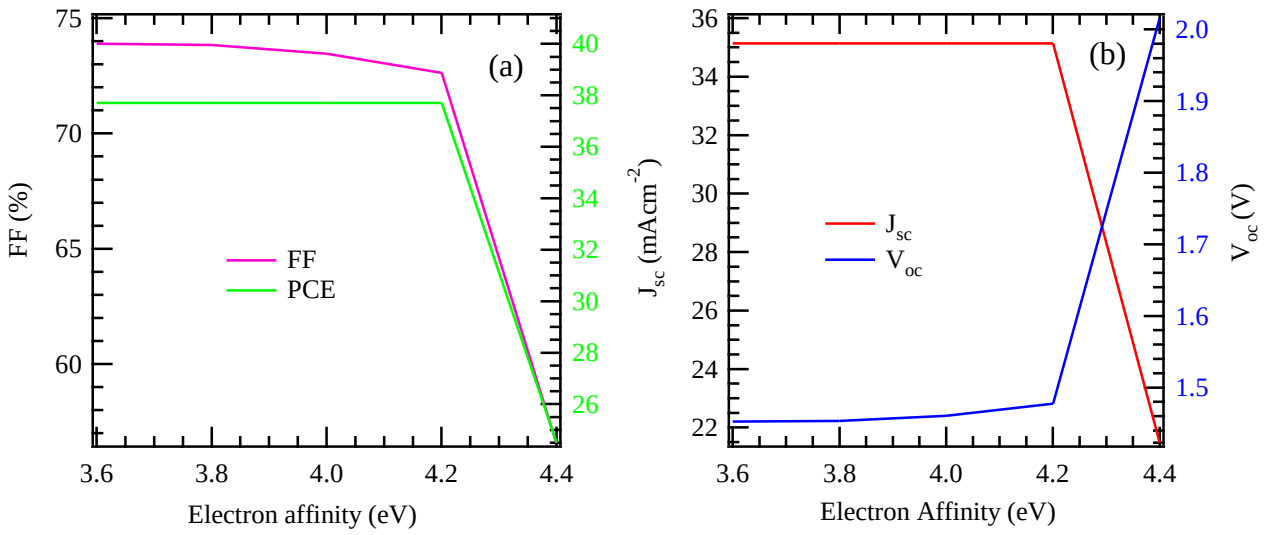

Figure 4.12: The impact of changing electron affinity on (a) FF and PCE (b) J_{sc} and V_{oc}

Figure 4.12a shows that when an electron affinity of 4.2 eV is obtained, a gradual decline in PCE occurs after an increase in PCE. Conversely, FF declines gradually from 3.6 eV to 4.2 eV and then drops off rapidly to approximately 57% at 4.4 eV. While the PCE values drop from 39.9% to 27.02% with an increase in EA, the FF consistently drops from 71.5% to 50.94%. Figure 4.12b illustrates how J_{sc} essentially stays constant up until an EA of 4.2 eV, at which point it abruptly decreases to 21.8 mA/cm^2. On the other hand, as Figure 4.12b shows, the V_{oc} increases linearly once the electron affinity is raised from 3.6 to 4.2 eV, increasing continuously throughout.

EA affects charge recombination processes, which in turn affects the stability of the cell. Increased charge recombination may result from a reduced EA in the PSCs, which would ultimately reduce PCE and stability. The quality of the interfaces between the various layers that make up the solar cell structure is also impacted by these phenomena. An ideal EA helps build better interfaces, reduce errors, and improve the device's overall performance. As a result, changing a material's electron affinity in a PSC can have a big impact on the device's overall functionality, stability, charge transfer, and efficiency.

4.4.14 The effect of band gap of the absorber on electrical output characteristics

A material's bandgap is essential for its use in solar cells, particularly PSCs. It has multiple direct effects on their electrical output; the bandgap establishes the range of light wavelengths that the material may effectively absorb (Zhang *et al.*, 2023). An ideal bandgap in photovoltaic cells guarantees absorption of visible and near-infrared light (Liu *et al.*, 2023). Ineffective absorption may result from departures from this range. When photons are absorbed,

the band gap's size influences how electron-hole pairs are created (Chatterjee *et al.,* 2023). To maximize efficiency, there must be a balance between minimal energy loss and effective absorption. To produce electrical energy, charge carriers holes and electrons must be transported to the electrodes efficiently.

Table 4.5: Impact of changing the absorber's band gap on the suggested solar cell

Band gap (eV)	**V_{oc} (V)**	**J_{sc} (mA/cm^2)**	**FF (%)**	**PCE (%)**
1.1	1.1868	42.96	75.54	38.52
1.3	1.5220	34.84	71.04	37.66
1.5	6.7227	22.75	17.69	33.02
1.7	8.6840	21.54	13.73	25.69
1.9	6.8362	16.42	17.37	19.49
2.1	4.3043	12.20	27.20	14.29
2.3	3.0495	9.40	37.67	10.79

Table 4.5 presents the performance characteristics of various bandgap solar cells, highlighting their influence on device metrics like PCE, V_{oc}, J_{sc}, and FF. It is obvious that a wider bandgap usually results in a higher potential difference, which raises V_{oc}, whereas a smaller photon count decreases J_{sc} by stimulating fewer electrons. When the bandgap of the material increases, FF slightly increases after initially decreasing with greater bandgaps. PCE peaks at 1.1 eV band gap, emphasizing how crucial it is to balance V_{oc}, J_{sc}, and FF for the best possible device architectural efficiency. Lower bandgaps show promise for achieving larger PCE and improved device operational performance, especially in the 1.1 eV to 1.3 eV range. The analysis highlights how difficult it is to maximize solar cell performance and how important it is to choose parameters carefully.

Effective charge transfer depends on carrier mobility and diffusion length, both of which are indirectly influenced by the bandgap. Band gap influences J_{sc} and V_{oc}, among other characteristics. While a narrower band gap can improve Jsc but may lower V_{oc} due to higher recombination, a wider band gap tends to increase V_{oc} but may limit J_{sc} due to reduced absorption. The band gap affects elements such as carrier mobility, recombination rates, and resistances, which in turn affects the FF and the solar cell's overall efficiency (Hossain *et al.*, 2023). In conclusion, the band gap has a major impact on the perovskite materials' electrical output properties, such as light absorption, charge production, transport, V_{oc}, J_{sc}, FF, and PCE. Consequently, determining the ideal bandgap is essential to optimizing PSC performance.

The physical and electrical characteristics of each layer, including thickness, doping concentrations, and most importantly, the band gap (Eg) of materials like $CH_3NH_3SnI_3$, were first determined in order to perform the bandgap energy optimization. The energy threshold needed to excite electrons from the valence band to the conduction band is determined by the band gap, which makes it crucial because it directly affects the photovoltaic (V_{oc}) that the solar cell generates when it is illuminated. Under each scenario, SCAPS-1D calculated the associated J-V characteristics of the solar cell by varying the bandgap of $CH_3NH_3SnI_3$ across a range of 1.1 eV to 2.3 eV, as shown in Table 4.5. The changes in J_{sc} with applied voltage (V) are illustrated by the J-V characteristics. The correctness of the simulations may then be verified by comparing the findings to theoretical predictions, which will also help to clarify how differences in the bandgap affect the performance of the solar cell. These simulations enhance our understanding of how material parameters affect device efficiency in photovoltaic applications and offer valuable insights into optimizing solar cell design.

4.4.15 The impact of donor density on solar device electrical characteristics

The number of dopants that contribute free electrons to produce excess negative charge carriers in a semiconductor device is measured by the donor density within the solar device (Morab *et al.,* 2023). The electrical properties the solar cell is notably influenced by this density. Higher donor densities raise the carriers' (free electrons) concentration, which may improve the semiconductor material's conductivity (Chauhan *et al.,* 2023). The donor density of a solar cell affects its V_{oc}. Higher donor densities can generally increase V_{oc} by reducing recombination losses and enabling more effective electron-hole pair separation. As more charge carriers become accessible for producing current, higher donor concentrations can increase photocurrent. The FF, which represents the solar cell's performance in relation to its theoretical maximum, is similarly influenced by donor density. FF can be improved by optimal donor densities because they lower resistive losses inside the cell. Donor density affects the solar cell's total efficiency.

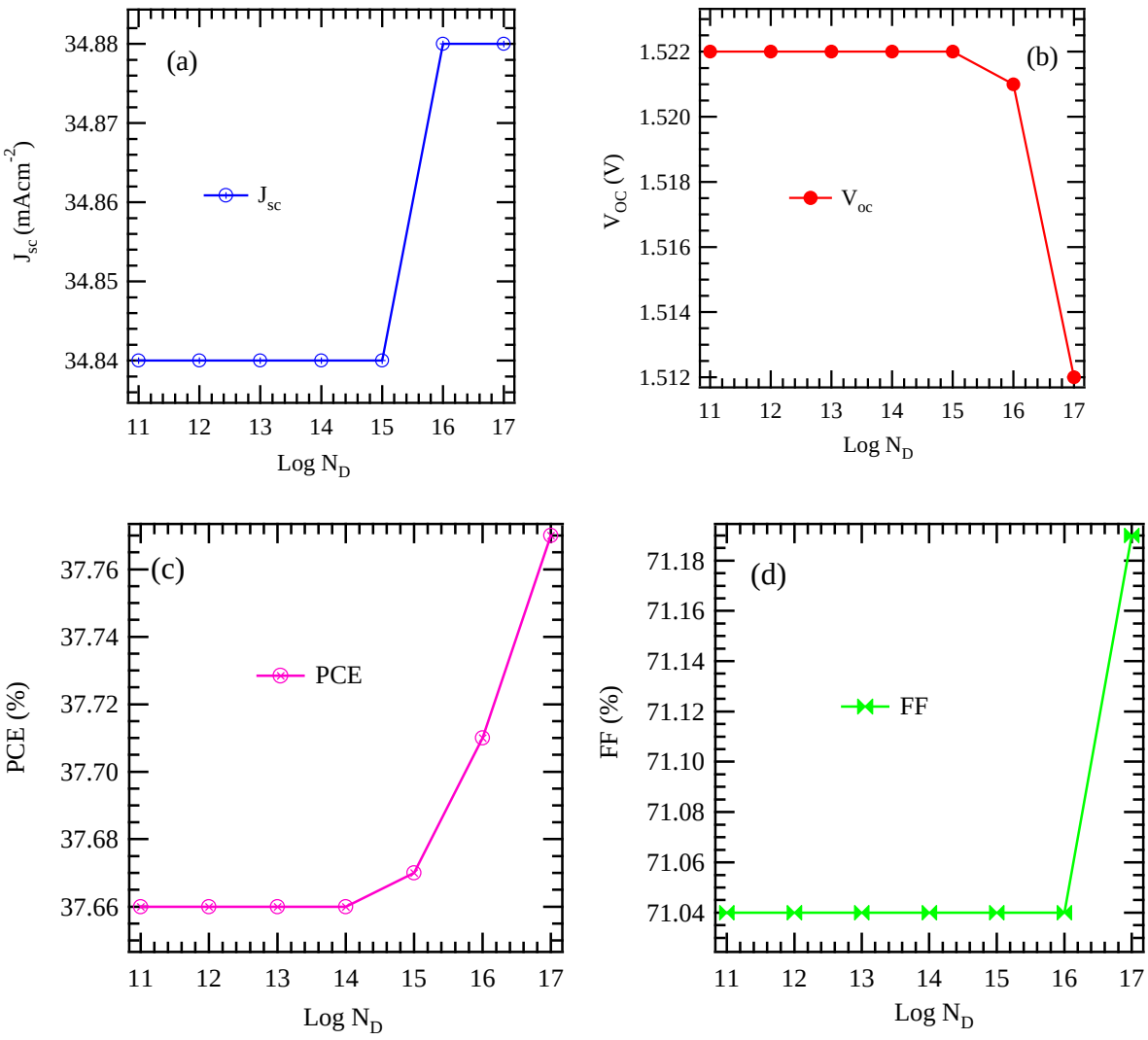

Figure 4.13: Impact of donor density on the suggested solar device's electrical output: (a) J_{sc}, (b) V_{oc}, (c) PCE, and (d) FF

The impact of donor density on the model cell's different electrical properties is shown in Figure 4.13. The J_{sc} appears to be constant in Figure 4.13a between donor densities of 10^{11} cm^{-3} and 10^{14} cm^{-3}. After that, it increases and eventually levels off at 10^{17} cm^{-3}. J_{sc} initially stays mostly unchanged as donor density increases, suggesting that higher donor density promotes charge carrier production independently of J_{sc}. J_{sc} increases significantly above a certain value before levelling off and becoming less affected by additional increases in donor density. The V_{oc} falls between donor densities of 10^{15} cm-3 and 10^{17} cm^{-3}, but it stays constant between donor densities of 10^{11} cm-^{3} and 10^{15} cm^{-3}, as Figure 4.13b illustrates. It is evident that going above a certain threshold increases recombination, which eventually lowers V_{oc}. This emphasizes the necessity of carefully injecting donor density to maximize device efficiency. Figure 4.13c shows that the PCE grows gradually to reach an optimal value of roughly 37.8% at 10^{17} cm^{-3}, after remaining constant between donor densities of 10^{14} cm^{-3} and

10^{14} cm^{-3}. This suggests that while an initial rise in donor density has no discernible effect on PCE, after a certain point, PCE begins to grow, indicating an area of donor density that is optimally efficient. In the end, Figure 4.13d shows that as donor density increases from 10^{11} cm-3 to 10^{16} cm^{-3}, FF is mostly constant. However, it then increases dramatically to reach a maximum at roughly 71.2% at 10^{17} cm^{-3}.

Donor concentrations that are properly controlled can improve carrier mobility, prevent recombination losses, and increase device efficiency. The fact that there is an ideal range for donor density must be acknowledged. Overly low concentrations may limit carrier mobility and conductivity, which can both lower the performance of the solar cell, while extremely high concentrations may increase recombination losses. As a result, optimizing donor density is essential for creating solar devices that work well. In order to modify these characteristics and achieve the required electrical performance in solar cell topologies, fabrication techniques and material engineering are critical components.

4.4.16 The impact of acceptor density on electrical parameters

If other parameters like mobility stay constant, higher acceptor densities typically result in higher conductivity. By adding more energy levels closer to the valence band, the density of acceptors modifies the band structure of the semiconductor, changing the energy gap and ultimately the semiconductor's electrical characteristics. A fundamental practice in semiconductor device engineering is manipulating acceptor density by doping procedures. This is necessary to enable fine control of electrical properties that are suited to particular applications. Figure 4.14a illustrates that as the density of acceptors rises from 10^{11} to 10^{15} cm^{-3}, the J_{sc} values stay essentially constant until they decrease between 10^{15} and 10^{17} cm^{-3}. Conversely, the V_{oc} value remains constant between 1×10^{11} and 1×10^{15} cm^{-3} prior to decreasing between 10^{15} and 10^{17} cm^{-3} as acceptor density increases (Figure 4.14b). Accordingly, when layer thickness and acceptor density rise, so do the electrical characteristics of methyl ammonium triiodide perovskite-based solar cells.

Doping semiconductor materials strategically uses acceptor components to tailor their properties. Increases in acceptor density have an effect on the doping concentration, which in turn affects how wide the depletion region is in semiconductor junctions or diodes. Therefore, acceptor density affects many different characteristics such as carrier concentration, conductivity, mobility, band structure, and more, and it has a major impact on the electrical behaviour and efficiency of semiconductor devices.

Conversely, Figure 4.14c depicts the relationship between the acceptor density and the PCE, with the PCE being constant between 10^{11} and 10^{14} cm^{-3}, exhibiting a minor decline at

10^{15} cm^{-3}, and then increasing to 37.76% at 10^{17} cm^{-3}. This fast increase enhances the electrical results of the device by suggesting better charge carrier pickup and lower recombination losses at greater acceptor densities. Figure 4.14d shows that FF stays steady at roughly 71.04% for the range of $10^{11}cm^{-3}$ to $10^{16}cm^{-3}$, suggesting that changes in NA within this range have minimal impact on the value of FF. This may indicate that other variables are more significant or that the system has reached a plateau; still, the FF approaches 71.16% when the N_A rise to $10^{15}cm^{-3}$. Higher doping concentrations after this point greatly improve the FF, maybe as a result of better electrical characteristics or lower recombination losses.

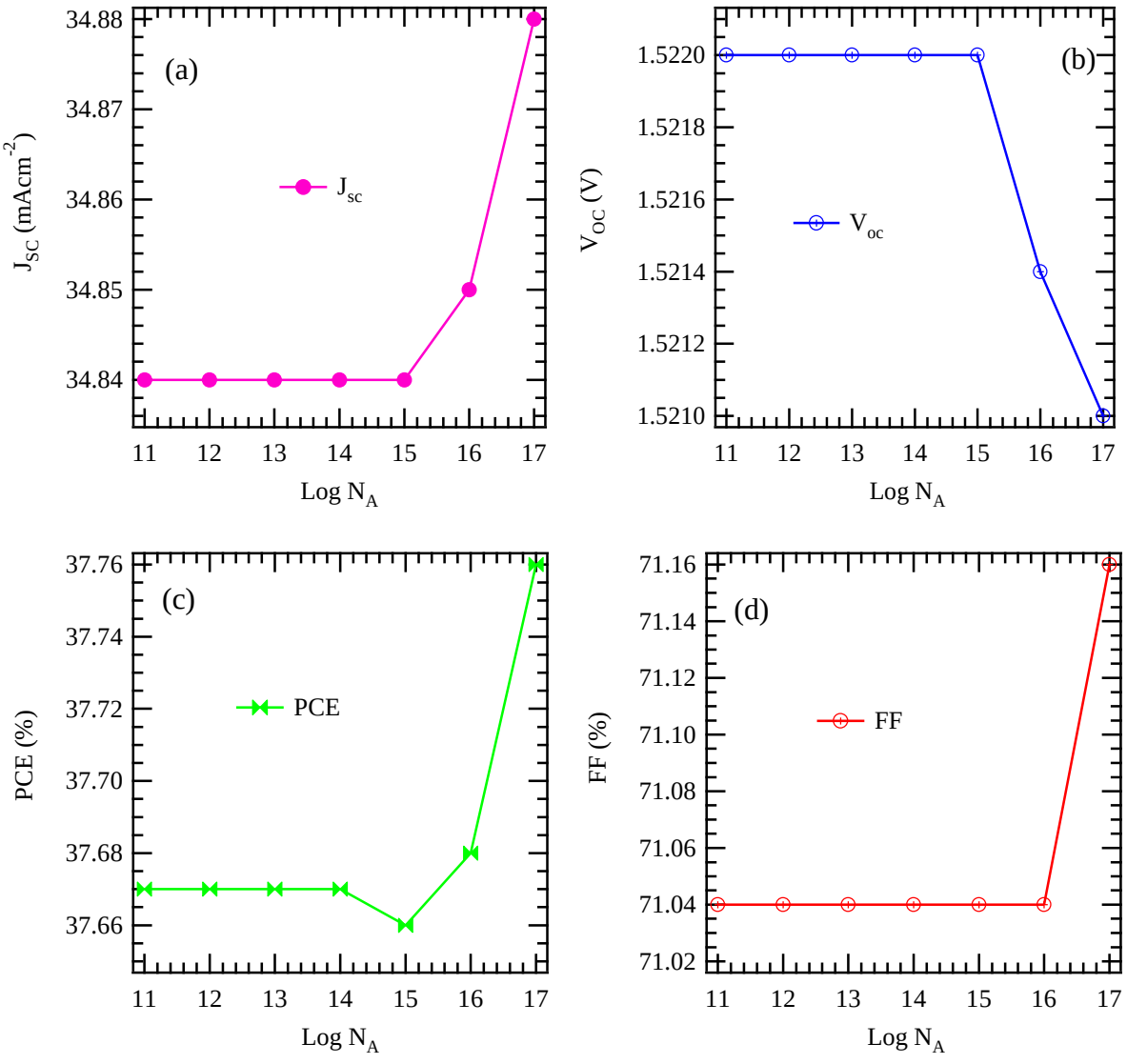

Figure 4.14: Acceptor density's impact on the proposed solar device's electrical output is shown in (a) J_{sc}, (b) V_{oc}, (c) PCE, and (d) FF

4.4.17 Effect of defect density on the absorber layer

Particularly in materials like $MAPbI_3$, methyl ammonium iodide (MAI) is essential to the creation of the perovskite structure. The final perovskite layer's defect density and crystallinity are determined by the quality and stoichiometry of MAI. Defects can be passivated by keeping the stoichiometric balance in check and making sure MAI is pure; on the other hand, an excess or lack of MAI can result in iodine vacancies or defects related to MAI, respectively. Various tactics have been devised to decrease the number of defects in PSCs. Enhancing MAI concentration is one practical strategy.

Defect development can be reduced by carefully controlling the MAI to PbI_2 ratio during solution preparation (Hwang, 2023). Furthermore, imperfections can be passivated with the aid of additive engineering, which entails adding tiny amounts of chemicals like cesium or formamidinium (Lee & Park, 2023). By improving crystal quality, post-treatment techniques including solvent annealing, thermal annealing, or vapour-assisted treatments can also help lower defect density. Defect density is another factor that affects PSC stability. Degradation may occur more quickly at high defect density when exposed to environmental stressors such heat, moisture, and UV light. Ion movement is facilitated by defects, which adds to PSC hysteresis and chronic instability. In conclusion, controlling the absorber layer's defect density is essential for enhancing the stability, performance, and efficiency of perovskite solar cells. This includes paying close attention to the quality and stoichiometry of MAI. To achieve low-defect perovskite layers and increase the overall efficacy of PSCs, innovative fabrication and post-treatment procedures must be used.

The link between defect density and J_{sc} is seen in Figure 4.15a. According to the graph, J_{sc} stays reasonably constant at about 34 mA/cm² when log Nt varies between 0^{11} cm^{-3} and 10^{15} cm^{-3}. Nonetheless, at 10^{15} cm^{-3}, J_{sc} sharply drops, almost to 0 mA/cm², and at 10^{17} cm^{-3}, Nt. This demonstrates the J_{sc} extreme sensitivity to changes in Nt above a particular threshold, pointing to a critical point at which an increase in Nt causes the device's performance to decline noticeably. The V_{oc} normally drops as fault density increases, as seen in Figure 4.15b. This happens as a result of greater Nt causing more recombination events, which lessen charge carrier separation and hence lower the V_{oc}.

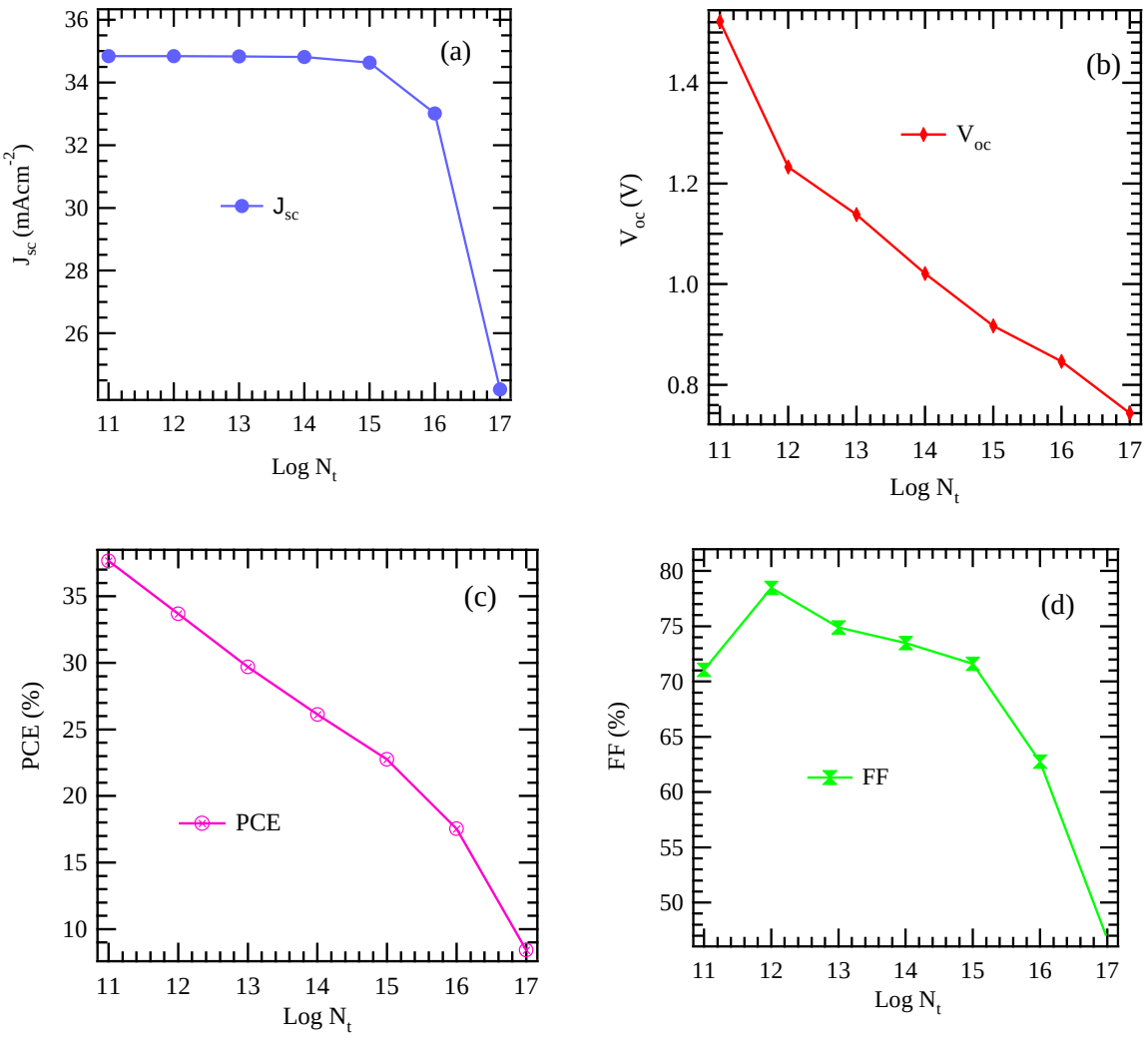

Figure 4.15: Impact of defect density on the suggested cell's electrical results: (a) J_{sc}, (b) V_{oc}, (c) PCE, and (d) FF

The effect of defect density on PCE is seen in Figure 4.15c. PCE gradually decreases between $10^{11}cm^{-3}$ and $10^{17}cm^{-3}$. There are a few possible explanations for this decrease in PCE, including higher defect density, larger-scale thermodynamic inefficiencies, and increased recombination losses. FF, which normally ranges from 50% to 75%, is a critical indicator of system efficiency, according to Figure 4.15d. This work investigates the relationship between FF and the logarithm of either defect density or particle count, covering values between 10^{11} and 10^{17} cm^{-3}. When Nt is $10^{11}cm^{-3}$, FF is almost 70% at first. It then gradually increases and peaks at roughly 75% at $10^{12}cm^{-3}$, suggesting improved performance as a result of ideal particle interactions at lower densities. FF decreases slightly as Nt increases to between 10^{12} cm^{-3} and 10^{15} cm^{-3}, but drops sharply beyond Nt of 10^{15} cm^{-3} to 10^{17} cm^{-3}, dropping to about 50% when Nt is 10^{17} cm^{-3}. This suggests a critical threshold where the cell structure performance deteriorates, possibly because of unfavourable exciton interactions. Comprehending these

dynamics is crucial in the domains of electronics and material science, where controlling particle concentration is key for maximizing efficiency.

4.5 Comparative analysis

Comparing several device configurations, Table 4.6 assesses each one's performance using metrics like V_{oc}, J_{sc}, FF, and PCE. Different layers or materials are used in each configuration to create various solar cells. The model cell suggested in this paper stands out among the mentioned configurations with the highest PCE of 37.66%. It is important to remember that these results are based on simulations, not actual data, suggesting that they are theoretical projections. The results offer important insights into potential material combinations and layer configurations that could improve solar cell efficiency in order to fabricate a robust physical cell, but since it is based on simulation, experimental verification is required to validate its actual performance. The low electrical performance of other similar lead-free solar cells, as shown in Table 4.6, suggests that the suggested solar cell structure has a greater chance of achieving higher operational performance.

Table 4.6: Comparative analysis of other $CH_3NH_3SnI_3$ device structures from literature

Configuration	**Method**	**V_{oc} (V)**	**J_{sc} (mA/cm^2)**	**FF (%)**	**PCE (%)**	**Ref.**
ITO/PEDOT: PSS/$MASnI_3$/PCBM/PEI/Al	Expt.	0.54	33.0	66	6.03	(Mehrabian *et al.*, 2023)
FTO/$CuAlO_2$/$CH_3NH_3SnI_3$/WO_3/Au	Simul.	0.99	33.43	81.05	26.74	(Sarkar *et al.*, 2024)
ITO/PEDOT: PSS/$CH_3NH_3PbI_3$/ZnO/Al	Expt.	0.974	-134	55.12	7.2	(Puspita, 2019)
FTO/c-TiO_2/mpTiO_2/$CH_3NH_3SnI_3$/Spiro-OMeTAD/Au	Expt.	0.92	22.65	67.74	6%	(Srivastava *et al.*, 2022)
FTO/PCBM/ $MAPbI_3$/Cu_2O/Au	Simul.	0.88	27.28918	81.05	19.46	(Deepthi Jayan, 2022)

FTO/PCBM/$CsPbI_3$/Cu_2O/Au	Simul.	1.1104	20.47125	64.47	14.66	(Deepthi Jayan, 2022)
FTO/ZnO/CdS/CZTS/MO	Simul.	0.64	32.96436	83.75	25.72	(Zyoud *et al.*, 2021)
ITO/ PC61BM /$CH_3NH_3SnI_3$/ PEDOT: PSS /Mo	Simul.	1.5220	34.84	71.04	37.66	This work

Lead-based perovskite solar cells FTO/PCBM/$MAPbI_3$/Cu_2O/Au and FTO/PCBM/$CsPbI_3$/Cu_2O/Au show excellent performance metrics and efficiency, but because of their lead toxicity, they pose serious risks to human health and the environment. Conversely, lead-free substitutes, as FTO/c-TiO_2/mp-TiO_2/$CH_3NH_3SnI_3$/Spiro-OMeTAD/Au, offer a more secure and environmentally friendly choice; however, they have fewer difficulties with efficiency and stability. In general, the development of non-toxic, stable, cost-effective, and efficient substitutes is essential to the advancement of solar cell technology in the direction of an energy-secure and independent future.

With a remarkable PCE of 25.72%, the simulation of the chalcogenide-based cell structure FTO/ZnO/CdS/CZTS/MO also shows a noteworthy V_{oc} of 0.64V, a J_{sc} of 32.96436 mA/cm², and an FF of 83.75%. These findings show the remarkable performance and bright future of chalcogenide-based solar cells in the mix of renewable energy sources; however, the model cell under investigation is more efficient than all the cells in Table 6 and provides inspiration for feasible solar cell fabrications for future scalability and production.

4.6 Conclusions

In this pioneering research, we have simulated a solar cell model achieving impressive power conversion efficiency (PCE) of 37.66%, surpassing the Shockley-Queisser limit of 35%. This success is largely attributed to the use of interfacial layers, especially conductive polymers, which significantly enhance charge extraction and boost overall device performance. The optimal thickness for the perovskite layer was determined to be 1000 nm, as thinner layers resulted in harmful exciton recombination. Additionally, the electron affinity was optimized at 4.2 eV; exceeding this value led to reduced efficiency. The study also reveals that the model cell exhibits high thermal tolerance, retaining around 95% of its power at 400 K, as indicated by Mott-Schottky capacitance analysis. Molybdenum (Mo) was identified as a superior back contact material due to its excellent electrical properties, cost-effectiveness, and abundance compared to gold, platinum, and silver. The research highlights the critical role of balancing shunt and series resistance for optimal photoelectric conversion, which is essential for high-

performance, scalable, and commercial solar cells. The donor and acceptor density for PCE and FF was found to be 10^{17} cm^{-3}, and the ideal operating temperature for the model cell was identified as 340 K. The inclusion of buffer layers such as CdS, ZnS, ZnSe, and V_2O_5 proved crucial, as these layers improve charge separation and transport, reduce recombination losses, and enhance energy band alignment and light absorption, significantly boosting overall efficiency. This research provides valuable insights into sustainable energy solutions, contributing to better climate adaptation and a reduced carbon footprint. These findings open new avenues for future innovations in solar cell technology, promising more efficient, reliable, and durable photovoltaic devices.

REFERENCES

Ahamed, T., Rahaman, I., Karmakar, S., Halim, M. A. & Sarkar, P. K. (2023). Thickness optimization and the effect of different hole transport materials on methylammonium tin iodide (CH 3 NH 3 SnI 3)-based perovskite solar cell. *Emergent Materials,* ***6***(1), 175-183.

Ahmed, S., Rahman, N., Haque, M. D., Ali, M. H. & Islam, A. Z. M. T. (2024). Performance investigation of MAPbI3/MASnI3 based all-perovskite tandem solar cell using SCAPS simulation. *Physica Scripta*, ***99***(5), 1-13.

Al Mahmud, J., Rahman, M. F., Kuddus, A., Ali, M. H., Islam, A. S., Haque, M. D., Al Ahmed, S. R., Mushtaq, M. & Ismail, A. B. M. (2023). Design and analysis of a SnS 2/WS 2/V 2 O 5 double-heterojunction toward high-performance photovoltaics. *Energy Advances,* ***2***(1), 1843-1858.

Ali, M. H., Islam, A. S., Haque, M. D., Rahman, M. F., Hossain, M. K., Sultana, N. & Islam, A. T. (2023). Numerical analysis of FeSi2 based solar cell with PEDOT: PSS hole transport layer. *Materials Today Communications,* ***34***(1), 1-15.

Amrillah, T., Prasetio, A., Supandi, A. R., Sidiq, D. H., Putra, F. S., Nugroho, M. A., Salsabilla, Z. & Azmi, R. (2023). Environment-friendly copper-based chalcogenide thin film solar cells: status and perspectives. *Materials Horizons,* ***10***(2), 313-339.

Arunachalam, J. & Sivaperuman, K. (2024). An investigation of the influence of various factors on the electrical performance of a (CuGaS2)-based thin-film solar cell using SCAPS-1D software. *Optik*, ***303***(1), 1-17.

Ašmontas, S. & Mujahid, M. (2023). Recent progress in perovskite tandem solar cells. *Nanomaterials,* ***13***(12), 1-43.

Baigorri, J., Zaversky, F. & Astrain, D. (2023). Massive grid-scale energy storage for next-generation concentrated solar power: A review of the potential emerging concepts. *Renewable and Sustainable Energy Reviews,* ***185***(1), 1-12.

Bandara, R. M. I., Silva, S. M., Underwood, C. C., Jayawardena, K. I., Sporea, R. A. & Silva, S. R. P. (2022). Progress of Pb-Sn mixed perovskites for photovoltaics: a review. *Energy & Environmental Materials,* ***5***(2), 370-400.

Biswas, S. K., Ahmed, M. M., Orthe, M. F., Sumon, M. S. & Sarker, K. (2023). Numerical Investigation of High Efficiency Cu_2SnSe_3 Thin Film Solar Cell with a Suitable ZnSe Buffer Layer Using SCAPS 1D Software. *European Journal of Electrical Engineering and Computer Science,* ***7***(8), 63-70.

Butcher, J. C. (2000). Numerical methods for ordinary differential equations in the 20th century. *Journal of Computational and Applied Mathematics,* ***125***(1-2), 1-29.

Chatterjee, K., Dutta, A., Mishra, S., Bairy, B., Sen, M. B., Gorai, A., Saha, S. K. & Akhtar, A. J. (2023). Impact of tailoring of the defect states and the band gap towards extreme photocatalytic performance and photo-induced conductivity in cobalt doped ZnO QD. *Ceramics International,* ***49***(20), 32768-32778.

Chauhan, P., Agarwal, S., Srivastava, V., Hossain, M. K., Pandey, R., Madan, J., Lohia, P., Dwivedi, D. & Amami, M. (2023). Kesterite CZTS based thin film solar cell: generation, recombination, and performance analysis. *Journal of Physics and Chemistry of Solids,* ***183***(1), 111631-11647.

Chee, A. K.-W. (2023). On current technology for light absorber materials used in highly efficient industrial solar cells. *Renewable and Sustainable Energy Reviews,* ***173***(1), 1-12.

Chen, X. H., Tee, K., Elnahass, M. & Ahmed, R. (2023). Assessing the environmental impacts of renewable energy sources: A case study on air pollution and carbon emissions in China. *Journal of Environmental Management,* ***345***(2023), 1-13.

Cho, H., Kim, J., Kim, M., An, H., Min, K. & Park, K. (2024). A review of problems and solutions in Ni-rich cathode-based Li-ion batteries from two research aspects: Experimental studies and computational insights. *Journal of Power Sources,* ***597***(2024), 1-18.

Cho, S., Pandey, P., Yoon, S., Ryu, J., Lee, D.-G., Shen, Q., Hayase, S., Song, H., Choi, H. & Ahn, H. (2023). Anchoring self-assembled monolayer at perovskite/hole collector interface for wide bandgap Sn-based solar cells with a record efficiency over 12%. *Surfaces and Interfaces,* ***42***(1), 103478.

Chowdhury, T. A., Zafar, M. A. B., Islam, M. S.-U., Shahinuzzaman, M., Islam, M. A. & Khandaker, M. U. (2023). Stability of perovskite solar cells: issues and prospects. *RSC Advances,* ***13***(1), 1787-1810.

Deepthi Jayan, K. (2022). Design and Comparative Performance Analysis of High-Efficiency Lead-Based and Lead-Free Perovskite Solar Cells. *physica status solidi (a),* ***219***(7), 1-14.

Duan, L., Walter, D., Chang, N., Bullock, J., Kang, D., Phang, S. P., Weber, K., White, T., Macdonald, D. & Catchpole, K. (2023). Stability challenges for the commercialization of perovskite–silicon tandem solar cells. *Nature Reviews Materials,* ***8***(1), 261-281.

Ebon, M. I. R., Ali, M. H., Haque, M. D. & Islam, A. Z. M. T. (2023). Computational investigation towards highly efficient Sb2Se3 based solar cell with a thin WSe2 BSF layer. *Engineering Research Express, **5***(2023), 1-23.

Fu, Q. & Jen, A. K. (2023). Perovskite solar cell developments, what's next? *Next Energy, **1***(1), 1-4.

Ganesh, G., Yasin, A., Misnon, I. I., Fakharuddin, A., Schmidt-Mende, L., Ab Rahim, M. H., Thomas, S. & Jose, R. (2023). Augmenting stability and performance in perovskite solar cells: A critical review on perovskite-polymer synergy. *Solar Energy, **257***(1), 266-306.

Gelderman, K., Lee, L. & Donne, S. W. (2007). Flat-Band Potential of a Semiconductor: Using the Mott–Schottky Equation. *Journal of Chemical Education, **84***(4), 1-4.

Ghosh, S., Bera, S., Sardar, S., Pal, S., Camargo, F. V., D'Andrea, C. & Cerullo, G. (2023). Role of Efficient Charge Transfer at the Interface between Mixed-Phase Copper-Cuprous Oxide and Conducting Polymer Nanostructures for Photocatalytic Water Splitting. *ACS Applied Materials & Interfaces, **15***(15), 18867-18877.

Hanna, M. Y., Majidi, M. A. & Nugraha, A. R. (2023). Computational study of III–V direct-gap semiconductors for thermoradiative cell applications. *Nanotechnology, **34***(31), 315705.

Hossain, M. K., Toki, G. I., Madan, J., Pandey, R., Bencherif, H., Mohammed, M. K., Islam, M. R., Rubel, M., Rahman, M. F. & Bhattarai, S. (2023). A comprehensive study of the optimization and comparison of cesium halide perovskite solar cells using ZnO and Cu 2 FeSnS 4 as charge transport layers. *New Journal of Chemistry, **47***(18), 8602-8624.

Hunde, B. R. & Woldeyohannes, A. D. (2023). Performance analysis and optimization of perovskite solar cell using SCAPS-1D and genetic algorithm. *Materials Today Communications, **34***(1), 1-13.

Hwang, I. (2023). Challenges in Controlling the Crystallization Pathways and Kinetics for Highly Reproducible Solution-Processing of Metal Halide Perovskites. *The Journal of Physical Chemistry C, **127***(50), 24011-24026.

Ibarra Michel, J., Dréon, J., Boccard, M., Bullock, J. & Macco, B. (2023). Carrier-selective contacts using metal compounds for crystalline silicon solar cells. *Progress in Photovoltaics: Research and Applications, **31***(4), 380-413.

Imani, S., Seyed-Talebi, S. M., Beheshtian, J. & Diau, E. W. G. (2023). Simulation and characterization of CH3NH3SnI3-based perovskite solar cells with different Cu-based hole transporting layers. *Applied Physics A, **129***(143), 1-13.

Ismail, M., Noman, M., Tariq Jan, S. & Imran, M. (2023). Boosting efficiency of eco-friendly perovskite solar cell through optimization of novel charge transport layers. *Royal Society open science, **10***(1), 1-30.

Jaffri, S. B., Ahmad, K. S., Abrahams, I., Almanqur, L. & Alharbi, Y. T. (2023). Semiconducting Y2O3-ZnO stacked nano-fibrous arrays for interfacial engineering in solar cells, electrical charge storage, and electrochemical water splitting. *Solar Energy,* **266**(1), 1-12.

Juarez-Perez, E. J., Momblona, C., Casas, R. & Haro, M. (2024). Enhanced power-point tracking for high-hysteresis perovskite solar cells with a galvanostatic approach. *Cell Reports Physical Science, **5***(3), 1-20.

Khan, J., Ahmad, R. T. M., Tan, J., Zhang, R., Khan, U. & Liu, B. (2023). Recent advances in 2D organic− inorganic heterostructures for electronics and optoelectronics. *SmartMat, **4***(2), 1-40.

Khelifi, W. & Luscombe, C. K. (2024). Recent Developments in Indacenodithiophene and Indacenodithienothiophene-based Donor-Acceptor Conjugated Polymers: From Design to Device Performance in Organic Electronics. *Progress in Polymer Science**, 151***(5), 1-32.

Kumar, P., You, S. & Vomiero, A. (2023). Recent progress in materials and device design for semitransparent photovoltaic technologies. *Advanced Energy Materials, **13***(39), 1-40.

Laidouci, A., Singh, V., Dakua, P. K. & Panda, D. K. (2023). Performance evaluation of ZnSnN2 solar cells with Si back surface field using SCAPS-1D: A theoretical study. *Heliyon, **9***(10)1-20.

Lee, C.-C., Zhang, J. and Hou, S. (2023). The impact of regional renewable energy development on environmental sustainability in China. *Resources Policy,* **80**(10), 1-40.

Lee, D.-K. & Park, N.-G. (2023). Additive engineering for highly efficient and stable perovskite solar cells. *Applied Physics Reviews, **10***(1), 1-8.

Li, H., Xie, G., Fang, J., Wang, X., Li, S., Lin, D., Wang, D., Huang, N., Peng, H. and Qiu, L. (2024a). Holistic dielectric and buffer interfacial layers enable high-efficiency perovskite solar cells and modules. *Nano Energ. **124***(8), 41-50.

Li, R.& Liu, X. (2022). 13 Hybrid Perovskite. *Emergent Micro-and Nanomaterials for Optical, Infrared, and Terahertz Applications**, Taylor & Francis Online**.363***(8), 29-41.

Li, X., Yu, H., Liu, Z., Huang, J., Ma, X., Liu, Y., Sun, Q., Dai, L., Ahmad, S. & Shen, Y. (2023). Progress and challenges toward effective flexible perovskite solar cells. *Nano-Micro Letters*, ***115***(10), 1-24.

Li, Y., Ma, Z., Hou, S., Liu, Q., Yan, G., Li, X., Yu, T., Du, Z., Yang, J. & Chen, Y. (2024b). Recent progress in hydrogen: From solar to solar cell. *Journal of Materials Science & Technology*, **176**(9), 236-257.

Liu, B., Wang, Y., Wu, Y., Dong, B. & Song, H. (2023). Novel broad spectral response perovskite solar cells: A review of the current status and advanced strategies for breaking the theoretical limit efficiency. *Journal of Materials Science & Technology*, ***140***(9), 33-57.

Mamta, Maurya, K. K. & Singh, V. N. (2021). Enhancing the performance of an Sb2Se3-based solar cell by dual buffer layer. *Sustainability*, ***13***(21), 1-12.

Mehrabian, M., Afshar, E. N. & Akhavan, O. (2023). TiO2and C60 transport nanolayers in optimized Pb-free CH3NH3SnI3-based perovskite solar cells. *Materials Science and Engineering: B*, **287**(15), 1-16.

Min, J., Choi, Y., Kim, D. & Park, T. (2024). Beyond Imperfections: Exploring Defects for Breakthroughs in Perovskite Solar Cell Research. *Advanced Energy Materials*, ***14***(6), 1-22.

Mohammad, A. & Mahjabeen, F. (2023). Promises and challenges of perovskite solar cells: a comprehensive review. *BULLET: Jurnal Multidisiplin Ilmu*, ***2*****(5),** 1147-1157.

Mohammed, M. K., Al-Mousoi, A. K., Kumar, A., Sabugaa, M. M., Seemaladinne, R., Pandey, R., Madan, J., Hossain, M. K., Goud, B. S. & Al-Kahtani, A. A. (2023). Harnessing the potential of Dion-Jacobson perovskite solar cells: Insights from SCAPS simulation techniques. *Journal of Alloys and Compounds*, ***963*****(10),** 171246- 171260.

Morab, S., Sundaram, M. M. and Pivrikas, A. (2023). Review on charge carrier transport in inorganic and organic semiconductors. *Coatings*, ***13***(9), 1-23.

Nazir, S., Ali, A., Aftab, A., Muqeet, H. A., Mirsaeidi, S. & Zhang, J.-M. (2023). Techno-Economic and Environmental Perspectives of Solar Cell Technologies: A Comprehensive Review. *Energies*, ***16***(13), 1-31.

Noh, M. F. M., Arzaee, N. A., Fat, C. C., Tiong, S. K., Teridi, M. A. M. & Zuhdi, A. W. M. (2023). Perovskite/CIGS Tandem Solar Cells: Progressive Advances from Technical Perspectives. *Materials Today Energy*, ***39***(11), 1-30.

Obaideen, K., Olabi, A. G., Al Swailmeen, Y., Shehata, N., Abdelkareem, M. A., Alami, A. H., Rodriguez, C. & Sayed, E. T. (2023). Solar energy: Applications, trends analysis,

bibliometric analysis and research contribution to sustainable development goals (SDGs). *Sustainability*, ***15***(2), 1-34.

Priyadarshini, P., Senapati, S. & Naik, R. (2023). Lead-free organic inorganic hybrid halide perovskites: an emerging candidate for bifunctional applications. *Renewable and Sustainable Energy Reviews,* ***186***(3), 113649.

Puspita, D. (2019). Optimation of Layers Thickness Design of Perovskite Solar Cell (PSC) Using GPVDM Simulation. *Computational and Experimental Research in Materials and Renewable Energy, **2***(2), 56-63.

Rehman, F., Syed, I. H., Khanam, S., Ijaz, S., Mehmood, H., Zubair, M., Massoud, Y. & Mehmood, M. Q. (2023). Fourth-generation solar cells: a review. *Energy Advances,* **2(**9), 1227–1532.

Sabri, S., Malek, R. & Kassmi, K. (2023). Improvement Efficiency of Solar Cells Using III-V Dual Junction: InGaP/GaAs. *Key Engineering Materials, **954***(9), 97-109.

Saha, J. and Panda, S. K. (2023). Overview and comparative analysis of bidirectional cascaded modular isolated medium-voltage AC–low-voltage DC (MVAC-LVDC) power conversion for renewable energy rich microgrids. *Renewable and Sustainable Energy Reviews, **174***(28), 113118.

Sarkar, D., Mottakin, M., Hasan, A. M., Islam, M. A., Haque, M. M., Selvanathan, V., Aminuzzaman, M., Alanazi, A. M. & Akhtaruzzaman, M. (2024). Numerical investigation of Aloe Vera-mediated green synthesized CuAlO2 as HTL in Pb-free perovskite solar cells. *Journal of Taibah University for Science, **18***(6), 1-13.

Song, D., Ramakrishnan, S., Xu, Y. & Yu, Q. (2023). Designing Effective Hole Transport Layers in Tin Perovskite Solar Cells. *ACS Energy Letters*, ***8***(10), 4162-4172.

Soonmin, H., Hardani, Nandi, P., Mwankemwa, B. S., Malevu, T. D. & Malik, M. I. (2023). Overview on different types of solar cells: an update. *Applied Sciences, **13***(4), 2051.

Soultati, A., Tountas, M., Armadorou, K. K., bin Mohd Yusoff, A. R., Vasilopoulou, M. & Nazeeruddin, M. K. (2023). Synthetic approaches for perovskite thin films and single-crystals. *Energy Advances, **2***(24), 1075-1115.

Srivastava, S., Singh, A. K., Kumar, P. & Pradhan, B. (2022). Comparative performance analysis of lead-free perovskites solar cells by numerical simulation. *Journal of Applied Physics, **131***(17), 1075-1115.

Subudhi, P. and Punetha, D. (2023). Pivotal avenue for hybrid electron transport layer-based perovskite solar cells with improved efficiency. *Scientific Reports, **13***(32), 1-15.

These, A., Koster, L. J. A., Brabec, C. J. & Le Corre, V. M. (2024). Beginner's Guide to Visual Analysis of Perovskite and Organic Solar Cell Current Density–Voltage Characteristics. *Advanced Energy Materials.**14**(21)*, 1-9.

Tobbeche, S., Kalache, S., Elbar, M., Kateb, M. N. & Serdouk, M. R. (2019). Improvement of the CIGS solar cell performance: structure based on a ZnS buffer layer. *Optical and Quantum Electronics, **51***(1-13), 1-13.

Uddin, M. N. & Afrin, P. (2024). Comparative performance analysis of poly (3-hexylthiophene-2, 5-dial) and [6, 6]-phenyl-C61 butyric acid methyl ester-based organic solar cells in bulk-heterojunction and bilayer structure using SCAPS. *Optik, **302**,(*44), 1-23.

Uddin, M. S., Hosen, R., Sikder, S., Mamur, H. & Bhuiyan, M. R. A. (2024). Photovoltaic performance enhancement of Al/ZnO: Al/i-ZnO/CdS/CIGS/Pt solar cell using SCAPS-1D software. *Next Energy, **2***(14), 1-11.

Vedel, C. D., Gunst, T., Smidstrup, S. & Georgiev, V. P. (2023). Shockley-Read-Hall recombination and trap levels in In 0.53 Ga 0.47 As point defects from first principles. *Physical Review B, **108***(9),. 1075-1115.

Wang, Z., Nayak, P. K., Caraveo-Frescas, J. A. & Alshareef, H. N. (2016). Recent developments in p-Type oxide semiconductor materials & devices. *Advanced Materials, **28***(20), 3831-3892.

Wright, M., Stefani, B. V., Jones, T. W., Hallam, B., Soeriyadi, A., Wang, L., Altermatt, P., Snaith, H. J., Wilson, G. J. & Bonilla, R. S. (2023). Design considerations for the bottom cell in perovskite/silicon tandems: a terawatt scalability perspective. *Energy & Environmental Science, **16***(43), 4164-4190.

Yang, S., Duan, Y., Liu, Z. & Liu, S. (2023). Recent advances in CsPbX3 perovskite solar cells: focus on crystallization characteristics and controlling strategies. *Advanced Energy Materials, **13***(33), 22-33.

Zeng, G., Pu, D., Huang, L., Guan, H., Zhou, S., Zhou, J., Shen, W., Li, G., Fang, G. & Ke, W. (2023). Enhancing the performance of tin-based perovskite solar cells through solvent purification of tin iodide. *Journal of Materials Chemistry A, **11***(56), 11245-11253.

Zhang, H., Liu, J., Xu, T., Ji, W. & Zong, X. (2023). Recent advances on small band gap semiconductor materials (≤ 2.1 eV) for solar water splitting. *Catalysts, **13***(4), 728-758.

Zheng, Y., Jiang, B., Gao, Z., Lin, G., Sang, N., Chen, L. & Li, M. (2019). Optimization of SnO2-based electron-selective contacts for Si/PEDOT:PSS heterojunction solar cells. *Solar Energy, **193***(15), 502-506.

Zhou, J., Zhang, G., Wang, W., Chen, Q., Zhao, W., Liu, H., Zhao, B., Ni, Z. & Lu, J. (2024). Phase-engineered synthesis of atomically thin te single crystals with high on-state currents. *Nature Communications, **15***(23), 1-10.

Zyoud, S. H., Zyoud, A. H., Ahmed, N. M., Prasad, A. R., Khan, S. N., Abdelkader, A. F. & Shahwan, M. (2021). Numerical modeling of high conversion efficiency FTO/ZnO/CdS/CZTS/MO thin film-based solar cells: Using SCAPS-1D software. *Crystals, **11***(12), 1-21.

CHAPTER FIVE

ADVANCEMENTS IN THE PHOTOVOLTAIC OPTIMIZATION OF A HIGH-PERFORMANCE PEROVSKITE SOLAR CELL BASED ON GRAPHENE OXIDE (GO) HOLE TRANSPORT LAYER

Abstract

The growing demand for efficient and sustainable green energy solutions has spurred the search for high-performance perovskite solar cells (PSCs). This study focuses on optimizing the performance of a cell with the configuration ITO/PC61BM/$CH_3NH_3SnI_3$/GO/Fe, using the SCAPS-1D device simulator. Graphene oxide (GO), known for its exceptional electrical conductivity and mechanical strength, was employed as a hole transport layer (HTL) to enhance charge transport and minimize recombination losses at interfaces. The ideal GO thickness was identified as 50 nm, while the optimal absorber layer thickness was found to be 1000 nm. A comparison of various HTL materials revealed that GO provided superior electrical performance. In-depth analyses of generation-recombination dynamics, carrier transport, and interfacial characteristics offered valuable insights into device operation. The built-in voltage (V_{bi}) was calculated to be 0.31 V from the band diagram at 300 K. The study also explored the influence of donor and acceptor densities on Mott-Schottky (MS) capacitance characteristics, as well as the effects of temperature on MS capacitance analysis. The optimized PSC achieved key performance metrics, including an open-circuit voltage (V_{oc}) of 1.3462 V, a short-circuit current density (J_{sc}) of 34.84 mA/cm², a fill factor (FF) of 77.32%, and a power conversion efficiency (PCE) of 36.27%. The device's quantum efficiency (QE) demonstrated impressive photon capture rates of 85% to 100% between 300 and 700 nm wavelengths. These findings indicate low recombination rates, efficient charge separation, strong light absorption, effective charge collection, low resistive losses, and excellent charge carrier extraction. The choice of HTL material is critical for optimizing device performance. Overall, this study enhances the understanding of PSC device physics and offers valuable guidance for developing advanced, eco-friendly solar energy technologies.

5.1 Introduction

One of the cutting-edge innovations in the field of renewable energy is perovskite solar cells. These cutting-edge gadgets use a unique material structure to transform sunlight into electricity. They derive their name from the mineral perovskite, and their remarkable qualities have demonstrated that they have substantial potential. Their high-power conversion efficiencies enable them to transform a significant amount of solar radiation into useful electricity (Chowdhury *et al.,* 2023). Perovskite materials are a more economical option than

conventional silicon-based solar cells since they are also inexpensive and may be produced utilizing low-temperature, solution-based techniques (Mohammad & Mahjabeen, 2023). PSCs are appealing for reasons more than just being economical and efficient. Their adaptability enables integration into a range of applications, including flexible devices and rooftop installations. Innovative solar energy solutions like portable power sources and building-integrated photovoltaics (BIPVs) are made possible by this versatility. PSCs do, however, confront significant difficulties in spite of their encouraging qualities. Other important considerations are stability and durability, as these materials deteriorate when exposed to moisture, oxygen, and UV light (Ahn & Choi, 2024). Concerns regarding toxicity and environmental effects are also raised by the fact that lead is present in many perovskite compositions (Khan *et al.,* 2024).

To solve these bottlenecks and realize PSCs' full potential, more research is required. A recent trend is looking into lead-free substitutes and creating sophisticated encapsulation methods to increase longevity and stability. Furthermore, significant advancements in device architecture and material engineering have resulted in increases in durability and efficiency (Elangovan *et al.,* 2024). It is anticipated that PSCs will become more significant in the global transition to clean and sustainable energy sources as research advances. The method of creating PSCs involves a complex layering technique using multiple materials. Typically, the front electrode of a structure starts off as a transparent conductive oxide layer. A light-absorbing perovskite layer is then positioned in between an HTL and an electron transport layer (ETL). The assembly is completed with a metal back electrode. This design, sometimes referred to as the n-i-p configuration, enables effective charge extraction and separation when sunlight is absorbed by the perovskite material (Pandiaraj *et al.*, 2024). To improve device performance, other designs such as the p-i-n structure have also been studied. Because of its great efficiency, affordability, and simplicity of construction, PSCs have drawn a lot of interest as a viable technology for the next generation of solar energy harvesting.

Graphene oxide (GO) and graphitic carbon nitride (g-C_3N_4) have the potential to be employed as hole transport layers (HTLs) in PSCs (Asghar *et al.,* 2024), g-C_3N_4 has an adjustable bandgap and excellent thermal stability, offering good electronic properties and efficient charge extraction, despite the fact that they have varied attributes that affect how well they perform (Akram *et al.,* 2024). To enhance its functionality, though, its low conductivity typically needs to be modified or doped. On the other hand, GO has good mechanical qualities, a large surface area, and high conductivity, which allow for effective charge extraction and hole transport (Znidi *et al.,* 2024). Functional groups in GO that include oxygen boost the

material's interaction with the perovskite layer, improving the stability and overall performance of the device (Zhao *et al.*, 2024). GO's hydrophilicity and possible deterioration under operating conditions can pose certain obstacles, but generally, its advantages make it a more desirable option for HTLs in PSCs, especially when seeking improved stability and performance (Azmi *et al.*, 2024).

GO serves as the HTL. GO's work function is well suited for hole extraction from the perovskite layer because of its well-known adjustable electronic characteristics, high specific surface area, and strong conductivity (Zang *et al.*, 2024). Depending on the level of oxidation, its band gap can be adjusted. By enhancing charge transfer and lowering recombination, it improves the stability and performance of the PSC (Lohia *et al.*, 2024; Mathew & Snigdhapriya, 2024). Due to its excellent electrical conductivity and affordability when compared to other metals like gold or silver, iron (Fe) was chosen as the back electrode in this arrangement (Zhong *et al.*, 2024). Fe's work function is in good alignment with GO's energy levels, which makes hole collecting more effective. Furthermore, the mechanical robustness of Fe guarantees the PSC's long-term stability and structural integrity (Si *et al.*, 2024). The unique structural characteristics of g-C_3N_4 and GO are shown in Figure 5.1 and are essential for a range of optoelectronic applications.

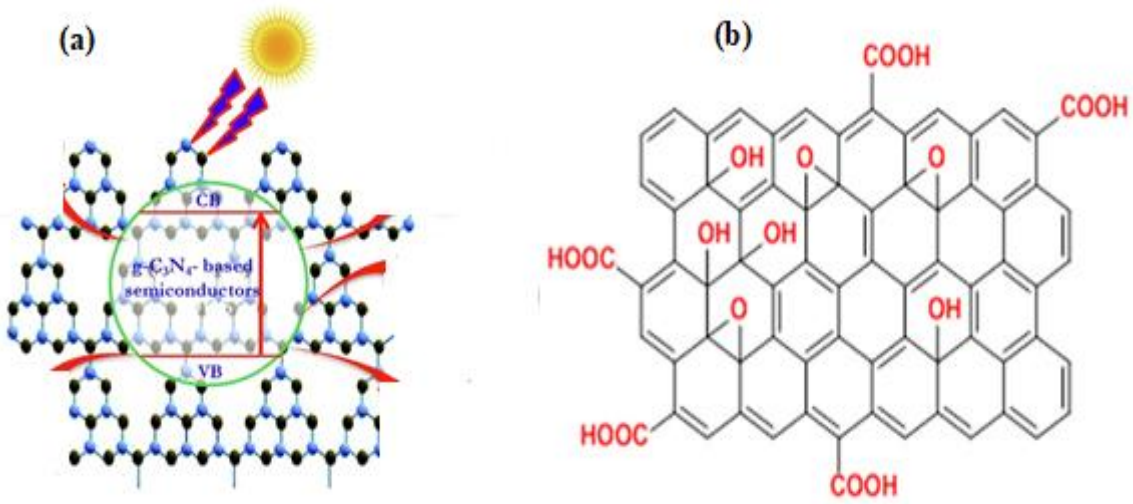

Figure 5.1: Structures of the g-C3N4 (a) and (b) GO molecules

(Cahyana *et al.*, 2019; Reddy *et al.*, 2019)

This study offers a novel approach to improve PSC performance by analysing the impact of different HTLs on device properties in detail. One obvious departure from conventional PSC structures is the usage of GO as an HTL in the arrangement. This work provides a thorough knowledge of the mechanisms influencing PSC performance, including the effect of HTL characteristics on charge carrier dynamics, recombination processes, and

overall device efficiency. It does this by employing sophisticated simulation approaches. ITO is the transparent conducting electrode used in the model cell. It was chosen because of its outstanding transparency in the visible spectrum and strong electrical conductivity (Jiao *et al.,* 2024). ITO reduces absorption losses, enabling light to enter the device efficiently and offering a conductive channel for charge carriers thanks to its broad band gap of roughly 3.5 to 4.3 eV (Wen *et al.,* 2024).

[6,6]-Phenyl-C_{61}-butyric acid methyl ester (PC61BM), a fullerene derivative well-known for its high electron mobility and superior electron transport capabilities, makes up the electron transport layer (ETL). $PC_{61}BM$, which has a band gap of about 1.8 eV, is a powerful ultraviolet light absorber that makes it easier to extract electrons from the perovskite layer effectively. This helps to transfer electrons to the ITO electrode and lower recombination losses (Khan, *et al.,* 2024). The absorber layer, which is the central component of the PSC, is composed of methylammonium tin iodide ($CH_3NH_3SnI_3$), a substitute for lead perovskite. This material has a high absorption coefficient that allows it to effectively absorb a wide range of sunlight and a band gap of about 1.3 to 1.4 eV, which makes it perfect for solar absorption (Nagar *et al.*,2021). In the visible spectrum, the ITO absorption coefficient is usually relatively low, often between 10^2 and 10^3 cm^{-1}. In the visible spectrum, PC61BM's absorption coefficient is comparatively modest, ranging from 10^3 to 10^4 cm^{-1}. Conversely, for visible light, $CH_3NH_3SnI_3$ has a high absorption coefficient, usually between 10^4 and 10^5 cm^{-1}. The mild GO absorption coefficient varies with the degree of reduction, typically between 10^3 and 10^4 cm^{-1}. In this layer, photon absorption creates electron-hole pairs, which are subsequently separated and transferred to the appropriate electrodes (Zhang *et al.,* 2024).

With careful material selection and architectural optimization, PSC performance can be significantly improved, as this study provides important insights. Through the use of GO as HTL, the study emphasizes how important interface engineering is for enhancing charge transfer and lowering recombination losses. The research investigates the intricate connections between layer thickness, carrier dynamics, and temperature impacts using the SCAPS-1D device simulator. Examining different HTL materials further demonstrates the significant influence material attributes have on device performance. This method emphasizes the potential of novel materials and in-depth simulations to propel the development of effective and sustainable solar energy technologies for fabrication into an extraordinary physical solar cell device. Extensive analyses have been conducted to provide insightful guidance for future PSC advancements. The results of this investigation greatly advance the growing corpus of

knowledge regarding PSCs and open the door to the creation of more effective and long-lasting solar energy systems.

5.2 Numerical simulation

The solar cell capacitance device simulator (SCAPS-1D), created by the Electronics and Information Systems Department at the University of Ghent in Belgium, was employed in this investigation. Using SCAPS-1D, the performance of the cell architecture is examined. By entering particular material parameters like band gap, absorption coefficient, carrier mobility, and layer thicknesses, SCAPS-1D recreates the electrical and optical behaviour of layered solar cell designs. Through this simulation, the PSC's potential efficiency, open-circuit voltage, short-circuit current, and fill factor can all be better understood, helping to optimize the design and comprehend how various layers interact to produce optimal performance (Mortadi *et al.*, 2024).

Standard test conditions (STCs) in this study include an air mass of 1.5 G, an irradiance of 1000 W m^{-2}, and a temperature of 300 K for all simulations. Figure 5.2a displays the cell structure that was examined in this study, while Figure 2b shows the energy level diagram for the several model PSC components, such as ITO, $PC_{61}BM$, MAI, GO, and Fe. Each material's valence band maximum (VBM) and conduction band minimum (CBM) are displayed in the diagram. The CBM and VBM for ITO are respectively -4.0 and -7.5 eV. $PC_{61}BM$ has a VBM of -6.0 eV and a CBM of -3.9 eV. The CBM and VBM of MAI ($CH_3NH_3SnI_3$), the perovskite layer, are -4.1 and -5.4 eV, respectively. In contrast, GO has a CBM of -1.9 eV and a VBM of -5.15 eV, whereas Fe has a CBM of -4.5 eV. Understanding this diagram requires an understanding of charge carrier dynamics. Electrons in the perovskite layer are stimulated from the VBM to the CBM upon light. Thereafter, these stimulated electrons move from the MAI, CBM to the $PC_{61}BM$, CBM, suggesting a favourable energy offset for the transfer of electrons. As seen in the diagram, electrons then go from $PC_{61}BM$ to the ITO electrode. The holes created in the MAI layer flow to the GO layer in terms of hole flow.

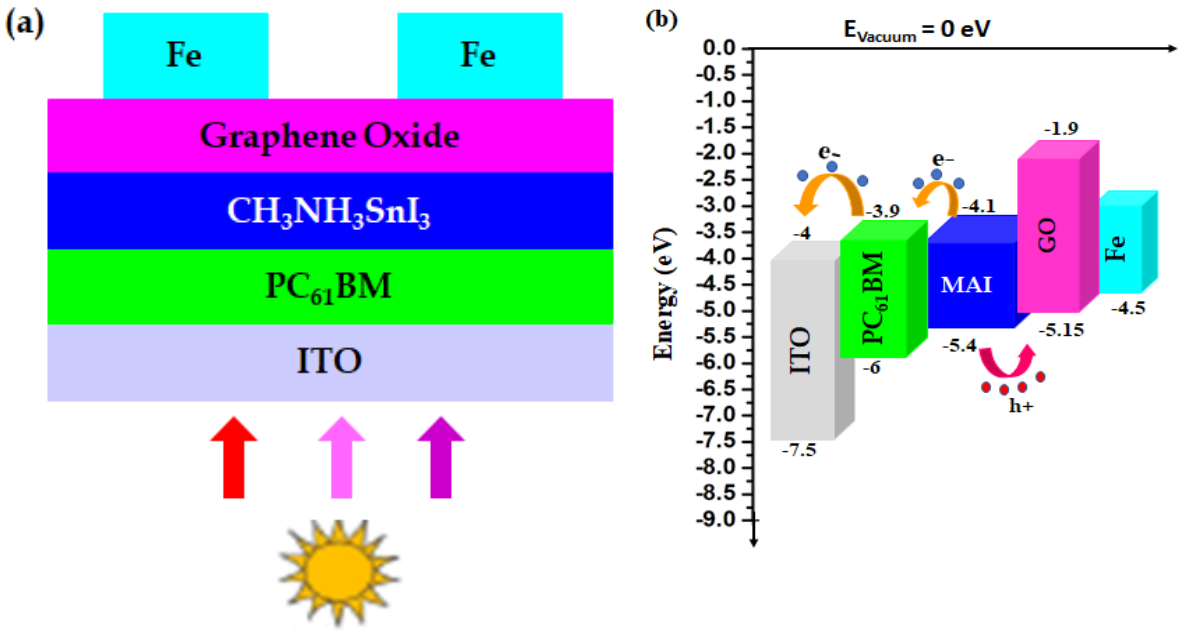

Figure 5.2: Model device structure (a) and the associated energy diagram (b)

This hole transfer is enabled by the energy level difference between the GO VBM at -5.15 eV and the MAI VBM at -5.4 eV. These holes finally travel from the GO electrode to the Fe electrode. For effective charge separation and transport, these energy levels must interact and align. Because of the well-aligned energy levels, the efficiency of the solar cell is increased and energy loss during electron and hole transmission is minimized. Appropriate alignments of these energy levels guarantee effective charge extraction and decrease recombination losses. All things considered, Figure 5.2b energy level diagram shows a well-thought-out PSC structure. Through careful energy level alignment, the electron and hole transport layers are both carefully chosen to maximize the device's performance.

For use in photovoltaics and other electronic devices, Table 5.1 presents a comparison of different HTL semiconductor materials according to their electrical and physical characteristics. The ideal thickness for the majority of GO, DPBTTT-14, P3HT, CuSCN, and Cu_2O is 50 nm, though this varies depending on the material. 200 nm is when NiO is thicker. A material's thickness can affect charge transport and light absorption efficiency, which can affect how well a device performs. The band gap in GO is 3.25 eV, which is broader and often linked to lower absorption of visible light, but in P_3HT and Cu_2O it ranges from 1.85 eV, indicating narrower gaps that boost light absorption. The ease with which a material can release an electron is indicated by its electron affinity. With their lower electron affinities (1.9 eV), GO and CuSCN may be more adept at electron injection (Ghorpade *et al.*, 2022). Cu_2O and DPBTTT-14, on the other hand, have higher electron affinities (3.2 eV), which may be useful

in other situations where strong electron binding is helpful. A material's capacity to retain electrical energy in an electric field is measured by its dielectric permittivity.

With high permittivity values of 10, materials like CuSCN and DPBTTT-14 are good at charge screening, which can enhance device performance by lowering charge recombination losses. The conduction band (CB) and valence band (VB) effective density of states (DOS) show which electronic states are available for charge carriers. P3HT, with 1.0×10^{22} cm^{-3}, the greatest CB density (Landgrave-Barbosa *et al.*, 2022), enhances device efficiency by supporting high charge carrier concentrations. In a similar vein, Cu_2O and P3HT both have high VB densities, which facilitate efficient hole transmission. The movement of holes and electrons is essential for the transfer of charge. The high electron mobility of GO (1×10^2 $cm^2/V{\cdot}s$) makes it stand out (Khelifi & Luscombe, 2024), P_3HT and CuSCN, on the other hand, have much smaller levels. Additionally, GO has a high hole mobility (3×10^2 $cm^2/V{\cdot}s$), which enhances its effectiveness in applications like solar cell devices that need fast hole transit.

Table 5.1: Basic input parameter of various materials used in the optimization of solar cell architecture

Parameters	**GO (**Al Dmour, 2023)	**$CH_3NH_3SnI_3$**	**PC61BM**	**ITO**	**DPBTTT-14 (**Kanoun *et al.*, 2019)	**P_3HT(**Azri *et al.*, 2019)	**CuSCN (**Azri *et al.*, 2019)	**Cu_2O** (Kanoun *et al.*, 2019)	**NiO** (Jimoh *et al.*, 2022)
Thickness (nm)	50	1000	50	90	50	50	50	50	200
Band gap Eg/Ev	3.25	1.3	2.1	3.500	2.16	1.85	3.4	2.17	2.17
Electron affinity x/eV	1.9	4.1	3.9	4.000	3.2	3.1	1.9	3.2	3
Dielectric permittivity	3	8.2	3.90	9.000	10	3.4	10	7.11	7.5
CB effective density of states/cm^{-3}	2.2×10^{21}	1×10^{18}	2.2×10^{19}	2.2×10^{18}	2.8×10^{19}	1.0×10^{22}	1.7×10^{19}	2.02×10^{17}	1.0×10^{19}
VB effective density of states /cm^{-3}	1.8×10^{19}	1×10^{18}	2.2×10^{19}	1.8×10^{19}	1.0×10^{19}	1.0×10^{22}	2.5×10^{21}	1.1×10^{19}	2.0×10^{18}
Electron mobility/cm^2/ V.s	1×10^{2}	1.6	1×10^{7}	2×10^{1}	2.83×10^{-3}	1×10^{-4}	1×10^{4}	200	200
Hole mobilitycm^2 /V.s	3×10^{2}	1.6	1×10^{7}	1×10^{1}	2.83×10^{-3}	1×10^{-3}	1×10^{1}	80	80

Donor concentration N_D/cm^{-3}	1×10^{16}	0	0.001	1×10^{21}	0	0	0	0	0
Acceptor concentration N_A/cm^{-3}	1×10^{16}	1×10^{15}	0.002	0	1×10^{18}	3.17×10^{-13}	1×10^{18}	1×10^{18}	2.0×10^{15}
Defect density/cm^{-3}	1×10^{14}	1×10^{11}	0	0	1×10^{14}	1×10^{14}	1×10^{14}	1×10^{14}	1×10^{14}

Donor concentration is relevant for materials doped to improve their electrical characteristics. The donor concentration of GO and other materials is 1×10^{16} cm^{-3}, whereas Cu_2O and P3HT exhibit distinct doping characteristics that impact their semiconductor behaviour. Acceptor concentration quantifies the locations that are available for hole capture. CuSCN and NiO are examples of materials with high acceptor concentrations (1×10^{34} cm^{-3}), which improves their p-type conductivity (Cetin *et al.,* 2018). Similar levels of structural defects are indicated by the defect density, which is constant for all materials at 1×10^{14} cm^{-3}. While materials like DPBTTT-14 offer advantages in electron affinity and mobility, making them ideal for varied technological requirements, GO, P3HT, and Cu_2O are generally preferable for semiconductor applications needing high DOS and moderate mobilities.

5.3 Results and discussion

To gain important insights into the suggested model device, in-depth evaluations of carrier transport, generation-recombination processes, and interfacial features have been optimized. A comprehensive analysis is conducted on the absorption model of the cell layers and the band diagram of the proposed solar cell. Mott-Schottky (MS) capacitance characteristics are examined in relation to the impacts of temperature and HTL donor and ETL acceptor densities, as well as the latter on MS capacitance analysis. To evaluate the performance of the model cell structure, a comprehensive comparative analysis has been conducted.

5.3.1 Comparative analysis

Prior research has examined many solar cell architectures similar to the one under investigation in order to forecast performance measures including V_{oc}, J_{sc}, FF, and PCE According to Liu et al. 2018 (Liu *et al.,* 2018) a strong FF of 80.0% and a PCE of 14.1% were achieved by the Glass/ITO/GO/PEDOT/$MAPbI_3$/PCBM/rhodamine 101/LiF/Au setup. In this case, PEDOT and GO serve as hole transport layers to decrease recombination and enhance

charge collection. While PC61BM promotes electron transport, the perovskite layer, $MAPbI_3$, absorbs light. Included in this configuration, rhodamine 101 improves charge separation or light absorption. LiF and Au serve as the last components of the structure, serving as the metal electrode and electron extraction, respectively. On the other hand, Cho et al. 2018 (Cho *et al.*, 2018), they suggested the Glass/ITO/PEDOT-GO/$MAPbI_3$/PC70BM/Al cell architecture, which showed moderate electrical results with a PCE of 12.76%.

Xie et al. (2020) investigated the Glass/ITO/MoO_3–RGO/$MAPbI_3$/PCBM/PCP/Ag architecture (Xie *et al.*, 2020), in which they combine rGO and molybdenum trioxide (MoO_3) to create an effective hole transport layer. An enhanced PCE of 18.15% was displayed by their model cell. Also, Patil and associates 2019 (Patil *et al.*, 2019), examined the Glass/FTO/Bl–TiO_2/rGO4–TiO_2/$(FAPbI_3)0.85(MAPbBr_3)0.15$/spiro-OMeTAD/Au structure, which has layers of TiO_2 modified with rGO_4 for improved light scattering and electron transport. 17.66% PCE was provided by the cell.

Table 5.2: Comparative analysis of various PSC structures based on graphene oxide material

Configuration	**Method**	**V_{oc} (V)**	**J_{sc} (mA/cm^2)**	**FF (%)**	**PCE (%)**	**Ref.**
Glass/ITO/GO/PEDOT:PSS/$MAPbI_3$/PCBM/rhodamine 101/LiF/Au	Expt.	0.97	18.20	80.00	14.10	(Liu *et al.*, 2018)
Glass/ITO/PEDOT:PSS–GO/$MAPbI_3$/PC70BM/Al	Expt.	1.03	17.92	71.00	12.76	(Cho *et al.*, 2018)
Glass/ITO/MoO3–RGO/$MAPbI_3$/PCBM/PCP/Ag	Expt.	1.12	21.18	77.00	18.15	(Xie *et al.*, 2020)
GO/CdTe	Simul.	0.4704	28.05	78.5	10.36	(Najim *et al.*, 2024)
Glass/FTO/Bl–TiO_2/rGO_4–TiO_2/$(FAPbI_3)0.85(MAPbBr_3)0.15$/spiro-OMeTAD/Au	Expt.	1.07	22.16	75.40	17.66	(Patil *et al.*, 2019)
FTO/GO/Cs2TiBr6/TiO_2	Simul.	0.541	12.70	75.6	6.54	(Thomas, 2023)
Glass/ITO/SnO_2/$MAPbI_3$–GO/spiro-OMeTAD/Au	Expt.	1.07	23.73	69.14	17.59	(Zhang *et al.*, 2018)
ITO/PC61BM/$CH_3NH_3SnI_3$/GO/Fe	Simul.	1.3462	34.84	77.32	36.27	This work

Also, Zhang et al. 2018 (Zhang *et al.*, 2018), demonstrated that an outstanding PCE of 17.59% was recorded by a model cell structure with the configuration Glass/ITO/SnO_2/$MAPbI_3$–GO/spiro-OMeTAD/Au, where SnO2 was utilized as the electron transport layer. Current GO-based modelling research by Najim et al. (2024) (Najim *et al.*, 2024) and Thomas (2023) (Thomas, 2023) yielded significantly low PCEs of 10.36 and 6.54%. In contrast, the model cell under investigation in this study, ITO/PC61BM/$CH_3NH_3SnI_3$/GO/Fe, uses a different strategy and uses a tin-based perovskite ($CH_3NH_3SnI_3$) as the light absorber. This configuration had an impressive PCE of 36.27% and outstanding performance metrics.

Performance metrics for several PSC setups are shown in Table 5.2, along with a variety of materials and their associated PCEs. This study's model cell architecture performs admirably, with a V_{oc} of 1.3462 V, a moderate J_{sc} of 34.84 mA/cm², an FF of 77.32%, and a PCE of 36.27%. This arrangement performs better than other structures documented in the literature. With remarkably high-performance metrics, this configuration stands out and indicates a great deal of promise for additional study and development in comparable material combinations to produce PSCs that are highly effective. Although they perform poorly in one or more performance criteria, other configurations also exhibit competitive efficiency. Given that every material and configuration has a distinct impact on the device's overall performance, this emphasizes the significance of material selection and interface engineering in maximizing PSC performance.

5.3.2 Optimization of different HTLs on the electrical parameters

The HTL affects important electrical metrics like V_{oc}, J_{sc}, FF, and PCE, and is essential in assessing the effectiveness and performance of PSCs. Much work has gone into optimizing HTLs with the goal of raising PSCs' stability and efficiency. Numerous HTL materials, both inorganic and organic, have been investigated for their possible application as HTLs; each presents unique benefits and difficulties. For instance, GO is well-known for having excellent PCE values due to its strong conductivity and favourable energy alignment. Another organic HTL, DPTTT-14, performs admirably but has a lower FF. Despite having a lower FF than GO, P3HT, a polymer that is frequently investigated, has high V_{oc} and PCE, which makes it a good candidate for HTL application.

Although they occasionally report lower FF and PCE compared to their organic equivalents, inorganic materials like CuSCN and Cu_2O are regarded for their stability and have demonstrated promising outcomes. NiO performs well as well; it is well-known for having

good thermal stability and appropriate band alignment. For the model cell structure, GO generally performs exceptionally well, making it a great option for HTL.

The effect of various HTLs on the electrical characteristics of PSCs is displayed in Table 5.3. Graphene Oxide (GO), DPTTT-14 (2,7-dialkyl[1]benzothieno[3,2-b][1]benzothiophene), P_3HT (Poly(3-hexylthiophene-2,5-diyl), CuSCN (Copper(I) Thiocyanate), Cu_2O (Copper(I) Oxide), and NiO (Nickel (II) Oxide) are among the HTLs whose performance is shown in the presented data. With a V_{oc} of 1.3462 V, a J_{sc} of 34.84 mA/cm², an FF of 77.32%, and a PCE of 36.27%, GO performs admirably. These numbers show that GO provides the most effective charge transport and collection, leading to the highest PCE of all the mentioned HTLs. With a much lower PCE of 20.98%, DPTTT-14, on the other hand, shows the lowest FF of 53.24% and the lowest V_{oc} of 1.1310 V. This implies that the efficiency of DPTTT-14's charge transmission or collecting is subpar.

Table 5.3: Performance metrics for optimization of various HTL components in the model cell

Hole Transport Layer	**V_{oc} (V)**	**J_{sc} (mA/cm^2)**	**FF (%)**	**PCE (%)**
GO	1.3462	34.84	77.32	36.27
DPTTT-14	1.1310	34.84	53.24	20.98
P_3HT	1.3951	34.84	74.53	36.23
CuSCN	1.2606	34.84	78.95	34.67
Cu_2O	1.2213	34.84	67.30	28.63
NiO	1.2272	34.84	75.60	32.32

With the greatest V_{oc} of 1.3951 V, an amazing FF of 74.53%, and a PCE of 36.23%, P3HT is a compelling contender for an HTL. It performs extremely similarly to GO. CuSCN's PCE is 34.67%, FF is 78.95%, and V_{oc} is 1.2606 V. Its greater FF produces a high PCE, while having a slightly lower V_{oc} than GO, demonstrating its efficacy as an HTL. Cu_2O performs moderately, with a PCE of 28.63%, FF of 67.30%, and V_{oc} of 1.2213 V. As a result, it is less effective than GO and P3HT. NiO exhibits modest performance as well, with a PCE of 32.32%, FF of 75.60%, and V_{oc} of 1.2272 V. Although it performs rather well, it is not as effective as GO and P3HT. GO is suggested as the HTL in conclusion because of its strong FF, high PCE of 36.27%, and high V_{oc}. These metrics demonstrate how much better GO is at enabling charge transmission and collection, which improves PSC performance. P3HT demonstrates encouraging outcomes as well, but GO performs somewhat better overall than P3HT.

5.3.3 Effect of temperature on the performance metrics of the cell structure

Temperature has a major effect on solar cell performance parameters. The V_{oc} is one of the main impacts, and it typically rises with temperature (An *et al.,* 2024). This decrease happens as a result of the solar cell's saturation current rising with temperature and the semiconductor material's bandgap narrowing, both of which add to the drop in V_{oc} (Ahmadi & Kim, 2024). On the other hand, at higher temperatures, the J_{sc} tends to somewhat increase. Higher intrinsic carrier concentration and enhanced light absorption at higher temperatures are the causes of this rise (Wang *et al.,* 2024). But as the temperature rises, the FF usually drops. This decline is caused by higher series resistance and increased recombination rates at higher temperatures (Afrin *et al.,* 2024).

As temperature rises, the solar cell's overall efficiency drops. Lower PCE may be attributed to the combined effects of lower V_{oc} and FF, which outweigh the small gain in J_{sc} (Zhang *et al.,* 2024). The solar cell's series and shunt resistances are impacted by temperature as well. Higher resistance in metallic contacts and other conductive channels causes series resistance, or R_S, to tend to grow. Concurrently, there is a chance that shunt resistance (R_{SH}) will drop, increasing leakage currents and decreasing efficiency even further (Muduli & Kale, 2024). Additionally, higher temperatures cause charge carriers to recombine more frequently, which reduces the amount of carriers available to generate current and lowers efficiency (Noman, Shahzaib, *et al.,* 2024). Furthermore, high temperatures can hasten the deterioration of perovskite and other components, lowering the solar cells' long-term durability and efficiency (Ahn & Choi, 2024).

Thermal cycling repeatedly has the ability to cause mechanical stress and layer delamination inside the cell structure (Chen *et al.,* 2024). By controlling the temperature of the solar cells, passive or active cooling devices can assist minimize performance losses caused by temperature effects (Sheikh *et al.,* 2024). It is also possible to improve overall performance and endurance across a variety of climatic circumstances by choosing materials with lower temperature coefficients and better thermal stability. Optimizing solar cell performance in real-world applications requires an understanding of the capacity to control temperature impacts.

The suggested solar cell architecture's performance is strongly impacted by temperature. Elevated temperatures have the potential to hasten the breakdown of the perovskite layer ($CH_3NH_3SnI_3$), thus diminishing stability and efficiency. Thermal stress can lead to crystallization problems and phase transitions in perovskite, which can impact charge transport and electronic characteristics (Yin *et al.,* 2024). Furthermore, higher temperatures might intensify interactions between the perovskite and the PC61BM and GO neighbouring

layers, resulting in undesired interfacial defects (Pandiaraj *et al.,* 2024). On the other hand, modest temperature rises can enhance charge carrier mobility and lower recombination losses, which will momentarily boost efficiency (Jiang *et al.,* 2024). For this reason, keeping the solar cell architecture stable and performing well requires maintaining an ideal operating temperature. Equation 5.1 links a PSC's metric and temperature characteristics (Ahmad *et al.,* 2023).

$$V_{0C} = \frac{nK_BT}{q}\left[In\left(\frac{I_L}{I_0}+1\right)\right] \quad (5.1)$$

Here, thermal voltage is represented by $\frac{K_BT}{q}$. I_L is for the current generated by light, and I_o is for the saturation current.

Chapter 3 page 87 covers the continuity and Poisson's equations, providing an in-depth explanation of their role in modelling charge carrier dynamics and electrostatic potential distribution in PSCs. The equations are mathematically derived and used to illustrate how electron and hole transport occurs, as well as their interactions with electric fields within the device. This discussion forms the basis for later analyses and simulations of PSC performance, highlighting the importance of these equations in optimizing the cell's overall efficiency.

The effect of temperature on a solar cell's V_{oc} is depicted in Figure 5.3a. V_{oc} rises first with increased temperature, peaking before declining as temperature rises further. Reduced recombination rates and increased carrier mobility at lower temperatures are responsible for the increase in V_{oc}, which enhances charge carrier separation and decreases non-radiative recombination. Better performance measurements for the solar cell result from this. On the other hand, V_{oc} maximizes at a certain ideal temperature. At this moment, the advantageous thermal energy that facilitates charge separation and the beginning of increased recombination rates as a result of temperature increases come into balance. V_{oc} starts to drop after this ideal temperature is exceeded. The main cause of this is that charge carriers recombine more frequently at higher temperatures. Temperature-dependent increases in the intrinsic carrier concentration in the semiconductor lead to increased recombination rates and decreased bandgap energy, which in turn lower V_{oc}.

Controlling the operating temperature is critical to maintaining optimal performance in solar cell design. Using cooling mechanisms or better-performing materials can help maintain the V_{oc} close to its optimal value. Moreover, choosing materials with appropriate thermal properties guarantees stable performance in a range of temperatures. This knowledge is especially important for PSCs, which are temperature-sensitive despite their high efficiency. Designing PSCs with better thermal stability can be guided by knowledge of how V_{oc} varies

with temperature. The negative impacts of temperature on V_{oc} can be lessened by employing techniques including surface passivation, adjusting the composition of perovskite layers, and utilizing hybrid materials. The relationship between temperature and V_{oc} highlights important factors for thermal control and material choice in solar cell design, guaranteeing reliable and effective operation at a variety of temperatures.

Figure 5.3b depicts how temperature affects a solar cell's J_{sc}. It is observed that J_{sc} is constant over a range of lower temperatures, suggesting that the performance of the cell is stable and unaffected by temperature within this range. This stability suggests effective processes for the generation and collection of charge carriers, which are unaffected by thermal effects up to a certain point. A sharp increase in J_{sc} occurs as the temperature rises and reaches a specific threshold. This sudden increase suggests a substantial alteration in the characteristics of the cell, most likely as a result of a phase transition in the perovskite material, a decrease in non-radiative recombination mechanisms, or improved charge carrier mobility brought on by higher thermal energy. The performance of the cell may be enhanced by this phase shift, which may result in a better crystalline structure and less recombination losses. J_{sc} stabilizes at a greater value over this threshold, suggesting that the solar cell achieves a new equilibrium state with improved performance.

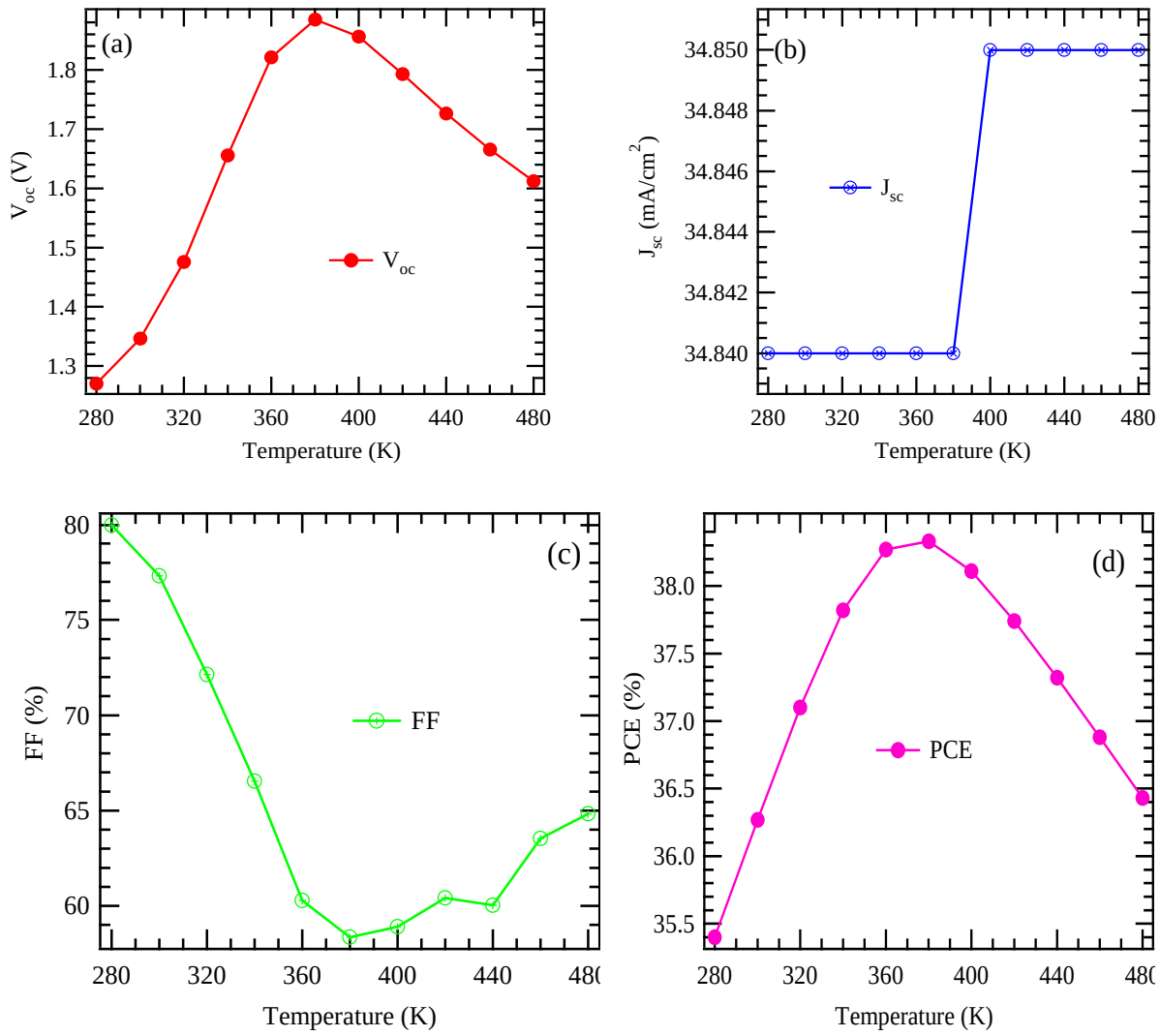

Figure 5.3: Effect of temperature on the performance metrics of the cell structure

Increased temperatures may improve material characteristics or charge carrier dynamics, as suggested by the greater constant value of J_{sc}. It is essential to comprehend J_{sc} temperature sensitivity in order to optimize solar cell design. Throughout the operational temperature range, performance should be maintained or improved by customizing the material composition and device architecture. Furthermore, putting thermal management techniques into practice could guarantee that the cell runs within its ideal temperature range. Figure 5.3b, in summary, emphasizes the critical role that temperature plays in solar cell performance. It displays stable J_{sc} at lower temperatures, a notable increase at a particular temperature threshold, and stabilization at a higher performance level beyond that. This knowledge is useful for selecting materials and developing design plans that maximize solar cell efficiency at different temperatures.

The impact of temperature on a cell structure's FF performance measures is shown in Figure 5.3c. According to the observed tendency, FF first decreases sharply as temperature rises, reaching a minimal point before progressively increasing once more. This trend suggests that temperature variations have a significant impact on the cell's efficiency. Reduced carrier mobility, altered material characteristics, or higher recombination rates could be the cause of the initial decline in FF. The temperature at which the cell has the greatest performance deterioration is represented by the lowest point. After this, the steady rise in FF points to possible recovery processes or stabilization inside the cell structure, either as a result of material phase transitions or heat stress adaption. The materials utilized in the cell construction, such as perovskite, which is known for its sensitivity to temperature fluctuations, are probably what are causing this temperature-dependent behaviour.

The way that temperature impacts FF is also influenced by the design and production process. Utilizing materials with improved thermal stability and practicing effective thermal management could lessen the precipitous drop in FF. Deeper research on material phase changes at varying temperatures, carrier mobility, and recombination rates would yield more insights into the underlying mechanisms. Furthermore, examining the hysteresis behaviour through structural cooling following heating may disclose the reversibility of the noted alterations. In general, these tendencies must be understood in order to optimize solar cell performance in a variety of climatic settings and guarantee stability and efficiency in real-world applications where temperature swings are frequent.

Conversely, Figure 5.3d illustrates how temperature affects a perovskite solar cell's power conversion efficiency (PCE). The figure demonstrates how the PCE greatly improves when the temperature rises from 280 K to about 370 K. Better solar performance at moderate temperatures can be due to increased charge carrier mobility and decreased recombination losses. The PCE peaks around 400 K, suggesting that this is the ideal temperature for the solar cell to operate at. The physics of the device and the characteristics of the material are best suited for effective energy conversion at this temperature range. Nevertheless, the PCE begins to drastically decrease above this ideal temperature. An increase in temperature can have a number of negative effects. For example, it can cause the perovskite materials to degrade thermally, which lowers their efficiency and crystallinity. It can also promote charge carrier recombination, which lowers the quantity of carriers available to generate current. Thermal instability can also result in phase segregation or ion migration, which negatively affects the performance of the device.

Figure 5 general pattern emphasizes how PCE depends on temperature, with performance metrics peaking at specific temperatures before declining. This emphasizes how crucial heat control is to PSC stability and good performance. When building and implementing PSCs in real-world settings with frequent temperature fluctuations, effective thermal management is essential. It is possible to produce PSCs that are more dependable and effective by improving the cell structure and materials to increase thermal stability.

5.4.4 Generation and recombination characteristics profiles

The perovskite material is highly efficient in producing these excitons because of its appropriate bandgap and high absorption coefficient (Elangovan *et al.,* 2024). Conversely, recombination is the process by which electrons and holes recombine and can happen via a variety of methods. When electrons and holes recombine, a key process in semiconductors known as "radiative recombination" occurs, which releases a photon and frequently serves as a loss mechanism in solar cells (Oni *et al.,* 2024). Conversely, non-radiative recombination happens without the release of photons and is usually brought on by imperfections or impurities in the perovskite material itself (Dudipala *et al.,* 2024). This non-radiative recombination can be an important loss mechanism in materials such as $CH_3NH_3SnI_3$, which may have a higher defect density than lead-based perovskites. Surface recombination occurs at the interfaces where the solar cell's layers meet. Effective interface engineering, like the application of GO; can lessen these losses by lowering recombination and passivating the interfaces (Oni *et al.,* 2024).

Each layer has varying degrees of success in reducing recombination. In order to effectively move electrons and keep them from recombining with holes in the layer of perovskites, PC61BM is necessary (H. Wang *et al.,* 2024). Successful extraction of charges and a decrease in recombination losses depend on its energy level alignment with the perovskite material (Ye *et al.,* 2024). Another crucial factor is the perovskite layer's superiority. Longer charge carrier lifetimes and fewer recombination centers are characteristics of a high-quality, flawless perovskite layer. By passivating defects at the perovskite/GO interface and facilitating effective hole extraction, the GO layer greatly reduces surface recombination (Shen *et al.,* 2024). The Fe electrode's appropriate contact and work function alignment guarantee low energy barriers and decreased recombination losses at the electrode interface (Jha *et al.,* 2024).

All things considered, a PSC's efficiency is mostly dictated by how well charge creation and recombination are balanced. Optimizing efficiency requires a high-quality perovskite material, well-engineered interfaces, and efficient charge transport layers like PC61BM and GO. The performance of PSCs can be greatly enhanced by reducing recombination through

careful material selection and interface engineering. Optimizing the design and fabrication procedures is crucial to improving the performance and efficiency of PSCs. This involves having a thorough understanding of these features within the particular configuration of the device.

Understanding generation and recombination properties is essential to semiconductor physics in order to analyse device performance, especially in applications like as solar cells and diodes. These analyses revolve around two essential equations: the Shockley equation and the Shockley-Read-Hall (SRH) recombination equation. When characterizing the J-V relationship of a p-n junction diode, the Shockley equation is essential. This formula is essential for assessing the effectiveness of gadgets like solar cells since it clarifies how the diode reacts to applied voltage (Mohandes & Moradi, 2024).

$$R_{SRH} = \frac{np - n_i^2}{\tau_{n,p}\left(p + n + 2n_i \cosh\left(\frac{E_i - E_t}{K_T}\right)\right)} \quad (5.2)$$

R_{SRH} , represents SRH recombination, where n and p denote the electron and hole concentration densities, respectively, whereas n_i refers to the intrinsic carrier concentration (cm^{-3}), τ and $\tau_{n,p}$ indicate the electron or hole lifetime (S), E_i represents the intrinsic fermi level (eV) and E_t is the trap energy level (eV),k is Boltzmann constant and T represents temperature.

The current flowing through the diode is represented by equation 5.6, where I is the saturation current, q is the charge of an electron, V is the voltage across the diode, k is Boltzmann's constant, and T is the absolute temperature. The Shockley equation captures the exponential relationship between current and voltage, which is important for comprehending how the diode functions under various conditions. Conversely, the Shockley-Read-Hall (SRH) recombination equation offers insights into the recombination processes that occur in semiconductors, particularly when non-radiative recombination centers are present. This equation is essential for comprehending how defects and impurities affect carrier dynamics within the semiconductor.

$$\frac{1}{\tau} = \frac{n_p}{n_n \tau n_{p+} n_p \tau p_n} + \frac{p_n}{p_{p\tau +} p_p \tau p_n} \quad (5.3)$$

From equation 5.3, τ denotes the carrier lifetime, while n_n and p_n represent the electron and hole densities at the recombination center, respectively. The terms τn_p and τp_n are the recombination times for electrons and holes, respectively. In order to maximize the efficiency of semiconductor devices, this equation aids in quantifying the impact of flaws and impurities on recombination rates. The Shockley equation mainly deals with the general electrical properties of diodes, but the SRH equation delves more deeply into the carrier recombination

mechanisms. Both equations are essential for constructing effective electrical and optoelectronic devices as well as for gaining a thorough understanding of semiconductor behaviour.

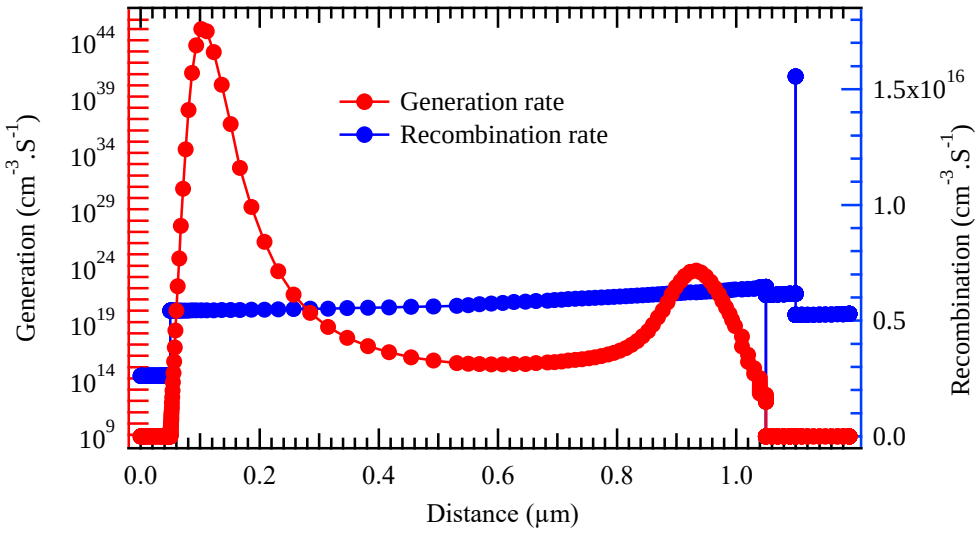

Figure 5.4: Generation-recombination characteristics

The production rate and recombination rate in a material as functions of depth are displayed in Figure 5.4. On different scales, these two rates are displayed on the y-axis. The recombination rate ranges from 0 to 1.6 x 10^{16} cm-3 s^{-1} on the right y-axis, whereas the generation rate ranges from 0 to 1044 $cm^{-3}s^{-1}$ on the left. Based on the plot, it can be shown that the generation rate curve peaks at a depth of 0.05 µm. This demonstrates unequivocally that at this level, generation outnumbers recombination by an astounding magnitude of 10^{25}. In general, recombination is quite abundant throughout the cell structure, particularly at a depth of 1.0 µm. This helps explain the cell's exceptional performance measurements that have been seen.

A semiconductor material's generation and recombination rates as a function of distance are shown in Figure 5.4. There are two separate curves displayed: the generation rate curve shows the speed at which electron-hole pairs form in the material, and the recombination rate curve shows the speed at which these pairs split up and disappear. A notable observation is the presence of a conspicuous peak in the generation rate curve at around 0.2 µm, indicating that this region experiences the highest rate of electron-hole pair formation.

The distribution of the recombination rate curve is wider; it begins at a relatively low value, rises steadily to a high of 0.6 µm, and then taper down towards the conclusion. It is clear that both rates vary with distance, with the recombination rate being dispersed over a wider area and the production rate being more localized. This figure shows a section close to an interface inside a semiconductor device. While processes like light absorption, thermal

excitation, or impact ionization can produce electron-hole pairs, band-to-band or trap-assisted recombination is most likely to be the dominant mechanism during the recombination process. It is implied from the discrepancy in the geographical distribution of the rates of generation and recombination that the produced carriers have a tendency to diffuse out of the generating zone before recombining. Factors such as carrier lifetime and movement affect its diffusion.

5.3 5 J-V and QE characteristics of the model cell structure

Analysing a PSC's performance and efficiency entails looking at its J-V (current density-voltage) and QE (quantum efficiency) properties using the structural model. The various parts of the cell structure each have a specific purpose. Because of its transparency and high conductivity, ITO is employed as the front electrode, which effectively allows light to enter the cell (Wen *et al.,* 2024). By serving as an ETL, PC61BM makes it easier for electrons to transfer from the perovskite layer to the electrode. The creation of electron-hole pairs and light absorption are carried out by the perovskite active layer, or $CH_3NH_3SnI_3$. Fe is utilized as the back electrode, and GO acts as the HTL to help move holes to the electrode.

The J-V curve is essential for assessing the PSC's performance since it offers important metrics such the J_{sc}, or the current density at zero voltage, which shows the maximum current the cell is capable of producing. The voltage that results from zero current is known as the V_{oc}, and it represents the highest voltage that a cell can produce. The FF, which represents the solar cell's quality, is the ratio of the maximum power output to the product of J_{sc} and V_{oc} (Khan *et al.,* 2024). The PCE, which displays the cell's total efficiency, is calculated as the electrical power output divided by the incident light power (Li *et al.,* 2024).

High transparency and conductivity from ITO in this combination enable the perovskite layer to absorb light efficiently. Recombination losses are decreased by PC61BM effective electron transport to ITO. When light is absorbed, the absorber layer, $CH_3NH_3SnI_3$, is essential for producing electron-hole pairs. While Fe functions as a strong back contact, GO aids in efficient hole transport and inhibits recombination at the back electrode. This structure usually exhibits a high PCE because of its good material qualities, high J_{sc} from effective light absorption and charge transfer, and appropriate V_{oc}.

QE, which is sometimes expressed as either internal quantum efficiency (IQE) or external quantum efficiency (EQE), quantifies how well the cell converts incident photons into electrons (Khalil *et al.,* 2024). When it comes to charge carrier collection, EQE is the ratio of charge carriers collected to photons incident on the cell, whereas IQE is the ratio of charge carriers collected to photons absorbed by the cell (Hossain *et al.,* 2024). In this configuration, EQE is contingent upon the $CH_3NH_3SnI_3$ absorption spectrum as well as the charge transport

efficiency of PC61BM and GO. Effective photon-to-electron conversion over a wide range is indicated by high EQE values (Li *et al.*, 2024), usually reaching its peak in the $CH_3NH_3SnI_3$ absorption range. Because it only takes into account absorbed photons, IQE typically has a greater value than EQE. High performance and efficiency are achieved by the optimization of light absorption, charge transfer, and collection in the solar cell architecture. While the QE characteristics should show high efficiency in converting absorbed photons to charge carriers, with EQE peaking in the absorption region of the photoactive absorber, the J-V characteristics should show high J_{sc}, moderate V_{oc}, and a decent FF, resulting in high PCE.

A model solar cell's J-V and QE characteristics are displayed in Figure 5.5, providing crucial information about the cell's operation. The relationship between the applied voltage across the solar cell and the current density is depicted by the J-V curve. When the voltage is zero, the curve begins at a high current density of 34 mA/cm², which represents the short-circuit state. This shows the highest current that the cell is capable of producing when it is illuminated. The current density stays mostly constant as the voltage rises, indicating high-quality material and few recombination losses. The current density does, however, abruptly decrease when the voltage gets closer to 0.95V, signifying the open-circuit condition, in which the voltage is at its highest but no current flows. Good diode behaviour and little series resistance losses are indicated by this steep decline. The J_{sc}, V_{oc}, FF, and PCE are important parameters that are obtained from the J-V curve and together they define the total performance of the solar cell.

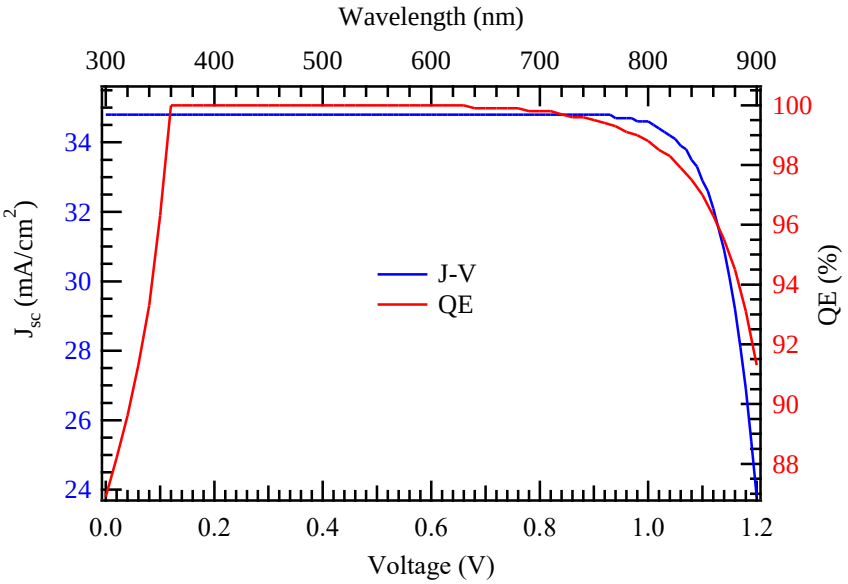

Figure 5.5: The J-V and QE characteristics of the model cell

The efficiency with which the solar cell transforms incident photons of various wavelengths into electrical current is shown by the QE curve. The QE has a high initial value and can reach 100%; it stays high over a large wavelength range. This suggests that over this

spectral range, the solar cell is quite effective at converting photons into electrical current. The high QE indicates efficient charge separation and absorption in the solar cell's active layer. At higher wavelengths, on the other hand, the QE decreases, suggesting a decrease in photon absorption or conversion efficiency. The spectral response, which displays the range of wavelengths the cell is responsive to, the peak QE, or wavelength at which the cell has the highest quantum efficiency, and the integrated QE, which gives an overall measure of efficiency across the spectrum, are important characteristics of the QE curve. In conclusion, the graph shows that the model solar cell performs exceptionally well in photovoltaic applications. The cell's high quantum efficiency across a wide range of wavelengths, along with its high open-circuit voltage and short-circuit current density, indicate that it is very effective at converting solar energy into electrical power. The J-V and QE curves' good overlap further suggests that there are few recombination losses and effective charge collection, which makes this solar cell structure a good option for highly efficient solar energy conversion.

5.3.6 Effect of optimizing back contacts on the electrical outcomes of the model cell

Improving different back contacts is essential to improving the electrical results of solar cells, including PCE, V_{oc}, J_{sc}, and FF. The choice of back contact materials and their characteristics, including work function, conductivity, and suitability for the absorber layer, can minimize recombination losses and greatly enhance charge carrier collection. Charge extraction and series resistance can be improved by using back contacts made of metals like gold, silver, or aluminum, or by adding passivating layers made of materials like TiO_2 or MoS_2. As a result, improving the back contact's thickness and surface roughness can enhance light absorption and reflection, increasing the solar cell's overall performance. The advancement of solar cell technologies, such as silicon-based and perovskite cells, depends on these optimizations in order to obtain higher efficiencies and more long-term stability.

Results of the optimization of back contact materials for the model PSC are shown in Table 5.4, which also highlights the various materials' performance characteristics. The materials Au, Ni, Pd, Co, and Pt had the greatest V_{oc}, each recording 2.8472 V, according to the data analysis. Al, on the other hand, has the lowest V_{oc} at 1.2212 V, while Fe has the lowest at 1.3462 V. The J_{sc}, which is around 34.84 mA/cm², is comparatively constant for all materials. The FF, which measures the amount of recombination losses and the effectiveness of charge collection, is highest for Fe at 77.32%. Compared to the majority of tested back contacts, which have an FF of 40.73%, this is a significant advantage. Al nevertheless has a comparatively high FF of 62.0%, but it is still about 15% below the FF that Fe recorded. Mo exhibits a low FF of

54.81% as well. Au, Ni, Pd, Co, and Pt lead with 40.40% in PCE. Fe comes next, with a still strong PCE of 36.27%.

Table 5.4: The Effect of optimizing back contacts on cell performance

Back contact	Work function (eV)	V_{oc} (V)	J_{sc} (mA/cm^2)	FF %)	PCE (%)
Fe	4.5	1.3462	34.84	77.32	36.27
Au	5.10	2.8472	34.84	40.73	40.40
Ni	5.15	2.8472	34.84	40.73	40.40
Pd	5.12	2.8472	34.84	40.73	40.40
Al	4.2	1.2212	34.85	62.00	26.39
Co	5.0	2.8472	34.84	40.73	40.40
Pt	5.65	2.8472	34.84	40.73	40.40
Mo	4.6	2.0592	34.84	54.81	39.32

Al has the lowest PCE (26.39%), whereas Mo demonstrates a competitive PCE of 39.32%. Based on these findings, it can be concluded that although though Au, Ni, Pd, Co, and Pt have the greatest V_{oc} and PCE values, their lower FF relative to Fe indicates that charge collection efficiency may still be improved. Fe, on the other hand, is notable for its effective charge extraction and low recombination losses due to its high FF of 77.32%.

Fe, despite not having the highest V_{oc} and PCE, makes a strong case as a back contact material with a work function of 4.5 eV. Fe has many benefits, chief among them being its high FF, indicating superior charge collection efficiency. Fe is also more affordable and readily available than precious metals such as Au, Pt, and Pd, which makes it a more economical option for larger-scale uses. Moreover, Fe might provide superior mechanical and chemical stability, extending the life and dependability of solar cell technology. Fe is suggested as a feasible back contact material for the suggested solar cell type due to its affordability, abundance, and possible stability benefits, particularly in situations where stability and cost are important considerations.

5.3.7 The band diagram of the model cell structure

A solar cell's band diagram sheds light on its energy levels and electron mobility (Mukhamale *et al.,* 2024). Sunlight strikes the semiconductor material on the solar panel, where it is absorbed, starting a series of operations (Xamidullayevich, 2024). Photogeneration of charge carriers is the process by which an electron in a semiconductor is excited to move from

the valence band to the conduction band after it has been absorbed by a photon (Nogueira *et al.,* 2025). A hole that is positively charged remains in the valence band as a result of this transition, which forms an electron-hole pair in which the electron is now free to travel in the conduction band (Shin & Pyun, 2024). The energy band structure of the semiconductor shows the relationship between energy levels and electron movement; electrons in the conduction band can move freely and contribute to electrical conductivity, while those in the valence band are bound to atoms. The presence of these electron-hole pairs allows current to flow through the material (Jouybar *et al.,* 2024). The energy differential between these two bands is known as the band gap, and it is a key factor in determining the solar cell's efficiency.

Cliffs or spikes in the energy band structure, particularly at the interfaces, can seriously affect a PSC's performance. These features are frequently caused by flaws at interfaces or by mismatched energy levels between various layers. The energy band diagrams provide an explanation for the energy offsets at these interfaces. The energy offset (ΔE) at the interface between two materials can be described by a key equation that includes the valence and conduction band boundaries. The difference between the perovskite layer's and the ETL's conduction band edges yields the CBO. This can be stated mathematically as:

$$\Delta E_C = E_C, \text{ETL} - E_C, \text{Perovskite} \quad (5.4)$$

In a similar manner, the difference between the perovskite layer's and the HTL's valence band edges determines the VBO:

$$\Delta E_v = E_C, \text{Perovskite} - E_v, \text{HTL} \quad (5.5)$$

These offsets may have a substantial effect on the device's performance. A conduction band spike, which might obstruct electron transport, is shown by a positive value ($\Delta EC > 0$) for the conduction band offset. On the other hand, a CBO, which can promote recombination at the interface, is indicated by a negative value ($\Delta EC < 0$). Comparably, for the VBO, a valence band spike with a positive value ($\Delta EV > 0$) acts as a barrier for hole transport and is commonly referred to as Hole Blocking (HBL), whereas a valence band cliff with a negative value ($\Delta EV < 0$) also facilitates recombination at the interface.

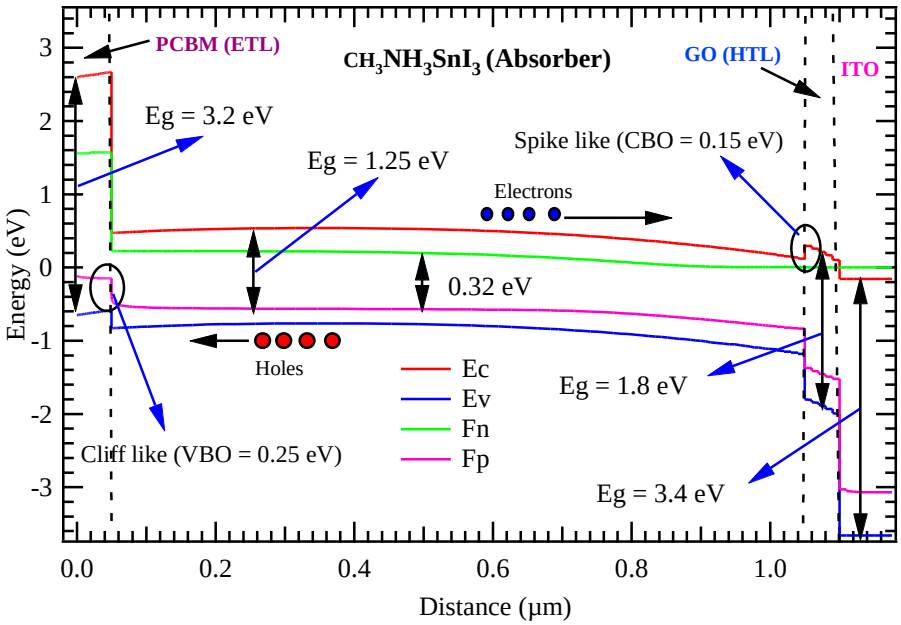

Figure 5.6: The band diagram of the model cell

Electron-hole pairs are produced in the model cell design when sunlight reaches the $CH_3NH_3SnI_3$ layer. While the holes are directed into the GO layer and gathered by the Fe electrode, the electrons travel to the $PC_{61}BM$ layer and subsequently to the ITO electrode. The ideal alignment of energy levels in the band diagram permits the efficient separation and movement of these charge carriers. This alignment improves the efficiency of sunlight's conversion to electrical energy and lowers energy losses.

The model PSC's energy band diagram, which shows the band alignments and energy levels of the different materials in the cell structure, is shown in Figure 5.6. The four main materials in the diagram are PCBM, $CH_3NH_3SnI_3$, GO, and ITO. Every component of the material contributes to the overall functioning of the cell by fulfilling a certain purpose. PCBM functions as the ETL and has a bandgap of 3.2 eV. With a bandgap of 1.25 eV, the perovskite absorber layer, $CH_3NH_3SnI_3$, is the core layer where light absorption takes place, producing electron-hole pairs. GO is the HTL and has a bandgap of 1.8 eV. Lastly, an electrode with a bandgap of 3.4 eV is employed: ITO. The conduction band edge (Ec), valence band edge (Ev), quasi-fermi level (Fp) for holes, and quasi-Fermi level (Fn) for electrons are the four energy band representations. The alignment of these energy levels in various materials is shown in the diagram. A cliff-like valence band offset (VBO) of 0.25 eV is seen at the interface between PCBM and $CH_3NH_3SnI_3$, whilst a spike-like conduction band offset (CBO) of 0.15 eV is observed at the $CH_3NH_3SnI_3$/GO contact. It is discovered that the device's built-in potential (V_{bi}), which is 0.32 eV, is essential for propelling the created electron-hole pairs inside the absorber layer to separate. Because electrons flow toward the ETL (PCBM) and holes toward

the HTL (GO), charge separation which is necessary for current generation under light is made easier. The diagram emphasizes how crucial the band offsets at the interfaces are, since they have a big impact on how charge carriers move and how well the device works as a whole. In general, the energy band diagram shows how various materials interact with one another and with their respective energy levels, offering a thorough understanding of the PSC's energy landscape. This knowledge is essential for improving the cell's performance and efficiency.

5.3.8 Theoretical absorption model of the cell layers

When sunlight hits the surface of a solar cell, light absorption starts. Anti-reflective coatings (ARCs) are found on many solar cells in order to optimize light entry and limit reflection (Jamaluddin *et al.*, 2024). The purpose of this layer is to increase light penetration into the cell by lowering the quantity of light that reflects off the surface. The front contact layer, which is frequently composed of transparent conductive materials like indium tin oxide (ITO), is encountered by light after it has passed through the ARC (Oni *et al.*, 2024). This layer is essential because it conducts electrical current from the ensuing active layers and allows light to pass through to them. The absorber layer, which is where actual light absorption and charge creation take place, is the central component of the solar cell. For example, this layer is usually made of a perovskite substance in PSCs. This substance is very good at absorbing light from the sun in a variety of wavelengths and transforming it into electron-hole pairs.

To produce an electrical current, these charge carriers must be effectively transferred to the electrodes when they are generated. Charge transfer layers (CTLs), which comprise HTLs and ETLs, are in charge of handling this task. Each layer has a distinct function in the particular model structure used in this work: ITO serves as the layer of front contact. It has electrical conductivity and is transparent to light, allowing it to reach the active layers. Although it absorbs very little light on its own, transparency is necessary for the best possible light ingress. The ETL is PC61BM. Its function is to ease the flow of electrons from the electrode to the perovskite layer. Due to its low absorption in the visible band, PC61BM largely facilitates light transmission to the photoactive layer. The principal absorber layer is $CH_3NH_3SnI_3$. Its high absorption coefficient indicates that it effectively creates electron-hole pairs and absorbs a sizable amount of incident sunlight.

Its great energy conversion efficiency is partly attributed to its broad absorption spectrum. Graphene oxide, or GO, is frequently employed as an HTL or interfacial layer. It controls hole transport and has a small effect on light absorption. But improving charge collection and overall cell efficiency is its main purpose. Fe functions as the layer of back contact. Its job is to finish the electrical circuit by gathering the electrons produced in the

$CH_3NH_3SnI_3$ layer. Its function is less about light absorption and more about effective current collecting. The link between the photon wavelength and the absorption coefficient is expressed by the equation 5.6.

$$\alpha = 4\pi k \frac{1}{\lambda} \quad (5.6)$$

In this context, α is the absorption coefficient (cm^{-1}), λ is the photon wavelength in nanometres (nm) whereas k is the extinction coefficient.

The light absorption properties in this solar cell structure are mostly determined by the CH3NH3SnI3 layer. To achieve great efficiency, this perovskite material excels in capturing a wide spectrum of sunlight (Dou *et al.*, 2024). The other layers are vital to maximizing the function of the cell even though they don't make a big difference in light absorption. The ITO layer controls light transmission into the cell, $PC_{61}BM$ handles electron transport, GO controls hole transport, and Fe gathers generated electrical current. Taken as a whole, these layers help the cell more efficiently convert sunlight into electrical energy.

The absorption properties of the several layers in the model PSC, namely GO, Indium ITO, $PC_{61}BM$, $CH_3NH_3SnI_3$, and GO, are displayed in Figure 5.7. The perovskite material shows the maximum absorption throughout the visible spectrum, demonstrating its critical function in efficiently harvesting solar energy. For photons to be converted into electrons, high absorption is necessary, which makes $CH_3NH_3SnI_3$ an important part of the solar cell's operation. A common fullerene derivative utilized as an electron acceptor is PC61BM. Its role in promoting electron transit and lowering recombination losses is highlighted by its moderate absorption level.

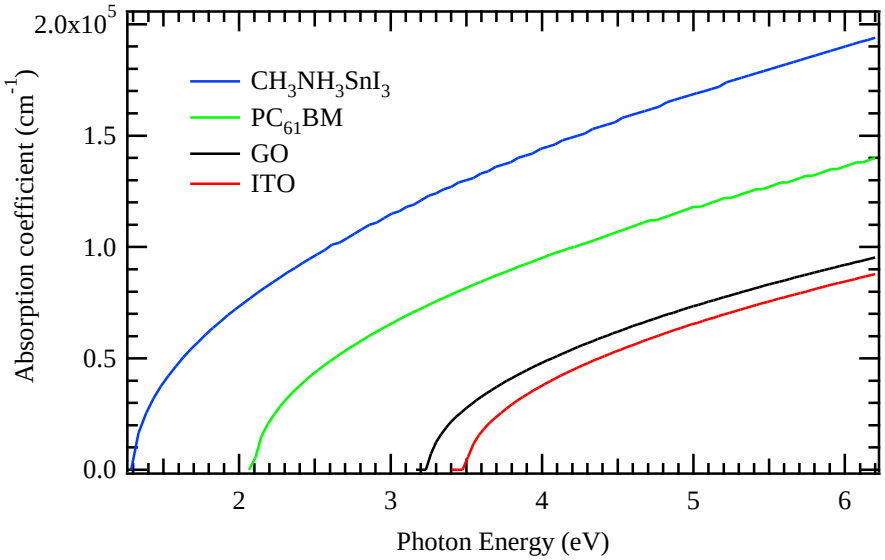

Figure 5.7: Absorption model of the cell layers

Due to its ability to efficiently transfer electrons produced in the perovskite layer to the electrodes, this property is essential for preserving the solar cell's efficiency. In contrast to $CH_3NH_3SnI_3$ and $PC_{61}BM$, GO exhibits reduced absorption. GO's superior electrical conductivity and flexibility, which boost charge transport and mechanical stability and improve the overall performance of the solar cell, make it valuable notwithstanding this fact. ITO has the lowest absorption of all the materials because its main function is to efficiently conduct electrons while letting light into the cell. Its conductivity and transparency are necessary for the solar cell to operate at its best. The different roles that these materials play within the solar cell are highlighted by their absorption characteristics. Gaining insight into these traits can help with future optimization and high-performance PSC design.

5.3.9 The impact of acceptor density on Mott-Schottky capacitance analysis

In PSCs, the ETL is essential to device performance, especially to the capacitance behaviour seen in MS analysis (Shao & Loi, 2020). The MS capacitance measurements are critical for extracting characteristics such as the V_{bi}, depletion region width, and carrier density. The acceptor density has a substantial impact on MS capacitance analysis (Ghahremanirad *et al.,* 2023). The capacitance-voltage (C-V) properties, in particular the slope and intercept of the MS plot ($1/C^2$ vs. V), are impacted by changes in the ETL acceptor density. The V_{bi}, which is derived from the MS plot's intercept, may change as acceptor density changes (Kirchartz *et al.,* 2012). A greater V_{bi} is usually the result of enhanced carrier recombination and separation efficiency at higher acceptor densities. The MS plot's slope indicates that the carrier density is inversely proportional to the carrier density in the depletion region (Zandi *et al.*, 2018). A larger carrier density is shown by a steeper MS plot slope, which is a function of acceptor density. Additionally, variations in acceptor density affect the width of the depletion region; a higher acceptor density typically decreases this width, which in turn affects the capacitance of the device as a whole (Zhao *et al.,* 2014). As a result of the larger concentration of mobile charge carriers caused by higher acceptor density, capacitance values rise. This changes the C-V curve and affects the precision of the derived parameters.

Achieving the intended PSC performance requires optimizing the acceptor density in the. An increase in acceptor density can improve the efficiency of charge extraction, hence enhancing device performance. Excessive acceptor density, however, can result in higher recombination losses, which would be detrimental to the FF and V_{oc}. Optimizing the acceptor density is crucial to preserving long-term performance and minimizing deterioration because the features of PSCs also impact their stability. Because different materials have different acceptor densities and electrical characteristics, choosing the right material such as TiO_3, SnO_3,

or ZnO is crucial. The findings of acceptor density and MS capacitance characteristics are also influenced by the fabrication process, which includes the annealing temperature and layer thickness (Weiss *et al.*, 2016). Researchers can increase the precision of retrieved electrical parameters, improve overall PSC performance, and guarantee device stability by comprehending and optimizing the acceptor density. The link between acceptor density and capacitance is provided by Equation 5.7 (You, 2005).

$$\frac{1}{C^2} = \frac{2(V - V_{fb})}{\epsilon\epsilon_0 q N_A} \qquad (5.7)$$

In this case, ϵ is the semiconductor's dielectric constant, ϵ_0 is the permittivity of free space, q is the elementary charge (charge of an electron), N_A is the acceptor density for a p-type semiconductor, and C is the capacitance per unit area of the depletion region.

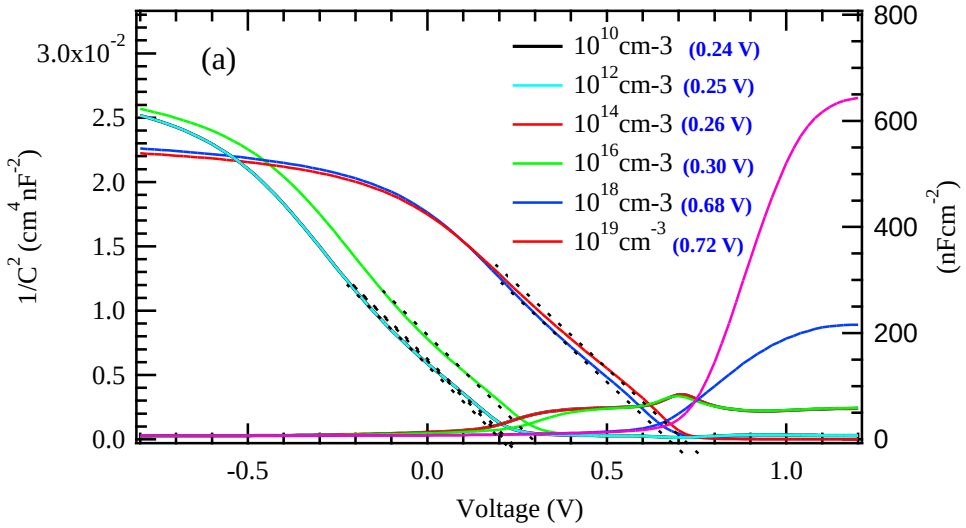

Figure 5.8: Effect of acceptor density on MS capacitance analysis

Acceptor density's effect on the MS capacitance analysis in the model PSC is shown in Figure 5.8. The applied voltage (V) is represented by the x-axis, while the inverse square of the capacitance ($1/C^2$) is displayed on the y-axis. The acceptor densities associated with each curve range from 10^{10} cm-3 to 10^{19} cm-3. The voltage at which the depletion region begins to form shown by the sharp spike in $1/C^2$ shifts to higher voltages as acceptor density rises. This shift suggests that in order to reach depletion, larger acceptor densities need a higher applied voltage. Higher acceptor densities are also associated with a rise in the V_{bi}, which is determined from the x-intercept of the linear section of the MS plot. With a distinct linear area, the capacitance exhibits a more typical MS behaviour at lower acceptor densities of 10^{10} cm-3 to 10^{16} cm^{-3}. The capacitance action, on the other hand, has many inflection points and becomes more complex at greater acceptor densities (10^{18} and 10^{19} cm^{-3}). Additional effects like altered

depletion widths, heightened recombination, or other transport layer effects could be the cause of this complexity.

The capacitance values can be used to infer the depletion width; higher acceptor densities are associated with thinner depletion regions, as indicated by higher capacitance values at a given voltage. Higher acceptor densities generally indicate better built-in electric fields, which may improve device performance by enhancing charge separation. On the other hand, the more complex capacitance behaviour at the highest densities suggests that very high acceptor densities could introduce negative effects like increased recombination. In conclusion, Figure 5.8 illustrates the relationship between the depletion zone, V_{bi}, and total capacitance as the acceptor density increases behaviour in PSCs.

5.3.10 Effect of donor density on MS capacitance analysis

The HTL in PSCs has a major effect on the overall functioning of the device since it is necessary for effective hole extraction and conveyance. The donor density of the is one of its important characteristics, and MS capacitance analysis can be used to investigate it. By analysing a semiconductor junction's capacitance-voltage (C-V) characteristics, this technique can reveal information on the device's Vbi and charge carrier density (Rajendran *et al.,* 2024). Equations 5.8 can be used in MS analysis to determine the relationship between a junction's capacitance (C) and applied voltage (V) (Huang *et al.,* 2024):

$$\frac{1}{C_{SC}^2} = \frac{2}{\epsilon\epsilon_0 e N_d}\left(E - E_{fb} - \frac{K_B T}{e}\right) \qquad (5.8)$$

In this context, C_{SC} is the space charge capacitance, B is the vacuum dielectric constant, e is the elementary charge, Nd is the charge carrier density, E_{fb} is the flat band potential (V_{fb}), K_B is the Boltzmann constant, T is the temperature, and E is the electrode potential.

The MS plot is influenced substantially by the donor density of the. This plot's steeper slope, which indicates a higher concentration of charge carriers, corresponds to a higher donor density (Bhattacharjee *et al.,* 2024). Conversely, a lower charge carrier concentration is reflected by a shallower slope that results from a lower donor density. Changes in the donor density can also have an impact on the V_{bi}, which is likewise provided by the voltage axis intercept of the MS plot (Yu *et al.,* 2024). The depletion region width in the is influenced by the donor density. A higher donor density narrows the depletion width, which affects the capacitance found in the analysis. Consequently, at a given voltage, an increase in donor density usually results in a decrease in junction capacitance because of the narrower depletion region (Gülnahar *et al.,* 2024). Conversely, a broader depletion region at lower donor densities leads to higher capacitance values.

It is useful to comprehend how donor density affects MS capacitance analysis in order to optimize PSCs. In order to improve charge extraction and transport and, ultimately, device efficiency, it aids in the selection of suitable HTL materials and doping techniques. Better performance and stability of PSCs can be achieved by optimizing the electrical properties of the HTL to provide desired device characteristics, which can be achieved by customizing the donor density through material selection, interface design, or additive engineering.

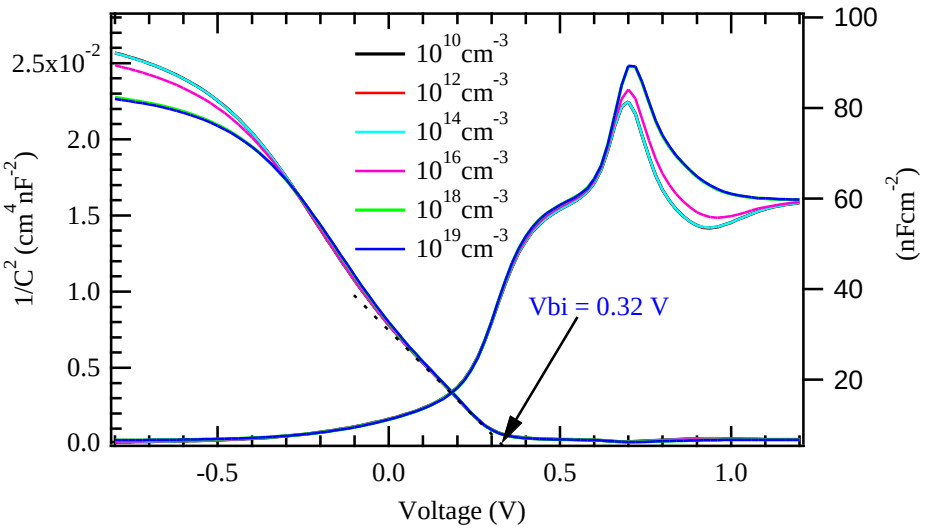

Figure 5.9: Effect of the donor density on MS capacitance analysis

The MS capacitance analysis for a solar cell with varying donor densities is shown in Figure 5.9. In a typical MS plot, the y-axis shows the reciprocal of the square of the capacitance ($1/C^2$), and the x-axis typically shows the voltage (V). A critical factor in solar cells that affects charge carrier separation and electric field distribution is the V_{bi}. Plots show that the V_{bi} is approximately 0.32 V and does not change much with different donor densities. This suggests that the capacitance is more affected by changes in donor density than V_{bi}. The MS plot shows notable variations when the donor density rises from 10^{10} cm^{-3} to 10^{19} cm^{-3}. The capacitance values are higher for lower donor densities (10^{10} cm-3 to 10^{14} cm^{-3}), indicating a lower carrier density in the depletion area.

On the other hand, the capacitance values fall at greater donor densities (10^{16} cm^{-3} to 10^{19} cm^{-3}), suggesting a larger carrier density in the depletion region. Donor density also affects the MS plot's slope, which represents the doping concentration. A higher doping concentration is indicated by a less steep slope, whereas a steeper slope denotes a lower doping concentration. Additionally, the plots demonstrate that the slope of the plot declines with increasing donor density, which is consistent with higher doping concentrations. The performance of the device is significantly impacted by these differences in donor density.

Elevated donor densities in the HTL have the potential to improve the overall performance of the solar cell by augmenting charge extraction and mitigating series resistance. Extremely high donor densities, however, may also result in higher recombination losses, which could offset these advantages. The MS analysis shows that the capacitance and doping profile of the solar cell are highly affected by changes in the HTL donor density. This in turn affects carrier dynamics and the way the electric field is distributed. Therefore, for the best solar cell efficiency, choosing the ideal donor density is essential to striking a balance between increased charge extraction and reducing recombination losses.

5.3.11 Effect of temperature on MS capacitance analysis

Temperature-related changes in the band gap of the semiconductor also affect the capacitance by altering the effective density of states (DOS) in the valence and conduction bands (Kumar *et al.,* 2024). Additionally, the semiconductor material's dielectric constant may change with temperature, affecting capacitance readings (Abid *et al.,* 2024). Temperature increases in PSCs can cause a number of measuring abnormalities that skew the data. These include mechanical stress brought on by component thermal expansion mismatches, increased hysteresis effects, and deterioration of the perovskite material. Reduced efficiency can result from higher temperatures because they can change the dynamics of charge carriers, increase dark current, and deteriorate layer interfaces. Measurement distortion can also be caused by variations in the bandgap of the perovskite material and an increase in electronic noise. To reduce these issues and guarantee accurate data, rigorous experimental design and efficient thermal control are crucial. Higher temperatures frequently cause leakage currents to become more noticeable, which could skew capacitance measurements (Husain *et al.,* 2024). Furthermore, temperature can alter the contact resistance between the semiconductor and the electrode, which can compromise the accuracy of the measurement. In different temperatures, the MS plot might show varied slopes and behaviours. The kind of semiconductor (n-type or p-type) and the variations in carrier concentration are related to these changes. Temperature-dependent reaction rates are explained by the Arrhenius equation (5.9) which may be used to examine how temperature affects PSC activation energy (Kim *et al.,* 2017).

$$k = A\ exp\left(\frac{E_a}{k_B T}\right) \tag{5.9}$$

The rate constant in this instance is denoted by k, the Boltzmann constant by K_B, the activation energy by Ea, the pre-exponential factor by A, and the temperature in Kelvin by T.

Temperature changes can modify the dielectric constant and the built-in potential in PSCs, which can impact the capacitance. These changes require a grasp of the general

relationship between capacitance and temperature. Temperature and capacitance are related in equation 5.10 (Atkins *et al.*, 2023).

$$C(T) = C_0 exp\left(\frac{-E_C}{k_B T}\right) \quad (5.10)$$

Here, C(T) is the capacitance at temperature T, C_0 is a pre-exponential factor related to capacitance, Ec is the characteristic energy for capacitance, K_B is the Boltzmann constant, T is the absolute temperature in Kelvins. As the temperature rises, the capacitance diminishes, demonstrating the temperature dependence of the dielectric properties and the V_{bi} in PSCs.

The linear portion of the plot, which is connected to the space-charge area, will be impacted by temperature as it influences these parameters. This change may have an effect on the doping concentration and V_{fb} determination. It is essential to calibrate measurements and account for temperature-induced fluctuations in order to interpret MS findings effectively while taking temperature effects into account. Analysing the data from measurements made at various temperatures can reveal important information about the behaviour and characteristics of the semiconductor.

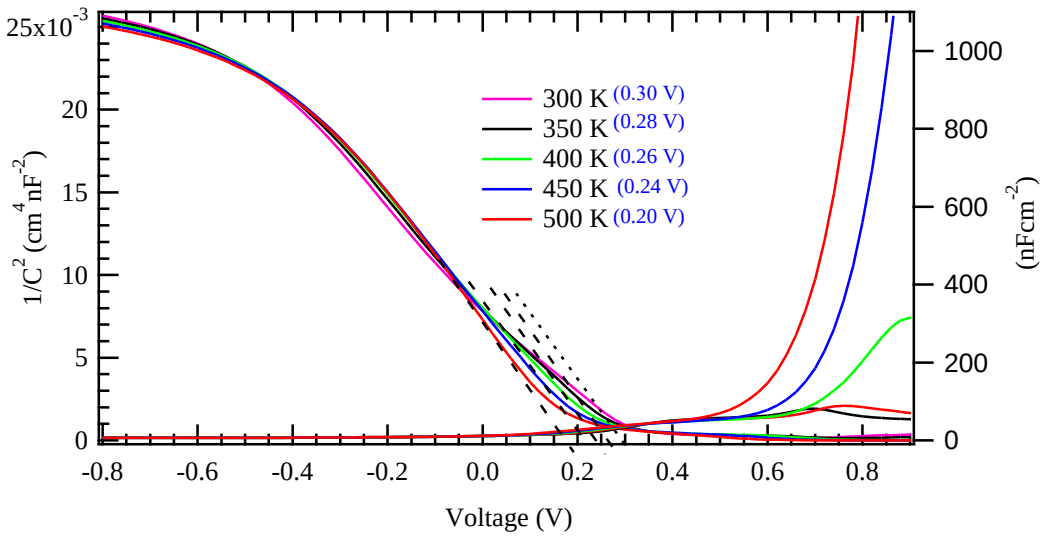

Figure 5.10: Effect of temperature on MS capacitance analysis

Capacitance-voltage (C-V) characteristics of semiconductor devices, such as solar cells, are examined by MS analysis, which offers important insights into parameters including doping concentration and the V_{bi} (Gülnahar *et al.*, 2024). The MS charts for a solar cell at various temperatures (300 K, 350 K, 400 K, 450 K, and 500 K) are displayed in Figure 5.10. A thorough examination of how temperature affects MS capacitance yields numerous important findings. As the temperature rises, the flat-band potential (V_{fb}) approaches lower voltages. This change suggests that the solar cell's intrinsic potential is temperature-dependent, with the flat-band potential rising with temperature. Second, as temperature rises, the MS plot's

slope, which is inversely proportional to the doping concentration (N_D), diminishes. This implies that at greater temperatures, the effective doping concentration rises. Changes in defect states inside the solar cell or increased carrier production are the causes of the increase in doping concentration. Furthermore, at a given voltage, the capacitance of the cell structure rises with temperature. Generally, elevated temperatures are correlated with higher capacitance values.

The higher thermal production of carriers, which results in a higher charge density in the depletion region, is the cause of the enhanced capacitance. Additionally, at higher temperatures, especially between 450 K and 500 K, the MS plots show more noticeable non-linearity and deviations from perfect linear behaviour. Defect states, higher carrier recombination, and other structural irregularities in the solar cell can all contribute to these variations. The precision of parameter extraction from the MS analysis, such as doping concentration and V_{bi}, is impacted by these variations. Lastly, modifications to the material properties of the solar cell, such as bandgap narrowing, elevated intrinsic carrier concentration, and modified defect states, are connected to the temperature dependency seen in the MS analysis. These modifications have an effect on the efficiency and V_{oc} of the solar cell as well as its overall performance.

In general, the MS capacitance analysis shows that temperature has a major effect on a solar cell's electrical properties. The capacitance rises, the effective doping concentration increases, and the flat-band potential decreases with temperature. Additionally, when the temperature rises, the MS plots show increased non-linearity and deviations, revealing intricate interactions between the material and structure of the solar cell (Sibu *et al.,* 2024). Optimizing solar cell performance under a range of operating situations requires an understanding of these impacts.

5.3.12 Nyquist plot for the model cell

The first step in creating a Nyquist plot is to obtain impedance data for the model cell over a range of frequencies. Examining the Nyquist plot's many properties can provide light on the electrochemical behaviour of the cell. Plots typically exhibit a line that approaches the real axis at high frequencies. This area often indicates the resistance of the cell and provides a clear indicator of the series resistance of the cell (R_S) (Zhu *et al.,* 2023). The plot frequently bends or forms a semicircle as the frequency drops. The cell's inductive or capacitive characteristics are shown by its curvature. On the other hand, the low-frequency behaviour can shed light on Warburg impedance or diffusion-related phenomena, which are important to comprehend for things like ion diffusion in electrochemical cells (Sriram *et al.,* 2024). All things considered,

the Nyquist plot is an effective diagnostic tool that aids in deciphering the intricate relationships and dynamics within a model cell, offering insightful data for both theoretical research and real-world applications (Pandey *et al.*, 2024).

The model cell's electrochemical impedance is depicted in the Nyquist plot. The charge transfer resistance between the HTL (GO) and the perovskite layer ($CH_3NH_3SnI_3$) is shown by a semicircle that is usually visible at high frequencies. Warburg impedance regions, which are indicative of diffusion-limited processes, are frequently seen in the plot at lower frequencies (Srivastava *et al.*, 2021). The low-frequency region sheds light on ion migration and overall cell performance, while the diameter of the semicircle provides information on the charge transfer resistance. By examining these factors, one may evaluate the stability and efficiency of the cell and improve material interfaces to maximize charge extraction and reduce resistive losses.

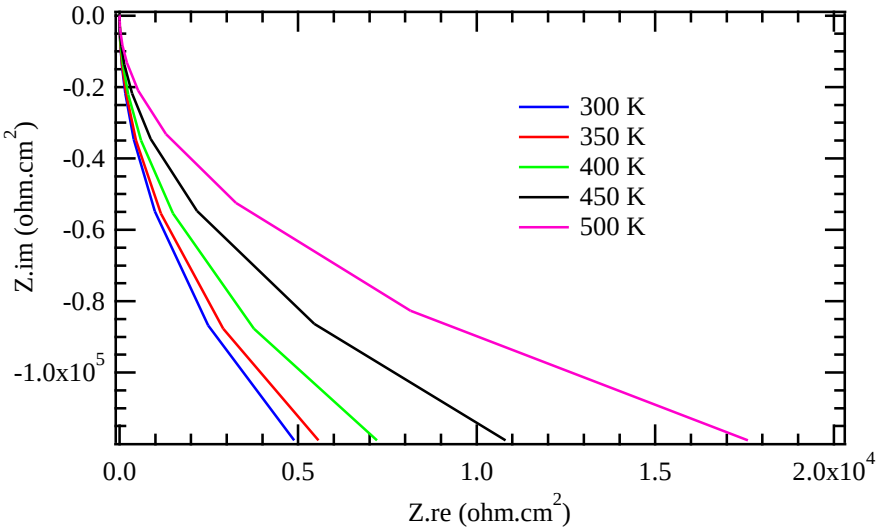

Figure 5.11: Nyquist plot for the model cell

The model solar cell's impedance response at different temperatures (300 K, 350 K, 400 K, 450 K, and 500 K) is displayed in Figure 5.11. With the real part of the impedance (Z') drawn on the x-axis and the imaginary part (Z") plotted on the y-axis, Nyquist plots are typically used to depict complicated impedance data. Each plotted curve represents the impedance response at a particular temperature. In a Nyquist plot, each semicircle is typically linked to a distinct physical process occurring within the solar cell, such as transport resistance, recombination, and charge transfer resistance. The semicircles shift to the left, indicating a discernible drop in overall impedance as the temperature rises from 300 K to 500 K. Lower impedance values are often the result of increased carrier mobility and less recombination resistance at higher temperatures. Impedance measurements across a range of frequencies are plotted, with the low-frequency response shown at the right end of each curve and the high-

frequency response shown at the left. Low frequencies represent slower processes such charge recombination, while high frequencies are primarily controlled by the resistance and capacitance of the bulk material and contacts.

The characteristic frequencies at which the impedance is primarily reactive are shown by the peaks in the imaginary part of the impedance (Z''). Changes in the temporal constants of the activities taking place inside the solar cell can be inferred from the shift in these peaks with temperature. The graphs show larger semicircles at lower temperatures (e.g., 300 K and 350 K), indicating higher overall impedance and implying slower recombination rates and more resistance to charge carriers. In contrast, the semicircles look much smaller at higher temperatures (e.g., 450 K and 500 K), indicating lower resistance and suggesting that charge carriers can move more freely but recombine more quickly. In conclusion, the Nyquist plot provides insights into the fundamental device physics that impact performance by showing how the solar cell's impedance varies with temperature. Fitting the Nyquist plot and obtaining quantitative data on these processes can be done with a comprehensive equivalent circuit model, which typically consists of components like resistors, capacitors, and constant phase elements. Understanding and maximizing the efficiency of solar cells under various operating situations depends on this approach.

5.4 Conclusions

The proposed device structure demonstrates exceptional performance, achieving a notable power conversion efficiency of 36.27% at an optimal absorber thickness of 1000 nm. This device reaches a peak quantum efficiency of 100% within the 360 to 700 nm wavelength range, indicating excellent photon absorption for enhanced power generation. The quantum efficiency varies from approximately 85% at 300 nm to 87% at 900 nm. Mott-Schottky capacitance analysis, influenced by temperature, reveals a built-in potential (V_{bi}) of 0.30 V at 300 K, which decreases significantly to 0.2 V at 500 K, suggesting that the device retains around 67% of its power at higher temperatures still an impressive performance. Altering the donor density from 10^{10} cm^{-3} to 10^{19} cm^{-3} does not significantly impact the Vbi, which remains steady at 0.32 V, indicating that increased donor density does not substantially affect the device's operation. Conversely, increasing the acceptor density from 10^{10} cm^{-3} to 10^{19} cm^{-3} raises the V_{bi} from 0.2 to 0.72 V, suggesting improved performance at higher acceptor densities. The band diagram analysis of the device indicates a consistent V_{bi} of 0.32 V. Overall, incorporating graphene oxide (GO) as the HTL enhances carrier mobility and reduces recombination losses, while using iron as the back contact improves electrical conductivity and device stability. Although based on simulation, this study offers valuable insights into the

mechanisms driving perovskite solar cell (PSC) performance. By examining generation-recombination dynamics, carrier transport, and interfacial engineering, the performance metrics of this cell are robust and could guide the development of highly efficient solar devices. This research supports the push towards sustainable energy, and future studies should aim to experimentally validate these results, explore new HTL materials, and address stability challenges to facilitate the scalability and commercialization of next-generation photovoltaic technologies.

REFERENCES

Abid, D., Mjejri, I., Oueslati, A., Guionneau, P., Pechev, S., Daro, N., & Elaoud, Z. (2024). A nickel-based semiconductor hybrid material with significant dielectric constant for electronic capacitors. *ACS omega*, ***9***(11), 12743-12752.

Afrin, P., Farjana, K., Vumije, A., & Uddin, M. N. (2024). An investigation on the impact of temperature variation over the performance of formamidinium tin iodide perovskite solar cell using SCAPS simulation. *AIP Advances*, ***14***(7) 1-38.

Ahmad, W., Noman, M., Tariq Jan, S., & Khan, A. D. (2023). Performance analysis and optimization of inverted inorganic CsGeI3 perovskite cells with carbon/copper charge transport materials using SCAPS-1D. *Royal Society open science*, ***510***(3), 1-37.

Ahmadi, Y., & Kim, K.-H. (2024). Modification strategies for visible-light photocatalysts and their performance-enhancing effects on photocatalytic degradation of volatile organic compounds. *Renewable and Sustainable Energy Reviews*, ***189****(8)*, 1-12.

Ahn, N., & Choi, M. (2024). Towards Long-Term Stable Perovskite Solar Cells: Degradation Mechanisms and Stabilization Techniques. *Advanced Science*, ***11***(4), 1-18.

Akram, M. Y., Ashraf, T., Tong, L., Yin, X., Dong, H., & Lu, H. (2024). Architecting High-Performance Photocatalysts: A Review of Modified 2D/2D Graphene/g-C3N4 Heterostructures. *Journal of Environmental Chemical Engineering*, ***12***(5), 1-9.

Al Dmour, H. (2023). SCAPS Numerical Analysis of Graphene Oxide/TiO2 Bulk Heterojunction Solar Cell Sensitized byN719 Ruthenium Dye. *East European Journal of Physics*, ***2312***(3), 555-561.

An, Y., Zhang, N., Zeng, Z., Cai, Y., Jiang, W., Qi, F., Ke, L., Lin, F. R., Tsang, S. W., & Shi, T. (2024). Optimizing crystallization in wide-bandgap mixed halide perovskites for high-efficiency solar cells. *Advanced Materials*, ***36***(17), 23-43.

Asghar, U., Qamar, M. A., Hakami, O., Ali, S. K., Imran, M., Farhan, A., Parveen, H., & Sharma, M. (2024). Recent Advances in Carbon Nanotube Utilization in Perovskite Solar Cells: A Review. *Micromachines*, ***15***(4), 529-560.

Atkins, P. W., De Paula, J., & Keeler, J. (2023). *Atkins' physical chemistry*. Oxford university press, 9***2***(8), 1-11.

Azmi, R., Zhumagali, S., Bristow, H., Zhang, S., Yazmaciyan, A., Pininti, A. R., Utomo, D. S., Subbiah, A. S., & De Wolf, S. (2024). Moisture-resilient perovskite solar cells for enhanced stability. *Advanced Materials*, ***36***(12), 22-53.

Azri, F., Meftah, A., Sengouga, N., & Meftah, A. (2019). Electron and hole transport layers optimization by numerical simulation of a perovskite solar cell. *Solar Energy*, ***181****(6)*, 372-378.

Bhattacharjee, S. K., Debnath, C., Hussain, S. A., Paul, P. K., & Bhattachrjee, D. (2024). Confirmation of charge carriers' types based on HOMO-LUMO positions in the active layer of a WORM memory device. *Journal of Materials Science: Materials in Electronics*, ***35***(2), 143-148.

Cahyana, A., Liandi, A., Yunarti, R., Febriantini, D., & Ardiansah, B. (2019). Green synthesis of dihydropyrimidine based on cinnamaldehyde compound under solvent-free using graphene oxide as catalyst. AIP Conference Proceedings, ***2168***(1), 1-8

Cetin, C., Chen, P., Hao, M., He, D., Bai, Y., Lyu, M., Yun, J. H., & Wang, L. (2018). Inorganic p-Type Semiconductors as Hole Conductor Building Blocks for Robust Perovskite Solar Cells. *Advanced Sustainable Systems*, ***2***(8-9), 1-32.

Chen, M., Dong, Y., Zhang, Y., Zheng, X., McAndrews, G. R., Dai, Z., Jiang, Q., You, S., Liu, T., & Harvey, S. P. (2024). Stress Engineering for Mitigating Thermal Cycling Fatigue in Perovskite Photovoltaics. *ACS Energy Letters*, ***9****(5)*, 2582-2589.

Cho, J. S., Jang, W., Mun, S. C., Yi, M., Park, J. H., & Wang, D. H. (2018). Tuning surface chemistry and morphology of graphene oxide by γ-ray irradiation for improved performance of perovskite photovoltaics. *Carbon*, ***139****(6)*, 564-571.

Chowdhury, T. A., Zafar, M. A. B., Islam, M. S.-U., Shahinuzzaman, M., Islam, M. A., & Khandaker, M. U. (2023). Stability of perovskite solar cells: issues and prospects. *RSC advances*, ***13***(3), 1787-1810.

Dou, D., Sun, H., Li, C., Gan, S., & Li, L. (2024). Perovskite-Based Indoor Photovoltaics and their Competitors. *Advanced Functional Materials*, ***39***(13), 1-28.

Dudipala, K. R., Le, T. H., Nie, W., & Hoye, R. L. (2024). Halide Perovskites and Their Derivatives for Efficient, High-Resolution Direct Radiation Detection: Design Strategies and Applications. *Advanced Materials*, ***36***(8), 1-22.

Elangovan, N. K., Kannadasan, R., Beenarani, B., Alsharif, M. H., Kim, M.-K., & Inamul, Z. H. (2024). Recent developments in perovskite materials, fabrication techniques, band gap engineering, and the stability of perovskite solar cells. *Energy Reports*, ***11****(6)*, 1171-1190.

Ghahremanirad, E., Almora, O., Suresh, S., Drew, A. A., Chowdhury, T. H., & Uhl, A. R. (2023). Beyond protocols: Understanding the electrical behavior of perovskite solar cells by impedance spectroscopy. *Advanced Energy Materials*, ***13***(30), 1-33.

Ghorpade, U. V., Suryawanshi, M. P., Green, M. A., Wu, T., Hao, X., & Ryan, K. M. (2022). Emerging chalcohalide materials for energy applications. *Chemical Reviews*, ***123***(1), 327-378.

Gülnahar, M., Mehmood, H., Canar, H. H., & Nasser, H. (2024). Analysis on the capacitance-voltage characteristics of metal-insulator-semiconductor capacitors based on thermally evaporated WOx on n-and p-type crystalline silicon. *Materials Science and Engineering: B*, ***304****(9)*, 1-30.

Hossain, M. J., Sun, M., & Davis, K. O. (2024). Photon management in silicon photovoltaic cells: A critical review. *Solar Energy Materials and Solar Cells*, ***267****(5)*, 1-21.

Huang, Y., Zhang, X., Li, L., Humayun, M., Zhang, H., Xu, X., Anthony, S. P., Chen, Z., Zeng, J., & Shtansky, D. V. (2024). Mott–Schottky Barrier Enabling High-Performance Hydrazine-Assisted Hydrogen Generation at Ampere-Level Current Densities. *Advanced Functional Materials*, ***26*** *(9)*, 1-13.

Husain, S., Harris, I., Gao, G., Li, X., Meisenheimer, P., Shi, C., Kavle, P., Choi, C. H., Kim, T. Y., & Kang, D. (2024). Low-temperature grapho-epitaxial La-substituted BiFeO3 on metallic perovskite. *Nature Communications*, *15*(1), 479-488.

Jamaluddin, N. I. I. M., Yusoff, M. Z. M., & Malek, M. F. (2024). Numerical Modelling of High Efficiency Silicon Solar Cell Using Various Anti Reflective Coatings (ARC). *Trends in Sciences*, ***21***(3), 7337-7337.

Jha, B. K., Chaule, S., & Jang, J.-H. (2024). Enhancing photocatalytic efficiency with hematite photoanodes: principles, properties, and strategies for surface, bulk, and interface charge transfer improvement. *Materials Chemistry Frontiers*, ***8***(10), 2197-2226.

Jiang, D., Sun, J., Ma, R., Wong, V. K., Yuan, J., Gao, K., Chen, F., So, S. K., Hao, X., & Li, G. (2024). Extracting charge carrier mobility in organic solar cells through space-charge-limited current measurements. *Materials Science and Engineering: R: Reports*, ***157****(8)*, 100772.

Jiao, P., Li, S., Zhu, G., Xu, H., Wang, K., Zhao, Y., Zhang, X., Jiang, K., Jiang, X., & Huang, Y. (2024). Effect of in layer thickness on the photoelectric properties of indium tin oxide (ITO)/In/ITO multilayer films. *Thin Solid Films*, ***789****(3)*, 140172.

Jimoh, O. M., Florence, I. N., Akinbolati, A., Nnachi, C., Ajani, C., Gyuk, P. M., Magaji, S., & Danladi, E. (2022). Investigating the Performance of Perovskite Solar Cells Using Nickel Oxide and Copper Iodide as P-type Inorganic layers by SCAPS-1D Simulation. *Phys. Access*,***65***(2) 37-50.

Jouybar, S., Naji, L., Sarabadani Tafreshi, S., & de Leeuw, N. H. (2024). A Density Functional Theory Study of the Physico-Chemical Properties of Alkali Metal Titanate Perovskites for Solar Cell Applications. *Molecules*, ***29***(14), 3355.

Kanoun, A.-A., Kanoun, M. B., Merad, A. E., & Goumri-Said, S. (2019). Toward development of high-performance perovskite solar cells based on CH3NH3GeI3 using computational approach. *Solar Energy*, ***182****(9)*, 237-244.

Khalil, A. A. A., Karmalawi, A. M., Abdelmageed, A. A., Al-shamiri, H. A., Shawkey, H. A., Kana, M. T. A., Swillam, M. A., & Kandel, H. M. (2024). Fast response fabricated MoS2-photodiode based thin film. *Journal of Materials Science: Materials in Electronics*, ***35***(8), 546.

Khan, A. D., Mustajab, M., Moeen, S., Imran, M., Ikram, M., Khan, Q., & Khan, M. (2024). Advancements in the stability, protection and lead-free strategies of perovskite solar cells: a critical review. *Environmental Science Advances*, ***3***(7), 1004-1029.

Khan, M. U., Shafiq, F., Janjua, M. R. S. A., Khalid, M., Yaqoob, J., Arshad, M., Alshehri, S. M., & Khan, R. A. (2024). Predicting benzodithiophene based donor materials with enhanced 19.09% PCE, open-circuit voltage and optoelectronic attributes for solar cell applications: Photochemical insights from DFT. *Journal of Photochemistry and Photobiology A: Chemistry*, ***446****(8)*, 115115.

Khelifi, W., & Luscombe, C. K. (2024). Recent Developments in Indacenodithiophene and Indacenodithienothiophene-based Donor-Acceptor Conjugated Polymers: From Design to Device Performance in Organic Electronics. *Progress in Polymer Science*, ***151****(2024)*, 1-40.

Kim, J., Park, N., Yun, J. S., Huang, S., Green, M. A., & Ho-Baillie, A. W. (2017). An effective method of predicting perovskite solar cell lifetime–Case study on planar CH3NH3PbI3 and HC (NH2) 2PbI3 perovskite solar cells and hole transfer materials of spiro-OMeTAD and PTAA. *Solar Energy Materials and Solar Cells*, ***162****(5)*, 41-46.

Kirchartz, T., Gong, W., Hawks, S. A., Agostinelli, T., MacKenzie, R. C., Yang, Y., & Nelson, J. (2012). Sensitivity of the Mott–Schottky analysis in organic solar cells. *The Journal of Physical Chemistry C*, ***116***(14), 7672-7680.

Kumar, M., Devi, M., Singh, D. V., Gupta, K., Raj, A., Pundir, S. K., Anshul, A., & Thakur, O. (2024). Advances in green energy conversion efficiency and interfacial engineering investigations of lead-free FASnI3-based PSC device. *Journal of Physics and Chemistry of Solids*, ***193***(9), 105-110.

Landgrave-Barbosa, F., Marmolejo-Valencia, A. F., Baray-Calderón, A., Hu, H., Aguilar-Cordero, J. C., Amador-Bedolla, C., & Ugalde-Saldivar, V. M. (2022). Impact of thickness of spin-coated P3HT thin films, over their optical and electronic properties. *Journal of Solid State Electrochemistry*,***26***(9) 649–661.

Li, C., Wu, Q., Liang, A., Chen, G., Chen, S., Su, Z., & Liang, G. (2024). Suppressing CuZn Deep-level Trap for Ultrafast Response in Kesterite Photodetector. *Surfaces and Interfaces*, ***52***(9), 104853-104858.

Li, Y., Ru, X., Yang, M., Zheng, Y., Yin, S., Hong, C., Peng, F., Qu, M., Xue, C., & Lu, J. (2024). Flexible silicon solar cells with high power-to-weight ratios. *Nature*, ***626***(7997), 105-110.

Liu, Q., Leng, C., & Yuan, J. (2018). A planar heterojunction perovskite solar cell modified by graphene oxide. IOP Conference Series: Materials Science and Engineering, ***458****(3)*, 1-8

Lohia, P., Singh, S., Srivastava, V., Agarwal, S., Dwivedi, D., Rai, S., Tighezza, A. M., & Hossain, M. K. (2024). Performance enhancement of organic perovskite solar cell with graphene oxide as electron transport layer. *Journal of Optics*, ***18****(9)*, 1-8.

Mathew, C. M., & Snigdhapriya, V. (2024). Computational analysis of ternary cation perovskite based solar cells employing transition metal chalcogenide, graphene derivatives, and SWCNT as hole transport layers. *Materials Today Communications*, ***39****(4)*, 109088-109095.

Mohammad, A., & Mahjabeen, F. (2023). Promises and challenges of perovskite solar cells: a comprehensive review. *BULLET: Jurnal Multidisiplin Ilmu*, ***2***(5), 1147-1157.

Mohandes, A., & Moradi, M. (2024). Improved performance of inorganic CsPbI3 perovskite solar cells with WO3/C60 UTL bilayer as an ETL structure: a computational study. *Physica Scripta*, ***99***(5), 1-30.

Mortadi, A., El Hafidi, E., Monkade, M., & El Moznine, R. (2024). Investigating the influence of absorber layer thickness on the performance of perovskite solar cells: a combined simulation and impedance spectroscopy study. *Materials Science for Energy Technologies*, ***7****(5)*, 158-165.

Muduli, S. P., & Kale, P. (2024). Effect of diffusion doping-induced defects on shunt resistance affecting Si-nanowire solar cell performance. *Journal of Materials Science: Materials in Electronics*, *35*(6), 430-442.

Mukhamale, S. V., Kartha, M. J., & Khirade, P. P. (2024). Experimental, theoretical and numerical simulation-based investigations on the fabricated Cu2ZnSn thin-film-based

Schottky diodes with enhanced electron transport for solar cell. *Scientific reports*, ***14***(1), 1-9.

Nagar, N., Shukla, R., Srivastava, A., Wadhwani, N., & Singh, N. Modeling and Simulation of Lead-free, formamidinium germanium-antimony halide (FA4GeSbCl12) based Solar Cell. Journal of Energy Chemistry, ***891***(6), 1-38.

Najim, A., Bajjou, O., Bakour, A., Moulaoui, L., & Rahmani, K. (2024). Numerical computing of CdTe-based solar cells with graphene oxide buffer layers using SCAPS-1D software. *Indian Journal of Physics*, ***98***(1), 67-77.

Nogueira, A. E., Ribeiro, L. S., Nogueira, F. G., & Torres, J. A. (2025). Semiconductors: An Introduction. In *Handbook of Semiconductors*. CRC Press, ***94***(8), 1-11.

Noman, M., Khan, Z., & Jan, S. T. (2024). A comprehensive review on the advancements and challenges in perovskite solar cell technology. *RSC advances*, ***14***(8), 5085-5131.

Noman, M., Shahzaib, M., Jan, S. T., Khan, Z., Ismail, M., & Khan, A. D. (2024). Optimizing band gap, electron affinity, & carrier mobility for improved performance of formamidinium lead tri-iodide perovskite solar cells. *Materials Science and Engineering: B*, ***300****(7)*, 1-14.

Oni, A. M., Mohsin, A. S., Rahman, M. M., & Bhuian, M. B. H. (2024). A comprehensive evaluation of solar cell technologies, associated loss mechanisms, and efficiency enhancement strategies for photovoltaic cells. *Energy Reports*, ***11****(5)*, 3345-3366.

Pandey, S. V., Prochowicz, D., Mahapatra, A., Pandiaraj, S., Alodhayb, A., Akin, S., & Yadav, P. (2024). The circuitry landscape of perovskite solar cells: An in-depth analysis. *Journal of Energy Chemistry*, ***94****(9)*, 393-413.

Pandiaraj, S., Aftab, S., Koyyada, G., Kabir, F., Hegazy, H., & Kim, J. H. (2024). Perovskite Photovoltaics: Exploring the Role of 2D and 1D Carbon-Based Interfacial Layers for Enhanced Stability and Efficiency. *Materials Today Energy*, ***44***(3)101629-101635.

Patil, J. V., Mali, S. S., Patil, A. P., Patil, P. S., & Hong, C. K. (2019). Highly efficient mixed-halide mixed-cation perovskite solar cells based on rGO-TiO2 composite nanofibers. *Energy*, ***189****(5)*, 116396-116400.

Rajendran, J., Raju, L., & Bojaraj, L. (2024). Analytical assessment of Schottky diodes based on CdS/Si heterostructure: current, capacitance, and conductance analysis using TCAD. *Indian Journal of Physics*, ***98***(9)2775–2784.

Reddy, K. R., Reddy, C. V., Nadagouda, M. N., Shetti, N. P., Jaesool, S., & Aminabhavi, T. M. (2019). Polymeric graphitic carbon nitride (g-C3N4)-based semiconducting

nanostructured materials: synthesis methods, properties and photocatalytic applications. *Journal of Environmental Management*, ***238****(2)*, 25-40.

Shao, S., & Loi, M. A. (2020). The role of the interfaces in perovskite solar cells. *Advanced Materials Interfaces*, ***7***(1), 1901469.

Sheikh, Y., Jasim, M., Qasim, M., Qaisieh, A., Hamdan, M. O., & Abed, F. (2024). Enhancing PV solar panel efficiency through integration with a passive Multi-layered PCMs cooling system: A numerical study. *International Journal of Thermofluids*, ***23***(4), 1-17.

Shen, X., Lin, X., Peng, Y., Zhang, Y., Long, F., Han, Q., Wang, Y., & Han, L. (2024). Two-Dimensional Materials for Highly Efficient and Stable Perovskite Solar Cells. *Nano-Micro Letters*, ***16***(1), 201-209.

Shin, H.-C., & Pyun, S.-I. (2024). Thermodynamic and electro-kinetic aspects of diffusion and migration (charge transfer) of electrons and holes across an np-type junction under bias and a photovoltaic cell under illumination. *Journal of Solid State Electrochemistry*, ***28***(3), 929-956.

Si, H., Zhao, X., Zhang, Z., Liao, Q., & Zhang, Y. (2024). Low-temperature electron-transporting materials for perovskite solar cells: Fundamentals, progress, and outlook. *Coordination Chemistry Reviews*, ***500****(1)*, 1-8.

Sibu, G. A., Gayathri, P., Akila, T., Marnadu, R., & Balasubramani, V. (2024). Manifestation on the choice of a suitable combination of MIS for proficient Schottky diodes for optoelectronics applications: A comprehensive review. *Nano Energy*, ***125***(8) 1-9.

Sriram, S., Olivan, L. A., White, R. J., & Rowe, A. R. (2024). Quantifying cathode biofilm resistance in a cdrAB modified Shewanella oneidensis MR-1 using electrochemical impedance spectroscopy. *Electrochimica Acta*, ***481****(20)*, 1-9.

Srivastava, P., Kumar, R., & Bag, M. (2021). The curious case of ion migration in solid-state and liquid electrolyte-based perovskite devices: Unveiling the role of charge accumulation and extraction at the interfaces. *Physical Chemistry Chemical Physics*, ***23***(18), 10936-10945.

Thomas, T. (2023). Simulation Study of Cs2TiBr6 Perovskite Solar Cells Using Graphene Oxide as a Novel HTL Layer Using SCAPS 1-D. *Renewable Energy Research and Applications*, ***4***(2), 159-169.

Wang, H., Zhang, C., Yao, Y., Cheng, C., & Wang, K. (2024). Non-Fullerene Organic Electron Transport Materials toward Stable and Efficient Inverted Perovskite Photovoltaics. *Small*, ***13***(4), 1-21.

Wang, S., Chen, C., Zhang, Z., Cai, Y., Zhang, Y., Gao, S., Chen, W., Guo, S., Abduryim, E., & Dong, C. (2024). Efficient thermoelectric properties and high UV absorption of stable zinc-doped all-inorganic perovskite for BIPV applications in multiple scenarios. *Solar Energy*, ***267****(1)*, 112240.

Weiss, T. P., Redinger, A., Rey, G., Schwarz, T., Spies, M., Cojocura-Mirédin, O., Choi, P.-P., & Siebentritt, S. (2016). Impact of annealing on electrical properties of Cu2ZnSnSe4 absorber layers. *Journal of Applied Physics*, ***120***(4),1-9.

Wen, H., Weng, B., Wang, B., Xiao, W., Liu, X., Wang, Y., Zhang, M., & Huang, H. (2024). Advancements in Transparent Conductive Oxides for Photoelectrochemical Applications. *Nanomaterials*, ***14***(7), 1-21.

Xamidullayevich, Y. A. (2024). Pplication Of Photovoltaic effects to Energy-Saving Materials Components of the Structure and Solar Cells. *The best intellectual research*, ***14***(2), 105-109.

Xie, B., Zhang, Y., Li, Y., Chen, W., Hu, X., & Zhang, S. (2020). Solution preparation of molybdenum oxide on graphene: A hole transport layer for efficient perovskite solar cells with a 1.12 V high open-circuit voltage. *Journal of Materials Science: Materials in Electronics*, ***31****(6)*, 6248-6254.

Ye, Y. C., Chen, L., Chen, X. M., Ma, C. Y., Lv, B. H., Wang, J. Y., Dou, W. D., Zhang, C., Ma, T. L., & Tang, J. X. (2024). Interfacial Energy Level Alignment and Defect Passivation by Using a Multifunctional Molecular for Efficient and Stable Perovskite Solar Cells. *Advanced Functional Materials*, ***34***(8), 1-10.

Yin, M., Yao, H., Qiu, H., Wu, C., Zhang, M., & Hao, F. (2024). A Revisit of Crystallization in Tin Halide Perovskite Thin Films: From Nucleation, Intermediate to Crystal Growth. *Advanced Functional Materials*, ***8***(9), 1-37.

You, C. (2005). *A high-speed, low power silicon germanium BiCMOS FPGA with new features for applications*. Rensselaer Polytechnic Institute ***38****(9)*, 6248-6254.

Yu, G., Liu, C., Wang, T., Wei, Y., Liu, W., Fu, W., Wu, X., Lin, P., Xu, L., & Cui, C. (2024). Sn-Doped Nb2O5 Films as Effective Hole-Selective Passivating Contacts for Crystalline Silicon Solar Cells. *Solar RRL*, ***8***(5), 1-8.

Zandi, O., Agrawal, A., Shearer, A. B., Reimnitz, L. C., Dahlman, C. J., Staller, C. M., & Milliron, D. J. (2018). Impacts of surface depletion on the plasmonic properties of doped semiconductor nanocrystals. *Nature Materials*, ***17***(8), 710-717.

Zang, L., Zhao, C., Hu, X., Tao, J., Chen, S., & Chu, J. (2024). Emerging Trends in Electron Transport Layer Development for Stable and Efficient Perovskite Solar Cells. *Small*, ***20***(1), 1-30.

Zhang, J., Li, T., Zheng, J., Xiao, Y., Li, X., Song, J., Cheng, C., Yang, W., & Chen, G. (2024). Hole transport layer in photoelectrochemical water splitting. *Solar RRL*, ***8***(1), 1-25.

Zhang, L., Deng, D., Lu, K., & Wei, Z. (2024). Optimization of charge management and energy loss in all-small-molecule organic solar cells. *Advanced Materials*, ***36***(22), 1-30.

Zhang, X., Ji, G., Xiong, D., Su, Z., Zhao, B., Shen, K., Yang, Y., & Gao, X. (2018). Graphene oxide as an additive to improve perovskite film crystallization and morphology for high-efficiency solar cells. *RSC advances*, ***8***(2), 987-993.

Zhao, C. X., Mao, A. Y., & Xu, G. (2014). Junction capacitance and donor-acceptor interface of organic photovoltaics. *Applied Physics Letters*, ***105***(6),1-6.

Zhao, K., Hu, Q., Cao, J., Qi, Y., Wei, P., Lu, Y., Cheng, J., & Xie, Y. (2024). Enhancing Efficiency and Stability in Carbon-Based Perovskite Solar Cells by Double Passivation with Ultralow-Cost Coal-Derived Graphene and Its Derivatives. *ACS Applied Materials & Interfaces*, ***16***(16), 20577-20586.

Zhong, S.-J., Chen, K.-Y., Wang, S.-L., Manshaii, F., Jing, N., Wang, K.-D., Liu, S.-C., & Zhou, Y.-L. (2024). Metal-based nanowires in electrical biosensing. *Rare Metals*, ***13***(6), 1-22.

Zhu, W., Wang, J., Luo, H., Luo, B., Li, X., Liu, S., & Li, C. (2023). Electrical Characterization and Analysis of Single Cells and Related Applications. *Biosensors*, ***13***(10), 907.

Znidi, F., Morsy, M., & Uddin, M. N. (2024). Recent advances of graphene-based materials in planar perovskite solar cells. *Next Nanotechnology*, ***5(9)***, 1-13.

CHAPTER SIX

GENERAL DISCUSSION, CONCLUSIONS, AND RECOMMENDATIONS

6.1. General Discussion

This work utilized the solar cell device simulator (SCAPS-1D) to analyse and optimize various high-performance perovskite solar cell (PSC) configurations, focusing on developing hole transport layer-free (HTL-free) and lead-free PSCs for enhanced solar energy capture, improved device efficiency, and better performance under diverse conditions. In this study, a novel HTL-free PSC of the configuration, ITO/PC61BM/$CH_3NH_3SnI_3$/Pt, was investigated. The objective was to enhance device performance by introducing buffer layers like cadmium sulphide (CdS) and optimizing ETLs. Mott-Schottky capacitance analysis provided crucial insights into the interface characteristics and charge carrier behaviour within the solar cell structure. Optimization of the back contacts played a key role in improving charge extraction and minimizing recombination losses. The simulation results were impressive, with a PCE of 38.11%, a J_{sc} of 35.32 mA/cm², an FF of 88.67%, and a V_{oc} of 1.2168 V. These findings demonstrate the potential of HTL-free PSCs to achieve high performance while reducing manufacturing costs.

Moreover, lead-Free PSC cell structure, ITO/PC61BM/$CH_3NH_3SnI_3$/PEDOT:PSS/Mo, aimed at optimising the thickness of the light-absorbing layer and assess the solar cell's temperature tolerance was thoroughly examined. The optimal thickness for the $CH_3NH_3SnI_3$ layer was determined to be 1000 nm, maximizing QE. Mott-Schottky capacitance analysis showed that the cell maintained 95% of its power output at 400 K, indicating excellent thermal stability. Key electrical parameters included a J_{sc} of 34.84 mA/cm², a V_{oc} of 1.5226 V, an FF of 71.04%, and a PCE of 37.66% at 300 K. The study also analysed the effects of different buffer layers (CdS, ZnS, ZnSe, and V_2O_5) and parasitic resistances on the cell's performance, offering valuable insights into developing lead-free solar energy technologies. In the third investigation, the PSC design with graphene oxide HTL (ITO/PC61BM/$CH_3NH_3SnI_3$/GO/Fe) was tested under various conditions. In this case, graphene oxide (GO), known for its exceptional electrical conductivity and mechanical properties, was used as the HTL to enhance charge transport and reduce recombination losses. The optimal thicknesses for GO and the absorber layer were determined to be 50 nm and 1000 nm, respectively. Comparative analysis of different HTL materials revealed that GO provided superior electrical performance. The optimised PSC achieved a V_{oc} of 1.3462 V, a J_{sc} of 34.84 mA/cm², an FF of 77.32%, and a PCE of 36.27%. The device also demonstrated strong photon capture efficiency, with quantum

efficiency (QE) ranging from 85% to 100% across wavelengths of 300 to 700 nm. These results highlight the importance of selecting appropriate HTL materials for optimal device performance and contribute to the development of advanced, eco-friendly solar energy technologies. Together, these studies underscore the potential of various PSC configurations to achieve high efficiency, thermal stability, and cost-effectiveness, advancing the pursuit of sustainable and scalable solar energy solutions.

6.2. Conclusions

This study highlights a pivotal breakthrough in the advancement of perovskite solar cell (PSC) technology, where material innovation, device engineering, and the use of advanced simulation tools are driving significant progress in solar energy. The shift from traditional lead-based PSCs to lead-free alternatives like $MASnI_3$ marks an important step toward sustainability, addressing both environmental and health concerns. The research emphasizes how careful design of device architectures, especially through interface engineering and the incorporation of novel materials such as graphene oxide (GO) and cadmium sulphide (CdS), has led to notable improvements in power conversion efficiency (PCE) and operational stability. This progress reflects a broader trend in renewable energy research, focusing not only on achieving high efficiencies but also on ensuring that these technologies are scalable, cost-effective, and environmentally friendly. The remarkable PCEs achieved in simulations, exceeding 38% in some instances, demonstrate the potential of these next-generation PSCs to outperform current photovoltaic technologies. The use of advanced simulation tools like SCAPS-1D plays a critical role in this development, enabling researchers to model and predict the behaviour of complex solar cell systems under various conditions. This capability is essential for refining material choices, optimizing band alignment, and improving charge transport mechanisms, all of which are key to enhancing PSC performance. The insights gained from this research not only contribute to the evolution of PSC technology but also support global efforts to decarbonize energy production. By advancing the design and fabrication of lead-free PSCs, this research helps facilitate the transition to a sustainable energy future, where solar power plays a central role in reducing dependence on fossil fuels and mitigating climate change. The ongoing exploration of innovative materials and device configurations will be crucial in unlocking the full potential of perovskite solar cells, ensuring their significance in the renewable energy landscape. Towards this end, the following conclusions can derived from this work:

i. The incorporation of CdS, ZnSe and TiO_2 buffer layers were effective in improving the methylammonium – based perovskite solar cell performance, resulting in a PCE exceeding 38% for both HTL-free and HTL-based configurations.

ii. In all the solar cell architectures investigated in this work, the PCE was above 35%, $J_{sc} > 34\ (mAcm^{-2}), V_{oc} > 1.2\ (V) and\ FF > 71\%,$ with the highest PCE and FF being recorded at 38.11% and 88.68%, respectively for the HTL-free cell structure.

iii. It is evident from the study that various solar cell architectures attained quantum efficiencies $> 90\%$ in the wavelength range 300 -700 nm indicating impressive solar capture for charge for effective charge transport and enhanced electricity generation

6.3. Recommendations

In order to assess how different material layers impact the performance of a solar cell architecture based on a methylammonium tin iodide photoactive layer, continued research into lead-free perovskite materials, is essential for developing high-performance, affordable and environmentally friendly perovskite solar cells. This is critical in evaluating the influence of interfaces on the electrical parameters of the solar cell architectures for possible scaling and manufacturing. The following recommendations can be deduced from this study.

i. Organic-based buffers such as fullerene, P3HT (poly(3-hexylthiophene), PEI (poly(ethyleneimine) and Spiro-OMeTaD should be investigated for the performance of cell architectures investigated in this work.

ii. Electrical outcomes such as PCE, J_{sc}, V_{oc}, and FF need to be determined for different photosensitizers – formamidinium tin iodide and chalcogenide-based perovskites in order to understand their performance in comparison to the cell devices evaluated in this work.

iii. Optical parameters such as absorption, bandgap and electron affinities should be simulated for the model cell structures using the density functional theory (DFT).

APPENDICES

Appendix I: SCAPS-1D graphical user interface

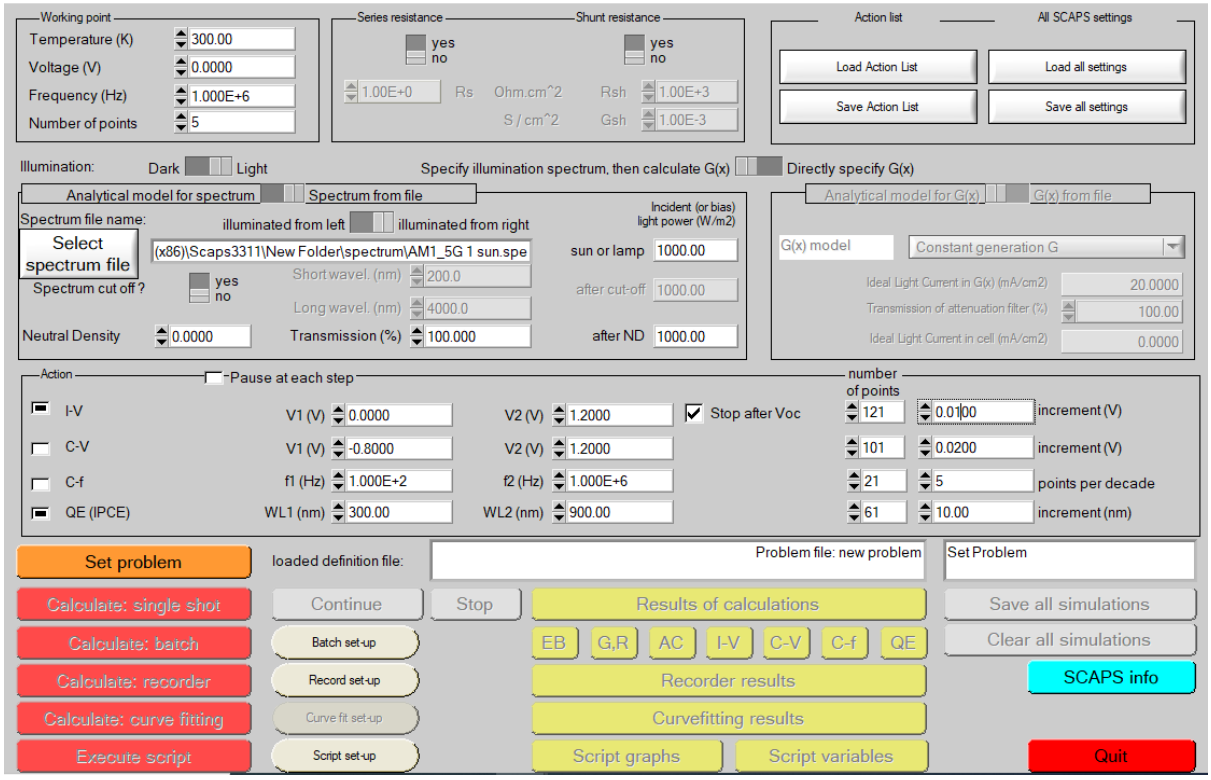

Appendix II: SCAPS-1D graphical user interface showing a solar cell architecture

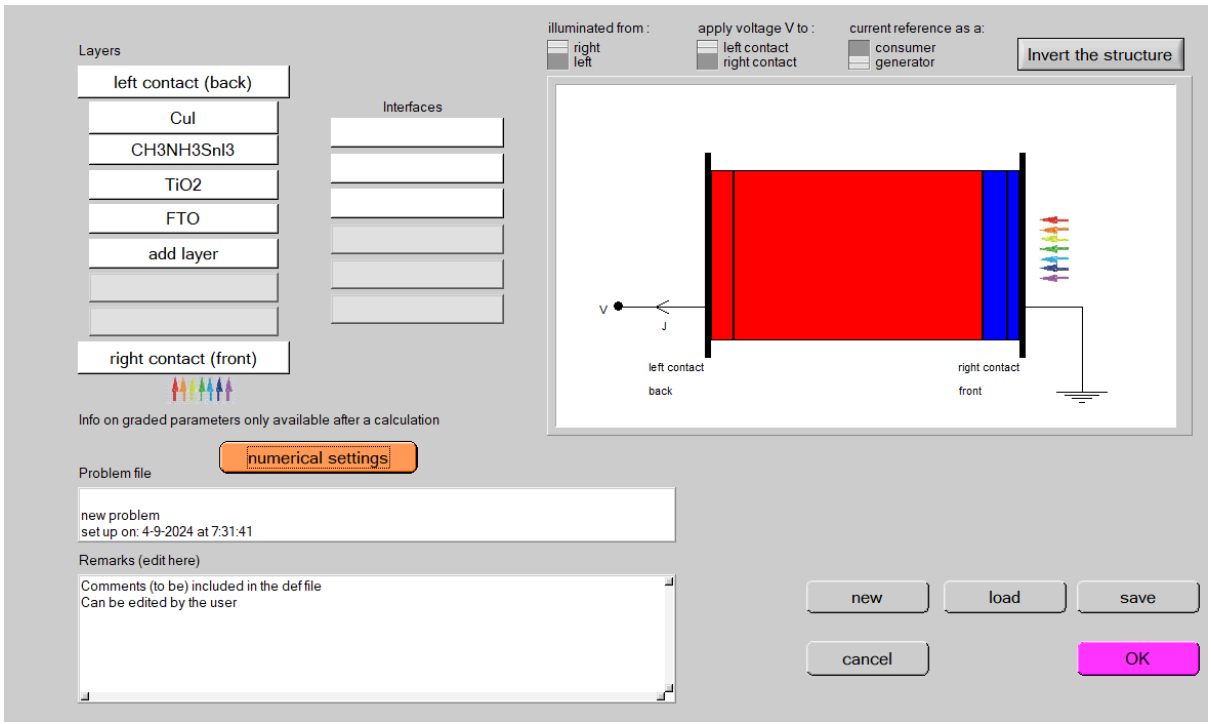

Appendix III: Publication 1

Hindawi
International Journal of Photoenergy
Volume 2023, Article ID 3801813, 35 pages
https://doi.org/10.1155/2023/3801813

Review Article

A Review of the Technological Advances in the Design of Highly Efficient Perovskite Solar Cells

George G. Njema and Joshua K. Kibet

Department of Chemistry, Egerton University, Njoro, Kenya

Correspondence should be addressed to Joshua K. Kibet; jkibet@egerton.ac.ke

Received 6 February 2023; Revised 24 March 2023; Accepted 10 July 2023; Published 7 August 2023

Academic Editor: Daniel T. Cotfas

The search for renewable and sustainable energy for energy security and better environmental protection against hazardous emissions from petro-based fuels has gained significant momentum in the last decade. Towards this end, energy from the sun has proven to be reliable and inexhaustible. Therefore, better light harvesting technologies have to be sought. Herein, the current trends in the development of perovskite solar cells with a focus on device engineering, band alignment, device fabrication with superior light harvesting properties, and numerical simulation of solar cell architectures are critically reviewed. This work will form the basis for future scientist to have a better scientific background on the design of highly efficient solar cell devices, which are cost-effective to fabricate, highly stable, and eco-friendly. This review presents thorough essential information on perovskite solar cell technology and tracks methodically their technological performance overtime. The photovoltaic (PV) technology can help to reduce pollution related to greenhouse gas emissions, criterion pollutant emissions, and emissions from heavy metals and radioactive species by nearly 90%. Following the introduction of highly efficient perovskite solar cell (PSC) technologies, the problems associated with stability, short life-time and lead-based perovskite solar cell configurations have significantly been minimized. The fabrication and simulation of perovskite solar cells has been made possible with advanced technologies and state-of-the-art computational codes. Furthermore, device simulation strategies have lately been used to understand, select appropriate materials, and gain insights into solar cell devices' physical behavior in order to improve their performances. Numerical simulation softwares such as the 1-dimenional solar cell capacitance simulator (SCAPS-1D), Silvaco ATLAS, and wx-analysis of microelectronic and photonic structures (wxAMPS) used to understand the device engineering of solar cells are critically discussed. Because of the need to produce charge collection selectivity, hole transport materials (HTMs) as well as electron transport materials (ETMs) constitute essential PSC components. In this work, the synthesis of inorganic HTMs, as well as their characteristics and uses in various PSCs comprising mesoporous and planar designs, are explored in detail. It is anticipated that the performance of inorganic HTLs on PSCs would encourage further research which will have a significant influence on the future designs and fabrication of highly efficient solar cells.

Appendix IV: Publication 2

Materials Today Communications 39 (2024) 108957

Contents lists available at ScienceDirect

Materials Today Communications

journal homepage: www.elsevier.com/locate/mtcomm

Numerical optimization of interface engineering parameters for a highly efficient HTL-free perovskite solar cell

George G. Njema [a], Joshua K. Kibet [a,*], Silas M. Ngari [a], Nicholas Rono [b]

[a] Department of Chemistry, Egerton University, Egerton, Kenya
[b] Fort Hare Institute of Technology, University of Fort Hare, Alice, South Africa

ARTICLE INFO

Keywords:
Buffer layers
HTL-free
Interface optimization
High performance
Mott-Schottky

ABSTRACT

Decarbonizing the world's energy system has set the stage in favor of renewable energy alternatives such as the more reliable, abundant, inexhaustible, and sustainable solar energy. However, the photovoltaic technology faces significant stability, longevity, and scalability challenges. These difficulties can be overcome by judicious optimization of interfacial engineering of the solar cell architecture that will decrease the cost of fabrication and enhance the solar cell performance and durability. Herein, a comprehensive analysis of a novel high-performance hole transport layer-free (HTL-free) perovskite solar cell (PSC) of the configuration, ITO/$PC_{61}BM$/$CH_3NH_3SnI_3$/Pt, was investigated by device simulation while optimizing electron transport materials, metal back contacts, front contact materials, and buffer layers. The focus is on enhancing device performance by introducing various types of buffer layers, such as cadmium sulphide (CdS) in the proposed solar cell model. By fine-tuning the ETL layers and manipulating perovskite acceptor and donor densities, better device performance was achieved. Furthermore, the Mott-Schottky capacitance analysis yielded critical insights into the interface properties and dynamics of charge carriers within the solar cell structure. Optimizing back contacts also play a critical role in charge extraction and reduced recombination losses. Leveraging a sophisticated simulation platform, SCAPS-1D, the study assesses how design strategies impact photovoltaic electrical outcomes such as open-circuit voltage (V_{oc}), power conversion efficiency (PCE), short-circuit current density (J_{sc}), and Fill factor (FF). The proposed HTL-free device posted remarkable results – PCE of 38.11 %, J_{sc} of 35.32 $mAcm^{-2}$, FF of 88.67 %, and V_{oc} of 1.2168 V. Accordingly, this work inspires the promising prospects of HTL-free PSCs in achieving robust solar harvesting capabilities while streamlining device affordability. Therefore, the proposed device architecture stimulates the journey towards affordable and high-performance scalable solar cell modules.

Appendix V: Publication 3

Contents lists available at ScienceDirect

Next Energy

journal homepage: www.sciencedirect.com/journal/next-energy

Performance optimization of a novel perovskite solar cell with power conversion efficiency exceeding 37% based on methylammonium tin iodide

George G. Njema, Joshua K. Kibet*, Silas M. Ngari

Department of Chemistry, Egerton University, Njoro, Kenya

ARTICLE INFO

Keywords:
Light harvesting
Interface properties
Quantum efficiency
Climate change
De-carbonization

ABSTRACT

The development of highly efficient lead-free solar cells is essential for sustainable energy production in the face of depleting fossil fuel resources and the negative effects of climate change. Perovskite solar cells (PSCs) containing lead pose considerable environmental and public health hazards, in addition to thermal stability and longevity challenges. Here, a novel lead-free solar cell design of the configuration, ITO/$PC_{61}BM$/$CH_3NH_3SnI_3$/PEDOT:PSS/Mo, is investigated for improved light harvesting capabilities, enhanced device performance, and better operational efficiency under various temperature conditions. The optimal thickness of the light-absorbing layer, $CH_3NH_3SnI_3$, was found to be 1000 nm for maximum quantum efficiency (QE). Further, the temperature tolerance of the solar cell was evaluated using Mott-Schottky (MS) capacitance analysis and showed that the model cell retains about 95% of its power at 400 K, demonstrating excellent thermal stability and robust performance. The solar cell also shows promising electrical output parameters, including a short-circuit current density (J_{sc}) of 34.84 mA/cm^2, open-circuit voltage (V_{oc}) of 1.5226 V, Fill factor (FF) of 71.04%, and an impressive power conversion efficiency (PCE) of 37.66% at 300 K. The effect of buffer layers such as CdS, ZnS, ZnSe, and V_2O_5 on the electrical outcomes of the model cell structure has been critically examined. Additionally, parasitic resistances and doping characteristics on the operational performance of the cell have been explored in detail. This work therefore, provides remarkable insights in the field of solar energy harvesting, offering potential sustainable energy generation solutions, supporting de-carbonization of the environment and climate change mitigation efforts towards an energy sustainable future.

Appendix VI: Research Permit

REPUBLIC OF KENYA

NATIONAL COMMISSION FOR SCIENCE, TECHNOLOGY & INNOVATION

Ref No: 972744

Date of Issue: 23/May/2024

RESEARCH LICENSE

This is to Certify that Mr.: George GEOEGE Njema of Egerton University, has been licensed to conduct research as per the provision of the Science, Technology and Innovation Act, 2013 (Rev.2014) in Nakuru on the topic: NUMERICAL ANALYSIS OF THE ELECTRICAL CHARACTERISTICS OF LEAD-FREE PEROVSKITE SOLAR CELL BASED ON METHYLAMMONIUM TIN IODIDE for the period ending : 23/May/2025.

License No: NACOSTI/P/24/35879

972744

Applicant Identification Number

Director General
NATIONAL COMMISSION FOR SCIENCE,TECHNOLOGY & INNOVATION

Verification QR Code

NOTE: This is a computer generated License. To verify the authenticity of this document, Scan the QR Code using QR scanner application.

See overleaf for conditions